DANIELLE CRISTINE MOTA FERREIRA

COMPLEXOS POLIELETRÓLITOS QUITOSANO-CARBOXIMETILCELULOSE: ESTUDO FÍSICO-QUÍMICO E APLICABILIDADE COMO CARREADORES DE VITAMINAS E ADSORVENTES DE POLUENTES

Tese apresentada à Universidade Federal de Viçosa, como parte das exigências do Programa de Pós-Graduação em Ciência e Tecnologia de Alimentos, para obtenção do título de *Doctor Scientiae*.

Orientador: Eduardo Basílio de Oliveira

Coorientadores: Jane Sélia dos Reis Coimbra
Alvaro Vianna Novaes de C. Teixeira

VIÇOSA - MINAS GERAIS
2023

Ficha catalográfica elaborada pela Biblioteca Central da Universidade Federal de Viçosa - Campus Viçosa

T
F383c
2023

Ferreira, Danielle Cristine Mota, 1993-
Complexos polieletrólitos quitosano-carboximetilcelulose: estudo físico-químico e aplicabilidade como carreadores de vitaminas e adsorventes de poluentes / Danielle Cristine Mota Ferreira. – Viçosa, MG, 2023.
1 tese eletrônica (154 f.): il. (algumas color.).

Inclui apêndices.
Orientador: Eduardo Basílio de Oliveira.
Tese (doutorado) - Universidade Federal de Viçosa, Departamento de Tecnologia de Alimentos, 2023.
Inclui bibliografia.
DOI: https://doi.org/10.47328/ufvbbt.2023.543
Modo de acesso: World Wide Web.

1. Colodais. 2. Química supramolecular. 3. Água - Purificação. I. Oliveira, Eduardo Basílio de, 1980-.
II. Universidade Federal de Viçosa. Departamento de Tecnologia de Alimentos. Programa de Pós-Graduação em Ciência e Tecnologia de Alimentos. III. Título.

CDD 22. ed. 541.345

Bibliotecário(a) responsável: Alice Regina Pinto Pires CRB-6/2523

DANIELLE CRISTINE MOTA FERREIRA

COMPLEXOS POLIELETRÓLITOS QUITOSANO-CARBOXIMETILCELULOSE: ESTUDO FÍSICO-QUÍMICO E APLICABILIDADE COMO CARREADORES DE VITAMINAS E ADSORVENTES DE POLUENTES

Tese apresentada à Universidade Federal de Viçosa, como parte das exigências do Programa de Pós-Graduação em Ciência e Tecnologia de Alimentos, para obtenção do título de *Doctor Scientiae*.

APROVADA: 30 de maio de 2023.

Assentimento:

gov.br Documento assinado digitalmente
DANIELLE CRISTINE MOTA FERREIRA
Data: 11/09/2023 11:34:37-0300
Verifique em https://validar.iti.gov.br

Danielle Cristine Mota Ferreira
Autora

gov.br Documento assinado digitalmente
EDUARDO BASILIO DE OLIVEIRA
Data: 11/09/2023 12:31:50-0300
Verifique em https://validar.iti.gov.br

Eduardo Basílio de Oliveira
Orientador

AGRADECIMENTOS

A Deus e à Nossa Senhora, por estarem sempre comigo, me guiando, iluminando cada passo meu e me abençoando. Obrigada por me darem a fé e a força necessária para lutar e enfrentar todos os obstáculos. Obrigada por tantos presentes divinos, por me darem talvez além do que posso merecer.

Obrigada aos meus amores, hoje anjos, Vô Raimundo, Vô Oscar e tio Edson, que tenho certeza que sempre estão olhando por mim e intercedendo a meu favor. Sem essa força divina, nenhuma conquista seria possível.

À minha mãezinha, pelo carinho, amor, incentivo e orações. Por ser a voz que tranquiliza meu coração, por sempre me motivar, entender minhas faltas e momentos de afastamento e me mostrar o quanto é importante estudar, mesmo não tendo ela a mesma oportunidade no passado. Ao meu paizinho querido, por me fazer entender que o futuro é feito a partir da constante dedicação no presente! Esse doutorado é prova do amor e apoio incondicional de vocês. Certamente não chegaria até onde estou sem os pais dedicados e amorosos que tive.

À minha irmã Grasy, a quem eu amo infinitamente, por sempre acreditar na minha capacidade de alcançar meus objetivos e por sempre vibrar comigo. Dedico a você, além desse trabalho, todo meu amor!

Ao meu namorado Caio César, pelo apoio incondicional, por entender minha ausência e me encher de amor. Obrigada mozi!

Aos melhores amigos que eu poderia ter encontrado! Michele, Gustavo, Lucas, Ana Paula, Kely, Davi, Toninho, Monique, Rafaela, Camila, José Roberto, Adamu. Ter vocês comigo é uma honra, poder contar com o apoio incondicional dos meus amigos nessa tese com certeza foi um privilégio. Sinto-me extremamente grata por todas as vezes que vocês me deram forças pra continuar. Esse título de doutorado não é só meu, ele com certeza é nosso!

A todos colegas da família LOP-LEMA, agradeço pelos ótimos momentos que passamos juntos, pela partilha de ansiedades, por um lado, e de gargalhadas, por outro.

Aos demais amigos e familiares, que de alguma forma, estiveram presente e/ou contribuíram para a concretização deste trabalho.

Agradeço muito ao Edu. Pela generosidade de ter aceitado ser meu orientador e por se tornar muito mais que isso. Obrigada por me ter sempre recebido com um cafezinho e sorriso contagiante, pelo estímulo, por estar sempre pronto para ajudar e por ter acreditado nas minhas capacidades e aceitado meus defeitos. Sua leitura atenta, reuniões e o seu profundo percurso

intelectual e humano, fez toda a diferença na minha trajetória. Vai sempre ser uma referência em minha vida.

Agradeço também à professora Jane, um exemplo de mulher e profissional, pelo excelente convívio, pelos valiosos ensinamentos e pela preciosa colaboração como co-orientadora desse trabalho.

Aos bolsistas de Iniciação Científica e aos estagiários que colaboraram na realização dos experimentos, Carol, Celine e Thaís.

O presente trabalho foi realizado com apoio da Coordenação de Aperfeiçoamento de Pessoal de Nível Superior – Brasil (CAPES) – Código de Financiamento 001.

À Fundação de Amparo à Pesquisa do Estado de Minas Gerais (FAPEMIG), pela concessão de recursos financeiros ao projeto (CAG - APQ-01457-18).

À Universidade Federal de Viçosa (UFV), ao Departamento de Tecnologia de Alimentos (DTA) e ao Programa de Pós-Graduação em Ciência e Tecnologia de Alimentos (PPGCTA), pela oportunidade e pelos recursos investidos durante o curso.

A todos que de alguma forma contribuíram para a realização deste trabalho.

Educação não transforma o mundo.

Educação muda as pessoas.

Pessoas transformam o mundo.

Paulo Freire

BIOGRAFIA

DANIELLE CRISTINE MOTA FERREIRA, filha de Maria Auxiliadora Mota Ferreira e João Ferreira Abdon Senei, nasceu em João Monlevade, Minas Gerais, em 01 de julho de 1993.

Em fevereiro 2011 iniciou a graduação em Bacharelado em Ciência e Tecnologia, na Universidade Federal dos Vales do Jequitinhonha e Mucuri, concluindo-o em julho de 2013. No mesmo ano deu início à Graduação em Engenharia de Alimentos, concluindo-a em julho de 2016. Durante a graduação foi bolsista de iniciação científica, entre março de 2013 e dezembro de 2015, sob a orientação da professora Franciele Maria Pelissari, do Departamento de Engenharia de Alimentos. Foi monitora da disciplina de Microbiologia, sob a supervisão da professora Lílian Pantoja, do Departamento de Ciência e Tecnologia.

Em janeiro de 2016 ingressou no Curso de Mestrado do Programa de Pós- Graduação em Ciência e Tecnologia de Alimentos, na UFVJM, concluindo-o em fevereiro de 2018.

Em março de 2018 ingressou no Curso de Doutorado do Programa de Pós- Graduação em Ciência e Tecnologia de Alimentos, na UFV, submetendo-se à defesa de sua tese em junho de 2023.

RESUMO

FERREIRA, Danielle Cristine Mota, D.Sc., Universidade Federal de Viçosa, maio de 2023. **Complexos polieletrólitos quitosano-carboximetilcelulose: estudo físico-químico e aplicabilidade como carreadores de vitaminas e adsorventes de poluentes.** Orientador: Eduardo Basílio de Oliveira. Coorientadores: Jane Sélia dos Reis Coimbra e Alvaro Vianna Novaes de Carvalho Teixeira.

A área de Ciência e Tecnologia de Alimentos e setores de pesquisa e desenvolvimento industrial têm buscado estratégias que visam à diversificação de produtos e processos. Embora existam estudos que descrevem a importância da interação entre polissacarídeos e sua aplicabilidade tecnológica, ainda são escassos nas bases de dados disponíveis, estudos amplos que contemplem aspectos físico-químicos e técnico-funcionais sobre a interação entre quitosano (CHS) e carboximetilcelulose (CMC). Nesse sentido, foram estudados o efeito da proporção de mistura de quitosano e carboximetilcelulose, da temperatura e do pH na formação de sistemas macro e micro-estruturados. Os resultados de FT-IR revelaram que os complexos formados por CHS e CMC foram promovidos pela interação eletrostática e, possivelmente, por pontes de hidrogênio. Na proporção de 1:2 (CHS/CMC) e à 25 °C, o potencial ζ do sistema foi próximo de zero e os macro-complexos polieletrólitos (macro-PECs) tiveram rendimento máximo, apresentaram estrutura altamente porosa e visualmente estáveis em solução aquosa por semanas. Macro-PECs foram, portanto, aplicados como adsorventes de corantes (Amarelo Crepúsculo, Azul de Metileno, Vermelho Congo e Safranina) e metais pesados (Cd^{2+} e Pb^{2+}). O modelo de adsorção de Langmuir sugeriu homogeneidade da superfície das partículas dos macro-PECs. A cinética de adsorção mostrou que os processos podem seguir o modelo de pseudo-primeira ou pseudo-segunda ordem. Já os micro-PECs se apresentaram como partículas coloidais dispersas, classificadas como amorfas e termicamente estáveis, eficazes no processo de entrega controlada de niacinamida, alcançando 4,85% e 80,78% e capacidade máxima de carga (LC) e ~~a~~ eficiência de encapsulamento (EE), respectivamente. O fator pH teve maior influência nas respostas (EE e LC) estudadas, sendo o processo de produção de estruturas carreadoras favorecido em valores de pH mais baixos (3,0). A utilização de tempos de processo mais curtos favoreceu a formação dos sistemas de carreamento em termos práticos e econômicos. O estudo de liberação *in vitro* de micro-PECs CHS/CMC de niacinamida, realizado em diferentes condições de pH, mimetizando a condição do trato gastrointestinal, indicou que a liberação máxima de niacinamida ocorreu após cerca de 4,5 h e as constantes do

modelo de ordem zero (K_0) foram baixas e semelhantes para todos os sistemas estudados, demonstrando uma baixa taxa de liberação e indicando que o processo de liberação de niacinamida dos micro-PECs CHS/CMC ocorre principalmente por difusão. O impacto promissor dos sistemas macro e micro-estruturados de quitosano e carboximetilcelulose em sistemas-modelo de adsorção de poluentes, em sistemas aquosos, e em sistemas-modelo de liberação controlada de compostos bioativos hidrofílicos apontou ampla gama de técnico-funcionalidades em diversos setores, como por exemplo indústria alimentícia, química, têxtil e farmacêutica.

Palavras-chave: Estruturas supramoleculares. Interação CHS-CMC. Sistemas coloidais. Tratamento de água poluída. Controle e liberação controlada.

ABSTRACT

FERREIRA, Danielle Cristine Mota, D.Sc., Universidade Federal de Viçosa, May, 2023. **Chitosan-carboxymethylcellulose polyelectrolyte complexes: physical-chemical study and applicability as carriers of vitamins and adsorbents of pollutants.** Adviser: Eduardo Basílio de Oliveira. Co-adviser: Jane Sélia dos Reis Coimbra and Alvaro Vianna Novaes de Carvalho Teixeira.

The Food Science and Technology area and industrial research and development sectors have sought strategies aimed at diversifying products and processes. Although there are studies that describe the importance of the interaction between polysaccharides and their technological applicability, the available databases are still scarce, broad studies that address physical-chemical and technical-functional aspects of the interaction between chitosan and carboxymethylcellulose. In this sense, the effect of the mixture proportion of chitosan and carboxymethylcellulose, temperature and pH in the formation of macro and micro-structured systems were studied. The FT-IR results revealed that the complexes formed by CHS and CMC were promoted by electrostatic interaction and, possibly, hydrogen bonds. At the ratio of 1:2 and 25 °C, the ζ potential of the system was close to zero and the macro-polyelectrolyte complexes (macro-PECs) had maximum yield, had a highly porous structure, and were visually stable in aqueous solution for weeks. Macro-PECs have therefore been effectively applied as adsorbents for dyes (Sunset Yellow, Methylene Blue, Congo Red, and Safranin) and heavy metals (Cd^{2+} and Pb^{2+}). The Langmuir adsorption model suggested surface homogeneity of macro-PEC particles. The adsorption kinetics showed that the processes can follow the pseudo-first or pseudo-second-order model. The micro-PECs, on the other hand, appeared as dispersed colloidal particles, classified as amorphous and thermally stable, effective in the process of controlled delivery of niacinamide, reaching 4.85% and 80.78% of maximum load capacity (LC) and efficiency encapsulation (EE), respectively. The pH factor had the greatest influence on the responses (EE and LC) studied, with the production process of carrier structures being favored at lower pH values (3.0). The use of shorter process times favored the formation of carrier systems in practical and economic terms. The in vitro release study of CHS/CMC micro-PECs of niacinamide performed under different pH conditions, mimicking the condition of the gastrointestinal tract, indicated that the maximum release of niacinamide occurred after about 4.5 hours and the model constants of zero order (K0) were low and similar for all systems studied, demonstrating a low release rate and indicating that the process of niacinamide release from CHS/CMC micro-PECs occurs mainly by diffusion. The promising impact of macro and

micro-structured systems of chitosan and carboxymethylcellulose in model systems of adsorption of pollutants in aqueous systems and in model systems of controlled release of hydrophilic bioactive compounds pointed to a wide range of technical functionalities in several sectors, such as example food, chemical, textile and pharmaceutical industries.

Keywords: Supramolecular Structures. CHS-CMC Interaction. Colloidal Systems. Polluted Water Treatment. Controlled Release.

LISTA DE ILUSTRAÇÕES

CAPÍTULO 1

CAPÍTULO 2

CAPÍTULO 3

CAPÍTULO 4

LISTA DE TABELAS

CAPÍTULO 1

CAPÍTULO 3

CAPÍTULO 4

LISTA DE ABREVIAÇÕES E SÍMBOLOS

AGU	Unidade de anidroglicose
μ_e	Mobilidade eletroforética
$(\bar{[\eta]})$	Viscosidade intrínseca média
CHS	Quitosano
CMC	Carboximetilcelulose
CrI	Índice de cristalinidade
DA	Grau de acetilação
DD	Grau de desacetilação
d_h	Diâmetro hidrodinâmico
DLS	Espalhamento dinâmico de luz
DRX	Difractometria de raios X
FT-IR	Espectroscopia de infravermelho por transformada de Fourier
PDI	Índice de polidispersão
PEC	Complexo polieletrólito
SEM	Microscopia eletrônica de varredura
TGA	Análise termogravimétrica
$\bar{M}_V$	Massa molar viscométrica média
XRD	Difractometria de raios X
ζ-potential	Potencial zeta
A	Precisão
q_{e0}	Capacidade de adsorção de macro-PEC fresco
Cd^{2+}	Cádmio
CR	Vermelho congo
t	Tempo de contato
C_0	Concentração inicial do poluente
%R	Porcentagem de remoção
C_d	Concentração de equilíbrio após a dessorção
q_D	Capacidade de dessorção de equilíbrio
K_f	Constante de Freundlich

C	Interceptação do gráfico de difusão intrapartícula
k_d	Constante de taxa de difusão intrapartícula
Pb^{2+}	Chumbo
LQ	Limite de Quantificação
LD	Limites de Detecção
m	Massa
Q_m	Capacidade máxima de adsorção
MB	Azul de metileno
Macro-PEC	Polyelectrolyte complex macroscópicos
k_1	Constante de velocidade de pseudo-primeira ordem
k_2	Constante de velocidade de pseudo-segundaordem
K_R	Constante de Redlich-Peterson
α	Constante de Redlich-Peterson
β	Constante de Redlich-Peterson
S	Safranina
SEM	Microscopia eletrônica de varredura
UV	Ultraviolet
V	Volume
YS	Amarelo crepúsculo
pH_{ZPC}	pH de carga zero
K_H	Constante Higuchi
K_0	Constante de ordem zero
K_1	Constante de primeira ordem
EE	Eficiência de encapsulação
K_{K-P}	Constante de Korsemeyer-Peppas
LC	Capacidade de carga
n	Expoente de difusão ou liberação
X_1	Tempo de processamento
X_2	pH
X_3	Concentração de niacinamida
Y_1	Eficiência de encapsulação
Y_1	Capacidade de carga

SUMÁRIO

1. INTRODUÇÃO

A busca por novos materiais é uma das estratégias que visam à diversificação e/ou melhoria de produtos e processos. Embora existam estudos que~~m~~ descrevem a importância da interação entre polissacarídeos e sua aplicabilidade tecnológica, ainda são escassas nas bases de dados disponíveis, estudos amplos que contemplem aspectos moleculares e técnico-funcionais sobre a interação entre quitosano e carboximetilcelulose.

Quitosano é um polissacarídeo biodegradável, biocompatível com tecidos humanos e atóxico, obtido pela desacetilação parcial da quitina, sendo essa encontrada nas carapaças de camarões, caranguejos e outros artrópodes marinhos, ou na parede celular de alguns fungos. Grupos amino (NH_2) existentes nas cadeias do quitosano podem ser protonados em meios aquosos ácidos, o que favorece a sua dispersão, possibilitando o aumento do espectro de utilização deste biopolímero em diversas aplicações industriais. O quitosano vem sendo empregado principalmente como excipiente para liberação controlada de fármacos e outras substâncias bioativas, e também como suporte para a fabricação de próteses ósseas e dérmicas. No setor alimentar, o quitosano é principalmente utilizado na produção de coberturas comestíveis para frutas e na fabricação de filmes para embalagens.

Carboximetilcelulose é um polissacarídeo hidrofílico, obtido a partir da modificação química da celulose, por meio da inserção parcial ou total de grupos carboximetil ($CH_2OCH_2COO^-$) que, em meio aquoso, encontram-se carregados negativamente. Por possuir propriedades não tóxicas, bioadesivas e sensíveis ao pH, a CMC possui várias aplicações nas indústrias alimentícia, farmacêutica, de papel, têxtil e petrolífera. Como resultado, por meio deste composto, pode-se obter gelificação *in situ*, materiais com sensibilidade a estímulos externos, sistemas com liberação controlada e com bioadesão. Na indústria alimentícia, a CMC é usada como estabilizador alimentar em bebidas à base de cacau, sorvetes e produtos de panificação. Em sorvetes, retarda o crescimento de cristais de gelo, e em xaropes e confeitos, retarda o crescimento de cristais de açúcar. Também provoca aumento da viscosidade podendo ser utilizado como aglutinante e espessante. Além disso, é um promissor agente de entrega de compostos ativos, uma vez que é capaz de absorver grandes quantidades de água ou outros fluidos desejáveis e liberá-los sob condições controladas.

Embora alguns estudos descrevam a importância da interação entre polissacarídeos e sua aplicabilidade tecnológica, não foram encontrados, nas bases de dados disponíveis, estudos amplos que contemplem aspectos cinéticos, moleculares e técnico-funcionais sobre a interação entre quitosano e carboximetilcelulose, principalmente sem a utilização de agentes reticulantes.

O presente trabalho buscou, portanto, novas aplicabilidades a esses polissacarídeos, além daquelas que já possui em outras áreas, com potencial para remediar poluição de sistemas aquosos, bem como para utilização em formulações alimentícias capazes de carrear e liberar de forma controlada compostos bioativos, tais como a niacinamida.

Tendo em vista o contexto apresentado, essa tese objetivou estudar a técnico-funcionalidade de sistemas macro e micro-estruturados formados por quitosano e carboximetilcelulose.

Dessa forma, o presente documento foi estruturado como segue:

i) Um capítulo intitulado "Revisão de literatura" em que é feita uma apresentação do quitosano e da carboximetilcelulose, além de estudos que propuseram a utilização dessas macromoléculas em diferentes aplicações. Na sequência, são apresentadas definições sobre adsorção e carreamento de compostos. Este capítulo objetiva fornecer bases teóricas para a compreensão de como o trabalho experimental visa responder à problemática apresentada. Além disso, espera-se demonstrar o caráter inovador da proposta e dos resultados de cada capítulo experimental.

ii) Em seguida, é apresentado o artigo científico intitulado por "*Polyelectrolyte complexes (PECs) obtained from chitosan andcarboxymethylcellulose: A physicochemical and microstructural study"* (https://doi.org/10.1016/j.carpta.2022.100197), publicado no periódico **Carbohydrate Polymer Technologies and Applications**. Os efeitos da proporção de mistura de quitosano (CHS) para carboximetilcelulose (CMC) (1:0; 4:1; 3:1; 2:1; 1:1; 1:2; 1:3; 1:4; 0:1), da temperatura (25; 45; 65; 85 ºC) e do pH (3,0; 3,5; 4,0; 4,5) foram analisados quanto à obtenção de complexos macro e micropolieletrólitos (PEC). Ambos, macro e micro-PECs (estruturas microscópicas dispersas), foram estudados por SEM, FT-IR, XRD e TGA.

iii) No terceiro capítulo é apresentado o artigo científico intitulado "*Chitosan/carboxymethylcellulose polyelectrolyte complexes (PECs) are an effective material for dye and heavy metal adsorption from water"* (doi: 10.1016/j.carbpol.2023.120977), publicado no periódico **Carbohydrate Polymers**. Nesse estudo, complexos polieletrolíticos macroscópicos de quitosano/carboximetilcelulose (CHS/CMC macro-PECs) foram produzidos e testados como adsorventes de seis poluentes frequentemente presentes em águas residuais: amarelo crepúsculo (YS), azul de metileno (MB), vermelho congo (CR) e safranina (S), cádmio (Cd^{2+}) e chumbo (Pb^{2+}). Foram realizados estudos sobre a

influencia do pH nos processos de adsorção, estudos de cinética e de isotermas de Langmuir, bem como capacidades de dessorção.

iv) Por fim, no quarto capítulo, é também apresentado um manuscrito de artigo científico com título provisório "*Microstructured chitosan/carboxymethylcellulose polyelectrolyte complexes as a novel and efficient material for carrying and controlled release of niacinamide"*, a ser submetido a um periódico de circulação internacional. Nesse capítulo, microcomplexos de polieletrólitos (micro-PECs) à base de quitosano e carboximetilcelulose, contendo niacinamida como componente ativo modelo, foram preparados por processamento de coacervação complexa. O desenho experimental Box-Behnken foi adotado para estudar os efeitos de três variáveis independentes – tempo de processamento, ou seja, X_1 (60, 120 e 180 min), pH, ou seja, X2 (3, 4 e 5) e concentração de niacinamida, ou seja, X_3 (0,02, 0,04 e 0,06 $g \cdot L^{-1}$), na eficiência de encapsulação (Y_1) e na capacidade de ligação (Y_2) de micro-PECs CMC/CHS à niacinamida. Em seguida, a digestibilidade *in vitro* dos micro-PECs contendo niacinamida foi avaliada usando um modelo gastrointestinal estático. Quatro modelos cinéticos foram ajustados aos dados de cinética de liberação de niacinamida: ordem zero, primeira ordem, Higuchi e Korsemeyer-Peppas.

Espera-se que os resultados apresentados possam se juntar a mais relatos da literatura da área e contribuir para difundir as aplicações desses biopolímeros. Dessa forma, o objetivo geral dessa tese foi caracterizar físico-químicamente e técnico-funcionalmente complexos polieletrólitos quitosano-carboximetilcelulose como carreadores para vitaminas e adsorventes de substâncias poluentes.

CAPÍTULO 1

REVISÃO DA LITERATURA

1. ESTRUTURAS SUPRAMOLECULARES

Estruturas supramoleculares resultantes da associação de duas ou mais espécies moleculares diferentes têm atraído a atenção de pesquisadores acadêmicos e industriais, ao longo das duas últimas décadas, devido especialmente às suas características diferenciadas e, geralmente, superiores às dessas espécies isoladamente, em termos de propriedades e aplicações. A engenharia e a formação de moléculas complexas, que utilizam de estratégias elaboradas visando a quebra e/ou formação de novas ligações moleculares, têm estimulado o estudo de novas associações de biopolímeros e dos mecanismos de suas interações para aplicações inovadoras.

O processo de formação de estruturas supramoleculares é normalmente realizado em soluções aquosas, pois permite que ocorra a mobilidade dos diferentes componentes necessários para a formação dos complexos. Em solução, o movimento browniano, fenômeno pelo qual partículas tendem a se mover em caminhos pseudoaleatórios ou estocásticos através do líquido, é o principal responsável pelo direcionamento dos componentes e, portanto, é a principal contribuição para colocar as moléculas em contato (Kashapov et al., 2022).

Trabalhos publicados nos último anos relatam a química supramolecular de sistemas contendo diferentes misturas de macromoléculas, incluindo polissacarídeos (Alsakhawy et al., 2022; Chen et al., 2023; Limpongsa et al., 2021; Martins et al., 2020; Quadrado & Fajardo, 2022; Rahman et al., 2021a, 2021b; Sinha et al., 2022; Tsai et al., 2014). Algumas dessas misturas, devido à sua capacidade de formar géis fortes mesmo em baixas concentrações, têm sido usadas, por exemplo, no preparo de comprimidos farmacêuticos para liberação controlada de fármacos (Quadrado & Fajardo, 2022), bem como para modificar as propriedades reológicas de doces, pudins, fibras dietéticas, entre outros (Barclay et al., 2019; Lu et al., 2019). Porém, a maioria dos recentes estudos encontrados nesse campo se restringem a apenas análises estruturais e reológicas do produto final, sem aprofundar no entendimento das interações entre os biopolímeros. Sabe-se que essas interações afetam expressivamente a microestrutura, a estabilidade, e as propriedades reológicas de sistemas compostos. O entendimento do mecanismo dessas interações é crucial no desafio de encarar sistemas de grande complexidade, produzindo descobertas que concernem às aplicações reais em vários segmentos, além de ser uma forma disponível de controlar os fatores críticos para o desenvolvimento de novos produtos multifuncionais.

2. POLISSACARÍDEOS

Os polissacarídeos correspondem a uma classe de biopolímeros constituídos por monômeros de açúcar, ligados entre si por ligações glicosídicas (Y. Xu et al., 2019). Para uso comercial, são isolados de plantas e animais, ou de metabólitos exógenos de algumas bactérias, onde atuam principalmente como elementos estruturais e de sustentação nas paredes celulares de plantas. Funcionalidades dos polissacarídeos, tais como sua capacidade de gelificação, têm sido estudadas, não apenas do ponto de vista científico, mas também por sua importância nas indústrias alimentícia, farmacêutica, biomédica, cosmética, de revestimento, pintura e afins (Nie et al., 2019). Na área alimentícia, os polissacarídeos (PS) geralmente modificam a matriz alimentar por meio de alterações nas propriedades reológicas, o que aumenta a retenção de água, leva ao espessamento da matriz e pode promover a formação de gel. Outras aplicações incluem a estabilização cinética de espumas; de emulsões e de materiais particulados suspensos (Matsuyama et al., 2021; Xiao et al., 2021), melhorando a palatabilidade; prevenindo ou reduzindo a formação de cristais de gelo em alimentos congelados (X. Sun et al., 2022). Já na área farmacêutica, PS atuam na liberação controlada, no aumento da biodisponibilidade de substâncias pouco solúveis em água e na proteção de compostos sensíveis à degradação (térmica, química e enzimática) (Gopinath et al., 2018).

2.1 Quitosano

O quitosano é um biopolímero de natureza catiônica classificado pela Food and Drug Administration (FDA) como Generally Recognised As Safe (geralmente reconhecido como seguro) (Yan et al., 2021). Possui elevada densidade de cargas positivas devido à protonação dos grupos amino de sua cadeia principal, em meio aquoso, quando em pH abaixo de seus valores de pKa (6,2-7,0). Somada a essa característica única entre os polímeros naturais, apresenta outras propriedades intrínsecas, como não-toxicidade, biocompatibilidade, propriedades antibacterianas e biodegradáveis, que explicam sua vasta aplicação tecnológica (Ali & Ahmed, 2018).

O quitosano é obtido a partir da quitina (Figura 1), sendo essa um biopolímero estrutural, que tem um papel análogo ao do colágeno nos animais superiores e da celulose nas plantas terrestres. Assim como as plantas produzem celulose em suas paredes celulares, insetos e crustáceos produzem quitina em suas cascas e carapaças (el Knidri et al., 2018). Em geral, as carapaças de crustáceos são compostas por 30 a 40% de proteínas, 30 a 50% de carbonato de

cálcio e fosfato e 20 a 30% de quitina, mas estas porcentagens variam dependendo da fonte, ou mesmo da espécie, da qual a quitina é isolada. Por exemplo, os resíduos de camarão *Crangon* são compostas por 10-38% de proteínas, 31-44% de minerais e 24–46% de quitina (Bajaj et al., 2011; Kumirska et al., 2010).

O processo de obtenção do quitosano envolve três etapas principais: desmineralização, desproteinização e desacetilação, como mostrado na Figura 1.

Figura 1 - Processo de obtenção do quitosano

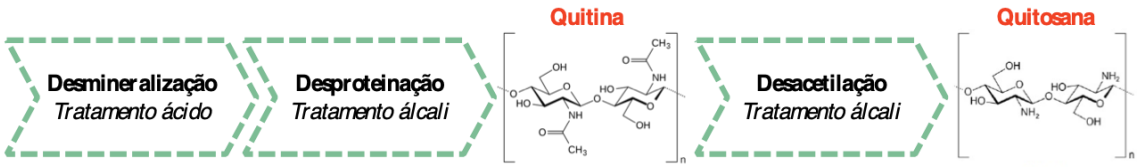

Na quitina, o grau de acetilação é tipicamente 0,9, indicando a presença de alguns grupos amino (a quitina pode sofrer pequena quantidade de desacetilação durante o processo de sua extração, podendo conter cerca de 5-15% de grupos amino) (el Knidri et al., 2018). Assim, o grau de N-acetilação, isto é, a proporção de 2-acetamido-2-desoxi-D-glucopiranose para 2-amino-2-desoxi-D-glucopiranose, é basicamente empregado para diferenciar a quitina do quitosano (Figura 2). Quando o grau de acetilação é maior que 50%, o polímero é chamado de quitina, e quando o grau de acetilação é menor que 50%, o polímero é denominado quitosano (Al-Rooqi et al., 2022).

Figura 2 - Diferenciação entre estruturas da quitina e quitosano

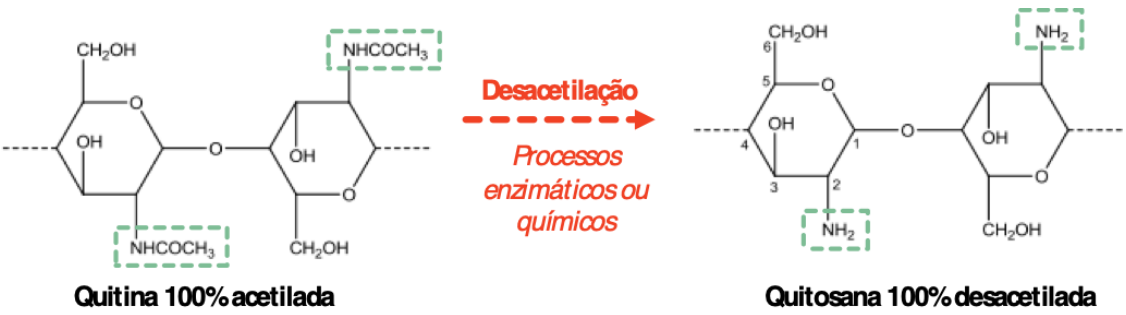

Como mencionado, quimicamente, o quitosano é constituído por duas subunidades, como a d-glucosamina e a N-acetil-d-glucosamina, ligadas linearmente entre si por meio de

ligações 1,4-glicosídicas. Estruturalmente, três grupos funcionais, isto é, grupos hidroxila primários e secundários e grupos amina, estão presentes em cada molécula repetitiva de quitosano. Esses grupos funcionais permitem que o quitosano seja mais propenso a sofrer modificações químicas. Além disso, esses grupos funcionais desempenham um importante papel em algumas características físico-químicas importantes do quitosano, incluindo a dispersibilidade e os atributos mecânicos gerais, como mencionado anteriormente (Mujtaba et al., 2019).

Apesar do quitosano ser insolúvel em água, pode-se dispersar em soluções aquosas de ácidos orgânicos (como por exemplo o ácido acético e fórmico), podendo também usar-se ácidos inorgânicos diluídos (tais como o ácido clorídrico, nítrico e perclórico). O valor de pKa situa-se normalmente entre 6,3 e 7, dependendo do grau de acetilação (el Knidri et al., 2018). A quantidade de grupos amino protonados ($-NH^{3+}$) afeta a dispersibilidade do quitosano, sendo que quanto maior for a quantidade, maior será o número de interações eletrostáticas repulsivas nas cadeias e, por consequência, maior será a solvatação. Essa é também a razão por que os polieletrólitos tem maior dispersibilidade em meio aquoso que os polímeros neutros. Além da repulsão eletroestática, há uma contribuição entrópica resultante da liberação dos contra-íons para o meio (Rinaudo, 2006).

Além da não-toxicidade e biocompatibilidade supracitadas, o quitosano pode ser degradado *in vivo* por várias enzimas, incluindo a lisozima (uma protease inespecífica presente em todos os tecidos de mamíferos) (Szymańska & Winnicka, 2015). Além disso, os produtos da degradação são oligossacáridos, composots não tóxicos, que podem ser excretados ou incorporados em glicosaminoglicanos e glicoproteínas. Estas propriedades tornam o quitosano adequada para uso alimentício. Ademais, o quitosano pode aumentar a penetração de compostos bioativos, colaborando na abertura das junções entre as células epiteliais (Mohammed et al., 2017). Essas propriedades fazem do quitosano um candidato ideal para uso na preparação de novos materiais para aplicações alimentícias.

2.2 Carboximetilcelulose

A carboximetilcelulose (CMC) é um polieletrólito aniônico produzido pela introdução de grupos carboximetil na molécula de celulose, como mostrado na Figura 3.

Figura 3 - Estruturas de oito possíveis unidades repetitivas presentes nas cadeias de carboximetilcelulose com até três grupos carboximetila por resíduo de glicose.

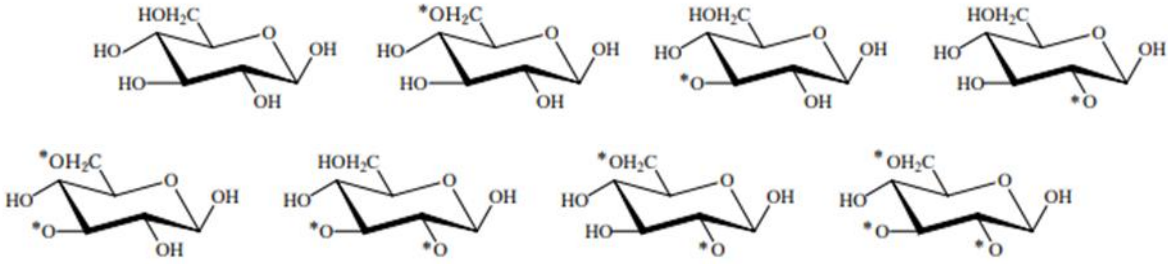

* Indica posições em que o grupo $CH_2COO\text{-}Na^+$ (ou $\text{-}CH_2COOH$) foi adicionado

A carboximetilcelulose é sensível à variação de pH e à força iônica, sendo o único polieletrólito derivado da celulose com essa característica (Arinaitwe & Pawlik, 2014). Industrialmente, é obtido a partir da reação em suspensão (*slurry process*) da celulose na presença de hidróxido de sódio e ácido monocloroacético. A CMC é usualmente comercializada na forma sódica (CMCNa) que, uma vez dissolvida em água, apresenta as características típicas de polieletrólitos. Suas propriedades e aplicações dependem, essencialmente, da viscosidade de suas soluções aquosas, do grau de substituição (DS) e da distribuição dos grupos carboximetil (da Silva et al., 2018).

A CMC pode ser obtida por meio de reação homogênea ou heterogênea. De modo geral, amostras de carboximetilcelulose obtidas por meio da reação heterogênea são constituídas por cadeias que podem conter até oito unidades repetitivas diferentes (Figura 3) e a distribuição dos substituintes inseridos depende da acessibilidade dos reagentes aos sítios reativos da macromolécula, sendo uma característica de difícil controle (Pinto et al., 2022).

2.3 Estruturas supramoleculares de quitosano e carboximetilcelulose

Complexos poliméricos podem ser obtidos por meio da interação entre dois ou mais polímeros, e a formação de estruturas supramoleculares a partir desses, geralmente na forma de sistemas coloidais ou suspensões, são obtidos por polimerização, agregação e/ou complexação, produzindo promissores materiais. Essas dispersões poliméricas constituem uma alternativa para superar as limitações dos componentes quando utilizados separadamente, ampliando a sua aplicação, tais como na preparação de filmes e materiais sintéticos, revestimentos, adesivos

para papel e produtos têxteis, floculantes, modificadores reológicos e para liberação de fármacos.

Considerando a necessidade de se entender a importância da presente tese e os recentes avanços relacionados ao uso de quitosano e carboximetilcelulose, torna-se essencial preparar uma revisão sobre o tema e sua possível aplicabilidade na indústria. A busca da literatura foi realizada no Science Direct, Wiley, Pubmed, e Taylor e Francis Online. A estratégia de busca envolveu os seguintes termos: “Chitosan”, “Carboxymethylcellulose”, “Adsorption”, “Encapsulation”, “Dye” e “Heavy Metal” presentes no título e/ou resumo e/ou palavras-chave, bem como seus similares. Foram considerados artigos de pesquisa publicados a partir de 2015, excluindo artigos repetidos e aqueles que não tiveram como objetivo a mistura entre quitosano e carboximetilcelulose (Fig. 4).

A partir da Figura 4, construiu-se as Tabelas 1 e 2, onde são apresentados alguns exemplos de estudos que propuseram a avaliação de estruturadas formadas a partir de CHS e CMC para adsorção (Tabela 1) e carreamento de compostos (Tabela 2), temas da presente tese, bem como outras aplicabilidades (Tabela 3). Foi constatado que, apesar dos fatores de características dos biopolímeros (estruturas, sítios reativos e densidade de carga), concentração, razão de mistura e condições de solvente (pH e força iônica) afetarem as interações dentro dos sistemas, causando diferenças significativas nos produtos finais, esses são muitas vezes pouco explorados. Além disso, como pode ser observado na Tabela 1, todos os recentes estudos encontrados utilizaram outras macromoléculas e/ou agentes reticulantes capazes de mudar radicalmente a físico-química de interação entre as macromoléculas.

Figura 4 – Artigos recentes (a partir de 2015) envolvendo os principais temas de pesquisa da presente tese.

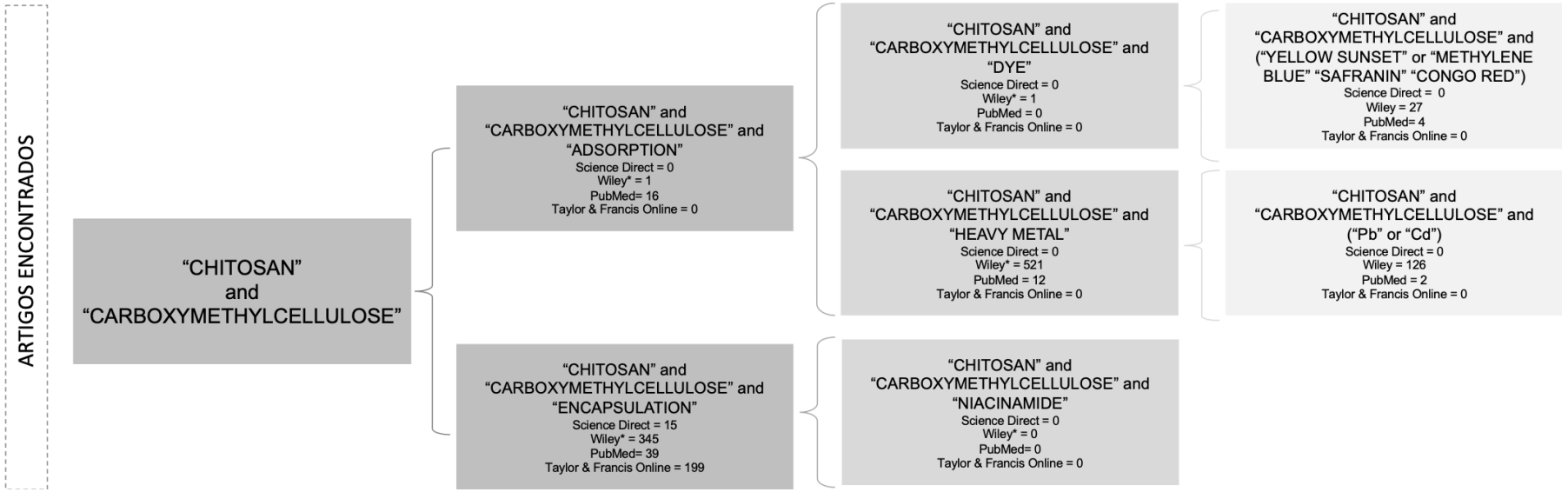

Tabela 1 - Descrição de estudos do quitosano (CHS) e carboximetilcelulose (CMC) atuando como carreadores de compostos ativos

Composto bioativo	Reagentes adicionais	Análises realizadas	Resultados alcançados	Referência
TiO_2 hidrofílico e ácido fenilbenzimidazol sulfônico (FA)	Reticulador ácido ferúlico CMC:CHS:FA em 1:2:4% em peso	Espectroscopia no infravermelho por transformada de Fourier (FT-IR); Calorimetria Exploratória Diferencial (DSC); Termogravimetria (TGA); Difração de raios-X (XRD);	Fator de proteção (FPS): 2,47; Classificação de estrelas: 3 a 2% de composto.	(Wongkom & Jimtaisong, 2017)
Salicilato de sódio (GQD)	Pontos quânticos de grafeno	FT-IR; Fotoluminescência (PL); Microscopia eletronica de varredura (SEM); Ponto de carga zero (pHpzc); Liberação *in vitro;* Toxicidade (Ensaio MTT).	Análises de FT-IR e PL confirmaram CHS-GQD dentro da matriz de CMC; Aumento da concentração de CMC gerou maior proteção contra o ambiente estomacal; Liberação controlada nas condições do trato gastrointestinal simulados; Estabilidade da dosagem por longo período; Baixa toxicidade contra células HT29 (ensaio MTT).	(Javanbakht & Shaabani, 2019)

Onicomicose	Nitrato de oxiconazol /escleroglucana/montmorilonita (MMT)	Propriedades mecânicas; Temperatura de transição vítrea; Ângulo de contato; Valor de opacidade; Liberação oxiconazol em função do tempo e da concentração de MMT.	Presença de MMT na matriz de hidrogel aumentou a temperatura de transição vítrea (63,72 °C para 76,75 °C) e valor da tensão de compressão (126,45 ± 8,83 kPa para 266,99 ± 6,60 kPa); Aumento de MMT: ↓ taxa de liberação: • 0% (p/p) de MMT: 70,33 ± 1,74% • 1% (p/p) de MMT: 63,92 ± 0,31% • 3 %(p/p) de MMT: 58,78 ± 1,45% • 5% (p/p) de MMT: 52,89 ± 0,21 %. Atividade antifúngica contra *Trichophyton mentagrophytes* e *Trichophyton rubrum* dermatófitos	(Kancı Bozoğlan et al., 2021)

Curcumina	Poli (ácido Iáctico-co-glicólico) (PLGA)	Distribuição de tamanho; MEV; Turbidez; Potencial zeta; Cinética de liberação; Citotoxicidade.	↑ pH (3 a 10): ↓ potencial zeta (+54 a -50 mV); Boa estabilidade coloidal; ↓ pH: liberação retardada ↑ pH neutro: liberação rápida EE: 98,8%	(Inphonlek et al., 2020)
Óleo de palma e β-caroteno		Eficiência de encapsulação (EE); Rendimento; Conteúdo de carotenóides; Morfologia; Comportamento térmico; Perfil de liberção.	Eficiência de encapsulamento: superior a 95%; Rendimento das micropartículas revestidas com quitosana/tripolifosfato de sódio: 55%; Rendimento das micropartículas revestidas com quitosana/carboximetilcelulose: 87%‘ Água e fluido gástrico: comportamento de liberação ideal; Fluido intestinal: baixa liberação; Aplicação em sistemas alimentares: maior liberação de carotenóides e baixa liberação de carotenóides após o armazenamento.	(Rutz et al., 2016)

Vancomicina (VM) no cólon	Ácido láurico	Rendimento; Eficiência de encapsulação; Morfologia e propriedades de mucoadesão; Absorção de água; Atividade antibacteriana contra *Staphylococcus aureus*	Proporção CH/CMC 1:3: maior capacidade de carga e EE (79.3 ± 3.9) pH 2.0: menor taxa de liberação e maior capacidade de absorção de água pH 7,4: maior tempo de permanencia no cólon.	(Cerchiara et al., 2016)
Bactérias probióticas	Genipapo	Viabilidade de Lactobacillus rhamnosus GG; FTIR; MEV; Potencial zeta; Grau de inchamento.	pH 7,4: maior inchamento pH 2,4: menor estabilidade Boa contagem de células viáveis (*Lactobacillus rhamnosus GG*) microencapsuladas	(Singh et al., 2017)

Cinamaldeído e o 2-aminobenzimidazole	Alginato de sódio e octaaminftalocianina de ferro	UV-Vis; FTIR; NMR; Distribuição de tamanho; DSC; EE; Perfil de liberação.	Tamanho de partícula: 10-30 nm; Estabilidade: até 40°C; EE: 48,77%; Taxa de liberação cumulativa: 83% em 60 h.	(Li et al., 2021)

Tabela 2 - Descrição de estudos de quitosano e carboximetilcelulose como adsorventes

Adsorvato	**Reagente adicionais**	**pH ótimo**	**q_e (mg/g)**	**Modelo isoterma**	**Modelo cinético**	**Referência**
Cd(II) e Cr(VI)	Polietilenoimina	5	470,0	Isoterma de Freundlich	Pseudo-segunda ordem	(S.-S. Li et al., 2020)
Cd(II)		2	347,0	Isoterma de Freundlich	Pseudo-segunda ordem	
Cr(VI)	N,N'-diisopropilcarbodiimida	2,5	115,78 ± 0,17	Isoterma de Langmuir	Pseudo-segunda ordem	(Andrade Neto et al., 2020)

Azul de metileno	Montmorilonita	8	2 g/L	Isoterma de Sips	Pseudo-primeira ordem e pseudo-segunda ordem	(Wang et al., 2020)
Azul de metileno (MB),	Óxido de grafeno, cloreto de dialildimetilamônio e ácido 2-acrilamido-2-metil-1-propanossulfônico	8	655,98	Isoterma de Langmuir	Pseudo-segunda ordem	(Mittal et al., 2021)
Alaranjado de metila (MO)		2	404,52	Isoterma de Langmuir		
Amarelo crepúsculo (AC)	-	2	212,83	Modelo de Freundlich	Pseudo-segunda ordem	(Zhao et al., 2020)
Azul de metileno (AM)		8	167,35	Modelo de Langmuir	Pseudo-primeira ordem	

Tabela 3 - Descrição de estudos de quitosano e carboximetilcelulose com demais aplicabilidades

Aplicabiliade	Reagentes adicionais	Análises realizadas	Principais resultados alcançados	Referencial
Hidrogéis termossensíveis	Escleroglucana Montmorilonita	FTIR, MEV, EDX, TEM, XRD, TGA e medições de inchaço	↑ MMT: ↑ temperatura de gelificação, ↑ estabilidade térmica; ↑ intumescimento: ambiente ácido; ↑ intumescimento mínimo: água destilada; Comportamento de intumescimento não Fickiano. ↑ inchaço: ↑ quantidade de MMT.	(Bozoğlan et al., 2020)
Esferas macroscópicas	Ácido cítrico como agente reticulante		pH 4,5: ↑ força e resistencia de até 0,071 N; Concentração: influência na forma e tamanho; Pós-aquecimento suave (35°C): ↑ estabilidade dos grânulos	(Altam et al., 2021)

Filmes	Curdlana	Propriedades mecânicas, Permeabilidade ao vapor de água; Absorção de água, Estabilidade térmica	Em comparação ao filme de CHS: ↑ Propriedades mecânicas, ↓ Permeabilidade, ↑ Estabilidade térmica	(Wang et al., 2019)

3. ADSORÇÃO

Com o rápido desenvolvimento da economia e da indústria moderna, os metais pesados e os poluentes orgânicos representam uma séria ameaça ao acesso sustentável à água potável, sendo o tratamento de águas residuais um dos principais focos de preocupação das indústrias alimentícia (Biswal et al., 2022; Schio et al., 2022; Sellaoui et al., 2021), têxtil (Luo et al., 2023), de petróleo (Wang et al., 2022; Wu et al., 2022), da pesquisa ambiental e do poder público.

Várias técnicas têm sido utilizadas na purificação de efluentes, sendo a adsorção considerada como um dos métodos mais eficientes e convenientes devido ao seu baixo consumo de energia, fácil operação e baixa poluição secundária (Sahid et al., 2021). Outros métodos usados para limpeza de águas poluídas incluem coagulação e/ou floculação (Ihaddaden et al., 2022; Nnaji et al., 2022; Sun et al., 2021), filtração através de membrana (Gao et al., 2022; Liu et al., 2022), irradiação (Hmamouchi et al., 2022), processos de oxidação (Kumar & Gupta, 2022), tratamentos biológicos (Liu et al., 2023), entre outros.

A adsorção pode ser definida como um fenômeno físico-químico no qual um componente (adsorvato ou adsorbato) em ~~uma~~ fase gasosa ou líquida é transferido para a superfície de uma fase sólida ou líquida condensada (adsorvente ou adsorbente). O processo de remoção das moléculas de adsorvato a partir da superfície do adsorvente é chamado dessorção (Wang & Guo, 2020b)

Os processos de separação por adsorção podem ser classificados em duas categorias básicas, a depender da interação entre a superfície sólida e a molécula. A adsorção química, ou quimissorção, resulta das interacoes mais específicas entre o adsorvente e a primeira camana de soluto adsorvido, envolvendo a partilha de elétrons. Normalmente é um processo irreversível, em que a dessorção da substância original leva em geral a uma modificação química da mesma. Já a fisissorção, ou adsorção física, ou ainda adsorção de Van der Waals, é prontamente reversível, caracterizada pelas fracas forças de atração intermoleculares entre as moléculas a serrem adsorvidas e a superfície do adsorvente. (Bushra et al., 2021)

A indústria química e de alimentos vêm fazendo uso da adsorção, por exemplo, na separação e purificação de produtos de alto valor agregado, na purificação de ar e gases e na reciclagem de águas residuárias contendo compostos indesejáveis, tais como corantes e metais pesados.

O mecanismo de remoção de corantes, conforme explicitado pela Figura 5, ocorre sequencialmente em quatro etapas (Bushra et al., 2021):

(1) difusão superficial das moléculas do corante (adsorvato) para a camada-limite de líquido existente ao redor do adsorvente;
(2) transporte do adsorvato por difusão através deste filme líquido até a entrada dos poros do adsorvente;
(3) difusão superficial das moléculas de corante para o interior do material através dos poros do adsorvente;
(4) adsorção dos íons/moléculas dos corantes em um sítio disponível do adsorvente por meio dos processos de quimissorção e/ou fisissorção (Figura 6).

Figura 5 - Etapas do processo de adsorção. (1) Difusão superficial através da camada limite; (2) transporte do adsorvato por difusão até a entrada dos poros do adsorvente; (3) difusão superficial para o interior do material adsorvente através dos poros; (4) adsorção dos íons/moléculas dos corantes em um dos sítios disponíveis do adsorvente por meio de quimissorção e/ou fisissorção.

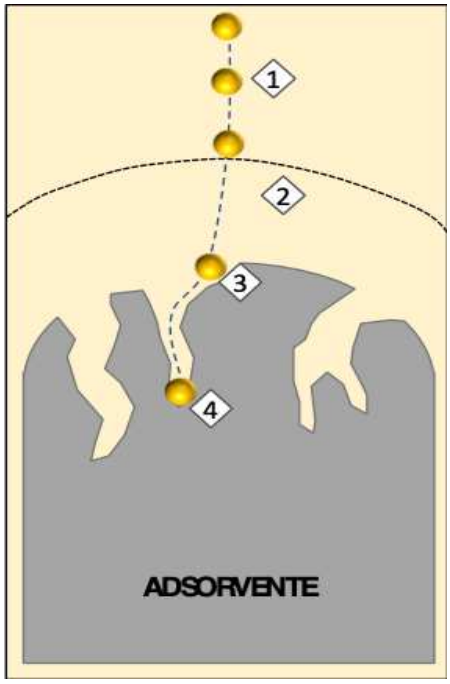

Fonte: Adaptado de Montanher et al., 2007.

Figura 6 - Diferença entre fisiossorção e quimiossorção

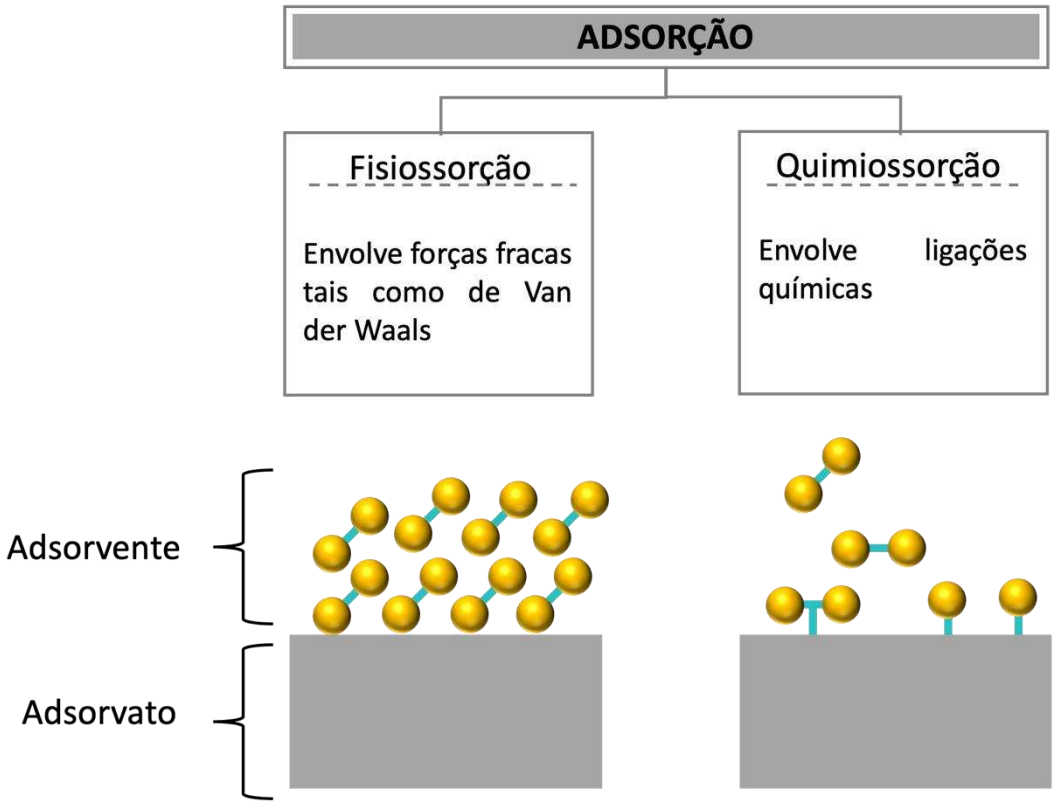

Diferentes tipos de adsorventes, tais como biossorventes, carvão ativado (Kwak et al., 2022), argilas e minerais (Zhang et al., 2021), polímeros, nanopartículas (Zhu et al., 2022) e compósitos (Duman et al., 2022) com alta capacidade de adsorção têm sido empregados com sucesso para remover poluentes de águas residuais. Porém, além da capacidade de remoção, o adsorvente deve ter alta disponibilidade, viabilidade econômica, capacidade regenerativa, além de responder às diretrizes ecológicas de tratamento de efluentes sem comprometer a qualidade da água.

3.1. Isotermas de adsorção

De acordo com Anastopoulos e Kyzas (2014), o modelo isotérmico de adsorção é uma ferramenta útil que fornece informações sobre a capacidade teórica máxima de adsorção e possíveis interações entre adsorventes e adsorbato. Tais informações podem ser representadas por meio de modelos teóricos, empíricos ou pela combinação desses que, por meio de equações, relacionam a massa adsorvida com a concentração do adsorvato restante na fase fluida. Os modelos de Langmuir e de Freundlich são os mais utilizados para descrever o equilíbrio de

adsorção de poluentes presentes em água, ainda existindo os de Dubinin-Radushkevich, Sip, Temkin e Redlich-Peterson, Halsey, Flory-Huggins, Elovich, e os Modelos Isotérmicos de Harkin-Jura.

3.1.1. Isoterma de Langmuir

O modelo de Langmuir é considerado o mais simples das isotermas de adsorção. Considera que, o sistema é ideal, e que as moléculas são adsorvidas e aderem à superfície do adsorvente, de forma homogênea, em sítios definidos e localizados, com a adsorção em monocamadas (Figura 7). Cada sítio pode acomodar somente uma molécula adsorvida e a energia da molécula é a mesma em todos os sítios da superfície (Chen et al., 2022; Langmuir, 1918).

Figura 7 – Esquematização dos processos adsortivos monocamada (teoria de Langmuir) e multicamadas (teoria de Freundlich).

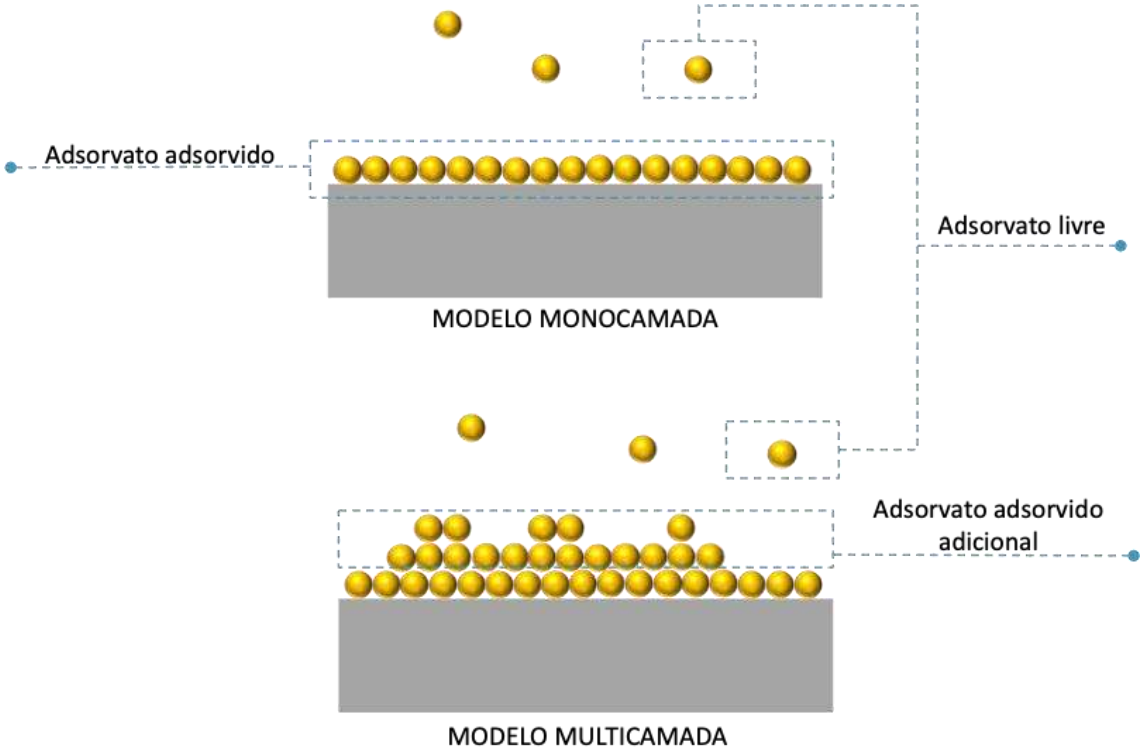

A forma matemática da isoterma de Langmuir (Equação 1) resulta da suposição de que quando uma solução está em contato com um material adsorvente e alcança o equilíbrio, a taxa

em que as espécies são adsorvidas na superfície é igual à taxa em que as espécies saem da superfície (Langmuir, 1918; Mozaffari Majd et al., 2022).

$$q_e = \frac{Q_{máx} K_l C_e}{1 + K_l C_e} \qquad \text{Equação 1}$$

Em que qe é a quantidade adsorvida da espécie no equilíbrio por unidade de massa de adsorvente ($mg \cdot g^{-1}$), Qmáx representa a quantidade máxima da espécie adsorvida ($mg \cdot g^{-1}$), Kl é a constante de adsorção de Langmuir relacionada ao equilíbrio química adsorvato/adsorvente ($L \cdot mg^{-1}$) e Ce é a concentração de equilíbrio do adsorvato ($mg \cdot L^{-1}$).

3.1.2. Isoterma de Freundlich

A isoterma de Freundlich é um modelo exponencial empírico, e foi uma das primeiras equações propostas para estabelecer uma relação entre a quantidade de material adsorvido e a concentração do material na solução. É aplicada em casos não ideais, pois considera superfícies heterogêneas e sorção em multicamadas, sugerindo que os sítios ligantes são diferentes quanto à capacidade de sorção. Sendo a superfície heterogênea, os sítios de adsorção possuem energias de adsorção diferentes e, por isso, nem sempre estão disponíveis. Esse modelo assume ainda que a energia da adsorção do adsorvato em um determinado sítio ativo está relacionada à existência de sítios adjacentes ocupados ou disponíveis (H. Freundlich, 1906; Mozaffari Majd et al., 2022).

O modelo de Freundlich assume que à medida que a concentração de adsorvato na solução aumenta, o mesmo acontece com a concentração de adsorvato na superfície do adsorvente. A equação do modelo de Freundlich é apresentada na Equação 2:

$$q_e = K_F \cdot C_e^{\frac{1}{n}} \qquad \text{Equação 2}$$

Em que K_F ($mg \cdot g^{-1}$) e n são constantes características do sistema, e estão relacionadas com a capacidade e a intensidade da adsorção, respectivamente. O índice F é uma indicação de que se trata de uma constante de Freundlich e Ce é a concentração de equilíbrio de soluto na solução. Em geral K_F avalia o aumento da capacidade de adsorção do adsorvente para um aumento na concentração do corante.

3.1.3. Isoterma de Redlich-Peterson R–P

O modelo de Redlich-Perterson corresponde ao modelo híbrido que integra três parâmetros em uma única equação empírica (Equação 3). A equação do modelo de Redlich-Perterson inclui relações de concentração exponencial no denominador e linear no numerador que mostram o equilíbrio de adsorção em uma ampla faixa de concentrações e podem ser usadas em sistemas de adsorção homogêneos e heterogêneos (Chen et al., 2022; Redlich & Peterson, 1959).

$$q_e = \frac{K_R \cdot C_e}{1 + \alpha_R C_e^{\beta R}} \qquad \text{Equação 3}$$

Em que K_Re $\alpha_R$são as constantes R–P; βR é o expoente que pode estar entre 0 e 1.

3.2. Cinética de adsorção

Cinética de adsorção é expressa como a taxa de remoção do adsorvato da fase fluida em relação ao tempo, a uma pressão ou concentração constante, envolvendo a difusão de um ou mais adsorbatos através dos macro-poros até as regiões mais interiores do adsorvente (Wang & Guo, 2020a).

O estudo da cinética ajuda a compreender o mecanismo de adsorção. Os dados obtidos são tipicamente analisados matematicamente usando modelos de pseudo-primeira e pseudo-segunda ordem para determinar o modelo cinético mais adequado para descrever um processo de sorção. O modelo de pseudo-primeira ordem corresponde a um processo controlado por difusão, sendo a equação de difusão intrapartícula (Equação 4). Já o modelo de pseudo-segunda ordem (Equação 5) assume que o processo é controlado pela reação de adsorção na interface líquido/sólido no adsorvente. Já modelo cinético de adsorção por difusão intrapartícula (Equação 6) assume que a difusão do filme líquido que cerca o adsorvente é desprezível e que a difusão intrapartícula é a única taxa que controla as etapas do processo de adsorção (Simonin, 2016).

$$q_t = q_e(1 - e^{-k_1 t}) \qquad \text{Equação 4}$$

$$q_t = \frac{k_2 {q_e}^2}{1+k_2 q_e t} \quad \text{Equação 5}$$

$$Q_t = k_d t^{0.5} + C \quad \text{Equação 6}$$

Em que k é a constante da taxa de adsorção ($h^{-1}(g{\cdot}mg^{-1})n^{-1}$); n é a ordem da adsorção com relação à concentração efetiva dos sítios de adsorção disponíveis na superfície do adsorvente; qe é a quantidade adsorvida no equilíbrio ($mg{\cdot}g^{-1}$) e qt é a quantidade adsorvida no tempo t ($mg{\cdot}g^{-1}$).

A adequação do processo cinético sugere que um mecanismo de adsorção química é baseado nos valores do coeficiente de correlação mais próximos da unidade obtida. Além disso, a condição de equilíbrio na sorção é alcançada quando a concentração do adsorvente permanece constante devido à transferência líquida zero do soluto adsorvido e dessorvido da superfície do sorvente.

3.3 Principais contaminantes de águas residuárias

A água é um recurso natural essencial à vida e desenvolvimento humano, bem como ao equilíbrio de qualquer ecossistema. Porém, com o rápido desenvolvimento da indústria moderna e da economia social, o descarte inadequado de poluentes representam uma séria ameaça ao acesso sustentável à água potável.

Os poluentes hídricos mais comuns incluem corantes (Hosny et al., 2023), metais pesados (Jiang et al., 2023), fenóis e fosfatos (Priya et al., 2022). Diferentes contaminantes causam riscos potenciais à saúde humana, bem como ao meio ambiente. O uso de metais pesados para diversas aplicações e atividades antrópicas (por exemplo, mineração, fundições, queima de combustíveis líquidos, lixiviação de metais e fundição) leva à sua liberação em fontes de água, podendo causar diversos problemas de saúde (Du e Li, 2023). Os corantes sintéticos são outra categoria de poluentes da água amplamente aplicados em diversos setores da indústria, tais como têxtil, gráfica, de couro, farmacêutica, de papel e alimentícia. Os corantes orgânicos são tóxicos, não degradáveis, bioacumulativos, recalcitrantes, carcinogênicos e mutagênicos e, portanto, prejudiciais os organismos aquáticos e a saúde humana (Hosny et al., 2023).

A seguir são descritas as principais características dos agentes poluentes estudados na presente tese.

3.3.1 Corantes

Segundo Damodaran et al. (2010) um corante é qualquer produto químico, natural ou sintético, capaz de conferir cor. A faixa de energia à qual o olho é sensível é chamada de luz visível. Luz visível, dependendo do indivíduo e sua sensibilidade, abrange comprimentos de onda de aproximadamente 380-770 nm (Figura 8). Corantes, portanto, são compostos capazes de absorver luz na região do visível, cuja finalidade é conferir cor sob condições pré-estabelecidas.

Figura 8 - Espectro eletromagnético. Fonte: Adaptado de Damodaran et al. (2010)

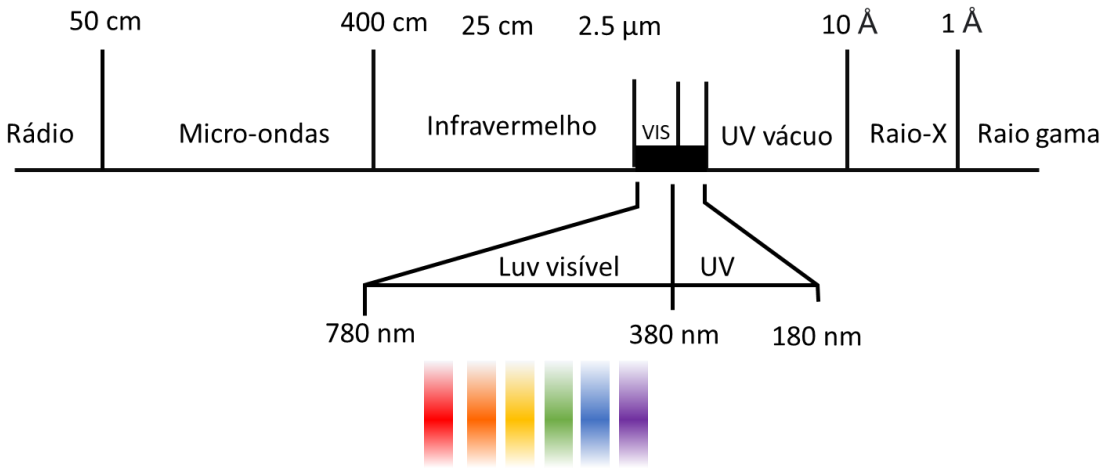

Os corantes consistem em compostos orgânicos insaturados e aromáticos formados por grupos cromóforos, auxocromos e estruturas aromáticas conjugadas. Os cromóforos, grupos químicos insaturados, são responsáveis pela coloração intrínseca dos corantes. Já os radicais químicos, auxocromos, são responsáveis pela intensificação da cor e fixação do corante no material (Berradi et al., 2019). Os radicais auxocromos possuem os grupos NH_2, OH, COOH ou SO_3H, podendo ser ácidos ou básicos. A Tabela 4 reúne os principais grupos cromóforos e auxocrômicos.

Tabela 4 - Grupos cromofóricos e auxocrômicos presentes em corantes.

Grupos cromóforos		**Grupos auxocromos**	
Azo	(-N=N-)	Amino	($-NH_2$)
Nitroso	(-NO or –N-OH)	Metilamino	($-NHCH_3$)
Carbonila	(>C=O)	Dimetilamino	($-N(CH_3)_2$)
Etilênico	(>C=C<)	Hidroxila	(-OH)
Nitro	($-NO_2$ ou =NO–OH)	alcoxila	(-OR)
Sulfureto	(>C=S)	Grupos doadores de elétrons	($-NO_2$)
Cetona-imina	(>C=NH)		($-CO_2H$)
Polimetina	(=HC-HC = CH–CH =)		($-SO_3H$)
Antraquinona			($-OCH_3$) Cl, Br, I, At
Ftalocianina	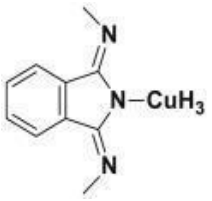		
Trifenilmetano	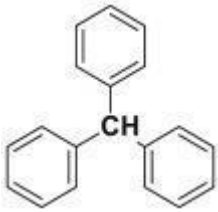		

Fonte: Adaptado de Berradi et al., 2019

A classificação dos corantes pode ser feita de acordo com sua constituição química ou de acordo com sua aplicabilidade (Figura 9). A classificação por estrutura química concentra-se na natureza do agrupamento cromóforo; essas classes incluem: trifenilmetano, ftaleína, trifenilmetil, nitrarado, atraquinona, azo, índigo, azina, xateno, nitro, oxazina, ftalocianina e triarilenetano, azo, antraquinona, índigo, xanteno, ftalocianina, nitrado e nitrosado, difenilmetano, trifenilmetano, azina, xateno, nitro, oxazina, diarilmetano e corantes poliméticos (Berradi et al., 2019).

Figura 9 - Classificação de corantes sintéticos. Fonte: Adaptado de Berradi et al, 2019.

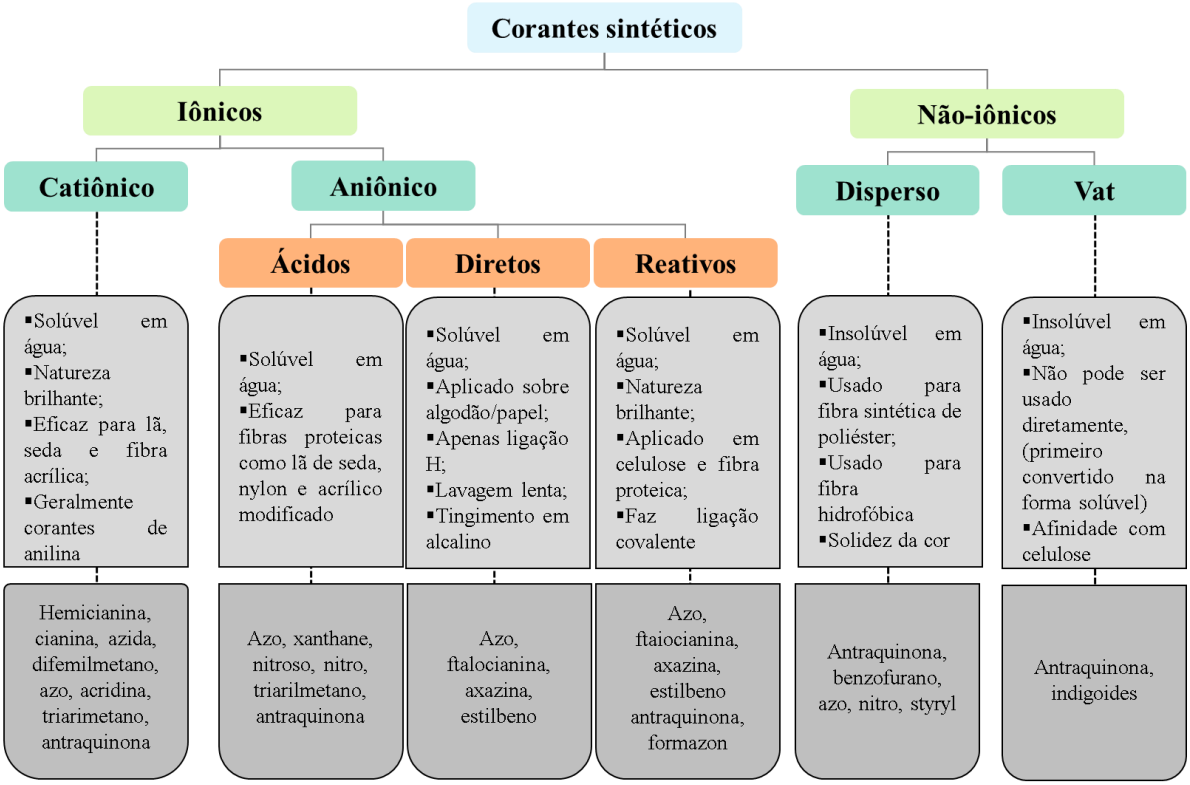

i.Azul de metileno

O azul de metileno (AM) é caracterizado por ser um corante catiônico, ou seja, em soluções aquosas, dissocia-se em ânions cloreto e cátions. Sua nomenclatura em química é definida por cloridrato de metiltiamina (ou cloreto de 3,7-bisdimetilaminofenotiazin-5-a), possui composição química $C_{16}H_{18}SN_3Cl.3H_2O$ e massa molecular de 319,85 $g \cdot mol^{-1}$ (Oladoye et al., 2022).

No que se refere ao seu grupo cromóforo, possui um anel contendo um átomo de enxofre e de nitrogênio e dois anéis aromáticos, cada um ligado a um átomo de nitrogênio que interage com dois grupos metila. Essa composição de sua estrutura, proporciona ao corante boa

resistência a processos de biodegradação (Hu, 2018). Sua forma de comercialização mais comum é a tri-hidratada, de acordo com a Figura 10.

Figura 10 - Fórmula estrutural do AM em sua forma tri-hidratada

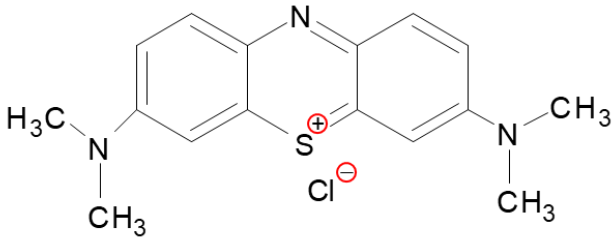

Apesar da ampla aplicabilidade, o corante azul de metileno, quando em excesso, apresenta comprovados efeitos nocivos em humanos e animais, tais como confusão mental, respiração não sistemática, sensação de queimação, necrose tecidual, quadriplegia, náusea, icterícia, entre outros (Vitskits et al., 2008). Considerando essa perigosa ameaça, faz-se crescente a necessidade de tratamentos eficazes nos resíduos industriais aquosos antes que esses sejam despejados diretamento no meio ambiente.

ii. Amarelo crepúsculo

Amarelo crepúsculo, também conhecido por outras nomeações como, amarelo crepúsculo FCF, amarelo alaranjado S, amarelo alimentar CI_3 e amarelo sol é um corante azo aniônico amplamente aplicado na indústria alimentícia para melhorar a aparência de alguns alimentos e bebidas, tais como queijo, bolos, doces, bebidas carbonatadas e suco de laranja. É ainda utilizado na indústria cosmética e de produtos farmacêuticos devido a ótima disposição de cor e baixo custo quando comparado com corantes naturais (Alqarni et al., 2018). Quimicamente é denominado como dissódico 6-hidroxi-5-[(4-sulfofenil) azo] 2-naftalenossulfononato (Figura 11) (Tajik e Beitollahi, 2022), sendo responsável por gerar coloração marrom avermelhada quando dissolvido em solução alcalina e coloração amarelo-alaranjada em água e soluções ácidas (Balram et al., 2022).

Figura 11 - Estrutura química amarelo crepúsculo.

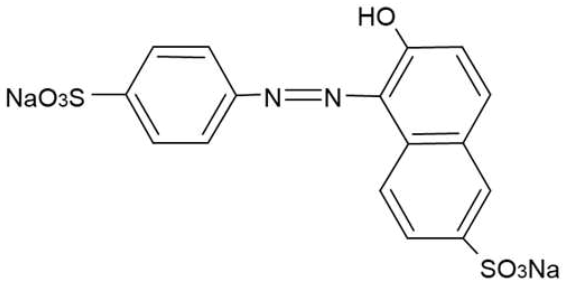

Apesar da comprovada eficiência de coloração em diversas matrizes, estudos tem demonstrado a possível associação do corante amarelo crepúsculo com vários efeitos adversos à saúde, tais como alergias, déficit de atenção, hiperatividade (Amchova et al., 2015), o que reforça a necessidade de se projetar um método conveniente, confiável e econômico para a remoção do mesmo de águas residuais antes que sejam lançadas no meio ambiente.

iii. Vermelho do Congo

O vermelho Congo (CR) é um corante azo aniônico, solúvel em água cuja cor e toxicidade estão relacionadas ao pH. A solução de CR adquire cor vermelha em pH neutro e alcalino e tende ao azul em pH mais baixo (Licona-Juárez et al., 2023). Este composto heterocíclico aromático induz alterações morfológicas e enfraquece a parede celular em concentrações subletais em fungos (Vuong et al., 2023).

Conforme mostra a Figura 12, a estrutura deste corante contém duas ligações azo como cromóforos submetidos à protonação sob condições ácidas. Presumivelmente, a forma aniônica (azoica) é mais tóxica que a forma protonada (Ahmad e Ansari, 2021).

É relatado que o CR é metabolizado em benzidina tendo, portanto, potencial para bioacumulação e sendo sua remoção da água dificultada. A toxicidade do CR pode causar danos ao sistema nervoso, irritação respiratória, diarréia, vômito, tontura, danos às mucosas e às membranas, sendo sua remoção de águas residuárias é muito importante (Cruz et al., 2023).

Figura 12 - Estrutura química do Vermelho do Congo.

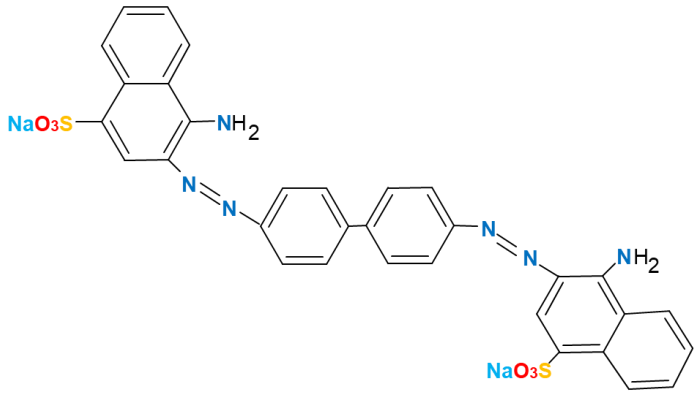

iv. Safranina

Safranina (S) (cloreto de 3, 7-diamino-2, 8-dimetil-5-fenilfenazina-5-io) (Figura13) é o corante sintético solúvel em água mais antigo conhecido. De coloração avermelhada, geralmente é usada para tingir algodão, fibras, couro, papel, seda, tanino e lã, sendo amplamente utilizado como corante nas indústrias alimentícia e têxtil (Çetinkaya et al., 2023).

Figura 13 - Estrutura química da Safranina.

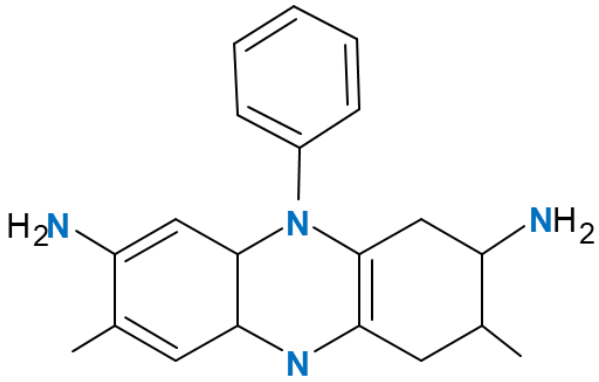

É documentado que a Safranina pode causar diversos efeitos agudos à saúde, como irritação e dor nas articulações, nos lábios e no estômago, podendo causar ainda vômito e diarréia (Bensalah et al., 2022). O estabelecimento de processos para eliminação deste corante em efluentes é de grande interesse do setor público e privado.

3.3.2 Metais pesados

Metais pesados são definidos como elementos metálicos de alta densidade (densidade superior a 4 g/cm^3) e massa atômica superior a 20. Constituem um grupo de aproximadamente 40 elementos, sendo extremamente tóxicos mesmo em magnitude muito baixa. Exemplos incluem chumbo (Pb), cadmium (Cd), cobre (Cu), zinco (Zn), cromo (Cr), chumbo (Pb), ferro (Fe), cobalto (Co), níquel (Ni) e manganês (Mn) (Mitra et al., 2022).

Embora alguns desses metais sejam essenciais para funções biológicas, como a geração e o funcionamento adequado de hormônios, enzimas, células e metabolismo; eles só são necessários para humanos em pequenas quantidades. Se os seus níveis no sistema circulatório aumentarem, isso poderá induzir efeitos negativos na saúde humana (Ahmadian et al., 2023).

Os metais pesados podem ser encontrados em seu estado elementar, o que indica que não sofreram modificações, ou em forma de complexos. Estes últimos são espécies químicas não degradáveis, por isso, uma vez colocados no meio ambiente, somente podem distribuir-se no ar, água, ou solo, às vezes mudando seu estado de oxidação, ou incorporando-se aos seres vivos. As atividades antropogênicas, tais como os processos de mineração, exercem um efeito considerável na concentração e mobilidade dos metais pesados no meio ambiente.

A seguir são apresentadas algumas características das espécies metálicas objeto desta tese.

i. Chumbo

O chumbo frequentemente se acumula no sangue, ossos, fígado, rins e cérebro humanos. Este metal pode perturbar a capacidade dos sistemas reprodutivo, hepático, endócrino, imunológico e digestivo. A exposição ao chumbo geralmente vem de tintas à base de chumbo, esgoto industrial e tubulações à base de chumbo. A exposição à tinta pode ocorrer através da ingestão direta de lascas de tinta ou, mais comumente, através da ingestão acidental de pó de chumbo (Huda et al., 2023).

O chumbo inorgânico (Pb) é o metal pesado mais extensivamente estudado. Hoje, ocorrem exposições elevadas em muitas profissões, mas também através, por exemplo, de água potável contaminada, medicamentos tradicionais, tinta com chumbo e solo e poeira em “pontos críticos” em torno de minas e fundições. O chumbo, frequentement,e se acumula no sangue, ossos, fígado, rins e cérebro humanos, podendo prejudicar a capacidade dos sistemas reprodutivo, hepático, endócrino, imunológico e digestivo (Bergdahl, et al., 2022).

ii. Cádmio

O cádmio é um elemento químico relativamente raro, de símbolo Cd, número atômico 48 e peso atômico 112. O cádmio não se encontra em estado livre na natureza, sendo encontrado unicamente na greenockita (CdS, sulfeto de cádmio). Geralmente, o cádmio se apresenta como mineral combinado com outros elementos, como o oxigênio, cloro e enxofre. Ele é geralmente obtido durante a produção de outros metais (zinco, cobre e chumbo) e oxida-se com facilidade (Wang et al., 2023).

Naturalmente, ele é absorvido pelos seres humanos através de certos alimentos ricos neste elemento, como patê, cogumelos, mariscos, cacau e algas secas. Entre os usos comerciais do cádmio podem ser citados o emprego como cobertura para prevenir a corrosão, em baterias níquel-cádmio, como reagente químico e pigmento (Souza-Arroyo et al., 2022).

Parte do cádmio encontrado no meio ambiente é liberado de forma natural nos rios pela decomposição das rochas e no ar através de incêndios florestais ou atividades vulcânicas. O restante é procedente das indústrias de produção de zinco, minérios de fosfato e produção de fertilizantes fosfatados artificiais, terminando geralmente nas águas residuais (Nordberg et al., 2018).

A ingestão prolongada de altas doses de Cd pode causar sérios danos a órgãos importantes, incluindo os pulmões e o fígado, e também levar ao câncer e outras doenças de saúde fatais (Galvez-Fernandez et al., 2021).

4. Carreamento de compostos

O carreamento de compostos é um método utilizado para aprisionar temporariamente uma substância ativa junto à um material carreador de modo a garantir a manutenção de suas principais características inalteradas por um determinado período de tempo (Mohammadian et al., 2020).

Muitos componentes naturais presentes em alimentos, tais como enzimas, carotenóides, vitaminas, polifenóis e óleos essenciais voláteis podem ser aprisionados em sistemas com diferentes diâmetros e distintas escalas, bem como nanoescala (0nm<d<1000 nm), microescala (d<1 cm) e macroescala (d> 1 cm), podendo esses existirem no estados sólido, líquido ou mesmo gasoso (Alu'datt et al., 2022).

Diversas são as razões para utilização do carreamento de compostos ativos em aplicações de alimentos e bebidas, dentre as quais podemos citar: (i) proteção do agente ativo aprisionado contra perdas de valor nutricional e/ou da bioatividade por interação com fatores

ambientais prejudiciais (por exemplo, calor, luz, ar e umidade); (ii) diminuição da evaporação e da taxa de transferência do agente central para o exterior; (iii) modificação das propriedades físicas das substâncias originais como por exemplo pela incorporação de substâncias líquidas em um sistema sólido seco para fácil manuseio; (iv) liberação controlada do material carreado; (v) mascaramento das propriedades organolépticas desagradáveis, como odor e sabor de alguns compostos; (vi) prevenção da incompatibilidade entre os componentes da mistura matriz (Alu'datt et al., 2022; Marcillo-Parra et al., 2021).

As tecnologias de encapsulamento podem ser classificadas de acordo com as técnicas utilizadas, tais como *spray drying* (Balci-Torun & Ozdemir, 2021), revestimento de leito fluidizado (Bellumori et al., 2021), lipossomas (Păvăloiu et al., 2021), complexação por inclusão, gelificação ionotrópica (Kairam et al., 2020) e coacervação complexa (Rosales et al., 2021). A última técnica citada foi utilizada no presente trabalho e é descrita na subsessão a seguir.

4.1. Coacervação complexa

O termo coacervação é utilizado na química coloidal que trata do processo de separação de fases líquidas induzida pela modificação do meio, como pH, temperatura, solubilidade, entre outros. A fase mais concentrada do componente coloidal é denominada coacervado e a outra fase, com poucas quantidades de coloides, é conhecida como fase de equilíbrio. No processo de coacervação simples, um único polímero está envolvido e os coacervados são formados devido a um mecanismo de desidratação causado pela adição de um sal ou líquido de dessolvatação no meio de reação. Quando a separação de fases associativa de dois ou mais polímeros em água ocorre pela interação eletrostática entre dois coloides de carga oposta diz-se que se trata de um processo de "coacervação complexa". Em muitos casos, os complexos formados são do tipo sólido (precipitado) (Eghbal & Choudhary, 2018).

A coacervação complexa pode ser usada para encapsulamento, formação de filmes de embalagem e produção de emulsões ou géis alimentares. Os coacervados formados também são usados como encapsulantes, aditivos, emulsificantes e modificadores de viscosidade na indústria alimentícia (Sing, 2017).

A coacervação tem sido cada vez mais utilizada para o carreamento de compostos de interesse industrial, bem como no desenvolvimento de materiais inovadores e funcionais pela interação de biopolímeros.

4.2. Cinética de liberação in vitro

4.3.

A cinética de liberação de um composto bioativo carreado é uma propriedade importante, uma vez que está diretamente relacionada à taxa e extensão da disponibilidade de absorção do agente ativo em seu alvo.

Modelos matemáticos são uma ferramenta importante para projetar formulações e avaliar processos de liberação de *in vitro* e *in vivo*, bem como permitir a interpretação quantitativa dos valores obtidos a partir de um ensaio de liberação.

4.2.1. Cinética de ordem zero

A dissolução de agentes ativos contidos em formas farmacêuticas não desintegrantes, que leva à sua liberação lenta, seguindo a cinética de liberação de ordem zero, pode ser expressa pela equação 6:

$$D_t + D_0 + K_0 t \qquad \text{Equação 6}$$

Em que D_t é a quantidade do composto ativo dissolvido no tempo t, D_0 é a quantidade inicial do composto na solução e K_0 é a constante de liberação de ordem zero (Bruschi, 2015).

Para cinética de ordem zero, a liberação de um agente ativo é apenas em função do tempo e o processo ocorre a uma taxa constante independente da concentração do agente ativo. O padrão de liberação de ordem zero são adequados para administração lenta e prolongada de compostos tais como, antibióticos e antidepressivos, fármacos para manutenção da pressão arterial, para controle da dor e como terapia do câncer (Doadrio et al., 2015).

4.2.2 Cinética de primeira-ordem

De maneira geral, o modelo cinético de primeira-ordem (equação 7) descreve a taxa de liberação do composto ativo de um sistema em função da concentração e do tempo, podendo descrever a dissolução de moléculas solúveis em uma matriz porosa.

$$ln\, Q_t = ln\, Q_0 + Q_1 t \qquad \text{Equação 7}$$

4.2.3 Modelo de Higuchi

O modelo desenvolvido por Higuchi descreve a taxa de liberação de compostos a partir de sistemas matriciais homogêneos submetidos a um meio difusor.

A Equação 8 descreve o modelo simplificado de Higuchi, que relaciona a concentração do agente ativo com a raiz quadrada do tempo, representando uma função linear.

$$Q_t = k_H\sqrt{t} \qquad \text{Equação 8}$$

Além disso, o modelo de Higuchi assume que: (i) a matriz contém uma concentração inicial de bioativo muito maior do que a solubilidade do mesmo; (ii) a difusão é unidirecional, pois os efeitos de borda são desprezíveis; (iii) a espessura da forma de dosagem é muito maior do que o tamanho das moléculas do fármaco, (iv) a difusividade do ativo é constante (Bruschi, 2015).

4.2.4 Modelo Hixson–Crowell

Hixson e Crowell (1931) descobriram que a área regular de um grupo de partículas é proporcional à raiz cúbica de seu volume. Usando essa relação, eles propuseram uma equação 9:

$$Q^{\frac{1}{3}} = Q_0^{\frac{1}{3}}(t) - K_{hc} \qquad \text{Equação 9}$$

Em que W_0 é a quantidade inicial do fármaco no sistema; Wi é o valor restante do fármaco no sistema no tempo t; e K_{HC} é a constante de incorporação, que relaciona superfície e volume.

Esta equação se aplica aos carreadores na forma de comprimidos, em que a dissolução ocorre em planos paralelos à superfície da forma farmacêutica; esta superfície diminui proporcionalmente ao longo do tempo e a forma geométrica mantém-se constante.

4.2.5 Modelo Korsmeyer–Peppas

O modelo de Korsmeyer–Peppas é geralmente usado para analisar a liberação de compostos ativos de microcápsulas poliméricas, quando o mecanismo de liberação não é bem

conhecido ou quando possa estar envolvido mais de um tipo de mecanismo de liberação. A equação 10, que descreve esse modelo, encontra-se a seguir:

$$Q = K_{K-P}(t^n) \qquad \text{Equação 10}$$

Em que K^{K-P} é a constante de Korsmeyer–Peppas, n é o expoente de liberação, que indica o mecanismo de taxa de liberação.

Diante das informações contidas nessa revisão de literatura, esta tese buscou estudar físico-químicamente complexos eletrólitos quitosano-carboximetilcelulose, bem como demonstrar sua aplicabilidade como carreadores de vitaminas e adsorvente de poluentes.

5. REFERÊNCIAS

Ahmad, R., Ansari, K. (2021). Comparative study for adsorption of congo red and methylene blue dye on chitosan modified hybrid nanocomposite. *Process Biochemistry*, v. 108, p. 90-102. https://doi.org/10.1016/j.procbio.2021.05.013

Ahmadian, M., Derakhshankhah, H., Jaymand, M. (2023). Recent advances in adsorption of environmental pollutants using metal–organic frameworks-based hydrogels. International Journal of Biological Macromolecules, 231, 15, https://doi.org/10.1016/j.ijbiomac.2023.123333.

Al-Rooqi, M. M., Hassan, M. M., Moussa, Z., Obaid, R. J., Suman, N. H., Wagner, M. H., Natto, S. S. A., & Ahmed, S. A. (2022). Advancement of chitin and chitosan as promising biomaterials. *Journal of Saudi Chemical Society*, *26*(6), 101561. https://doi.org/10.1016/j.jscs.2022.101561

Ali, A., & Ahmed, S. (2018). A review on chitosan and its nanocomposites in drug delivery. *International Journal of Biological Macromolecules*, *109*, 273–286. https://doi.org/10.1016/j.ijbiomac.2017.12.078

Alqarni, S.A.; Hussein, M.A.; Ganash, A.A. (2018). Highly sensitive and selective electrochemical determination of sunset yellow in food products based on AuNPs/PANI-co-PoAN-co-PoT/GO/Au electrode. *Chemistry Select*, v. 3, pp. 13167-13177.

Alsakhawy, M. A., Abdelmonsif, D. A., Haroun, M., & Sabra, S. A. (2022). Naringin-loaded Arabic gum/pectin hydrogel as a potential wound healing material. *International Journal of Biological Macromolecules*, *222*, 701–714. https://doi.org/10.1016/j.ijbiomac.2022.09.200

Altam, A. A., Zhu, L., Huang, W., Huang, H., & Yang, S. (2021). Polyelectrolyte complex beads of carboxymethylcellulose and chitosan: The controlled formation and improved properties. *Carbohydrate Polymer Technologies and Applications*, *2*. https://doi.org/10.1016/j.carpta.2021.100100

Altam, A. A., Zhu, L., Huang, W., Huang, H., & Yang, S. (2021). Polyelectrolyte complex beads of carboxymethylcellulose and chitosan: The controlled formation and improved properties. *Carbohydrate Polymer Technologies and Applications*, *2*. https://doi.org/10.1016/j.carpta.2021.100100

Alu'datt, M. H., Alrosan, M., Gammoh, S., Tranchant, C. C., Alhamad, M. N., Rababah, T., Alzougl, R., Alzoubi, H., Ghatasheh, S., Ghozlan, K., & Tan, T.-C. (2022). Encapsulated-based films for bioactive compounds and their application in the food industry: A roadmap for food-derived functional and healthy ingredients. *Food Bioscience*, *50*(PA), 101971. https://doi.org/10.1016/j.fbio.2022.101971

Amchova, P.; Kotolova, H.; Ruda-Kucerova, J. (2015). Health safety issues of synthetic food colorants. *Regul. Toxicol. Pharmacol*., 73 pp. 914-922.

Andrade Neto, J. C., Pereira, G. J., & Morandim-Giannetti, A. (2020). Lignocellulosic derivative and chitosan bioadsorbent: Synthesis, characterization, and performance in chromium adsorption. *Journal of Applied Polymer Science*, *137*(40), 49208. https://doi.org/10.1002/app.49208

Arinaitwe, E., & Pawlik, M. (2014). Dilute solution properties of carboxymethyl celluloses of various molecular weights and degrees of substitution. *Carbohydrate Polymers*, *99*, 423–431. https://doi.org/10.1016/j.carbpol.2013.08.030

Bajaj, M., Winter, J., & Gallert, C. (2011). Effect of deproteination and deacetylation conditions on viscosity of chitin and chitosan extracted from Crangon crangon shrimp waste. *Biochemical Engineering Journal*, *56*(1–2), 51–62. https://doi.org/10.1016/j.bej.2011.05.006

Balci-Torun, F., & Ozdemir, F. (2021). Encapsulation of strawberry flavour and physicochemical characterization of the encapsulated powders. *Powder Technology*, *380*, 602–612. https://doi.org/10.1016/j.powtec.2020.11.060

Balram, D.; Lian, K.Y.; Sebastian, N.; Al-Mubaddel, M.T. (2022). Noman Ultrasensitive detection of food colorant sunset yellow using nickel nanoparticles promoted lettuce-like spinel Co3O4 anchored GO nanosheets . *Food Chem. Toxicol*., 159, p. 112725.

Barclay, T. G., Day, C. M., Petrovsky, N., & Garg, S. (2019). Review of polysaccharide particle-based functional drug delivery. *Carbohydrate Polymers*, *221*(January), 94–112. https://doi.org/10.1016/j.carbpol.2019.05.067

Bellumori, M., de Marchi, L., Mainente, F., Zanoni, F., Cecchi, L., Innocenti, M., Mulinacci, N., & Zoccatelli, G. (2021). A by-product from virgin olive oil production (pâté) encapsulated by fluid bed coating: evaluation of the phenolic profile after shelf-life test and in vitro gastrointestinal digestion. *International Journal of Food Science and Technology*, *56*(8), 3773–3783. https://doi.org/10.1111/ijfs.15068

Bensalah, J., Habsaoui, A., Dagdag, O., Lebkiri, A., Ismi, I., Rifi, E. H., Zarrouk, A. (2021). Adsorption of a cationic dye (Safranin) by artificial cationic resins Amberlite®IRC-50: Equilibrium, kinetic and thermodynamic study. Chemical Data Collections, 35, 100756. doi:10.1016/j.cdc.2021.100756

Bergdahl, I. A., Skerfving, S. Chapter 19 - Lead, Handbook on the Toxicology of Metals (Fifth Edition), Academic Press, 2022, p. 427-493, https://doi.org/10.1016/B978-0-12-822946-0.00036-2.

Berradi, M., Hsissou, R., Khudhair, M., Assouag, M., Cherkaoui, O., El Bachiri, A., & El Harfi, A. (2019). Textile finishing dyes and their impact on aquatic environs. *Heliyon*, 5(11), e02711. doi:10.1016/j.heliyon.2019.e027

Berradi, M.; Hsissou, R.; Khudhair, M.; Assouag, M.; Cherkaoui, O.; Bachiri,A.; Harfi, A. (2019). Textile finishing dyes and their impact on aquatic environs. *Heliyon,* v. 5. https://doi.org/10.1016/j.heliyon.2019.e02711.

Biswal, A. K., Sahoo, M., Kumar Suna, P., Panda, L., Lenka, C., & Kumari Misra, P. (2022). Exploring the adsorption efficiency of a novel cellulosic material for removal of food dye from water. *Journal of Molecular Liquids*, *350*, 118577. https://doi.org/10.1016/j.molliq.2022.118577

Bozoğlan, B. K., Duman, O., & Tunç, S. (2020). Preparation and characterization of thermosensitive chitosan/carboxymethylcellulose/scleroglucan nanocomposite hydrogels. *International Journal of Biological Macromolecules*, *162*, 781–797. https://doi.org/10.1016/j.ijbiomac.2020.06.087

Bruschi, M. L. (2015). Mathematical models of drug release. In *Strategies to Modify the Drug Release from Pharmaceutical Systems* (1st ed., pp. 63–86). Woodhead Publishing. https://doi.org/10.1016/b978-0-08-100092-2.00005-9

Bushra, R., Mohamad, S., Alias, Y., Jin, Y., & Ahmad, M. (2021). Current approaches and methodologies to explore the perceptive adsorption mechanism of dyes on low-cost

agricultural waste: A review. *Microporous and Mesoporous Materials*, *319*(March), 111040. https://doi.org/10.1016/j.micromeso.2021.111040

Cerchiara, T., Abruzzo, A., Parolin, C., Vitali, B., Bigucci, F., Gallucci, M. C., Nicoletta, F. P., & Luppi, B. (2016). Microparticles based on chitosan/carboxymethylcellulose polyelectrolyte complexes for colon delivery of vancomycin. *Carbohydrate Polymers*, *143*, 124–130. https://doi.org/10.1016/j.carbpol.2016.02.020

Çetinkaya, S., Kaya, S., Aksu, A., Çetintaş, H. I., Jalbani, N. S., Erkan, S., Marzouki, R. (2023). Equilibrium and DFT modeling studies for the biosorption of Safranin O dye from water samples using Bacillus subtilis biosorbent. Journal of Molecular Structure, v.1276. https://doi.org/10.1016/j.molstruc.2022.134761.

Chen, R., Williams, P. A., Chong, D., Luo, S., Chen, J., & Liu, C. (2023). The interaction of pectin with wheat starch and its influence on gelatinization and rheology. *Food Hydrocolloids*, *136*, 108288. https://doi.org/10.1016/j.foodhyd.2022.108288

Chen, X., Hossain, M. F., Duan, C., Lu, J., Tsang, Y. F., Islam, M. S., & Zhou, Y. (2022). Isotherm models for adsorption of heavy metals from water - A review. *Chemosphere*, *307*(P1), 135545. https://doi.org/10.1016/j.chemosphere.2022.135545

Cruz, E. D., Missau, J., Collinson, S. R., Tanabe, E. H., Bertuol, D. A. (2023). Efficient removal of congo red dye using activated lychee peel biochar supported Ca-Cr layered double hydroxide. *Environmental Nanotechnology, Monitoring & Management*, v. 20, https://doi.org/10.1016/j.enmm.2023.100835.

da Silva, G. M., da Rocha, R. F. P., da Costa, M. P. M., Ferreira, I. L. de M., & Delpech, M. C. (2018). Evaluation of viscometric properties of carboxymethylcellulose and gellan. *Journal of Molecular Liquids*, *268*, 201–205. https://doi.org/10.1016/j.molliq.2018.07.062

DAMODARAN, S.; PARKIN, K.L.; FENNEMA, O.R. Química de Alimentos de Fennema. Trad. Brandelli et al. Porto Alegre: Artmed, 2010. 900p.

Doadrio, A. L., Conde, A., Arenas, M. A., Hernández-López, J. M., de Damborenea, J. J., Pérez-Jorge, C., Esteban, J., & Vallet-Regí, M. (2015). Use of anodized titanium alloy as drug carrier: Ibuprofen as model of drug releasing. *International Journal of Pharmaceutics*, *492*(1–2), 207–212. https://doi.org/10.1016/j.ijpharm.2015.07.046

Du, C., Li, Z. (2023). Contamination and health risks of heavy metals in the soil of a historical landfill in northern China. *Chemosphere,* v. 313. https://doi.org/10.1016/j.chemosphere.2022.137349

Duman, O., Polat, T. G., & Tunç, S. (2022). Development of poly(vinyl alcohol)/β-cyclodextrin/P(MVE-MA) composite nanofibers as effective and selective adsorbent and

filtration material for the removal and separation of cationic dyes from water. *Journal of Environmental Management*, *322*(July), 116130. https://doi.org/10.1016/j.jenvman.2022.116130

Eghbal, N., & Choudhary, R. (2018). Complex coacervation: Encapsulation and controlled release of active agents in food systems. *LWT - Food Science and Technology*, *90*(May 2017), 254–264. https://doi.org/10.1016/j.lwt.2017.12.036

el Knidri, H., Belaabed, R., Addaou, A., Laajeb, A., & Lahsini, A. (2018). Extraction, chemical modification and characterization of chitin and chitosan. *International Journal of Biological Macromolecules*, *120*, 1181–1189. https://doi.org/10.1016/j.ijbiomac.2018.08.139

Galvez-Fernandez, M., Grau-Perez, M., Garcia-Barrera, T., Ramirez-Acosta, S., Gomez-Ariza, J. L., Perez-Gomez, B., … Martin-Escudero, J. C. (2021). Arsenic, cadmium, and selenium exposures and bone mineral density-related endpoints: The HORTEGA study. *Free Radical Biology and Medicine*, v. 162, p. 392–400. doi:10.1016/j.freeradbiomed.202

Gao, N., Liang, F., Wang, X., & Li, B. (2022). Loose composite nanofiltration membrane with in-situ immobilized β-FeOOH film for effective dyes degradation and separation. *Colloids and Surfaces A: Physicochemical and Engineering Aspects*, *654*(July). https://doi.org/10.1016/j.colsurfa.2022.130115

Gopinath, V., Saravanan, S., Al-Maleki, A. R., Ramesh, M., & Vadivelu, J. (2018). A review of natural polysaccharides for drug delivery applications: Special focus on cellulose, starch and glycogen. *Biomedicine and Pharmacotherapy*, *107*(April), 96–108. https://doi.org/10.1016/j.biopha.2018.07.136

H. Freundlich. (1906). Over the adsorption in solution. *J. Phys. Chem.*, *57*, 1100–1107.

Hmamouchi, S., el Yacoubi, A., Massit, A., Berradi, M., el Hezzat, M., Sallek, B., & Chafik El Idrissi, B. (2022). Photocatalytic decomposition of methylene blue dye using sand-graphite composite under visible light irradiation. *Materials Today: Proceedings*, *xxxx*. https://doi.org/10.1016/j.matpr.2022.09.044

Hosny, N. M., Gomaa, I., Elmahgary, M. G. (2023). Adsorption of polluted dyes from water by transition metal oxides: A review. *Applied Surface Science Advances*, v.15. https://doi.org/10.1016/j.apsadv.2023.100395

Hosny, N. M., Gomaa, I., Elmahgary, M. G. (2023). Adsorption of polluted dyes from water by transition metal oxides: A review, *Applied Surface Science Advances*, v. 15. https://doi.org/10.1016/j.apsadv.2023.100395

Hu, X.-S.; Liang, R.; Sun, G. (2018). Super-adsorbent hydrogel for removal of methylene blue dye from aqueous solution. *Journal of Materials Chemistry* A, v. 6, n. 36, p. 17612–17624.

Huda, B. N., Wahyuni, E. T., Mudasir, M. (2023). Simultaneous adsorption of Pb(II) and Cd(II) in the presence of Mg(II) ion using eco-friendly immobilized dithizone on coal bottom ash. South African Journal of Chemical Engineering, v. 45, p. 315-327, https://doi.org/10.1016/j.sajce.2023.06.007

Ihaddaden, S., Aberkane, D., Boukerroui, A., & Robert, D. (2022). Removal of methylene blue (basic dye) by coagulation-flocculation with biomaterials (bentonite and Opuntia ficus indica). *Journal of Water Process Engineering*, *49*(March), 102952. https://doi.org/10.1016/j.jwpe.2022.102952

Inphonlek, S., Sunintaboon, P., Leonard, M., & Durand, A. (2020). Chitosan/carboxymethylcellulose-stabilized poly(lactide-co-glycolide) particles as bio-1 based drug delivery carriers. *Carbohydrate Polymers*, 242.

Javanbakht, S., & Shaabani, A. (2019). Encapsulation of graphene quantum dot-crosslinked chitosan by carboxymethylcellulose hydrogel beads as a pH-responsive bio-nanocomposite for the oral delivery agent. *International Journal of Biological Macromolecules*, *123*, 389–397. https://doi.org/10.1016/j.ijbiomac.2018.11.118

Jiang, H., Wu, S., Zhou, J. (2023). Preparation and modification of nanocellulose and its application to heavy metal adsorption: A review. *International Journal of Biological Macromolecules,* v. 236. https://doi.org/10.1016/j.ijbiomac.2023.123916

Kairam, N., Kandi, S., Choudhary, A., & Sharma, M. (2020). Development of flaxseed and garlic oil hydrogel beads by novel ionotropic gelation method. *Journal of Food Processing and Preservation*, *44*(10), 1–9. https://doi.org/10.1111/jfpp.14821

Kancı Bozoğlan, B., Duman, O., & Tunç, S. (2021). Smart antifungal thermosensitive chitosan/carboxymethylcellulose/scleroglucan/montmorillonite nanocomposite hydrogels for onychomycosis treatment. *Colloids and Surfaces A: Physicochemical and Engineering Aspects*, *610*. https://doi.org/10.1016/j.colsurfa.2020.125600

Kashapov, R., Razuvayeva, Y., Ziganshina, A., Lyubina, A., Amerhanova, S., Sapunova, A., Voloshina, A., Nizameev, I., Salnikov, V., & Zakharova, L. (2022). Formation of supramolecular structures in aqueous medium by noncovalent interactions between surfactant and resorcin[4]arene. *Colloids and Surfaces A: Physicochemical and Engineering Aspects*, *648*(March), 129330. https://doi.org/10.1016/j.colsurfa.2022.129330

Kumar, D., & Gupta, S. K. (2022). Electrochemical oxidation of direct blue 86 dye using MMO coated Ti anode: modelling, kinetics and degradation pathway. *Chemical Engineering and Processing - Process Intensification*, *181*(July), 109127. https://doi.org/10.1016/j.cep.2022.109127

Kumirska, J., Czerwicka, M., Kaczyński, Z., Bychowska, A., Brzozowski, K., Thöming, J., & Stepnowski, P. (2010). Application of spectroscopic methods for structural analysis of chitin and chitosan. *Marine Drugs*, *8*(5), 1567–1636. https://doi.org/10.3390/md8051567

Kwak, C. H., Lim, C., Kim, S., & Lee, Y.-S. (2022). Surface modification of carbon materials and its application as adsorbents. *Journal of Industrial and Engineering Chemistry*, *116*, 21–31. https://doi.org/10.1016/j.jiec.2022.08.043

Langmuir, I. (1918). The Adsorption of Gases on Plane Surfaces of Mica. *Journal of the American Chemical Society*, *40*(9), 1361–1403. https://doi.org/10.1021/ja01269a066

Li, J., Guo, M., Wang, Y., Ye, B., Chen, Y., & Yang, X. (2021). Preparation of biological sustained-release nanocapsules and explore on algae-killing properties. *Journal of Advanced Research*, *31*, 87–96. https://doi.org/10.1016/j.jare.2020.12.006

Li, S.-S., Wang, X.-L., An, Q.-D., Xiao, Z.-Y., Zhai, S.-R., Cui, L., & Li, Z.-C. (2020). Upon designing carboxyl methylcellulose and chitosan-derived nanostructured sorbents for efficient removal of Cd(II) and Cr(VI) from water. *International Journal of Biological Macromolecules*, *143*, 640–650. https://doi.org/10.1016/j.ijbiomac.2019.12.053

Licona-Juárez, K. C., Bezerra, A. V. S., Oliveira I. T. C., Massingue, C. D., Medina, H. R., Rangel, D. E. N. (2023). Congo red induces trans-priming to UV-B radiation in Metarhizium robertsii. *Fungal Biology.* https://doi.org/10.1016/j.funbio.2023.06.005

Limpongsa, E., Soe, M. T., & Jaipakdee, N. (2021). Modification of release and penetration behavior of water-soluble active ingredient from ball-milled glutinous starch matrix via carboxymethylcellulose blending. *International Journal of Biological Macromolecules*, *193*, 2271–2280. https://doi.org/10.1016/j.ijbiomac.2021.11.059

Liu, S., Wang, Z., Feng, X., & Pyo, S. H. (2023). Refractory azo dye wastewater treatment by combined process of microbial electrolytic reactor and plant-microbial fuel cell. *Environmental Research*, *216*(P2), 114625. https://doi.org/10.1016/j.envres.2022.114625

Liu, Z., Qiang, R., Lin, L., Deng, X., Yang, X., Zhao, K., Yang, J., Li, X., Ma, W., & Xu, M. (2022). Thermally modified polyimide/SiO2 nanofiltration membrane with high permeance and selectivity for efficient dye/salt separation. *Journal of Membrane Science*, *658*(March), 120747. https://doi.org/10.1016/j.memsci.2022.120747

Lu, X., Chen, J., Guo, Z., Zheng, Y., Rea, M. C., Su, H., Zheng, X., Zheng, B., & Miao, S. (2019). Using polysaccharides for the enhancement of functionality of foods: A review. *Trends in Food Science and Technology*, *86*(April 2018), 311–327. https://doi.org/10.1016/j.tifs.2019.02.024

Luo, Y., Wang, Y., Hua, F., Xue, M., Xie, X., Xie, Y., Yu, S., Zhang, L., Yin, Z., Xie, C., & Hong, Z. (2023). Adsorption and photodegradation of reactive red 120 with nickel-iron-layered double hydroxide/biochar composites. *Journal of Hazardous Materials*, *443*, 130300. https://doi.org/10.1016/j.jhazmat.2022.130300

Marcillo-Parra, V., Tupuna-Yerovi, D. S., González, Z., & Ruales, J. (2021). Encapsulation of bioactive compounds from fruit and vegetable by-products for food application – A review. *Trends in Food Science and Technology*, *116*(August 2020), 11–23. https://doi.org/10.1016/j.tifs.2021.07.009

Martins, A. F., Vlcek, J., Wigmosta, T., Hedayati, M., Reynolds, M. M., Popat, K. C., & Kipper, M. J. (2020). Chitosan/iota-carrageenan and chitosan/pectin polyelectrolyte multilayer scaffolds with antiadhesive and bactericidal properties. *Applied Surface Science*, *502*. https://doi.org/10.1016/j.apsusc.2019.144282

Matsuyama, S., Kazuhiro, M., Nakauma, M., Funami, T., Nambu, Y., Matsumiya, K., & Matsumura, Y. (2021). Stabilization of whey protein isolate-based emulsions via complexation with xanthan gum under acidic conditions. *Food Hydrocolloids*, *111*. https://doi.org/10.1016/j.foodhyd.2020.106365

Mitra, S., Chakraborty, A. J., Tareq, A. M., Emran, T., Bin, Nainu, F., Khusro, A., Idris, A. M., Khandaker, M. U., Osman, H., Alhumaydhi, F. A., Simal-Gandara, J. (2023). Impact of heavy metals on the environment and human health: novel therapeutic insights to counter the toxicity. *J. King Saud. Univ. - Sci.*, 34. Article 101865, 10.1016/J.JKSUS.2022.101865

Mittal, H., al Alili, A., Morajkar, P. P., & Alhassan, S. M. (2021). GO crosslinked hydrogel nanocomposites of chitosan/carboxymethyl cellulose – A versatile adsorbent for the treatment of dyes contaminated wastewater. *International Journal of Biological Macromolecules*, *167*, 1248–1261. https://doi.org/10.1016/j.ijbiomac.2020.11.079

Mohammadian, M., Waly, M. I., Moghadam, M., Emam-Djomeh, Z., Salami, M., & Moosavi-Movahedi, A. A. (2020). Nanostructured food proteins as efficient systems for the encapsulation of bioactive compounds. *Food Science and Human Wellness*, *9*(3), 199–213. https://doi.org/10.1016/j.fshw.2020.04.009

Mohammed, M. A., Syeda, J. T. M., Wasan, K. M., & Wasan, E. K. (2017). An overview of chitosan nanoparticles and its application in non-parenteral drug delivery. *Pharmaceutics*, *9*(4). https://doi.org/10.3390/pharmaceutics9040053

Mozaffari Majd, M., Kordzadeh-Kermani, V., Ghalandari, V., Askari, A., & Sillanpää, M. (2022). Adsorption isotherm models: A comprehensive and systematic review (2010−2020). *Science of the Total Environment*, *812*. https://doi.org/10.1016/j.scitotenv.2021.151334

Mujtaba, M., Morsi, R. E., Kerch, G., Elsabee, M. Z., Kaya, M., Labidi, J., & Khawar, K. M. (2019). Current advancements in chitosan-based film production for food technology; A review. *International Journal of Biological Macromolecules*, *121*, 889–904. https://doi.org/10.1016/j.ijbiomac.2018.10.109

Nie, J., Pei, B., Wang, Z., & Hu, Q. (2019). Construction of ordered structure in polysaccharide hydrogel: A review. Carbohydrate Polymers, 205(March 2018), 225–235. https://doi.org/10.1016/j.carbpol.2018.10.033

Nnaji, P. C., Anadebe, V. C., Ezemagu, I. G., & Onukwuli, O. D. (2022). Potential of Luffa cylindrica seed as coagulation-flocculation (CF) agent for the treatment of dye wastewater: Kinetic, mass transfer, optimization and CF adsorption studies. *Arabian Journal of Chemistry*, *15*(2), 103629. https://doi.org/10.1016/j.arabjc.2021.103629

Nordberg, G. F., Åkesson, A., Nogawa, K., Nordberg, M. Chapter 7 - Cadmium, Handbook on the Toxicology of Metals (Fifth Edition), Academic Press, 2022, p.141-196, https://doi.org/10.1016/B978-0-12-822946-0.00006-4.

Oladoye, P. O. et al. Methylene blue dye: Toxicity and potential elimination technology from wastewater. Results in Engineering, Department of Chemistry and Biochemistry, Florida International University, 11200 SW 8th St, Miami, FL, 33199, USA, v. 16, n. 100678, p. 1-1, set./2022.

Păvăloiu, R. D., Sha'at, F., Neagu, G., Deaconu, M., Bubueanu, C., Albulescu, A., Sha'at, M., & Hlevca, C. (2021). Encapsulation of polyphenols from lycium barbarum leaves into liposomes as a strategy to improve their delivery. *Nanomaterials*, *11*(8), 1–13. https://doi.org/10.3390/nano11081938

Pinto, E., Aggrey, W. N., Boakye, P., Amenuvor, G., Sokama-Neuyam, Y. A., Fokuo, M. K., Karimaie, H., Sarkodie, K., Adenutsi, C. D., Erzuah, S., & Rockson, M. A. D. (2022). Cellulose processing from biomass and its derivatization into carboxymethylcellulose: A review. *Scientific African*, *15*, e01078. https://doi.org/10.1016/j.sciaf.2021.e01078

Priya, E., Kumar, S., Verma, C., Sarkar, K., Maji, P. K. (2022). A comprehensive review on technological advances of adsorption for removing nitrate and phosphate from waste water. *Journal of Water Process Engineering*, v. 49. https://doi.org/10.1016/j.jwpe.2022.103159

Quadrado, R. F. N., & Fajardo, A. R. (2022). Vapor-induced polyelectrolyte complexation of chitosan/pectin: A promising strategy for the preparation of hydrogels for controlled drug delivery. *Journal of Molecular Liquids*, *361*. https://doi.org/10.1016/j.molliq.2022.119604

Rahman, S., Konwar, A., Majumdar, G., & Chowdhury, D. (2021a). Guar gum-chitosan composite film as excellent material for packaging application. *Carbohydrate Polymer Technologies and Applications*, *2*. https://doi.org/10.1016/j.carpta.2021.100158

Rahman, S., Konwar, A., Majumdar, G., & Chowdhury, D. (2021b). Guar gum-chitosan composite film as excellent material for packaging application. *Carbohydrate Polymer Technologies and Applications*, *2*. https://doi.org/10.1016/j.carpta.2021.100158

Redlich, O., & Peterson, D. L. (1959). A useful adsorption isotherm. *J. Phys. Chem.*, *63*, 1024.

Rinaudo, M. (2006). Chitin and chitosan: Properties and applications. *Progress in Polymer Science (Oxford)*, *31*(7), 603–632. https://doi.org/10.1016/j.progpolymsci.2006.06.001

Rosales, T. K. O., Pessoa da Silva, M., Lourenço, F. R., Aymoto Hassimotto, N. M., & Fabi, J. P. (2021). Nanoencapsulation of anthocyanins from blackberry (Rubus spp.) through pectin and lysozyme self-assembling. *Food Hydrocolloids*, *114*(December 2020). https://doi.org/10.1016/j.foodhyd.2020.106563

Rutz, J. K., Borges, C. D., Zambiazi, R. C., da Rosa, C. G., & da Silva, M. M. (2016). Elaboration of microparticles of carotenoids from natural and synthetic sources for applications in food. *Food Chemistry*, *202*, 324–333. https://doi.org/10.1016/j.foodchem.2016.01.140

Schio, R. da R., da Boit Martinello, K., Netto, M. S., Silva, L. F. O., Mallmann, E. S., & Dotto, G. L. (2022). Adsorption performance of Food Red 17 dye using an eco-friendly material based on Luffa cylindrica and chitosan. *Journal of Molecular Liquids*, *349*, 118144. https://doi.org/10.1016/j.molliq.2021.118144

Sellaoui, L., Dhaouadi, F., Li, Z., Cadaval, T. R. S., Igansi, A. v., Pinto, L. A. A., Dotto, G. L., Bonilla-Petriciolet, A., Pinto, D., & Chen, Z. (2021). Implementation of a multilayer statistical physics model to interpret the adsorption of food dyes on a chitosan film. *Journal of Environmental Chemical Engineering*, *9*(4), 105516. https://doi.org/10.1016/j.jece.2021.105516

Simonin, J. P. (2016). On the comparison of pseudo-first order and pseudo-second order rate laws in the modeling of adsorption kinetics. *Chemical Engineering Journal*, *300*, 254–263. https://doi.org/10.1016/j.cej.2016.04.079

Sing, C. E. (2017). Development of the modern theory of polymeric complex coacervation. *Advances in Colloid and Interface Science*, *239*, 2–16. https://doi.org/10.1016/j.cis.2016.04.004

Singh, P., Medronho, B., Alves, L., da Silva, G. J., Miguel, M. G., & Lindman, B. (2017). Development of carboxymethyl cellulose-chitosan hybrid micro- and macroparticles for

encapsulation of probiotic bacteria. *Carbohydrate Polymers*, *175*, 87–95. https://doi.org/10.1016/j.carbpol.2017.06.119

Sinha, D., Seth, S., Das, A., Bhattacharyya, U. K., Ghosh, K., Nandi, A., Banerjee, P., & Ray, S. (2022). Tuned Gum ghatti and pectin for green synthesis of novel wound dressing material: Engineering aspects and in vivo study. *Journal of Drug Delivery Science and Technology*, *76*. https://doi.org/10.1016/j.jddst.2022.103730

Souza-Arroyo, V., Fabián, J. J., Bucio-Ortiz, L. L., Miranda-Labra, R. U., Gomez-Quiroz, L. E., Gutiérrez-Ruiz, M. C. (2022). The mechanism of the cadmium-induced toxicity and cellular response in the liver. *Toxicology*, v. 480. https://doi.org/10.1016/j.tox.2022.153339

Sun, X., Wu, Y., Song, Z., & Chen, X. (2022). A review of natural polysaccharides for food cryoprotection: Ice crystals inhibition and cryo-stabilization. *Bioactive Carbohydrates and Dietary Fibre*, *27*. https://doi.org/10.1016/j.bcdf.2021.100291

Sun, Y., Li, D., Lu, X., Sheng, J., Zheng, X., & Xiao, X. (2021). Flocculation of combined contaminants of dye and heavy metal by nano-chitosan flocculants. *Journal of Environmental Management*, *299*(August). https://doi.org/10.1016/j.jenvman.2021.113589

Szymańska, E., & Winnicka, K. (2015). Stability of Chitosan—A Challenge for Pharmaceutical and Biomedical Applications. *Marine Drugs*, *13*(4), 1819–1846. https://doi.org/10.3390/md13041819

Tajik, S.; Beitollahi, H. (2022). Hydrothermal synthesis of CuFe2O4 nanoparticles for highly sensitive electrochemical detection of sunset yellow. *Food and Chemical Toxicology*, v. 165, p. 113048.

Tsai, R. Y., Chen, P. W., Kuo, T. Y., Lin, C. M., Wang, D. M., Hsien, T. Y., & Hsieh, H. J. (2014). Chitosan/pectin/gum Arabic polyelectrolyte complex: Process-dependent appearance, microstructure analysis and its application. *Carbohydrate Polymers*, *101*(1), 752–759. https://doi.org/10.1016/j.carbpol.2013.10.008

Vuong, N-M-T., Nguyen, P-T., Nguyen, T-K-O., Nguyen, D-B., Tran, T-M-D., Oanh, L . T. K., Nguyen, T-H., Pham, T.T., Lin, K-Y. A., Bui, X-T. (2023). Application of nano zero-valent iron particles coated by carboxymethyl cellulose for removal of Congo red dye in aqueous solution. *Case Studies in Chemical and Environmental Engineering*, 100469, https://doi.org/10.1016/j.cscee.2023.100469.

Wang, H., Luo, W., Guo, R., Li, D., & Xue, B. (2022). Effective adsorption of Congo red dye by magnetic chitosan prepared by solvent-free ball milling. *Materials Chemistry and Physics*, *292*(October), 126857. https://doi.org/10.1016/j.matchemphys.2022.126857

Wang, J., & Guo, X. (2020a). Adsorption kinetic models: Physical meanings, applications, and solving methods. *Journal of Hazardous Materials*, *390*, 122156. https://doi.org/10.1016/j.jhazmat.2020.122156

Wang, J., & Guo, X. (2020b). Adsorption isotherm models: Classification, physical meaning, application and solving method. *Chemosphere*, *258*, 127279. https://doi.org/10.1016/j.chemosphere.2020.127279

Wang, K., Du, L., Zhang, C., Lu, Z., Lu, F., & Zhao, H. (2019). Preparation of chitosan/curdlan/carboxymethyl cellulose blended film and its characterization. *Journal of Food Science and Technology*, *56*(12), 5396–5404. https://doi.org/10.1007/s13197-019-04010-2

Wang, R., Sang, P., Guo, Y., Jin, P., Cheng, Y., Yu, H., Xie, Y., Yao, W., Qian, H. (2023). Cadmium in food: Source, distribution and removal, *Food Chemistry*, v. 405, https://doi.org/10.1016/j.foodchem.2022.134666.

Wang, W., Ni, J., Chen, L., Ai, Z., Zhao, Y., & Song, S. (2020). Synthesis of carboxymethyl cellulose-chitosan-montmorillonite nanosheets composite hydrogel for dye effluent remediation. *International Journal of Biological Macromolecules*, *165*, 1–10. https://doi.org/10.1016/j.ijbiomac.2020.09.154

Wongkom, L., & Jimtaisong, A. (2017). Novel biocomposite of carboxymethyl chitosan and pineapple peel carboxymethylcellulose as sunscreen carrier. *International Journal of Biological Macromolecules*, *95*, 873–880. https://doi.org/10.1016/j.ijbiomac.2016.10.069

Wu, J., Sha, C., Li, D., Shen, C., Tang, H., & Huang, S. (2022). Spatial and seasonal variation and sources of deposition fluxes of polycyclic aromatic hydrocarbons (PAHs) in Shanghai. *Environmental Science and Pollution Research*, 75258–75270. https://doi.org/10.1007/s11356-022-20348-1

Xiao, N., He, W., Zhao, Y., Yao, Y., Xu, M., Du, H., Wu, N., & Tu, Y. (2021). Effect of pH and xanthan gum on emulsifying property of ovalbumin stabilized oil-in water emulsions. *LWT*, *147*. https://doi.org/10.1016/j.lwt.2021.111621

Xu, Y., Wu, Y. ji, Sun, P. long, Zhang, F. ming, Linhardt, R. J., & Zhang, A. qiang. (2019). Chemically modified polysaccharides: Synthesis, characterization, structure activity relationships of action. *International Journal of Biological Macromolecules*, *132*, 970–977. https://doi.org/10.1016/j.ijbiomac.2019.03.213

Yan, D., Li, Y., Liu, Y., Li, N., Zhang, X., & Yan, C. (2021). Antimicrobial properties of chitosan and chitosan derivatives in the treatment of enteric infections. *Molecules*, *26*(23). https://doi.org/10.3390/molecules26237136

Zhang, T., Wang, W., Zhao, Y., Bai, H., Wen, T., Kang, S., Song, G., Song, S., & Komarneni, S. (2021). Removal of heavy metals and dyes by clay-based adsorbents: From natural clays to 1D and 2D nano-composites. *Chemical Engineering Journal*, *420*(P2), 127574. https://doi.org/10.1016/j.cej.2020.127574

Zhao, J., Xing, T., Li, Q., Chen, Y., Yao, W., Jin, S., & Chen, S. (2020). Preparation of chitosan and carboxymethylcellulose-based polyelectrolyte complex hydrogel via SD-A-SGT method and its adsorption of anionic and cationic dye. *Journal of Applied Polymer Science*, *137*(34), 48980. https://doi.org/10.1002/app.48980

Zhu, G., Wang, Y., Tan, X., Xu, X., Li, P., Tian, D., Jiang, Y., Xie, J., Xiao, H., Huang, X., Chen, Y., Su, Z., Qi, J., Jia, S., & Zhang, S. (2022). Synthesis of cellulose II-based spherical nanoparticle microcluster adsorbent for removal of toxic hexavalent chromium. *International Journal of Biological Macromolecules*, *221*(June), 224–237. https://doi.org/10.1016/j.ijbiomac.2022.09.016

CAPÍTULO 2

POLYELECTROLYTE COMPLEXES (PECS) OBTAINED FROM CHITOSAN AND CARBOXYMETHYLCELLULOSE: A PHYSICOCHEMICAL AND MICROSTRUCTURAL STUDY

Ferreira, D. C. M.; Ferreira, S. O.; Alvarenga, E. S.; Soares, N. F.; Coimbra, J. S. R.; Oliveira, E. B. Polyelectrolyte complexes (PECs) obtained from chitosan and carboxymethylcellulose: A physicochemical and microstructural study. 2. Carbohydrate Polymer Technologies and Applications. 3. (2022). https://doi.org/10.1016/j.carpta.2022.100197

Highlights

- Chitosan forms macro and micro-PECs with carboxymethylcellulose;
- Interaction is due to a combination of electrostatic interactions and hydrogen bonds.
- Temperature of 25°C and mixing ratio of 1:2 favors macro-PECs
- Amorphous characteristics and thermal stability indicate can be suitable for encapsulating, controlled release of bioactives and adsorption.

Graphical abstract:

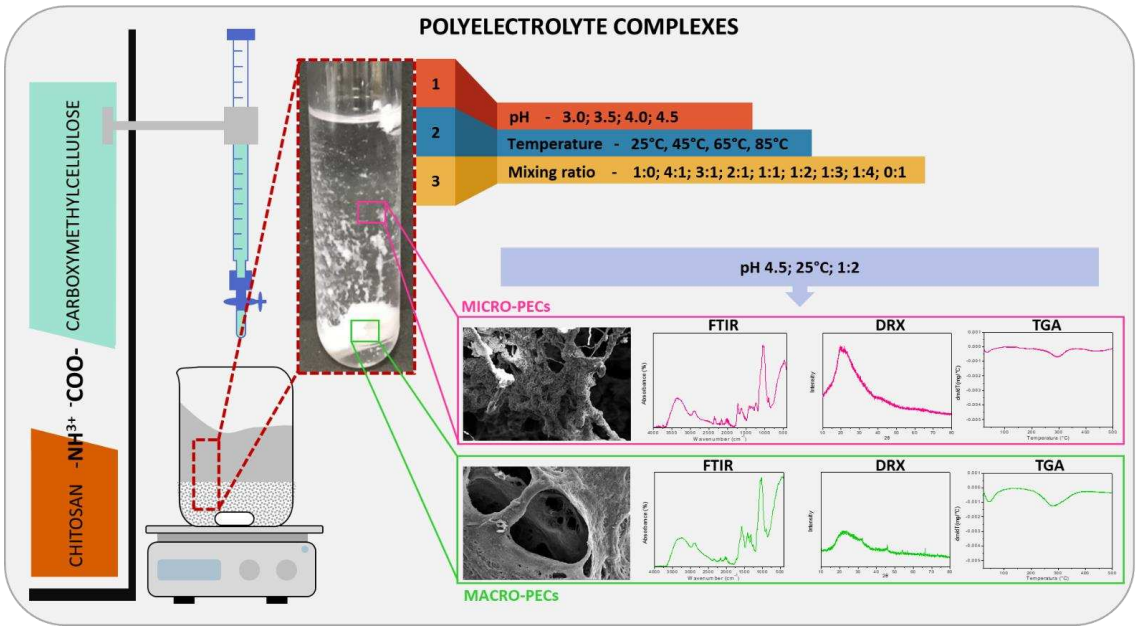

Carbohydrate Polymer Technologies and Applications 3 (2022) 100197

Contents lists available at ScienceDirect

Carbohydrate Polymer Technologies and Applications

journal homepage: www.sciencedirect.com/journal/carbohydrate-polymer-technologies-and-applications

Polyelectrolyte complexes (PECs) obtained from chitosan and carboxymethylcellulose: A physicochemical and microstructural study

Danielle Cristine Mota Ferreira [a], Sukarno Olavo Ferreira [b], Elson Santiago de Alvarenga [c], Nilda de Fátima Ferreira Soares [a], Jane Sélia dos Reis Coimbra [a], Eduardo Basílio de Oliveira [a,*]

[a] Equipe de Estudo de Materiais Alimentares (E^2MA), Departamento de Tecnologia de Alimentos (DTA), Universidade de Viçosa (UFV), CEP 36570-900, Viçosa, MG, Brazil
[b] Departamento de Física (DPF), Universidade Federal de Viçosa (UFV), CEP 36570-900, Viçosa, MG, Brazil
[c] Departamento de Química (DEQ), Universidade Federal de Viçosa (UFV), CEP 36570-900, Viçosa, MG, Brazil

ARTICLE INFO

Keywords:
CHS-CMC interaction
Macro-and Micro-PECs formation
Supramolecular structures
Food Hydrocolloids

ABSTRACT

Effects of chitosan (CHS) to carboxymethylcellulose (CMC) mixing ratio (1:0; 4:1; 3:1; 2:1; 1:1; 1:2; 1:3; 1:4; 0:1), temperature (25; 45; 65; 85 °C), and pH (3.0; 3.5; 4.0; 4,5) on obtaining of macro- and micro-polyelectrolyte complexes (PEC) were investigated. Mixing ratio 1:2 and 25 °C maximized the biopolymers' interactions and the formation of macro-PECs (macroscopic structures), independent of the pH. Both macro- and micro-PECs (dispersed microscopic structures) were studied by SEM, FT-IR, XRD and TGA. Micro-PECs had a more homogeneous appearance, whereas macro-PECs presented porous network structures interspersed with heterogeneous-sized vacuoles. Attractive electrostatic interactions and hydrogen bonds were involved in PECs formation. Macro-PECs were amorphous, which is desirable for encapsulating technologically relevant compounds. Finally, macro-PECs had low thermal degradation rates, and micro-PECs were thermally more stable than the forming biomolecules separately. Therefore, both macro- and micro-PECs formed by CHS and CMC appeared as green materials for different techno-functionalities, some of which are currently being studied by our team.

1. Introduction

Supramolecular structures resulting from the association of two or more different molecular species have drawn attention from academic and industrial researchers over the last two decades, especially due to their differentiated physicochemical characteristics and techno-functionality, which are generally superior to those of species alone. Such characteristics have stimulated the study of new associations of biopolymers and the mechanisms of their interactions for innovative applications (Zhang, Wang, Zhu & Zacharia, 2016.). Among the types of supramolecular structures, the polyelectrolyte complexes (PECs) stand out, resulting from the association between two highly charged polyelectrolytes (one positive and another negative) (Kulkarni et al., 2016; Meka et al., 2017). The formation of PECs, many times knowed like "self-assembly", is influenced both by the chemistry of the mixed cationic and anionic colloids, as well as by external conditions such as pH, ionic strength and temperature conditions (Hubbe, 2021; Y Zhang et al., 2015., 2018). Features such as high encapsulation efficiency, relatively lower processing cost, possibility of using food-grade coating materials, and room temperature synthesis make the polyelectrolytic complexation technique highly applicable in the food, agrochemical and related industries (Marciel, Chung, Brettmann & Lorraine, 2016; Shah & Leon, 2021).

PECs can be formed in different ways. Primary PECs are those formed immediately after mixing dispersions containing macromolecules with opposite charges. In primary complexation, very fine particles (micro-PECs) are quickly formed, increasing the turbidity in the reagent dispersion. If the complexation process is continued, the microparticles agglutinate so that larger particles, or intracomplexes, are formed. During this process, new electrostatic interactions can be formed and/or changes in polymer chains conformation can occur. When these intermediate complexes aggregate, intercomplexes are formed, and macroscopic structures obtained as compact precipitates (macro-PECs) (Meka et al., 2017). Among technologically relevant polysaccharides with potential to form strategic polyelectrolyte complexes, chitosan and some cellulose derivatives deserve attention.

Chitosan [poly-β(1→4)−2-amino-D-glucopyranose], whose amino group is a weak base in acidic aqueous media, is a non-branched, cationic polysaccharide, obtained by the deacetylation of chitin,

* Corresponding authors.
E-mail addresses: danielle.mota@ufv.br (D.C.M. Ferreira), eduardo.basilio@ufv.br (E.B. de Oliveira).

https://doi.org/10.1016/j.carpta.2022.100197

Available online 4 March 2022

List of symbols and abbreviations

AGU	Anhydroglucose unit
μ_e	Electrophoretic mobility
$(\overline{[\eta]})$	Average intrinsic viscosity
CHS	Chitosan
CMC	Carboxymethylcellulose
CrI	Crystallinity index
DA	Degree of acetylation
DD	Degree of deacetylation
d_h	Hydrodynamic diameter
DLS	Dynamic light scattering
FT-IR	Fourier-Transformed Infrared spectroscopy
NaCMC	Sodium Carboxymethylcellulose
PDI	Polydispersity index
PEC	Polyelectrolyte complex
SEM	Scanning electron microscopy
TGA	Thermogravimetric analysis
$\overline{M}_V$	Viscometric-avarage molar mass
XRD	X-ray diffractometry
ζ-potential	Zeta potential
τ	Turbidity

extracted from arthropods exoskeletons, extensively studied as a constituent of several technologically relevant complexes with natural or synthetic anionic polyelectrolytes (Ibrahim & Basma, 2017; Ibrahim, Nada & Eid, 2018; Islam, Bhuiyan & Islam, 2017), such as carboxymethylcellulose (Cerchiara et al., 2016a), dextran sulfate (Yucel Falco, Falkman, Risbo, Cárdenas & Medronho, 2017), hyaluronic acid (Valverde et al., 2019), collagen (M Li et al., 2019.), and xanthan gum (Aguiar, de, Silva, Rodas & Bertran, 2019).

Modified celluloses are another class of polysaccharides that stands out for their technological characteristics (Ibrahim et al., 2018). Chemically, natural cellulose [poly-β(1→4)-D-glucopyranose] is a non-branched homopolymer, electrically neutral, and also widespread in nature, since it is the major cell walls constituents of vegetal cells (Klemm, Heublein, Fink & Bohn, 2005). As cellulose is not water soluble, chemical modifications are usually made to introduce functional groups in its structure (by reaction with the cellulose hydroxyl groups), forming derivatives such as esters, ethers, and alcoholates. These derivatives are useful due to their greater microbiological stability, thermal and mechanical resistance, improved solubility, physical stability, and ion exchange efficiency (Klemm et al., 2005; Mischnick & Momcilovic, 2010). Carboxymethylcellulose (CMC) is one of the most commonly used cellulose ethers in the food, pharmaceutical and medical industry (Du et al., 2009; Duhoranimana et al., 2017). CMC is an anionic polyelectrolyte produced by introducing carboxymethyl groups into the cellulose molecule. It is sensitive to pH and ionic strength variation, being the only cellulose-derived polyelectrolyte with this characteristic (Arinaitwe & Pawlik, 2014). Industrially, CMC is obtained from the suspension reaction (slurry process) of cellulose, sodium hydroxide and monochloroacetic acid. CMC is commonly used as its sodium salt (CMC—Na) which, once dissolved in water, presents the typical characteristics of polyelectrolytes. Its properties and applications essentially depend on the viscosity of its aqueous solutions, the degree of substitution (DS) and the distribution of the carboxymethyl groups (da Silva et al., 2018).

The first report on the formation of complex polyelectrolytes is from Fukuda and Kikuchi (1979). In their first work, a short communication, the authors reported how a new chemical reaction of dilute aqueous solutions of sodium carboxymethylcellulose and chitosan led to a water-insoluble precipitate. The authors reported that the yield of the precipitate formed was influenced by pH, the ratio between biopolymers and the order of mixing, and that this precipitate was insoluble, even when subjected to high temperatures, in most organic products. In the following work (Fukuda, 1980), IR spectroscopic studies, elementary analyses, color reaction with toluidine blue, solubility assessment, and blood clotting tests *in vitro* were performed to better elucidate the formation of macro-PEC. More recent studies on the application of chitosan-carboxymethylcellulose complexes may be found in scientific databases. Cerchiara et al. (2016) prepared polyelectrolyte complexes based on chitosan and carboxymethylcellulose for colon delivery of vancomycin. The authors studied three different CHS/CMC weight ratios (3:1, 1:1 and 1:3) and prepared the microparticles by spray drying. Microparticles with a 1:3 ratio showed the best yield, encapsulation efficiency and drug loading. At pH 7.4, the release of vancomycin was prolonged, increasing the permanence of the drug in the colon. Roy, Ferri, Giraud, Jinping and Salaün (2018) prepared microcapsules from a CHS-based oil-in-water single emulsion, followed by the addition of a NaCMC dispersion. The microcapsules formed were added to glutaraldehyde, which, in addition to act as a crosslinking agent, hardened the wall and increased the encapsulation efficiency and yield. The optimal process conditions were identified in aqueous solution pH (5.5) and CH/NaCMC mass ratio (1:1). These studies remained restricted to only the final encapsulation products, without exploring the interactions underlying the biopolymer complexation or probing an understanding of formation of the macro- and micro-PECs. Furthermore, these few studies explored strategies and experimental protocols to select the best operational conditions, often based on purely empirical choices. A deeper physicochemical and microstructural knowledge of such PECs would be of pivotal importance, as this is intimately linked to the stability and technological properties of these composite systems. This is a challenging task, facing highly complex systems, but with a great potential of yielding discoveries that concern real applications across multiple segments in life sciences, *e.g.*, design of drug delivery systems (Xue et al., 2021) and tissue engineering (Mallick, Singh, Rastogi & Srivastava, 2018).

Therefore, this work aimed to investigate the influence of pH, temperature, and mixing ratio on the PECs formed between chitosan and carboxymethylcellulose, searching how the combinations of the factors lead to the formation of macro- and/or micro-PECs. Firstly, visual and Tyndall effect analyses were applied to identify the complex formation. Next, turbidity and ζ potential measurements were used to classify the system according to the inferred attractive interaction between the biopolymers in forming complexes. Dynamic light scattering (DLS), Fourier transform infrared spectroscopy (FT-IR) and X-ray diffraction (XRD) were used to assess the microstructure and the nature of the interactions between CHS and CMC. SEM was used to assess macro- and micro-PECs morphology. Their thermal stability was investigated based on TGA measurements.

2. Material and methods

2.1. Materials

Chitosan (low molecular weight, Sigma-Aldrich Corporation, USA; Product ID = 448,877) from fresh shrimp shells of *Pandalus boralis* and carboxymethylcellulose (Sigma-Aldrich Corporation, USA; Product ID = 419,311) were bought from Sigma-Aldrich Corporation (USA). Other analytical-grade chemicals were used without any purification: hydrochloric acid (Sigma-Aldrich, Brazil, 37 wt.% in H_2O) and sodium hydroxide (Sigma-Aldrich, Brazil. Deionized water was obtained from a Milli-Q system (18.2 MΩ·cm^{-1}, 25 °C; Reference *A*+, Millipore, Italy) was used in all experiments.

2.2. Polysaccharides preliminary characterization

2.2.1. Chitosan (CHS)

Before use, chitosan was washed three times with deionized water, to

reduce the water-soluble chitooligosaccharides content and salts residues. Washed chitosan was recovered using a vacuum filtration system, with qualitative paper (Cat No 1004 125, Whatman) (Leite Milião et al., 2022; Soares et al., 2019). Then, the remaining solid chitosan was frozen, lyophilized (Terroni, LS 3000, Brazil), and stored at 7 ± 2 °C (Consul, Pratice 410, Brazil).

Chitosan powder was analyzed using an FT-IR spectrophotometer (600-IR, Varian, USA) equipped with an attenuated reflectance accessory (GladiATR, PIKE Technologies, USA). Next, the degree of acetylation (DA) was estimated from the empirical relationship between normalized absorbances of the peaks at wavenumbers 1320 and 1420 cm^{-1} (Brugnerotto et al., 2001; Kasaai, 2008). The degree of deacetylation (DD) was obtained by simple difference [DD(%) = 100% – DA (%)]. The DD value of the chitosan used in the present study was estimated as 76.7% (for details, see Supplementary Material; Figure SM1).

Chitosan was dispersed in acetate buffer solution (0.2 M acetic acid + 0.1 M sodium acetate; pH 4.41; ionic strength 0.1 M) at varying concentrations [0.0, 0.05, 0.10, 0.15, 0.20, and 0.25 g•(100 mL^{-1})], and flow times for each of the resulting dispersions were measured in a Cannon-Fenske viscometer (model 513 20, Schott, Germany). Acetate buffer solution was used to ensure the dispersion of all chitosan present in aqueous media. Then, the average intrinsic viscosity ($[\overline{\eta}]$) was calculated as described in detail elsewhere (Amorim et al., 2016; Soares et al., 2019). From these experimental data, the viscometric-average molar mass ($\overline{M}_V$) was estimated to be 364 ± 10 kDa (for details, see Supplementary Material; Figure SM2).

2.2.2. Carboxymethylcellulose (CMC)

For the CMC degree of substitution (DS), the average number of hydroxyl groups substituted with carboxymethyl groups per anhydroglucose unit (AGU) was calculated. One gram of dry CMC—Na was dispersed in 500 mL of distilled water and stirred until a clear dispersion was obtained. For a reliable quantitative DS determination, all the carboxyl groups must be converted into their protonated form before the titration is started. Hence, the dispersion of CMC—Na was acidified to pH 3.2 by adding a solution of HCl 0.01 M. Then, a conductimetric titration with NaOH 0.025 M was performed at 25 °C. During the analysis the dispersion conductivity was continuously measured. A typical plot reporting the change in conductivity registered during the conductimetric titration is shown in the Supplementary Material; Figure SM4. From the plateau length, the amount of carboxylic groups per gram of CMC—Na, and thus the biopolymer DS, have been calculated (Capitani, Porro & Segre, 2000). The DS measured following this protocol was 0.59 ± 0.03.

For the $\overline{M}_V$ assessment, CMC dispersions at different concentrations [0.0; 0.05, 0.1, 0.15, 0.2, and 0.25 g•(100 g•L^{-1})] were prepared in sodium chloride 0.1 M, and the subsequent procedure was the same applied when characterizing chitosan (Section 2.2.1). From these experimental data, the viscometric-average molar mass ($\overline{M}_V$) was estimated to be 794 ± 8 kDa (for details, see Supplementary Material; Figure SM3).

2.3. Preparation of CHS and CMC acidic dispersions

First, a hydrochloric acid solution (1.0 mM; pH 3.0) was prepared. Then, chitosan (0.1 g•100 mL^{-1}) was added to this solution in order to obtain a chitosan stock dispersion (CSD). The resulting system was stirred for12 h using a magnetic stirrer (MA-039, Marconi, Brazil) at 25.0 ± 2 °C. After this, the pH was measured, checked, and readjusted to the targeted values (3.0, 3.5, 4.0, and 4.5; details are given in Section 2.4). An identical procedure was performed for the preparation of CMC dispersions. All eight dispersions were placed in closed flasks and stored in a refrigerator (Consul, PRATICE 410, Brazil) at 7 °C, until use in the subsequent experiments.

2.4. CHS/CMC polyelectrolyte complex obtaining

Complex formation between the CHS and CMC (CHS/CMC) was studied at different pHs (3.0, 3.5, 4.0 or 4.5), temperatures (25, 45, 65 or 85 °C), and mixing ratio of 4:1 (CHS4-CMC), 3:1 (CHS3-CMC), 2:1 (CHS2-CMC), 1:1 (CHS-CMC), 1:2 (CHS-CMC2), 1:3 (CHS-CMC3) and 1:4 (CHS-CMC4), in a factorial design, totaling 144 experimental conditions, including control treatments (CHS-0 and CMC-0). For the temperature of 25 °C, appropriate volumes of CMC dispersions were added drop-wise with adapted burette-magnetic stirrer into the previously prepared CHS dispersion. The mixtures were stirred for 10 min. For the other mixtures, appropriate volumes of CHS and CMC dispersions were blended, stirred for 10 min, and immersed in a thermostatic bath (Schott, CT 53, Germany) at 45, 65 or 85 °C for 2 h. After this processes, all 144 experimental systems were investigated using visual analysis, Tyndall scattering effect analysis. Systems classified as cloudy dispersion with macro-PECs were analyzed for turbidity. Those with higher incidences of turbidity and, consequently, higher amounts of micro-PECs, were analyzed for size (DLS) and FT-IR.

2.5. Experimental verification of chitosan CHS/CMC polyelectrolyte complex formation

2.5.1. Visual and Tyndall effect analyses

The formation of micro and macro-PECS obtained from CHS/CMC was preliminarily investigated using visual analysis and Tyndall scattering effect analysis, respectively. In this last one, the aqueous dispersion was illuminated with a laser beam (λ = 650 nm ± 10) (Laser & Led Light, China). Samples were evaluated and classified by visual observations as: (i) clear dispersion - no light scattering, (ii) clear dispersion with macro-PECs - little or no light scattering or (iii) cloudy dispersion with macro-PECs - with an intense scattering of light. These observations allowed the construction of a state diagram of the mixtures as a function of CHS/CMC mass mixing ratio, pH and temperature was constructed. Only the cloudy dispersions with macro-PECs were taken for turbidity measurements.

2.5.2. Macro-PECs yield assessment

For yield calculation, the dispersions obtained as described in Section 2.4 were centrifuged at 3000 g for 15 min (5430, Eppendorf, Germany). The micro and macro-PECs were collected and lyophilized (Terroni, LS 3000, Brazil) for subsequent characterizations. The freeze-dried macro-PECs were weighed (AUY220, Shimadzu, Japan) and the macro-PECs yield was then calculated using the Eq. (1):

$$CY_{CM}\ (\%) = \frac{m_i}{m_0} \tag{1}$$

in which, CY_{CM} is the macro-PEC yield, m_0 is the total biopolymer mass in the dispersion mixtures and m_i is the mass of the freeze-dried macro-PEC phase.

2.5.3. Turbidimetry

The cloudy dispersions cited in Section 2.5.1 were immediately poured into quartz cuvettes and the turbidity at 600 nm was rapidly measured in a spectrophotometer (Varian, Cary 50 Probe, EUA) (Weinbreck et al., 2003. Yang et al. 2012, You et al., 2018). Turbidity was defined as seen in Eq. (2):

$$\tau = \left(\frac{1}{L}\right) ln\left(\frac{I_o}{I}\right) \tag{2}$$

where L is the optical path length (1 cm), I is the intensity of light transmitted through the dispersion in the cuvette, and I_0 is the incident light intensity.

2.5.4. ζ-potential

The ζ-potential was estimated against pH and mixing ratio change of individual biopolymer dispersions CHS, CMC and their mixture formulations. For this analysis, samples of 1 mL of the dispersions and mixtures were placed in a cuvette placed within the equipment and exposed to a constant electric field, at 25.0 ± 0.1 °C (Zsizer Nano-ZS, Malvern Instruments, United Kingdom). The speed and the direction of the particle movement due to the electric field allowed the calculation of the electrophoretic mobility (Eq. (3)). Then, the Smoluchowski model (Eq. (4)) for the double electrical layer was considered to calculate the ζ potential values.

$$\mu_e = \frac{v}{\left|\vec{E}\right|} \tag{3}$$

$$\zeta = \frac{\eta \mu_e}{\varepsilon_0 \varepsilon_r} \tag{4}$$

In Eqs. (3) and (4), μ_e is the electrophoretic mobility, v is the speed of particles, $\vec{E}$ is the electric field, ε_r is the dielectric constant of the medium, ε_0 is the permittivity of free space, ζ is the zeta potential and η is the viscosity of the medium.

2.5.5. Particle size distribution

The hydrodynamic average diameter (d_h) and particle distribution index (PDI) were evaluated by dynamic light scattering (DLS) (Zsizer Nano-ZS, Malvern Instruments, United Kingdom). For this analysis, colloidal dispersions were diluted (1:10) with a single channel micropipette (K1–1000B, Kasvi, Brazil), using as diluent the same acid solution employed to prepare each original dispersions. Then, each system to be analyzed was placed in a cuvette and analyses were all carried out at 25.0 ± 0.1 °C.

Hydrodynamic diameter distributions were obtained by means of the amplitude of the decay rate A(Γ), obtained by fitting the normalized temporal intensity correlation functions, $g^{(2)}(t)$, through a NNLS (Non-Negative Least Square) algorithm, according to Eq. (5) Galván et al., 2018). Then, Γ distribution was turned to d_h using sequentially Eqs. (6) and ((7):

$$g^{(2)}(t) = 1 + \beta\left[\int_0^\infty A(\Gamma)\mathrm{e}^{-\Gamma t}\mathrm{d}t\right]^2 \tag{5}$$

$$\Gamma = \left(\frac{4\pi n_i}{\lambda}\sin\frac{\theta}{2}\right)^2 \cdot D \tag{6}$$

$$D = \frac{k_B T}{3\pi\eta d_h} \tag{7}$$

In Eqs. (5)–(7), A and β are constants that depends on the number of coherence areas in the detector, Γ is the decay rate, n_i is the index of refraction of the dispersion, λ is the wavelength of the laser, θ is the angle of detection, D is the mass diffusivity of the dispersed particles, k_B is the Boltzmann constant, T is the absolute temperature, η is the viscosity of the medium, and d_h is the average hydrodynamic diameter of dispersed particles. Polydispersity index (PDI) was calculated for each size distribution estimated according to Eq. (8) (Soares et al., 2019):

$$PDI = \left(\frac{SD}{d_h}\right)^2 \tag{8}$$

In Eq. (8), SD is the standard deviation corresponding to each d_h value.

2.6. Physicochemical characterization of CHS/CMC polyeletrolyte complexes

For the following analyses, the colloidal dispersions obtained as described in Section 2.4 were centrifuged at 3000 *g* for 15 min (5430, Eppendorf, Germany), and the aqueous phase containing micro-PECs was collected and stored. Macro-PECs remaining within the centrifuge tubes slid easily to Petri plates, without any detectable mechanical deformation, and then lyophilized (Terroni, LS 3000, Brazil). After that, the dried material was stored for further characterization.

2.6.1. Fourier-transformed infrared (FT-IR) spectroscopy analyses

FT-IR spectroscopy was used to examine the molecular interactions between CHS and CMC in the macro and micro-PECs, such as electrostatic interactions and hydrogen bonding. CHS, CMC and their freeze-dried mixtures (macro and micro-PECs) were carried out using a spectrophotometer (660-IR, Varian, USA) equipped with an attenuated reflectance accessory (GladiATR, PIKE Technologies, USA) over the region of 400–4000 cm^{-1}, with 16 scans and 4 cm^{-1} of spectral resolution. This analysis was conducted to observe changes of the functional groups before and after interactions between polymer matrixes as an indication of complex formation.

2.6.2. X-ray diffractometry (XRD) analyses

The XRD patterns of CHS, CMC and their freeze-dried mixtures (macro and micro-PECs) were determined by an X-ray diffractometer (D8 Advance, Bruker, Karlsruhe, Germany) equipped with Cu-Kα radiation (λ = 0.1542 nm) at 40 kV and 40 mA. The scan data were recorded from angles from 10° to 80° at a scanning rate of 0.1 degree per second. XRD was used to analyze the degree of crystallinity and examine the presence of amorphous characteristics. The diffractograms obtained were compared under the proposed experimental conditions and the observed differences were used as an indication of complex formation. The crystallinity index (CrI) for chitosan was obtained as proposed by Osorio-Madrazo et al. (2010)) as seen in Eq. (9):

$$CrI = A_C - A_t \tag{9}$$

In Eq. (9), A_C is the crystalline contribution area and A_t is the total diffractogram area.

2.6.3. Thermal gravimetric analyses

Thermal gravimetric analysis was performed using a thermal gravimetric analyzer (SHIMADZU, model 60H, Japan). Freeze-dried samples (macro- and micro-PECs) (3–5 mg) were weighed in the TGA microbalance and heated at 20 °C/min from 25 to 500 °C. Nitrogen gas was used as heating medium with a 20 mL/min flow rate. CHS, CMC and complexes powders were analyzed for their thermal behavior.

2.6.4. Microstructure - Scanning electron microscopy (SEM) analyses

Scanning electron microscopy (SEM) was used to obtain the morphology of macro- and micro-PECs. Samples were fixed in a sample holder, covered with gold (15 nm thick) (Quorum, Q150RS, United Kingdom) (Freitas-Silva, Diniz & da Silva, 2021), and analyzed using a LEO 1430VP scanning electron microscope (Carl Zeiss, United Kingdom) at 15 kV.

2.7. Data analyses

Minitab® 19.1 software was used to develop the experimental plan based on a multilevel factorial experiment. Visual, Tyndall Effect and FT-IR and X-ray diffraction analyses were evaluated qualitatively. Variance (ANOVA) followed by Tukey's test at a significance level of 5% was used to compare the influence of pH and temperature variables on the turbidity of the systems.

3. Results and discussion

3.1. Visual and Tyndall effect analyses results

The appearance of the dispersions of CHS and CMC was checked just

before and after they were used for preparation of mixtures. The effects of pH, temperature and mixing ratio CHS/CMC on the phase behavior of CHS-CMC mixed dispersions are depicted in Fig. 1.

From these results, it is clear that the analyzed parameters were critical in the complexation process, as also reported by other authors (Carvalho et al., 2021; H Zhang et al., 2016.). Pure CHS and CMC (CHS-0 and 0-CMC) dispersions presented clear dispersions at all pH and temperatures. The interaction between CHS and CMC is fast, triggering the formation of macro and micro-PECs upon mixing at all pHs and temperatures. According to Webster et al. (1997), there are three different types of PECs: (1) water-soluble complexes formed by macroscopically homogeneous systems containing smaller PEC aggregates; (2) cloudy colloidal systems with suspended PEC particles and (3) biphasic systems of supernatant liquid and precipitated complexes. Based on this classification, the systems resulting from the CHS and CMC mixtures were evaluated by visual observation and grouped in a phase diagram

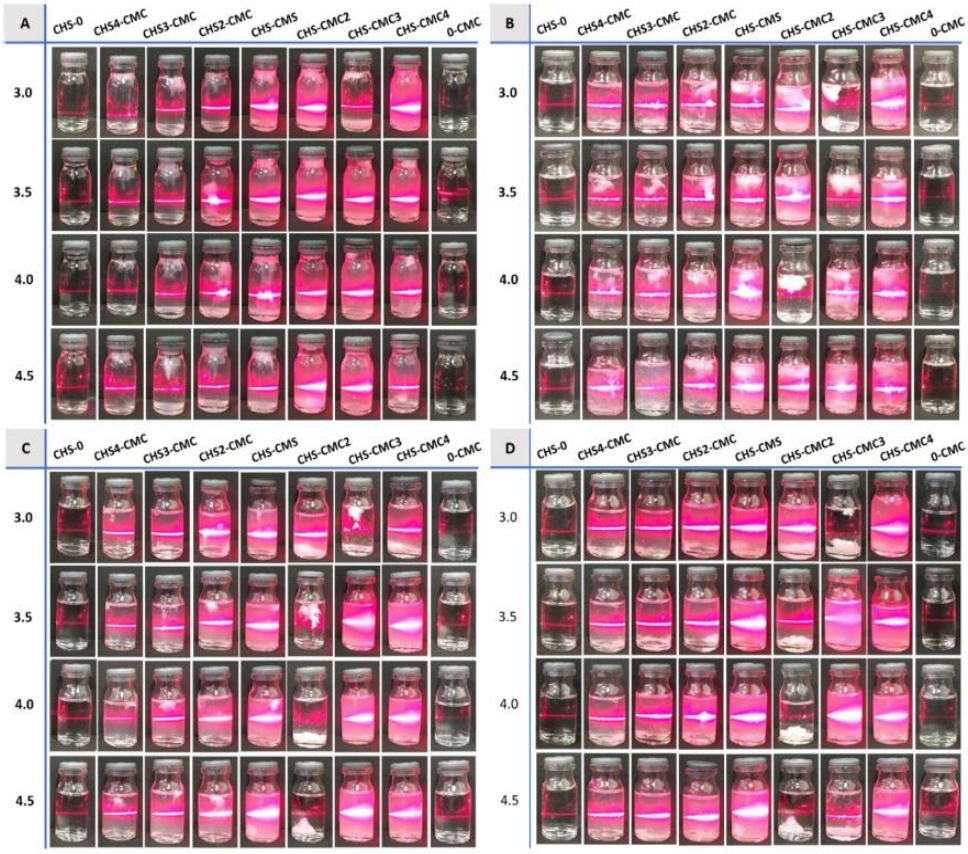

E	pH	CHS-0	CHS4-CMC	CHS3-CMC	CHS2-CMC	CHS-CMC	CHS-CMC2	CHS-CMC3	CHS-CMC4	0-CMC
25°C	3.0	□	◉	◉	◉	◉	◉	■	◉	□
	3.5	□	◉	◉	◉	◉	◉	◉	◉	□
	4.0	□	◉	◉	◉	◉	◉	◉	◉	□
	4.5	□	◉	◉	◉	◉	◉	◉	◉	□
45°C	3.0	□	◉	◉	◉	◉	◉	■	◉	□
	3.5	□	◉	◉	◉	◉	◉	■	◉	□
	4.0	□	◉	◉	◉	◉	■	◉	◉	□
	4.5	□	◉	◉	◉	◉	◉	◉	◉	□
65°C	3.0	□	◉	◉	◉	◉	◉	■	◉	□
	3.5	□	◉	◉	◉	◉	■	◉	◉	□
	4.0	□	◉	◉	◉	◉	■	◉	◉	□
	4.5	□	◉	◉	◉	◉	■	◉	◉	□
85°C	3.0	□	◉	◉	◉	◉	◉	■	◉	□
	3.5	□	◉	◉	◉	◉	■	◉	◉	□
	4.0	□	◉	◉	◉	◉	■	◉	◉	□
	4.5	□	◉	◉	◉	◉	■	■	◉	□

Fig. 1. – Appearance and Tyndall effect of CHS, CMC and their mixtures in different ratios and pHs at (A) 25 °C, (B) 45 °C, (C) 65 °C and (D) 85 °C. (E) is a state diagram summarizing schematically what is seen in (A)-(D): □: clear dispersion, ◉: macro-PECs and cloudy colloidal dispersion and ■: macro-PECs and

(Fig. 1E).

Thermodynamically favorable interactions between macromolecules in dispersion lead to a decrease in the Gibbs free energy of the whole system. The decrease in Gibbs free energy and the consequent formation of PECs come from the balance between enthalpic and entropic contributions; this last reflects the release of water and counter-ions as well as the changes in mobility and flexibility of biopolymers chains. It should be considered that in the spontaneous complexation observed between CHS and CMC, there is a competition between attractive electrostatic forces (which tend to bring oppositely charged macromolecules close to each other) and entropy effects (which tend to keep them in a more dispersed configuration within the system). Theoretically, charged polyelectrolytes would aggregate primarily due to electrostatic interactions to form electrically neutral (or close to neutral), lower-entropy micro-PECs, but this would go against the Second Law of Thermodynamics. Thus, one may claim that the formation of PECs should be enthalpically driven. Nonetheless, this simplified explanation (which was largely generalized until a few decades ago) is currently taken with caution (Fu & Schlenoff, 2016).

It is now well-known that the formation of PECs is also greatly favoured by the release of counterions and solvation water molecules interacting with each polyelectrolyte chain before the complexation. During complexation, in order to increase the system's configurational entropy, thereby decreasing the Gibbs free energy, these counterions and water molecules are released. Soon after, they are replaced by the oppositely charged polyelectrolyte's groups, making the complexation spontaneous (Rathee, Sidky, Sikora & Whitmer, 2018). These aspects will be further discussed in Section 3.3. On the other hand, one must keep in mind that characteristics of polymer chains, such as rigidity and hydrophobicity, can change mechanical and dynamic properties of PECs, and should be taken into account when calculating the thermodynamic equilibrium. In summary, each biopolymers duo would requires specific, quantitative thermodynamic investigations (commonly through nano- or microcalorimetry assays) to determine if their complexation is entropically- or enthalpically-driven.

Some CHS-CMC3 mixtures (pH 3.0 at 25 °C; pH 3.0 and 3.5 at 45 °C; pH 3.0 at 65 °C; pH 3.0 and 4.5 at 85 °C) showed, in addition to the macro-PECs, the formation of a clear dispersion, indicating, probably indicating the maximum intensity of interaction between the existing chitosan and CMC structural charges. The same behavior was observed for some CHS-CMC2 systems (pH 4.0 at 45 °C; pH 3.5, 4.0 and 4.5 at 65 °C and 85 °C). Overall, dispersions with higher concentrations of CMC, i.e., CHS-CMC2 and CHS-CMC3, had a greater tendency to form less cloudy dispersions, evidencing the lesser formation of micro-PECs and greater formation of macroscopic complexes, a fact confirmed by the tubidimetry analysis (presented and discussed in Section 3.2). This result strongly suggests that, for the other CHS-CMC ratios, CHS probably has a larger average linear charge density compared to CMC.

When complexation is carried out in nonstoichiometric mixing ratios and under dilute conditions, the reaction mixture develops a scattering effect when interacting with visible light, known as Tyndall effect. This behavior can be ascribed to the micro-PECs, which is believed to consist of a neutral core surrounded by the polyelectrolyte in excess, which acts as a stabilizer and prevents the PECs from aggregating (Kabanov & Zezin, 1984). This phenomenon, shown in Figs. 1 (A, B, C and D), was more evident in systems with higher proportions of CMC than CHS (*i.e.*, CHS-CMC4, CHS-CMC3, CHS-CMC2) and at room temperature, corroborating inferences from visual analysis and state diagrams.

3.2. Turbidity and macro-PECs yield results

Turbidity measurement is a simple and direct indicator for polyelectrolyte complex formation, as this phenomenon is accompanied by drastic changes of the system's turbidity Fig. 2. shows the changes in turbidity and macro-PECs yield of CHS-CMC mixtures at different pHs, temperatures and CHS-CMC ratios. The turbidity of the mixtures was much higher than pure either CHS or CMC dispersions, indicating that CHS and CMC formed colloidal PECs. This is in line with Fukuda and

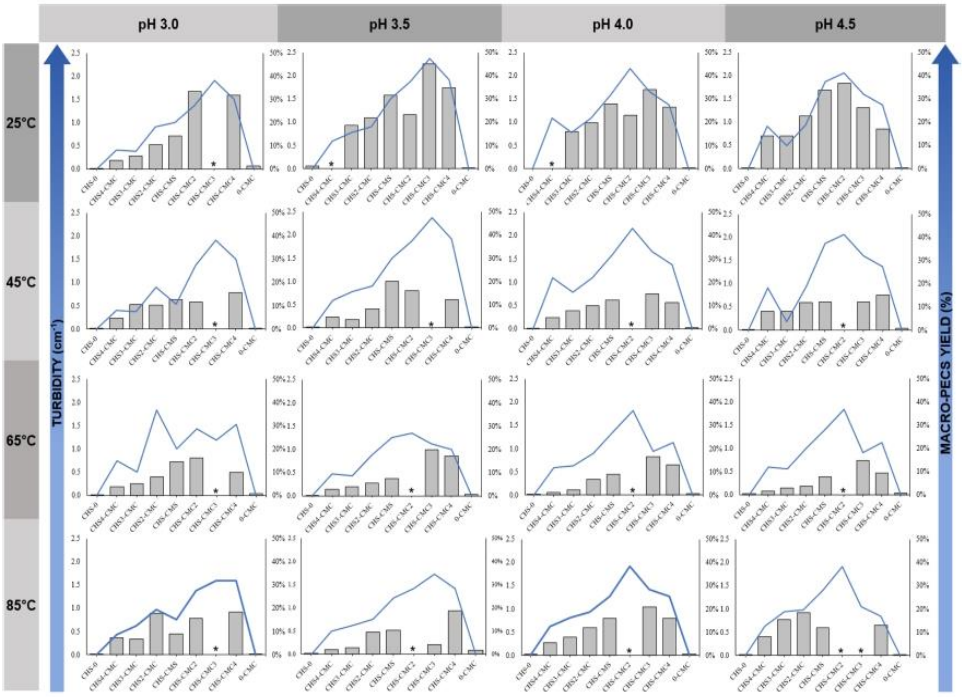

Fig. 2. - Turbidity (left vertical axis) and macro-PECs yield (right vertical axis) of CHS-CMC mixed dispersions, at different biopolymers rations, as a function of pH and temperature (▬ macro-PECs yield, ▬ turbidity). *Systems with no formation of turbid dispersion during eye inspection were not analyzed for turbidity..

Kikuchi (1979), who studied interactions between CHS and CMC at pH 2.5 and 5.0, and showed that at pH < 2.0, there was no formation of precipitates after mixing CHS and CMC dispersions, and that at pH > 5.3, precipitate/gels were generated.

In terms of composition, turbidity was lower in systems containing less CHS than CMC, whatever the pHs and temperatures. At a given CHS-CMC ratio, turbidity was lower at higher temperatures, meaning that colloidal particles formation was more favoured at 25 °C and 45 °C than at 65 °C and 85 °C, which suggests an exothermic process. These findings corroborate the visual analysis depicted in Fig. 1. On the other hand, no clear trend could be inferred from Fig. 2 concerning the effects of pH

In the CHS-0 absorption spectrum, bands at 1648 cm^{-1} were previously related to the the amide group of acetylated chitosan units. A band at 1580 cm^{-1} corresponds to the NH curvature of amine and amide II. (Kasaai, 2008; Soares et al., 2019). Other relevant peaks highlighted in the Fig. 6A are: 1418 cm^{-1}, attributed mainly to the -CH_2 bending; 1150 cm^{-1}, attributed to the antisymmetric stretch C—O-C and C—N stretch; 1024 cm^{-1}, attributed to the skeletal vibration of C—O stretching (Lawrie et al., 2007). Also, a strong peak attributable to the deprotonated –COO^- group was observed at 1589 cm^{-1} (Duhoranimana et al., 2017). The existence of a band at 1627 cm^{-1} confirms the presence of the –COO^- group. The bands around 1412 cm^{-1} and 1319 cm^{-1} correspond to the shear vibrations of –CH_2 and bending of –OH, respectively. The band at 1014 cm^{-1} is due to elongation of –CH—O-CH_2 (Wongvitvichot, Pithakratanayothin, Wongkasemjit & Chaisuwan, 2021).

To verify more quantitatively whether these observed trends were significant, interaction plots were built, considering the three independent variables and the effects of their interactions on the turbidity of the systems. The main effects plots (Fig. 3A) shows the adjusted means for each level of each categorical variable. As the lines are not horizontal, the main effects are present on all these variables. The factorial experiment analysis results confirmed that the main effects are all statistically significant, with those related to the pH factor being the least pronounced. However, as the interaction effects were statistically significant, these main effects graph can be misleading. The interaction plots (Fig. 3B) shows the adjusted mean turbidity value versus the pH, temperature and mixing ratio combinations. These results indicate apparent interaction effects because the lines are not parallel, implying that the relationship between the turbidity value and each factor depends on the definition of another factor. The factorial experiment analysis results indicated that the interaction effects for *Temperature*Mixing ratio, Mixing ratio*pH,* and *pH*Temperature* were statistically significant.

The Tukey test (Table SM1) applied to the general averages of turbidity comparing systems at different pH values indicated that systems at pH 3 have significantly lower average turbidity, suggesting a smaller formation of micro-PECs. At this pH, the chitosan amino groups (pK_a = 6.3–7.2) are predominantly protonated/charged (–NH_3^+), but more than 50% of the CMC carboxyl groups (pK_a = 3.5–3.65) (Dogsa et al., 2014; Xiong, Deng, Li, Li & Zhong, 2020) are protonated/uncharged (–COOH), so some repulsive forces between polysaccharides may exist. At pH 3.5, deprotonated, negatively charged carboxyl groups start to predominate over their protonated/uncharged counterparts, whereas the majority of the chitosan amino groups are still protonated

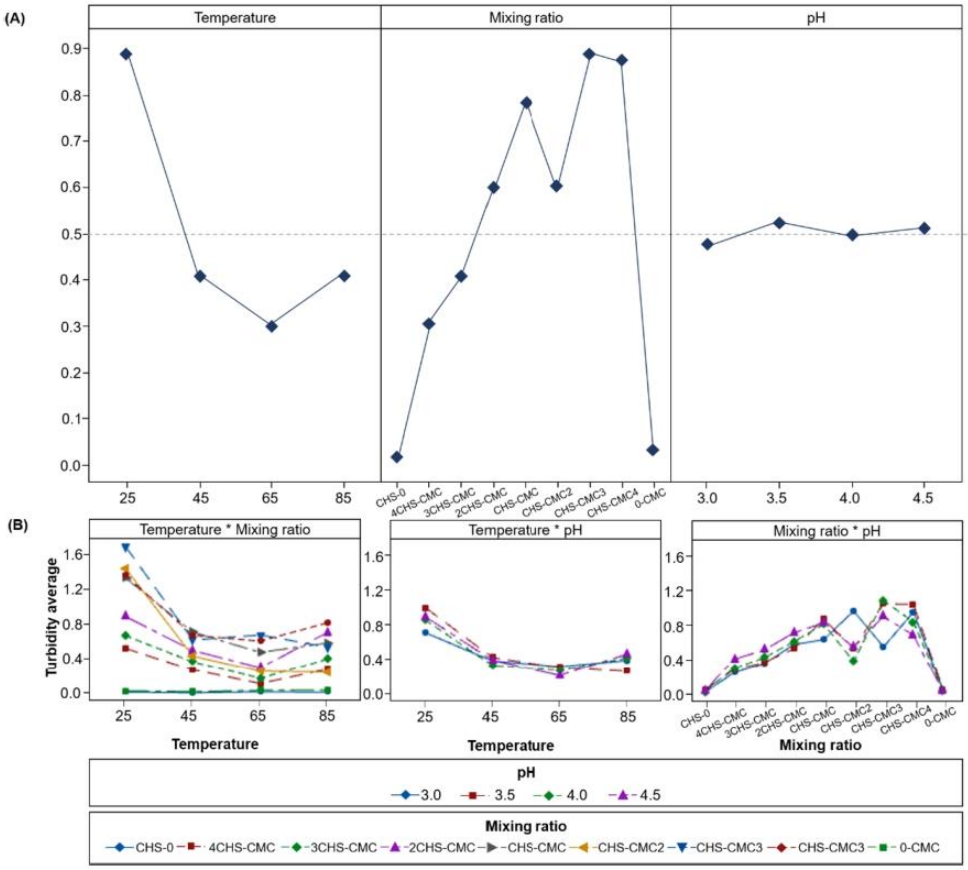

Fig. 3. – (A) Main effects and (B) interaction plots for turbidity.

and therefore positively charged. This also occurs at pH values of 4.0 and 4.5. Mixtures that presented a clear liquid phase and an evident macroscopic precipitate (and, therefore, did not have their turbidity evaluated) also presented a higher macro-PEC yield (Fig. 2), since the macroscopic separation of phases occurred when the endpoint of ionic complexation was reached. Thus, one can infer that the ratio corresponding to the maximum yield was found at the electrical equivalence point (EEP), at which the total net charge is practically zero. Indeed, the highest macro-PEC yields were observed for mixtures with a higher CMC mass ratio, in accordance with the visual and Tyndall effect results previously presented. Greater CMC mass ratios were associated with stronger heteropolymer interactions.

When the Tukey test was applied to compare systems at the temperatures studied (25, 45, 65 and 85 °C) (Table SM2), it indicated that the turbidity was higher in the systems at 25 °C. According to Vuillemin, Michaux, Muniglia, Linder and Jasniewski (2019), higher temperatures favor the compacting of the CHS structure, making the loads less available for interactions, and inducing less complex formation, which is consistent with the results of our present study. Besides, in general, at higher temperatures, a prevalence of hydrophobic interactions is more likely (Xiao, Wang, Xu & Huang, 2019a), which seems to contradict the hypothesis initially raised, according to which electrostatic interactions prevail in the complexation between CHS and CMC.

3.3. ζ potential of CHS/CMC polyeletrolyte complexes

As the results presented and discussed so far indicated that the increase in temperature does not positively affect the formation of micro and macro-PECs, only systems at room temperature were analyzed for the ζ potential.

In aqueous media, pH is a key factor affecting the ζ potential of supramolecular structures formed between polyelectrolyte, since the pH of the environing solvent influences the proportion of amino and carboxyl groups charged on biopolymers' chains. Moreover, the mixing ratio directly affects the electric charge balance between the polyelectrolytes and, consequently, the intensity of interaction and complexation (Xiao, Wang, Xu & Huang, 2019b). Results of ζ potentials of the CHS, CMC, and their mixtures as a function of medium pH are depicted in Fig. 4, along with the complex yield.

CHS-0 carried positive charges since the pK_a of amino groups is at pH 6.3–7.2, depending on its degree of acetylation (Q. Z Wang et al., 2006.). Its charge density declined with pH increase (ζ potential from +62.43 to +44.77 mV, at pH 3 and 4.5 respectively), similarly to what was reported by Vuillemin et al. (2019) for CHS 0.02% w/v in acetic acid. 0-CMC was negatively charged, since the pK_a of carboxyl groups is at pH 3.5–4.0) (Xiong et al., 2020)(Q. Z Wang et al., 2006.), and its charge densities (moduli) increased with pH increase (ζ potential from −6.65 to −39.97 mV, at pH 3 and 4.5 respectively). In other words, at higher pH values, the anionic character of CMC is enlarged due to dissociation of the carboxylic groups.

According to Fig. 4, the ζ potential values of the dispersed CHS (in CHS-0) were +62.43 mV, +56.33 mV, +23.70 mV and +44.77 mV, for pHs 3.0, 3.5, 4.0 and 4.5 respectively, whereas for dispersed CMC (in 0-CMC) the values were −6.65 mV, −7.10 mV, −20.57 and −39.97 mV for pHs 3.0, 3.5, 4.0 and 4.5. On the assumption that PECs formation would be favoured by the complete charge neutralization, their compositions of electrical equivalence point (EPP) can be denoted by $a\bullet[CHS] = b\bullet[CMC]$, where [CHS] and [CMC] are respectively the mean molar concentrations of chitosan (polycation) and carboxymethylcellulose (polyanion), a is the density of protonated of chitosan's amino groups, and b is the density of dissociated CMC carboxyl groups (density = average number of amino or carboxyl groups per biopolymer chain). If the active number of loading sites available for interaction was directly related to the mass concentration of biopolymers, the theoretical CMC to CHS mix ratio for complete charge neutralization should be 1:9.4, 1:7.9, 1:1.2 and 1:1.1 for pHs 3.0, 3.5, 4.0 and 4.5, respectively. These calculations were compatible only for mixtures at pH 4.0 and 4.5. The ζ potential values were positive until the ratio CHS-CMC2 in media with pH 3.0, 3.5 or 4.0,

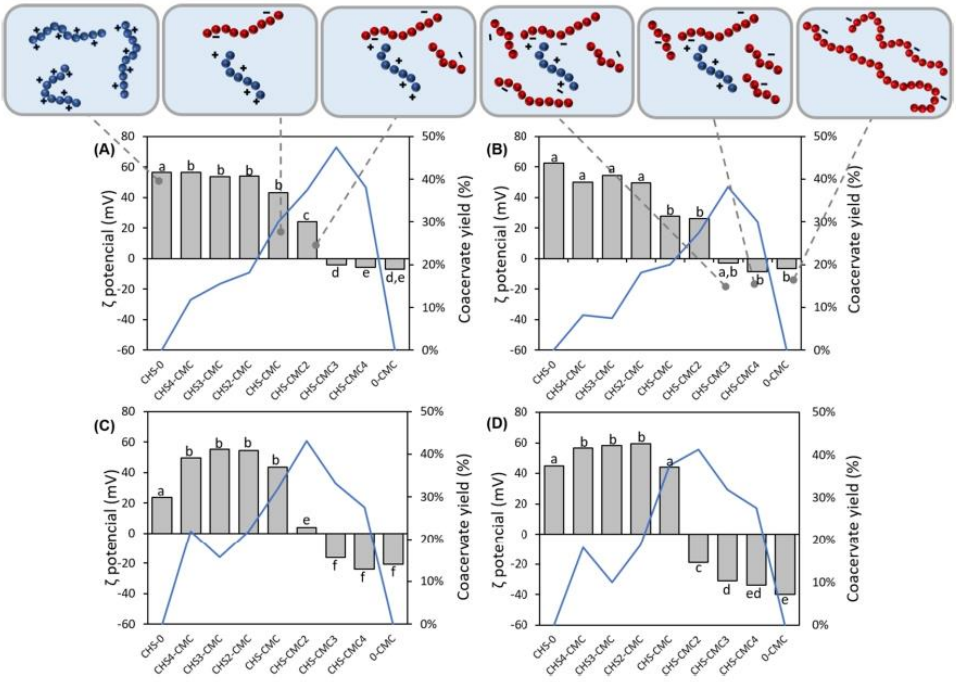

Fig. 4. - ζ potential and macro-PECs yield of CHS-CMC systems as a function of ratio at (a) pH 3.0, (b) pH3.5, (c) pH 4.0 and (d) pH 4.5.

indicating that CHS was in excess at these pH values, and this could be ascribed to its absolute charge density higher than that of CMC. When excessive CMC was added to CHS dispersion, for instance, CHS-CMC3 at pH 4.5, the ζ potential decreased to −12 mV because of excess CMC molecules, triggering electrostatic repulsions between similarly charged complexes and decreasing the turbidity (Fig. 2). It should be emphasized that, in addition to the total charge density, steric factors, local charge distribution on the polysaccharide chains, the positions of charged groups in the chains, and chain flexibility also affect the complexation stoichiometry (Picone & Cunha, 2013).

The secondary structure of polysaccharides is generally limited by the degree of rotational freedom of the glycosidic bond, specified by two dihedral angles, Φ and Ψ (Berglund et al., 2016). This rotational freedom is often limited by steric hindrances and, for charged polysaccharides such as CHS and CMC, also by electrostatic forces (Fu & Schlenoff, 2016). Keeping this in mind, it can be hypothesized that the assemblage of CHS and CMC chains during the formation of PECs can be considered as the net effect of three processes:

(i) entropic effects during the release of water and counter-ions bound on the biopolymer chains' surfaces;
(ii) an approaching of two oppositely charged biopolymer chains', forming a supramolecular PEC through cooperative effects, including conformational changes favorable for oppositely charged binding, in a somewhat ordered way;
(iii) additional assemblage of PECs mentioned in (ii), mainly due to the attraction between local clusters of either negative or positive charges in such supramolecular structures, but less orderly than in the first stages, due to progressive increase of steric hindrances, caused by voluminous groups and lateral chains (specially in CMC);

Our experimental results are in agreement with these hypotheses. In fact, at pH 4.5, the ζ potentials were positive until the CHS-CMC ratio was 1:1. At pH values of 3.0, 3.5 and 4.0, in addition to the 0-CMC control, the CHS-CMC3 and CHS-CMC4 mixtures showed negative ζ potentials. At pH 4.5, the mixtures CHS-CMC2, CHS-CMC3 and CHS-CMC4 showed negative ζ potentials, meaning that the CMC became excessive. Complete charge neutralization, *i.e.*, the electrical equivalence point (EPP) occurred in biopolymer ratios between 1:2 and 1:3 at pH 3.0, 3.5 and 4.0, and between 1:1 and 1:2 at pH 4.5. These results were also consistent with the turbidity and macro-PECs yield differences among the systems, even indicating that electrostatic interactions stabilized the complexes formed between CHS and CMC, and the most intensive interaction occurred at the point where the electrical charge of the complexes was close to the neutrality (zero). In addition, the CHS-CMC, CHS-CMC2, CHS-CMC3 and CHS-CMC4 systems were closer to electrical neutrality and significantly different from the others and, therefore, were further analyzed and compared in terms of dispersed particle size distributions.

3.4. Size distributions of CHS/CMC micro-polyeletrolyte complexes

The CHS:CMC ratio affected the particle size distribution (Fig. 5).

All studied mixtures showed a monomodal size distribution, with a peak under 2000 nm. The increase in the amount of CMC in the proportion of 1: 1 (CHS-CMC) to 1: 2 (CHS-CMC2) caused a decrease in the average diameter of the particles, corroborating the ζ potential results, as in this proportion, interactions between CHS positive charges and CMC negative charges were favored. Thus, the nonpredominance of repulsive interactions in such system resulted in the aggregation of polyelectrolytic complexes. The increase in the ratio from 1:2 (CHS-CMC2) to 1:3 (CHS-CMC3) caused an excess in the negative charges of the systems. In this last system, some of the CMC molecules interacted

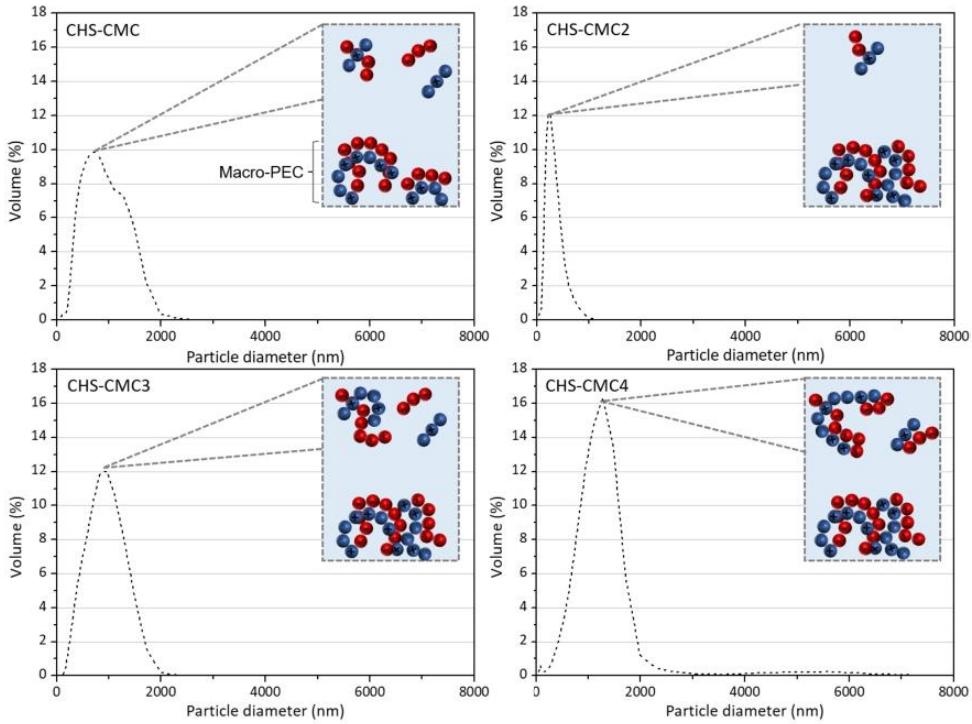

Fig. 5. - Intensity-weighted size distribution, average hydrodynamic diameter (d_h) and polydispersity index (PDI) of mixed samples at different CHS:CMC ratios. The illustrations show the inferred interactions between the polysaccharides.

with the CHS, precipitating and forming the macro-PECs. The other molecules with excess of negative charges acted in such a way as to prevail the repulsive interactions, thus increasing the average diameter of the micro-PECs. This observation is in accordance with the ζ potential results, for which the CHS-CMC2 system was closer zero. This result is also in line with the remaining previous results, since the system CHS-CMC2 showed a higher yield value for macro-PECs.

3.5. FT-IR spectroscopy features of CHS/CMC polyelectrolyte complexes

Intermolecular interactions between chitosan and carboxymethycellulose were also studied through FT-IR. Since the CHS-CMC, CHS-CMC2, CHS-CMC3 and CHS-CMC4 systems, at 25 °C, had a higher concentration of complexes, only the systems at room temperature were submitted to such analyses. The FT-IR spectra of CHS, CMC and physical mixture are shown in Fig. 6A. In general, the spectra profile was similar at all pH values, for the same mixtures, but a difference in the intensity of the observed bands was observed.

We intended to apply FT-IR to study CHS /CMC interactions, since a change in NH_3 vibration can be expected when groups $–NH_3^+$ interact electrostatically with the negatively charged locations of the CMC. The changes observed in the spectra obtained for the products of interactions between the two studied biopolymers, especially in the characteristic regions of the possible complexing sites of biopolymers, can be associated with the formation of links between them. However, because they have highly similar backbones, the FT-IR spectra of the prepared chitosan-carboxymethyl cellulose mixtures were very similar to those of the biopolymers separately, presenting bands degenerated by the overlapping of chemically similar groups. This caused broad and intense bands, despite the varying degree of interaction between the functional groups in the two polyelectrolytes. Then, the spectra of the mixtures of biopolymers, both from the macro-PECs phase and from the micro-PECs phase, showed the most characteristic peaks of CHS and CMC. As the concentration of the two biopolymers separately in the mixture is reduced (the total polysaccharide concentration remains constant), this may be the probable cause of the decrease in the intensity of intensity of the mixtures' spectra. In addition, the degree of mixing must be taken into account. If two components are mixed micro-homogeneously, then the absorbances of the individual components are approximately additive. If the sample is micro-heterogeneous, *i.e.*, there is demixing at the microscopic scale, then the intensities are additive, leading to dramatic flattening of the band (Mayerhöfer, 2004). According to our results, the dispersed phase showed a greater decline in absorbance amplitudes, suggesting the formation of more microstructured complexes. In the liquid phase, there was a shift in the absorbance band from 1266 cm^{-1} to 1235 cm^{-1}, in the 1589 cm^{-1} band (previously attributed to the $–COO^-$ group), and a change of shape of the band with a peak at 1739 cm^{-1}, suggesting a strong electrostatic interaction between the $–NH_3^+$ groups of chitosan and the $–COO^-$ groups of CMC, compatible with the complexation between these biopolymers. Finally, the spectra of the macro-PECs and micro-PECs formed showed a broad band at approximately 3000–3500 cm^{-1}, indicating enhanced hydrogen bonding compared to CHS and CMC separately. Such findings indicate that hydrogen bond interactions were also involved in the interaction between CHS and CMC.

3.6. X-Ray diffractometry features of CHS/CMC polyelectrolyte complexes

Fig. 6A illustrates the diffractograms of the CHS-CMC PECs (macro- and micro-) and their individual components.

Materials with crystalline and amorphous structures present, in the X-ray diffractogram, sharp and wide scattering peaks, respectively (Khoshakhlagh, Koocheki, Mohebbi & Allafchian, 2017). CHS exhibited

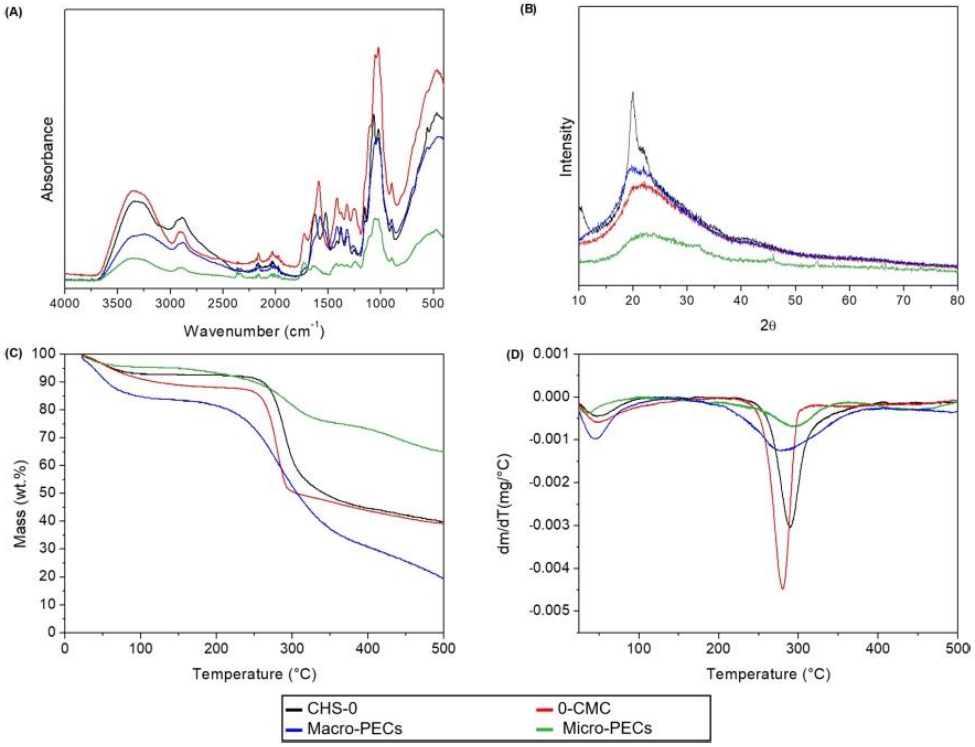

Fig. 6. – (A) FT-IR spectra, (B) X-ray diffraction patterns, (c) TG and (d) DTG thermograms of chitosan, carboxymethylcellulose, macro-PEC and micro-PECs.

two peaks, at 10.32° and 19.95°, and a shoulder at 21,66°, which correspond to the (110), (020) and (120) planes, respectively, showing the semicrystalline structure of the polymer, as already reported in the literature (Antonino et al., 2017; Jampafuang, Tongta & Waiprib, 2019; Phung Hai & Sugimoto, 2018). The degree of crystallinity of chitosan was 0,3558. This value also agrees with the degree of deacetylation of the chitosan employed in our experiments (DD = 76.7%). Indeed, even though the non-acetylated chitin is highly uniform and crystalline, the increase in DD causes the chitosan molecular chain to become more homogenized, increasing its crystallinity (Cheng et al., 2020).

For CMC, on the other hand, a broad diffused hump was observed centered at approximately $2\theta = 22{,}18°$, indicating that its structure was amorphous. These peaks disappeared upon the CHS-CMC complexation, and a new peak was generated at 21.86°. These variations indicated that the original structures of both CHS and CMC were not conserved when they formed supramolecular complexes, and a new structuration appeared through their interaction. After the complex formation between CHS and CMC, the crystalline regions observed in the pure polyelectrolytes were disrupted. The absence of new, well-defined diffraction signals is indicative of the non-formation of organized regions within the PEC structure. As demonstrated by Ramakrishnan, Adzahan, Yusof and Muhammad (2018), this characteristic is desirable when the complexes are destined to the encapsulation of both water-soluble and fat-soluble compounds. Materials in the crystalline state have highly organized molecular structure, difficulting to introduce other molecules within their arrangement. The opposite is true for materials in the amorphous state (Lim & Roos, 2018). Furthermore, amorphous structures, such as those presented by the carbohydrates in the present study, after removing water, can pass through the glass transition and enter the metastable rubber state, easening the controlled release of entrapped compounds through diffusion phenomena (Fernandes et al., 2017; Li, Roos & Miao, 2016).

3.7. Thermogravimetric features of CHS/CMC polyelectrolyte complexes

Thermogravimetric analysis (TGA) was performed for samples of chitosan, carboxymethylcellulose, for the macro-PECs formed in a 1:2 ratio obtained after centrifugation, and for the micro-PECs (Fig. 6C and 6D). All samples were degraded in two stages.

For CHS, an endothermic event occurred between 25 and 92 °C with a related mass loss of about 10%, attributed to water loss (See Supplementary Material; Figure SM5). The second event, observed between 257 and 321 °C (peak at 289 °C), promoted a higher rate of weight loss, corresponding to a total mass loss of 60.36%, and attributed to the depolymerization and decomposition of the acetyl and amine groups producing volatile compounds, also known as combustion products (CO, CO_2, and other low molecular weight derivatives). Similar thermal behavior was previously reported for CHS (Acosta-Ferreira et al., 2020; Corazzari et al., 2015). It is also possible to identify through the DTG curve a maximum thermal decomposition rate of 0.003 mg/ °C. The presence of mass at the end of the process indicates that CHS, as well as CMC and the studied complexes), contain a fraction of non-volatile components.

For CMC, the first event occurred between 27 and 122 °C, corresponding to the melting temperature, with a related mass loss of 11.85% due to the evaporation of free adsorbed and bound water in the cellulosic structure (Biswal & Singh, 2004). The second thermal event was observed between 255 and 300 °C (peak at 280 °C), corresponding to the decarboxylation of CMC—Na and pyrolysis of the cellulosic structure (Pettignano, Charlot & Fleury, 2019). At the end of the process, the CMC showed a total loss of 60.65% and a maximum thermal decomposition rate of 0.004 mg/ °C.

The thermograms for the macro and micro-PECs kept some similarities with those of the separate biopolymers, with two thermal events. For the macro-PECs, the first event was observed in the temperature range of 26–86 °C (peak at 44.8 °C), with 16% mass loss. As in the previous cases, the loss of mass at this stage may be related to the cleavage of some saccharide rings, the disintegration of macromolecular chains, and the volatilization of some degradation products (Xiao et al., 2019b). The second event was observed between 198 and 366 °C (peak at 283 °C) with a mass loss of 80.64%. The maximum thermal decomposition rate was 0.001 mg/ °C. For the micro-PECs, the first event was observed in the temperature range of 26–76.80 °C (peak at 33 °C), with 5.74% mass loss, and the second event was observed between 149 and 344 °C (peak at 295 °C), with 35.1% mass loss. The maximum thermal decomposition rate was 0.0006 mg/ °C.

Furthermore, it can be observed that at the end of the degradation study at 500 °C, the residual masses of 39.64%, 39.35%, 64.9% and 19.36% were left for chitosan, carboxymethylcellulose, micro-PECs and macro-PECs, respectively. The results, therefore, show that when compared to the macro-PECs, micro-PECs obtained from the CHS/CMC complexation showed greater thermal stability and less mass loss with time/temperature, which may be related to the structural changes indicated already discussed.

Presumably, the thermal stability of both macro- and micro-PEC systems depends on their network specificities. In particular, the total surface area in micro-PECs is much larger than that of macro-PECs. Therefore, in micro-PECs, biopolymer chains recovering them can be considered stabilizers for the those located in the core. These superficial chains absorb a great part of the thermal energy arriving and attenuate its diffusion through the core of the complexes. As a consequence, the core chains remain with low motility, and greater structural thermostability.

The freeze-dried macro-PECs showed greater weight loss than the biopolymers separately. This observation may be related to the attraction between the $-NH_3^+$ and $-COO^-$ groups. CHS in acidic solution has a semicrystalline structure, whose chains may adopt an extended double helix conformation, forming a structure of stacked sheets with accessible charges (R. Y Zhang, Zaslavski, Vasilyev, Boas & Zussman, 2018.). On the other hand, in aqueous media, CMC polymer chains tend to be in a stretched helical shape, and the –OH groups tend to come out of the helix, also being available for self-assembly (J Wang & Somasundaran, 2005.). When in their native state, macromolecules are in a lower energy conformation, requiring more energy for thermal decomposition (Xiao et al., 2019b). After complexation, the original conformation of CHS and CMC were modified, thus requiring less energy to decompose them. Even so, they showed a more moderate slope compared to the mass decreases of CHS and CMC, and moderate heat resistance, suggesting adequate thermal stability of the complexes for application in encapsulation, films and other practical uses.

3.8. Microstructural features of CHS/CMC polyeletrolyte complexes

As shown in Fig. 7, the SEM morphology of dispersed phases the CHS-CMC2 system at pH 4.5, after centrifugation, exhibited aggregate forms.

As verified by the size distribution analysis, CHS-CMC2 micro-PECs appeared as larger aggregates, which is proven here by the display on the images of associations of particles with irregular shapes. On the other hand, when compared to the micro-PECs, the macro-PECs presented a denser network structure. Moreover, the macro-PECs showed a highly porous, interconnected, and three-dimensional network, interspaced by heterogeneously sized vacuoles. It is worth mentioning that the freeze-drying process contributes to the formation of such pores in the structures due to sublimation of ice crystals. This last feature is especially relevant, as such vacuoles may provide location for the entrapment of bioactive compounds, intending either to protect them or to enable their controlled release.

4. Conclusions

This research investigated the formation and behavior of

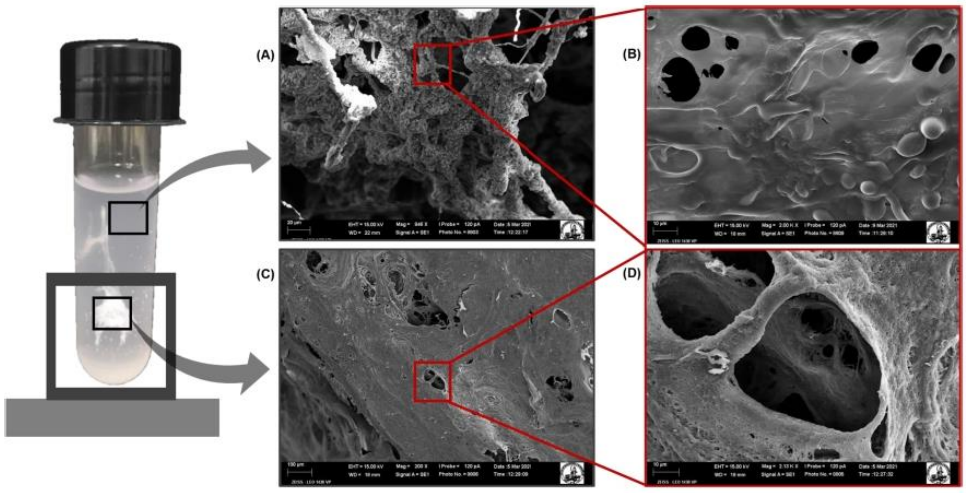

Fig. 7. – SEM images of (A, B) micro-PECs and (C, D) macro-PECs. Original images are shown separately in the Supplementary Material to better visualize the scales and magnification.

supramolecular structures obtained from the mixture between CHS (cationic polyelectrolyte) and CMC (anionic polyelectrolyte). The combination of the aforementioned biopolymer dispersions, at all pH values, mixing ratios and temperatures studied led to the formation of macro- and microstructured polyelectrolytes complexes, namely respectively macro- and micro-PECs. Macro-PECs were macroscopically visible and visually stable structures in aqueous solution for weeks, suggesting that they have potential application in areas such as adsorption of contaminants, as for instance dyes and heavy metals, and in tissue engineering as platforms for tissue repair. On the other hand, micro-PECs presented themselves as dispersed colloidal particles, identified as amorphous and thermally stable, with potential applicabilities in areas such as encapsulation and controlled release of thermosensitive bioactives, such as vitamins, antioxidants, phytosterols, and probiotics. Some of these putative techno-functionalities are currently under study by our team.

CRediT authorship contribution statement

Danielle Cristine Mota Ferreira: Conceptualization, Investigation, Formal analysis, Validation, Writing – original draft, Writing – review & editing. **Sukarno Olavo Ferreira:** Formal analysis, Resources. **Elson Santiago de Alvarenga:** Formal analysis, Resources. **Nilda de Fátima Ferreira Soares:** Formal analysis, Resources. **Jane Sélia dos Reis Coimbra:** Conceptualization, Resources, Funding acquisition. **Eduardo Basílio de Oliveira:** Conceptualization, Validation, Writing – review & editing, Supervision, Resources, Project administration, Funding acquisition.

Declaration of Competing Interest

The authors declare that they have no known competing financial interests or personal relationships that could have appeared to influence the work reported in this paper.

Acknowledgments

The authors are thankful to: Brazilian research agencies CAPES (88882.437265/2019–01; financial code 001) and FAPEMIG (APQ-01457–18), for their financial support; *D.Sc.* Cristiane do Carmo Cesario, Mr. Kleryton Luiz Alves De Oliveira, *D.Sc.* Lucas de Souza Soares and *M. Sc.* Talita Reis Teixeira e Silva, for their kind and constant technical and scientific support.

Supplementary materials

Supplementary material associated with this article can be found, in the online version, at doi:10.1016/j.carpta.2022.100197.

References

Acosta-Ferreira, S., Castillo, O. S., Madera-Santana, J. T., Mendoza-García, D. A., Núñez-Colín, C. A., Grijalva-Verdugo, C., et al. (2020). Production and physicochemical characterization of chitosan for the harvesting of wild microalgae consortia. *Biotechnology Reports*, 28. https://doi.org/10.1016/j.btre.2020.e00554

Aguiar, A. E., de, O., Silva, M., Rodas, A. C. D., & Bertran, C. A. (2019). Mineralized layered films of xanthan and chitosan stabilized by polysaccharide interactions: A promising material for bone tissue repair. *Carbohydrate Polymers, 207*, 480–491, 10.1016/j.carbpol.2018.12.006.

Amorim, M. L., Ferreira, G. M. D., Soares, L., de, S., Soares, W. A., dos, S., et al. (2016). Physicochemical aspects of chitosan dispersibility in acidic aqueous media: effects of the food acid counter-anion. *Food Biophysics, 11*(4), 388–399, 10.1007/s11483-016-9453-4.

Antonino, R. S. C. M. D. Q., Fook, B. R. P. L., Lima, V. A. D. O., Rached, R.Í. D. F., Lima, E. P. N., Lima, R. J. D. S., et al. (2017). Preparation and characterization of chitosan obtained from shells of shrimp (Litopenaeus vannamei Boone). *Marine Drugs, 15*(5), 1–12, 10.3390/md15050141.

Arinaitwe, E., & Pawlik, M. (2014). Dilute solution properties of carboxymethyl celluloses of various molecular weights and degrees of substitution. *Carbohydrate Polymers, 99*, 423–431. https://doi.org/10.1016/j.carbpol.2013.08.030

Berglund, J., Angles d'Ortoli, T., Vilaplana, F., Widmalm, G., Bergenstråhle-Wohlert, M., Lawoko, M., et al. (2016). A molecular dynamics study of the effect of glycosidic linkage type in the hemicellulose backbone on the molecular chain flexibility. *Plant Journal, 88*(1), 56–70, 10.1111/tpj.13259.

Biswal, D. R., & Singh, R. P. (2004). Characterisation of carboxymethyl cellulose and polyacrylamide graft copolymer. *Carbohydrate Polymers, 57*(4), 379–387, 10.1016/j.carbpol.2004.04.020.

Brugnerotto, J., Lizardi, J., Goycoolea, F. M., Argüelles-Monal, W., Desbrières, J., & Rinaudo, M. (2001). An infrared investigation in relation with chitin and chitosan characterization. *Polymer, 42*(8), 3569–3580, 10.1016/S0032-3861(00)00713-8.

Capitani, D., Porro, F., & Segre, A. L. (2000). High field NMR analysis of the degree of substitution in carboxymethyl cellulose sodium salt. *Carbohydrate Polymers, 42*(3), 283–286. https://doi.org/10.1016/S0144-8617(99)00173-3

Carvalho, S. G., dos Santos, A. M., Silvestre, A. L. P., Meneguin, A. B., Ferreira, L. M. B., Chorilli, M., et al. (2021). New insights into physicochemical aspects involved in the formation of polyelectrolyte complexes based on chitosan and dextran sulfate. *Carbohydrate Polymers, 271* (March). 10.1016/j.carbpol.2021.118436.

Cerchiara, T., Abruzzo, A., Parolin, C., Vitali, B., Bigucci, F., Gallucci, M. C., et al. (2016a). Microparticles based on chitosan/carboxymethylcellulose polyelectrolyte complexes for colon delivery of vancomycin. *Carbohydrate Polymers, 143*, 124–130, 10.1016/j.carbpol.2016.02.020.

Cerchiara, T., Abruzzo, A., Parolin, C., Vitali, B., Bigucci, F., Gallucci, M. C., et al. (2016b). Microparticles based on chitosan/carboxymethylcellulose polyelectrolyte

complexes for colon delivery of vancomycin. *Carbohydrate Polymers, 143*, 124–130, 10.1016/j.carbpol.2016.02.020.

Cheng, J., Zhu, H., Huang, J., Zhao, J., Yan, B., Ma, S., et al. (2020). The physicochemical properties of chitosan prepared by microwave heating. *Food Science and Nutrition, 8* (4), 1987–1994, 10.1002/fsn3.1486.

Corazzari, I., Nisticò, R., Turci, F., Faga, M. G., Franzoso, F., Tabasso, S., et al. (2015). Advanced physico-chemical characterization of chitosan by means of TGA coupled on-line with FTIR and GCMS: Thermal degradation and water adsorption capacity. *Polymer Degradation and Stability, 112*, 1–9, 10.1016/j.polymdegradstab.2014.12.006.

da Silva, G. M., da Rocha, R. F. P., da Costa, M. P. M., Ferreira, I. L., de, M., & Delpech, M. C. (2018). Evaluation of viscometric properties of carboxymethylcellulose and gellan. *Journal of Molecular Liquids, 268*, 201–205, 10.1016/j.molliq.2018.07.062.

Dogsa, I., Tomšič, M., Orehek, J., Benigar, E., Jamnik, A., & Stopar, D. (2014). Amorphous supramolecular structure of carboxymethyl cellulose in aqueous solution at different pH values as determined by rheology, small angle X-ray and light scattering. *Carbohydrate Polymers, 111*, 492–504. https://doi.org/10.1016/j.carbpol.2014.04.020

Du, B., Li, J., Zhang, H., Huang, L., Chen, P., & Zhou, J. (2009). Influence of molecular weight and degree of substitution of carboxymethylcellulose on the stability of acidified milk drinks. *Food Hydrocolloids, 23*(5), 1420–1426, 10.1016/j.foodhyd.2008.10.004.

Duhoranimana, E., Karangwa, E., Lai, L., Xu, X., Yu, J., Xia, S., et al. (2017). Effect of sodium carboxymethyl cellulose on complex coacervates formation with gelatin: Coacervates characterization, stabilization and formation mechanism. *Food Hydrocolloids, 69*, 111–120, 10.1016/j.foodhyd.2017.01.035.

Fernandes, R. V., de, B., Silva, E. K., Borges, S. V., de Oliveira, C. R., Yoshida, M. I., et al. (2017). Proposing novel encapsulating matrices for spray-dried ginger essential oil from the whey protein isolate-inulin/maltodextrin blends. *Food and Bioprocess Technology, 10*(1), 115–130, 10.1007/s11947-016-1803-1.

Freitas-Silva, L., Diniz, N., & da Silva, L. C. (2021). Morphoanatomical and biochemical changes in Zeyheria tuberculosa exposed to glyphosate drift. *Botany, 99*, 91–98.

Fu, J., & Schlenoff, J. B. (2016). Driving forces for oppositely charged polyion association in aqueous solutions: Enthalpic, entropic, but not electrostatic. *Journal of the American Chemical Society, 138*(3), 980–990, 10.1021/jacs.5b11878.

Fukuda, H. (1980). Polyelectrolyte complexes of chitosan with sodium carboxymethylcellulose. *In Bulletin of the Chemical Society of Japan, 53*(4), 837–840. https://doi.org/10.1246/bcsj.53.837

Fukuda, H., & Kikuchi, Y. (1979). Polyelectrolyte complexes of sodium carboxymethylcellulose with chitosan. Die Makromolekulare Chemie, 180(6), 1631–1633. 10.1002/macp.1979.021800629.

Galván, Z. R. N., Soares, L., de, S., Medeiros, E. A. A., Soares, N., de, F. F., et al. (2018). Rheological properties of aqueous dispersions of xanthan gum containing different chloride salts are impacted by both sizes and net electric charges of the cations. *Food Biophysics, 13*(2), 186–197, 10.1007/s11483-018-9524-9.

Hubbe, M. A. (2021). Contributions of polyelectrolyte complexes and ionic bonding to performance of barrier films for packaging: A review. *In BioResources* (Vol. 16,(Issue 2), 4544–4605, 10.15376/biores.16.2.hubbe.

Ibrahim, N. A., & Basma, M. (2017). Chitosan -based composite materials: Fabrication and characterization, in: Handbook of composites from renewable materials. In V. K. Thakur, M. K. Thakur, & M. R. Kessler (Eds.), *Physico-Chemical and mechanical characterization* (3rd ed, pp. 103–136). (Eds.): Wiley ScrivenerUS.

Ibrahim, N. A., Nada, A. A., & Eid, B. M. (2018). Polysaccharide-based polymer gels and their potential applications. *In Polymer Gel: Synthesis and Characterization (Issue December, pp. 97–126). Springer Singapore*. https://doi.org/10.1007/978-981-10-6083-0_4

Islam, S., Bhuiyan, M. A. R., & Islam, M. N. (2017). Chitin and chitosan: Structure, properties and applications in biomedical engineering. *Journal of Polymers and the Environment, 25*(3), 854–866. https://doi.org/10.1007/s10924-016-0865-5

Jampafuang, Y., Tongta, A., & Waiprib, Y. (2019). Impact of crystalline structural differences between α-and β-chitosan on their nanoparticle formation via ionic gelation and superoxide radical scavenging activities. *Polymers, 11*(12), 1–16, 10.3390/polym11122010.

Kabanov, V. A., & Zezin, A. B. (1984). A new class of complex water-soluble polyelectrolytes. *Die Makromolekulare Chemie, 6*(S19841), 259–276. https://doi.org/10.1002/macp.1984.020061984120

Kasaai, M. R. (2008). A review of several reported procedures to determine the degree of N-acetylation for chitin and chitosan using infrared spectroscopy. *Carbohydrate Polymers, 71*(4), 497–508. https://doi.org/10.1016/j.carbpol.2007.07.009

Khoshakhlagh, K., Koocheki, A., Mohebbi, M., & Allafchian, A. (2017). Development and characterization of electrosprayed Alyssum homolocarpum seed gum nanoparticles for encapsulation of D-limonene. *In Journal of Colloid and Interface Science (Vol. 490). Elsevier Inc*. https://doi.org/10.1016/j.jcis.2016.11.067

Klemm, D., Heublein, B., Fink, H. P., & Bohn, A. (2005). Cellulose: Fascinating biopolymer and sustainable raw material. *Angewandte Chemie - International Edition, 44*(22), 3358–3393, 10.1002/anie.200460587.

Kulkarni, A. D., Vanjari, Y. H., Sancheti, K. H., Patel, H. M., Belgamwar, V. S., Surana, S. J., et al. (2016). Polyelectrolyte complexes: Mechanisms, critical experimental aspects, and applications. Artificial cells. *Nanomedicine and Biotechnology, 44*(7), 1615–1625, 10.3109/21691401.2015.1129624.

Lawrie, G., Keen, I., Drew, B., Chandler-Temple, A., Rintoul, L., Fredericks, P., et al. (2007). Interactions between alginate and chitosan biopolymers characterized using FTIR and XPS. *Biomacromolecules, 8*(8), 2533–2541, 10.1021/bm070014y.

Leite Milião, G., Souza Soares, L.de, Balbino, D. F., Almeida Alves Barbosa, É.de, Bressan, G. C., Carvalho Teixeira, A. V. N.de, et al. (2022). pH influence on the mechanisms of interaction between chitosan and ovalbumin: A multi-spectroscopic approach. *Food Hydrocolloids*, 123. https://doi.org/10.1016/j.foodhyd.2021.107137

Li, M., Han, M., Sun, Y., Hua, Y., Chen, G., & Zhang, L. (2019). Oligoarginine mediated collagen/chitosan gel composite for cutaneous wound healing. *International Journal of Biological Macromolecules, 122*, 1120–1127. https://doi.org/10.1016/j.ijbiomac.2018.09.061

Li, R., Roos, Y. H., & Miao, S. (2016). Flavor release from spray-dried amorphous matrix: Effect of lactose content and water plasticization. *Food Research International, 86*, 147–155, 10.1016/j.foodres.2016.06.003.

Lim, A. S. L., & Roos, Y. H. (2018). Amorphous wall materials properties and degradation of carotenoids in spray dried formulations. *Journal of Food Engineering, 223*, 62–69. https://doi.org/10.1016/j.jfoodeng.2017.12.001

Mallick, S. P., Singh, B. N., Rastogi, A., & Srivastava, P. (2018). Design and evaluation of chitosan/poly(L-lactide)/pectin based composite scaffolds for cartilage tissue regeneration. *International Journal of Biological Macromolecules, 112*, 909–920, 10.1016/j.ijbiomac.2018.02.049.

Marciel, A. B., Chung, E. J., Brettmann, B. K., & Lorraine, L. (2016). Bulk and nanoscale polypeptide based polyelectrolyte complexes Amanda. *Advances in Colloid and Interface Science, 239*, 187–198.

Mayerhöfer, T. G. (2004). Modelling IR-spectra of single-phase polycrystalline materials with random orientation - A unified approach. *Vibrational Spectroscopy, 35*(1–2), 67–76. https://doi.org/10.1016/j.vibspec.2003.11.011

Meka, V. S., Sing, M. K. G., Pichika, M. R., Nali, S. R., Kolapalli, V. R. M., & Kesharwani, P. (2017). A comprehensive review on polyelectrolyte complexes. *Drug Discovery Today, 22*(11), 1697–1706, 10.1016/j.drudis.2017.06.008.

Mischnick, P., & Momcilovic, D. (2010). Chemical structure analysis of starch and cellulose derivatives. *In Advances in Carbohydrate Chemistry and Biochemistry* (Vol. 64). https://doi.org/10.1016/S0065-2318(10)64004-8. Issue C). Elsevier Inc.

Osorio-Madrazo, A., David, L., Trombotto, S., Jean-Michael, L., Peniche-Covas, C., & Domard, A. (2010). Kinetics study of the solid-state acid hydrolysis of chitosan: evolution of the crystallinity and macromolecular structure. *Biomacromolecules, 11*, 1376–1386.

Pettignano, A., Charlot, A., & Fleury, E. (2019). Solvent-free synthesis of amidated carboxymethyl cellulose derivatives: Effect on the thermal properties. *Polymers, 11* (7). https://doi.org/10.3390/polym11071227

Phung Hai, T. A., & Sugimoto, R. (2018). Fluorescence control of chitin and chitosan fabricated: Via surface functionalization using direct oxidative polymerization. *RSC Advances, 8*(13), 7005–7013, 10.1039/c8ra00287h.

Picone, C. S. F., & Cunha, R. L. (2013). Chitosan-gellan electrostatic complexes: Influence of preparation conditions and surfactant presence. *Carbohydrate Polymers, 94*(1), 695–703, 10.1016/j.carbpol.2013.01.092.

Ramakrishnan, Y., Adzahan, N. M., Yusof, Y. A., & Muhammad, K. (2018). Effect of wall materials on the spray drying efficiency, powder properties and stability of bioactive compounds in tamarillo juice microencapsulation. *Powder Technology, 328*, 406–414, 10.1016/j.powtec.2017.12.018.

Rathee, V. S., Sidky, H., Sikora, B. J., & Whitmer, J. K. (2018). Role of associative charging in the entropy-energy balance of polyelectrolyte complexes. *Journal of the American Chemical Society, 140*(45), 15319–15328, 10.1021/jacs.8b08649.

Roy, J. C., Ferri, A., Giraud, S., Jinping, G., & Salaün, F. (2018). Chitosan–carboxymethylcellulose-based polyelectrolyte complexation and microcapsule shell formulation. *International Journal of Molecular Sciences, 19*(9). https://doi.org/10.3390/ijms19092521

Shah, S., & Leon, L. (2021). Structural dynamics, phase behavior, and applications of polyelectrolyte complex micelles. *Current Opinion in Colloid and Interface Science, 53*, Article 101424, 10.1016/j.cocis.2021.101424.

Soares, L.de S., Perim, R. B., de Alvarenga, E. S., Guimarães, L.de M., Teixeira, A. V. N.de C., Coimbra, J. S.dos R., et al. (2019). Insights on physicochemical aspects of chitosan dispersion in aqueous solutions of acetic, glycolic, propionic or lactic acid. *International Journal of Biological Macromolecules, 128*, 140–148, 10.1016/j.ijbiomac.2019.01.106.

Valverde, A., Pérez-Álvarez, L., Ruiz-Rubio, L., Pacha Olivenza, M. A., García Blanco, M. B., Díaz-Fuentes, M., et al. (2019). Antibacterial hyaluronic acid/chitosan multilayers onto smooth and micropatterned titanium surfaces. *Carbohydrate Polymers, 207*, 824–833. July 201810.1016/j.carbpol.2018.12.039.

Vuillemin, M. E., Michaux, F., Muniglia, L., Linder, M., & Jasniewski, J. (2019). Gum Arabic and chitosan self-assembly: Thermodynamic and mechanism aspects. *Food Hydrocolloids, 96*(May), 463–474, 10.1016/j.foodhyd.2019.05.048.

Wang, J., & Somasundaran, P. (2005). Adsorption and conformation of carboxymethyl cellulose at solid-liquid interfaces using spectroscopic, AFM and allied techniques. *Journal of Colloid and Interface Science, 291*(1), 75–83, 10.1016/j.jcis.2005.04.095.

Wang, Q. Z., Chen, X. G., Liu, N., Wang, S. X., Liu, C. S., Meng, X. H., et al. (2006). Protonation constants of chitosan with different molecular weight and degree of deacetylation. *Carbohydrate Polymers, 65*(2), 194–201, 10.1016/j.carbpol.2006.01.001.

Wongvitvichot, W., Pithakratanayothin, S., Wongkasemjit, S., & Chaisuwan, T. (2021). Fast and practical synthesis of carboxymethyl cellulose from office paper waste by ultrasonic-assisted technique at ambient temperature. *Polymer Degradation and Stability, 184*, Article 109473, 10.1016/j.polymdegradstab.2020.109473.

Xiao, J. X., Wang, L. H., Xu, T. C., & Huang, G. Q. (2019a). Complex coacervation of carboxymethyl konjac glucomannan and chitosan and coacervate characterization. *International Journal of Biological Macromolecules, 123*, 436–445, 10.1016/j.ijbiomac.2018.11.086.

Xiao, J. X., Wang, L. H., Xu, T. C., & Huang, G. Q. (2019b). Complex coacervation of carboxymethyl konjac glucomannan and chitosan and coacervate characterization. *International Journal of Biological Macromolecules, 123*, 436–445, 10.1016/j.ijbiomac.2018.11.086.

Xiong, W., Deng, Q., Li, J., Li, B., & Zhong, Q. (2020). Ovalbumin-carboxymethylcellulose complex coacervates stabilized high internal phase emulsions: Comparison of the effects of pH and polysaccharide charge density. *Food Hydrocolloids, 98*, Article 105282 (August 2019)10.1016/j.foodhyd.2019.105282.

Xue, W., Liu, B., Zhang, H., Ryu, S., Kuss, M., Shukla, D., et al. (2021). Controllable fabrication of alginate/poly-L-ornithine polyelectrolyte complex hydrogel networks as therapeutic drug and cell carriers. *Acta Biomaterialia*, 10.1016/j.actbio.2021.11.004.

Yucel Falco, C., Falkman, P., Risbo, J., Cárdenas, M., & Medronho, B. (2017). Chitosan-dextran sulfate hydrogels as a potential carrier for probiotics. *Carbohydrate Polymers, 172*, 175–183. https://doi.org/10.1016/j.carbpol.2017.04.047

Zhang, H., Wang, C., Zhu, G., & Zacharia, N. S. (2016). Self-healing of bulk polyelectrolyte complex material as a function of pH and salt. *ACS Applied Materials and Interfaces, 8*(39), 26258–26265, 10.1021/acsami.6b06776.

Zhang, R. Y., Zaslavski, E., Vasilyev, G., Boas, M., & Zussman, E. (2018a). Tunable pH-responsive chitosan-poly(acrylic acid) electrospun fibers. *Biomacromolecules, 19*(2), 588–595, 10.1021/acs.biomac.7b01672.

Zhang, Y., Batys, P., O'Neal, J. T., Li, F., Sammalkorpi, M., & Lutkenhaus, J. L. (2018b). Molecular origin of the glass transition in polyelectrolyte assemblies. *ACS Central Science, 4*(5), 638–644, 10.1021/acscentsci.8b00137.

Zhang, Y., Yildirim, E., Antila, H. S., Valenzuela, L. D., Sammalkorpi, M., & Lutkenhaus, J. L. (2015). The influence of ionic strength and mixing ratio on the colloidal stability of PDAC/PSS polyelectrolyte complexes. *Soft matter, 11*(37), 7392–7401, 10.1039/c5sm01184a.

Supplementary Material (SM) I - "Polyelectrolyte complexes obtained from chitosan and carboxymethylcellulose: a physicochemical and microstructural study"

Danielle Cristine Mota Ferreira[a,1], Sukarno Olavo Ferreira[b], Elson Santiago de Alvarenga[c], Nilda de Fátima Ferreira Soares[d], Jane Sélia dos Reis Coimbra[e], Eduardo Basílio de Oliveira[a,2]

[a] Equipe de Estudo de Materiais Alimentares (E²MA), Departamento de Tecnologia de Alimentos (DTA), Universidade de Viçosa (UFV), CEP 36570-900, Viçosa, MG, Brazil.

[b] Departamento de Física (DPF), Universidade Federal de Viçosa (UFV), CEP 36570-900, Viçosa, MG, Brazil.

[c] Departamento de Química (DEQ), Universidade Federal de Viçosa (UFV), CEP 36570-900, Viçosa, MG, Brazil.

[d] Laboratório de Embalagens (LABEM), Departamento de Tecnologia de Alimentos (DTA), Universidade de Viçosa (UFV), CEP 36570-900, Viçosa, MG, Brazil.

[e] Laboratório de Operações Unitárias (LOP), Departamento de Tecnologia de Alimentos (DTA), Universidade de Viçosa (UFV), CEP 36570-900, Viçosa, MG, Brazil.

Corresponding authors:

✉Eduardo Basílio de Oliveira, Departamento de Tecnologia de Alimentos (DTA), Universidade Federal de Viçosa (UFV), Campus Universitário, Postal code 36570-900, Viçosa, MG, Brazil; phone: +55 31 3899 2228; e-mail: eduardo.basilio@ufv.br.

✉ Danielle Cristine Mota Ferreira, Departamento de Tecnologia de Alimentos (DTA), Universidade Federal de Viçosa (UFV), Campus Universitário, Postal code 36570-900, Viçosa, MG, Brazil; phone: +55 31 97111 8854; e-mail: danimotaferreira@gmail.com.

ABBREVIATIONS AND SYMBOLS

CHS	Chitosan
CMC	Carboxyethylcellulose
DTA	Differential thermal analysis
FT-IR	Fourier-Transformed Infrared spectroscopy
TG	Thermogravimetric analysis
K_{MHS}	Constant of Mark-Houwink-Sakurada relationship ($dL \cdot g^{-1}$)
$\bar{M}_V$	Viscometric-average molar mass (kDa)
θ	Scattering angle (^{o})
λ	Wave-length (nm)
η_{sp}	Specific viscosities (dimensionless)
η_r	Relative viscosity (dimensionless)
$[\eta]_H$	Huggins intrinsic viscosity ($dL \cdot g^{-1}$)
$[\eta]_K$	Kraemer intrinsic viscosity ($dL \cdot g^{-1}$)
$\bar{[\eta]}$	Average intrinsic viscosity ($dL \cdot g^{-1}$)

I. The degree of deacetylation (DD) of chitosan

The degree of deacetylation of chitosan was obtained by analyzing the FTIR spectrum (Figure SM1) of chitosan, from the peaks between 1320 and 1420 cm^{-1} obtained in the FTIR spectrum, which show the conversion of N-acetylglycosamine units into amino groups, and using if equation SM1.

Figure SM1 – FT-IR spectra from chitosan to 450 - 4000 cm^{-1}.

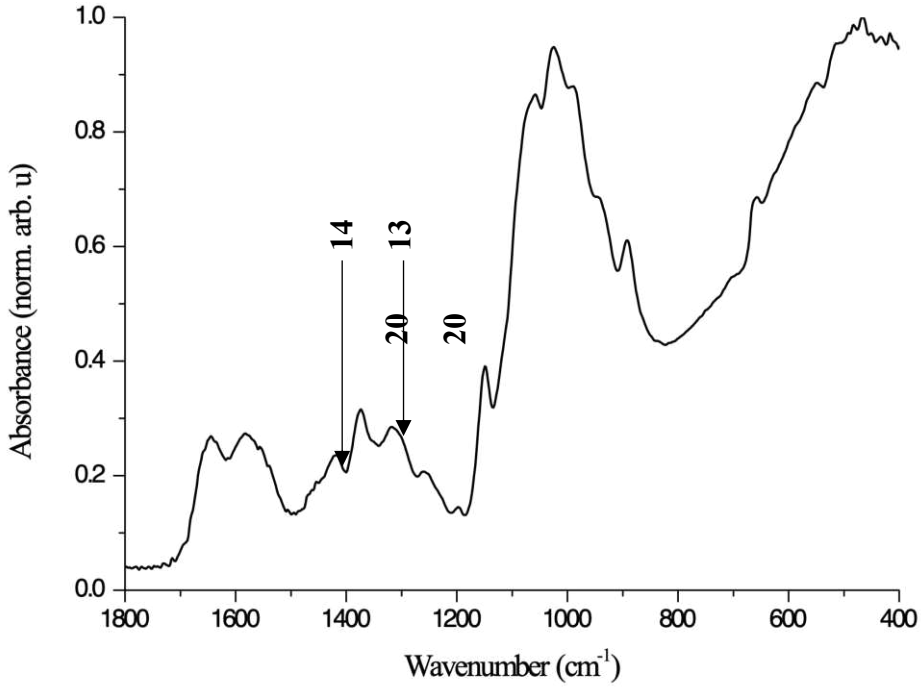

$$DD = 100 - \frac{(A_{1320}/A_{1420}) - 0.3822}{0.03133} \qquad \textit{Equation SM1}$$

A_{1320} and A_{1420} correspond to the absorbance of glucosamine.

II. Chitosan viscometric-avarage molar mass

From the flow times of chitosan dispersions [0.1, 0.2, 0.3, 0.4, and 0.5g·(100 mL)$^{-1}$ in acetate buffer [0,5 g·(100 mL)$^{-1}$], measured in a Cannon-Fenske viscometer (model 513 20, Schott, Germany), specific (ηsp) (Equation SM2) and relative viscosities (ηr) (Equation SM2) were calculated.

$$\eta_{sp} = \frac{t - t_0}{t_0} \qquad \textit{Equation SM1}$$

$$\eta_r = \eta_{sp} + 1 \qquad \textit{Equation SM2}$$

Where, *t* is the flow time of the chitosan dispersions and *t0* is the flow time of acetate buffer solution, in Equations SM1 and SM2.

Then, the average intrinsic viscosity ($[\eta]$) was calculated as the average between the Huggins ($[\eta]_H$) and Kraemer ($[\eta]_K$) intrinsic viscosities (Figure SM2), which were obtained by extrapolating Equations SM3 and SM4.

$$\frac{\eta_{sp}}{c} = [\eta]_H + k_1[\eta]^2 c \qquad \textit{Equation SM3}$$

$$\frac{ln\,(\eta_r)}{c} = [\eta]_K + k_1'[\eta]^2 c \qquad \textit{Equation SM4}$$

Figure SM2 – Adjustment of Huggins and Kraemer empirical models adjusted to viscometric-average experimental data from chitosan aqueous dispersions. (●) $\frac{\eta_{sp}}{c} = k_1[13.43]^2 \cdot c + [5.329]$; $R^2 = 0.982$, (○) $\frac{ln\,\eta_r}{c} = k'_1[-3.435]^2 \cdot c + [5.459]$; $R^2 = 0.934$.

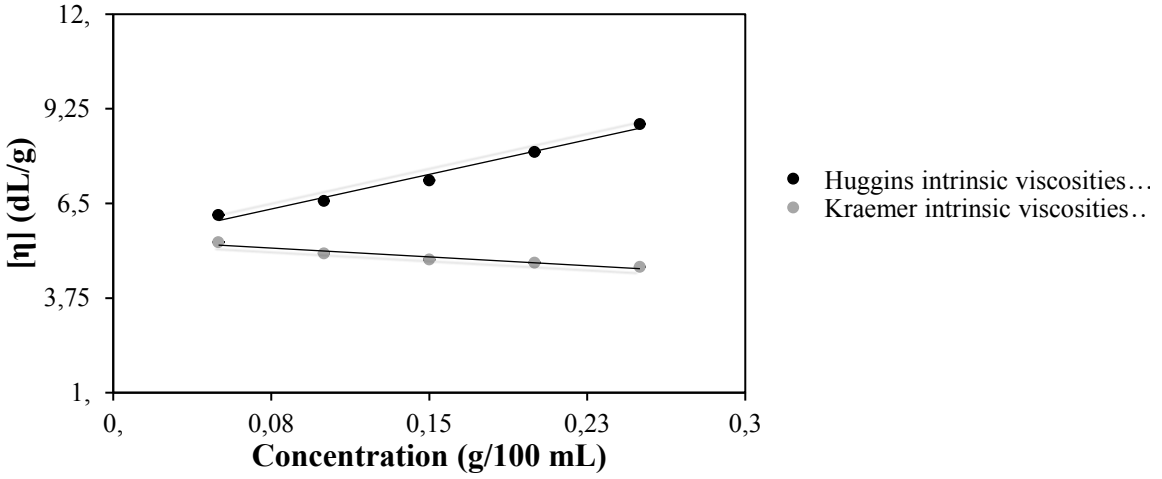

Applying Kasaai (2007) (equations SM5 and SM6), the values of the constants *a* (0.93) and *k* (3.63 × 10^{-5} dL·g^{-1}), from the MHS equation were calculated and obtained as viscosimetric average molar mass for the chitosan used in this work, the value of 364 ± 10 kDa.

$$a = \left(0.6202 + \frac{0.699x}{0.4806+x}\right) + [0.003(T-20)] + 0.06 * C_{ureia} \quad \textit{Equation SM5}$$

$$log\, K * 10^{-5} = -5.7676a + 5.9232 \quad \textit{Equation SM6}$$

$x = DA/(pH \cdot \mu)$, T tempetature in °C e C_{ureia} the concentration of urea in $mol \cdot L^{-1}$.

III. Carboxymethylcellulose viscometric-avarage molar mass

IV.

From the flow times of carboxymethylcellulose dispersions [0.05, 0.10, 0.15, 0.2, and 0.25] g·(100 mL)$^{-1}$ in sodium chloride 0.1 M, measured in a Cannon-Fenske viscometer (model 513 20, Schott, Germany), the average specific viscosities $\left(\bar{\eta}_{sp}\right)$ was measured.

Based on these data, a graph $C = f(C)$ and $ln\left(\bar{\eta}_{sp} + 1\right)/C = f(C)$. In Figure SM3, the regression adjustments for the constructed graph data are shown, using Huggins and Kraemer equations, as proposed by Kasaai (2007), for the calculation of intrinsic viscosity, [η].

Mean molecular weight was then estimated from intrinsic viscosity [η] by the Mark-Houwink equation;

$$[\eta] = kM^a \qquad \textit{Equation SM6}$$

where M is mean molecular weight and k and a are constants assigned values of 0.91 and 1.23 x 10^{-5} for NaCMC (Alvarez-Lorenzo et al., 2001; Vázquez et al., 1995)

Figure SM3 - Adjustment of Huggins and Kraemer equations to experimental data on carboxymethylcellulose

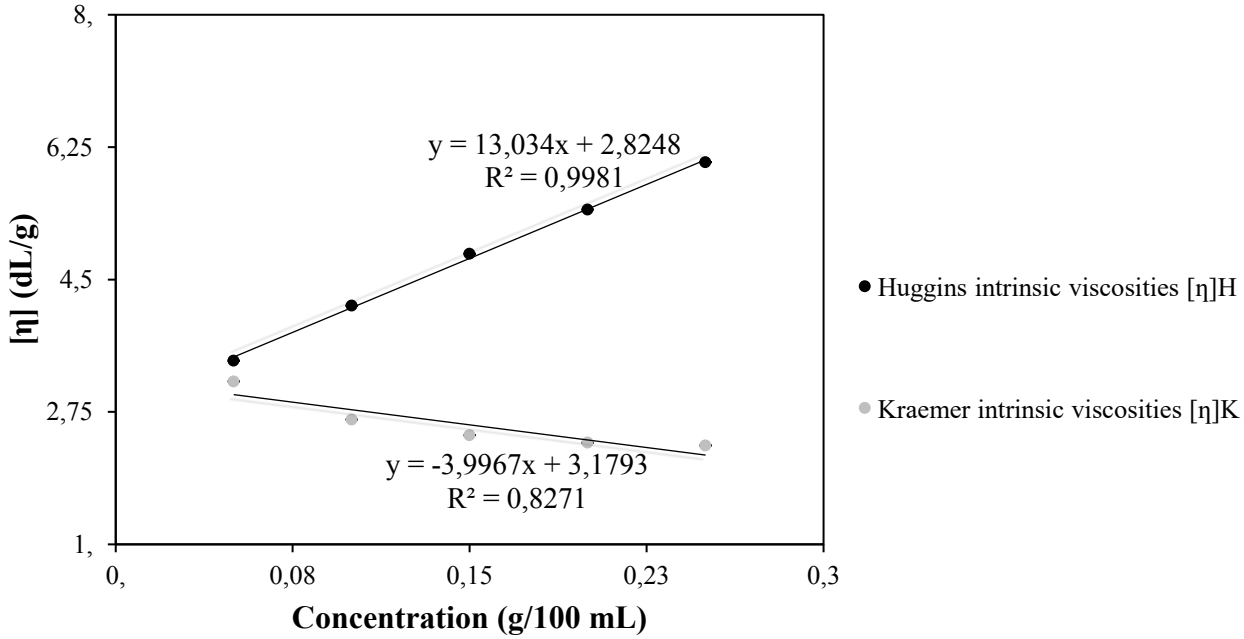

The Mark-Huggins-Sakurada constants used were those obtained by Kurata et al., 1975, for 0.1 M NaCl solvente (a = 0.91, K = 1.23*10^{-5}). From MHS equation were calculated and

obtained as viscosimetric average molar mass for the chitosan used in this work, the value of 794 ± 8 kDa.

V. Carboxymethylcellulose degree of substitution (DS)

Figure SM4 - Conductimetric titration.

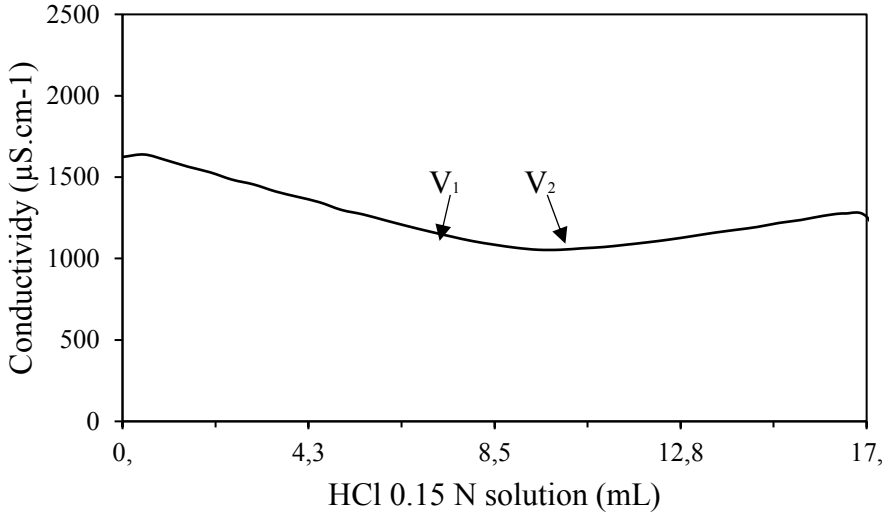

The degrees of substitution of the carboxymethylchitosan were calculated with the equation SM7.

$$DS = \frac{162A}{W - 58A}$$

where: DS is the degree of substitution; 162 is the molecular weight of the anhydrous glucose unit (AGU); A is the value obtained by subtracting V_1 and V_2 (L), where v_1 is the volume of base added to reach the first inflexion point; v_2 is the volume of base added to reach the second inflexion point, 58 is the increase in mass of the carboxymethyl groups added by AGU and and W (g) is the mass of sample used.

Figure SM5 - TG and DTG thermograms of of chitosan (A, B), carboxymethylcellulose (C, D), micro-PECs and (E, F) and for the macro-PECs (G,H).

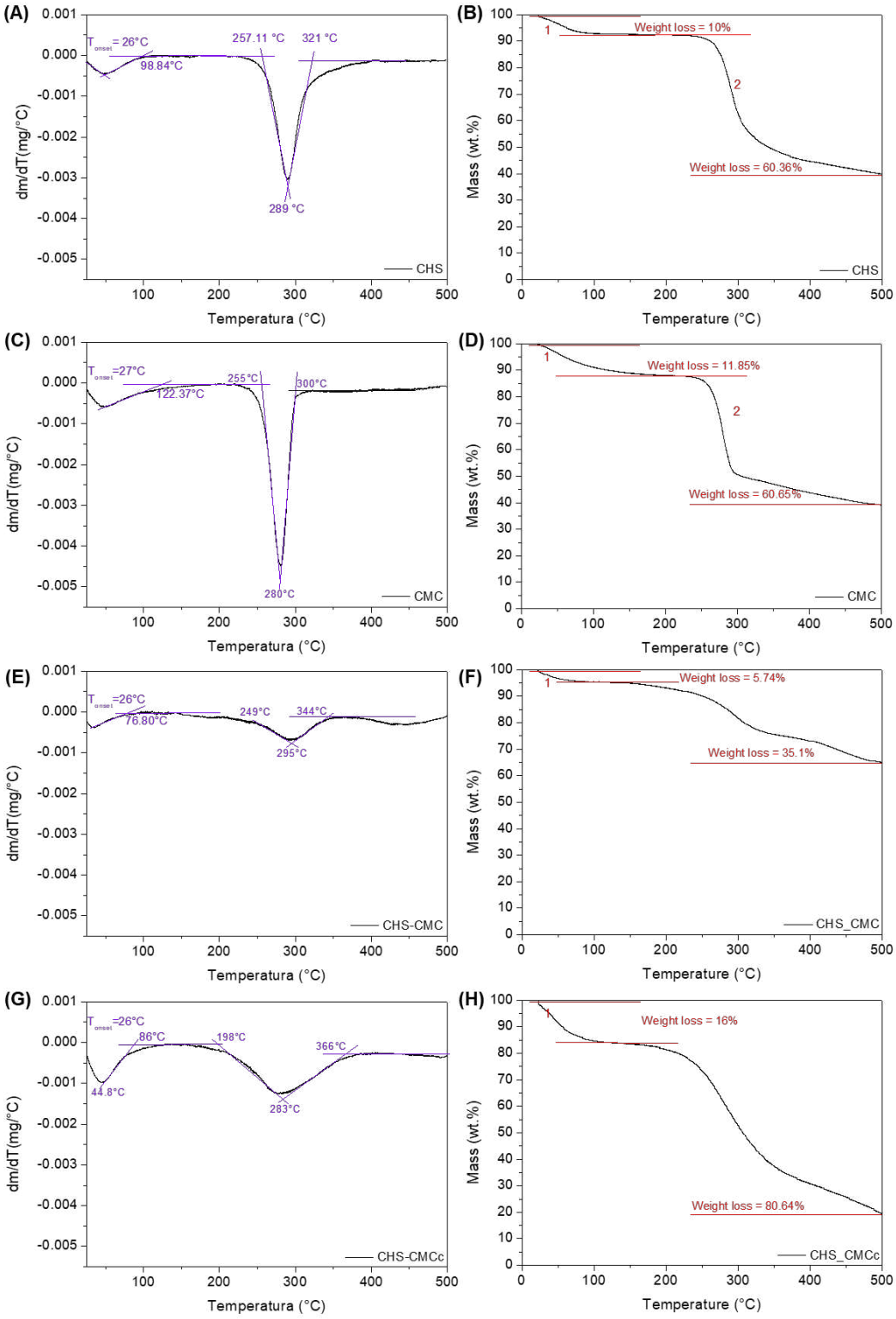

Figure SM6 - Figure 7A – Original image

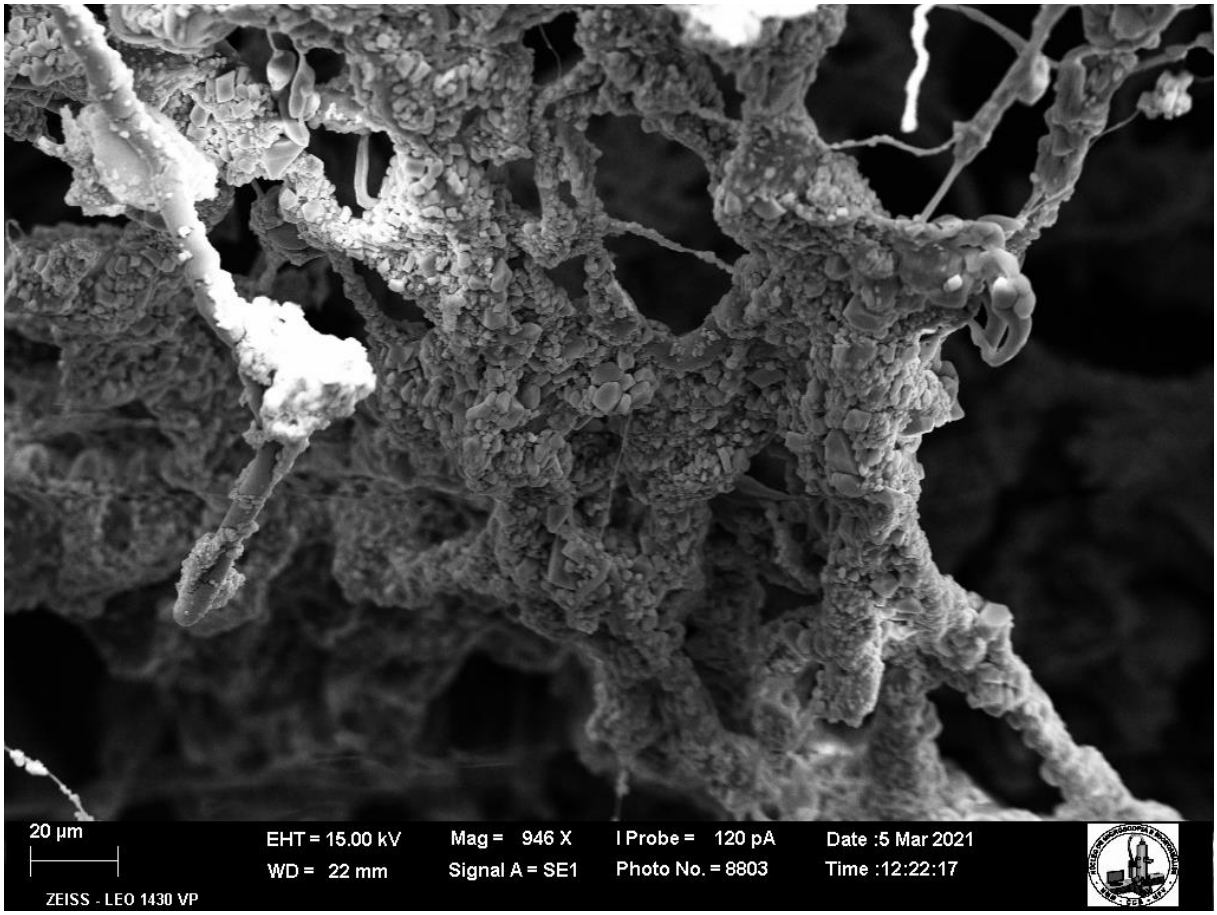

Figure SM7 - Figure 7B – Original image

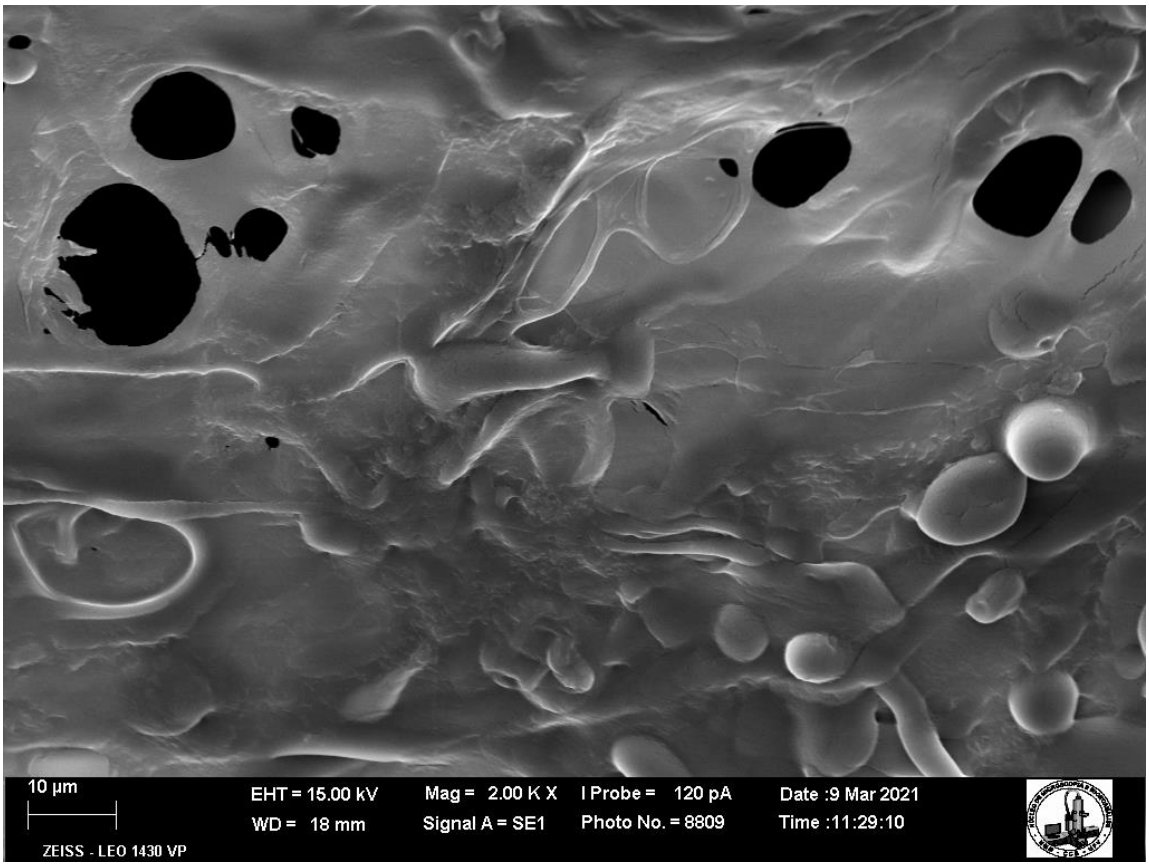

Figure SM8 - Figure 7C – Original image

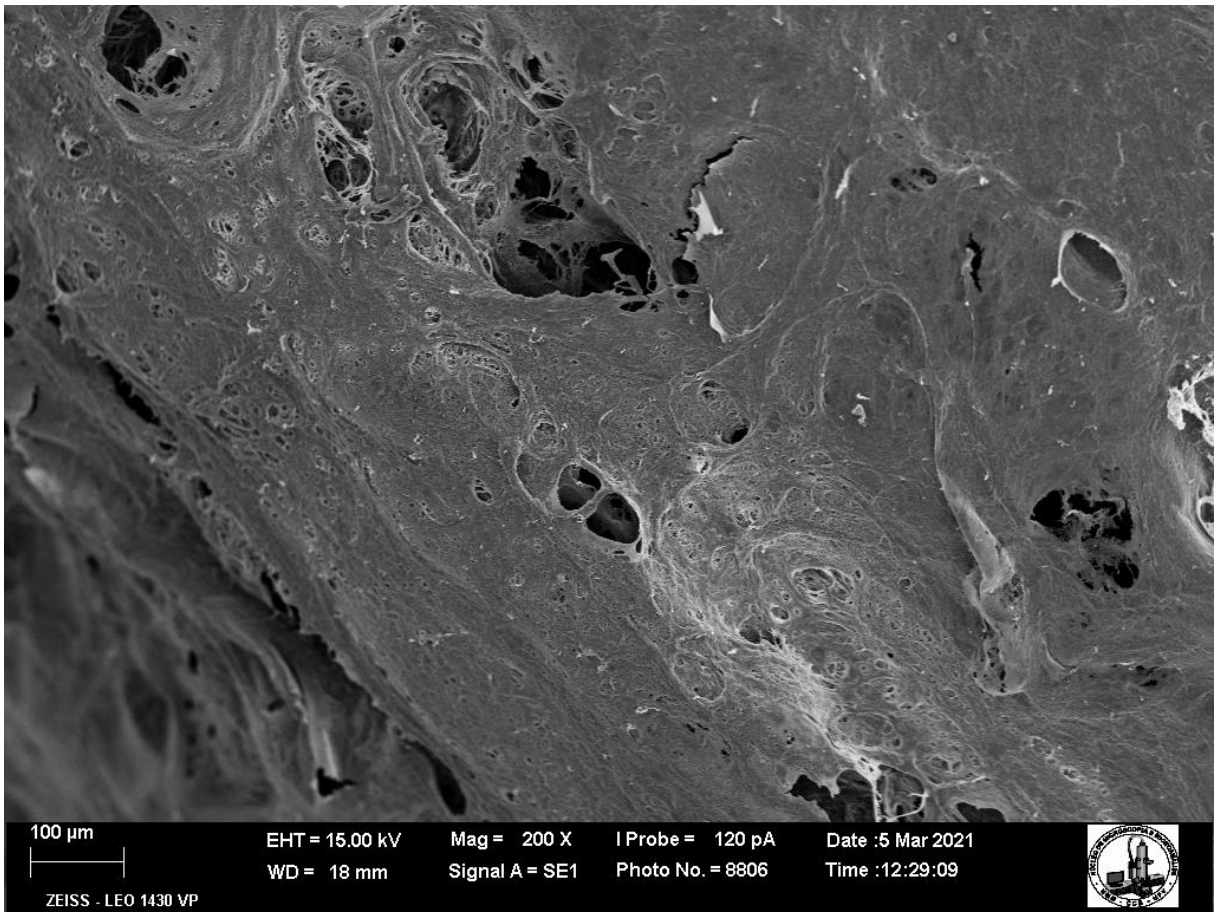

CAPÍTULO 3

CHITOSAN/CARBOXYMETHYLCELLULOSE POLYELECTROLYTE COMPLEXES (PECS) ARE AN EFFECTIVE MATERIAL FOR DYE AND HEAVY METAL ADSORPTION FROM WATER

Ferreira, D. C. M.; Ferreira, dos Santos, T. C..; Coimbra, J. S. R.; Oliveira, E. B. Chitosan/carboxymethylcellulose polyelectrolyte complexes (PECs) are an effective material for dye and heavy metal adsorption from water. Carbohydrate Polymers, 315, (2023). https://doi.org/10.1016/j.carbpol.2023.120977

Graphical abstract:

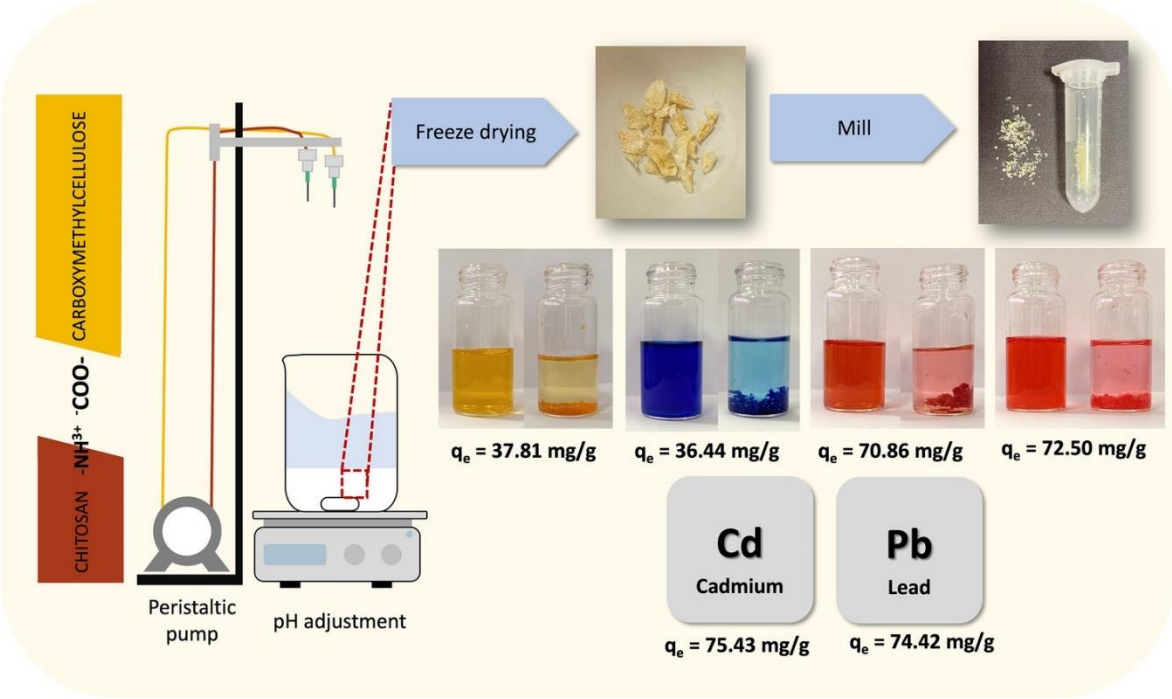

Carbohydrate Polymers 315 (2023) 120977

Contents lists available at ScienceDirect

Carbohydrate Polymers

journal homepage: www.elsevier.com/locate/carbpol

Chitosan/carboxymethylcellulose polyelectrolyte complexes (PECs) are an effective material for dye and heavy metal adsorption from water

Danielle Cristine Mota Ferreira [a,*], Thaís Cristina dos Santos [a], Jane Sélia dos Reis Coimbra [b], Eduardo Basílio de Oliveira [a,*]

[a] Equipe de Estudo de Materiais Alimentares (E²MA), Departamento de Tecnologia de Alimentos (DTA), Universidade de Viçosa (UFV), CEP 36570-900 Viçosa, MG, Brazil

[b] Laboratório de Operações Unitárias (LOP), Departamento de Tecnologia de Alimentos (DTA), Universidade de Viçosa (UFV), CEP 36570-900 Viçosa, MG, Brazil

ARTICLE INFO

Keywords:
Anionic dyes
Cationic dyes
Charged polysaccharides
Pollutants
Transition metal cations
Wastewater treatment

ABSTRACT

Granular macroscopic chitosan/carboxymethylcellulose polyelectrolytic complexes (CHS/CMC macro-PECs) were produced and tested as adsorbents for six pollutants often present in wastewaters: sunset yellow (YS), methylene blue (MB), Congo red (CR) and safranin (S), cadmium (Cd^{2+}) and lead (Pb^{2+}). The optimum adsorption pH values at 25 °C were 3.0, 11.0, 2.0, 9.0, 10.0, and 9.0 for YS, MB, CR, S, Cd^{2+}, and Pb^{2+}, respectively. Kinetic studies indicated that the pseudos-econd order model best represented the adsorption kinetics of YS, MB, CR, and Cd^{2+}, whereas the pseudo-first order model was the most suitable for S and Pb^{2+} adsorption. The Langmuir, Freundlich, and Redlich-Peterson isotherms were fitted to experimental adsorption data, with the Langmuir model providing the best fit. The maximum adsorption capacity ($q_{máx}$) of CHS/CMC macro-PECs for the removal of YS, MB, CR, S, Cd^{2+}, and Pb^{2+} was 37.81, 36.44, 70.86, 72.50, 75.43, and 74.42 mg/g, respectively (corresponding to 98.91 %, 94.71 %, 85.73 %, 94.66 %, 98.46 %, and 97.14 %). Desorption assays showed that CHS/CMC macro-PECs can be regenerated after adsorbing any of the six pollutants studied, with possibility of reuse. These results provide an accurate quantitative characterization of the adsorption of organic and inorganic pollutants on CHS/CMC macro-PECs, indicating a novel technological applicability of these two inexpensive, easy-to-obtain polysaccharides for water decontamination.

1. Introduction

In times when nature began to charge the bill for humanity's carelessness with the environment, the rational use of water resources in industrial processes has become one of the main concerns of industries, environmental research, and public authorities. Many of these activities generate a large volume of effluents, which often do not receive proper treatment, contaminating reservoirs and water stations, thus harming the environment (Chowdhury et al., 2022). Among the contaminants, dyes and heavy metals stand out since they are pollutants with relevant applications in the textile, leather, food, or pharmaceutical industries (Sultana et al., 2022). Considering their chronic toxicity and low biodegradability, improper disposal of dyes and heavy metals represents a critical threat to the environment and ecosystems, requiring the development of effective and economically viable technologies to adequately treat effluents containing such compounds.

In recent years, different methods have been proposed for the elimination or at least the reduction of dyes and heavy metals from wastewater, including coagulation/flocculation (Gadekar & Ahammed, 2016), ion exchange (Lahiri et al., 2022), membrane separation (Fortunato et al., 2021; Qu et al., 2022), adsorption (Alves et al., 2020; Xu et al., 2022), advanced oxidation (Bravo-Yumi et al., 2022),

Abbreviations: q_{e0}, Adsorption capacity of fresh macro-PEC; CMC, Carboxymethylcellulose; CHS, Chitosan; CR, Congo red; C_0, Dye initial concentration in solution; %R, Dye removal percentage; C_d, Equilibrium concentration after desorption; q_D, Equilibrium desorption capacity; K_f, Freundlich constant (represents the adsorption capacity); C, Intercept of intraparticle diffusion plot; k_d, Intraparticle diffusion rate constant; Pb^{2+}, Lead; LQ, Limit of Quantification; LD, Limits of Detection; n, Freundlich constant (intensity of adsorption); Q_m, Maximum capacity; MB, Methylene blue; PEC, Polyelectrolyte complex; k_1, Pseudo first order rate constant; k_2, Pseudo-second order rate constant; K_R, α, β, Redlich–Peterson constants; S, Safranin; SEM, Scanning electron microscopy; YS, Yellow sunset; pH_{ZPC}, pH corresponding to zero-point charge.

* Corresponding authors.
E-mail addresses: danielle.mota@ufv.br (D.C.M. Ferreira), eduardo.basilio@ufv.br (E.B. de Oliveira).

https://doi.org/10.1016/j.carbpol.2023.120977
Received 7 January 2023; Received in revised form 23 April 2023; Accepted 30 April 2023
Available online 4 May 2023

photocatalytic degradation (Elemike et al., 2017) and bioremoval (Elgarahy et al., 2021). Among these methods, adsorption continues to attract great attention due to its high efficiency, economic viability, and relative ease of operation. Conceptually speaking, adsorption is a surface phenomenon that removes chemical species from the fluid phase, with a consequent concentration on the surface of a given substrate, usually a solid (Amran & Zaini, 2021). Adsorbent materials should be economically viable, easily accessible, environmentally harmless, and highly removable and reusable. In addition, it is essential to use materials with minimum environmental impact, coming from abundant natural sources and being biodegradable and nontoxic. Furthermore, the complexity of wastewater (pH, temperature, and presence of mixed pollutants) can reduce treatment efficiency and negatively affect the regeneration of adsorbents, which should also be considered when choosing appropriate adsorbents for wastewater treatment (Aragaw & Bogale, 2021). Among the various materials used to fabricate adsorbents, polysaccharides, a broad class of carbohydrate polymers originating from natural sources, are promising candidates for such applications. They present diverse functional groups on their chains, allowing high adsorptive performance, high porosity, renewability, biodegradability, biocompatibility, and possible combination (Qi et al., 2021).

Sodium carboxymethyl cellulose (CMC) is a cellulose derivative soluble in water. Due to the deprotonation of carboxyl groups, it becomes negatively charged when dissolved in water (Ren et al., 2016). CMC has been explored for different purposes, such as food thickeners (Kowalska & Krzton-Maziopa, 2015), bioengineering (Capanema et al., 2018), dressings (Das et al., 2015), adsorption (Kono et al., 2013), and drug carriers (He et al., 2021). Chitosan (CHS), a polysaccharide composed mainly of glucosamine and *N*-acetylglucosamine units, is the only natural polysaccharide that is positively charged in aqueous media and has been applied in the removal of pollutants due to its availability, low cost, and high biodegradability (Sadiq et al., 2021). However, due to thermal stability and mechanical property limitations, this polysaccharide is often mixed with other polymers or crosslinking agents to form composites with improved physicochemical and techno-functional properties (Ferreira et al., 2022).

Ferreira et al. (2022) studied the combination of CHS and CMC dispersions and found that all pH values (3.0, 3.5, 4.0, or 4.5), mixing ratios (4:1, 3:1, 2:1, 1:1, 1:2, 1:3, and 1:4) and temperatures (25, 45, 65, or 85 °C) studied led to the formation of either macro- or microstructured polyelectrolyte complexes (PECs), namely, macro-PECs and micro-PECs, respectively. Macro-PECs appeared as granular, macroscopically visible structures, stable for weeks in an aqueous solution, suggesting that they have potential applications in the adsorption of contaminants, such as dyes and heavy metals. Indeed, Tang et al. (2020) studied modified magnetic Fe_3O_4/alkaline Ca-bentonite (MACB-CC) manufactured by modifying magnetic Fe_3O_4/alkaline Ca-bentonite (MACB) with both CMC and CHS via the Schiff base reaction for pollutant removal. The adsorbent exhibited stable magnetic separation ability and excellent adsorption for doxycycline (96 %). Additionally, Zhao et al. (2020) studied CHS and CMC hydrogels prepared by semi-dissolution/acidification/sol-gel transition (SD-A-SGT). The hydrogels formed showed good adsorption capacity for both cationic and anionic dyes. These reports illustrate the potential of CMC-CHS complexes for adsorption processes, opening doors for more systematic and quantitative investigations on this subject. On the other hand, to the best of our knowledge, complexes formed between CMC and CHS, without adding other reagents, complexing agents, or chemical modifications, have not been studied for adsorptive processes.

Therefore, the novelty brought by the present study is the demonstration of the applicability of supramolecular structures based on CHS and CMC, formed by a simple and direct method, as inexpensive and ecologically harmless adsorbents for the removal of dyes and heavy metals from water. Four organic dyes – sunset yellow (YS), methylene blue (MB), Congo red (CR), and safranin (S) – with azo- and/or condensed rings (see their molecular structures in Supplementary Materials) were studied here due to their ubiquity in many industrial wastewaters. In addition, similar to these dyes, many heavy metals are often present in industrial effluents, are nondegradable and highly toxic, and can accumulate within organisms along the food chain. Lead (Pb^{2+}) and cadmium (Cd^{2+}) are toxic heavy metals that frequently exist as cationic inorganic ions in industrial wastewater, so they were also taken as adsorbates in the present study. Due to the nonstopping growing need for natural, alternative, and low-cost materials (such as the carbohydrate-based supramolecular complexes studied here) to reduce or eliminate contaminants and, consequently, to improve the living conditions of populations through environmental protection and pollution control, we strongly believe that this report is of strategic technological potential. Furthermore, the results reported may contribute to the techno-economical value of two readily available polysaccharides also possessing recognized safety.

2. Materials and methods

2.1. Materials

Chitosan (low molecular weight, Sigma–Aldrich Corporation, USA; Product ID = 448877) from fresh shrimp shells *Pandalus boralis* and carboxymethylcellulose (Sigma–Aldrich Corporation, USA; Product ID = 419311) were purchased from Sigma–Aldrich Corporation (USA). Chitosan powder was washed three times with deionized water to remove water-soluble chitooligosaccharides and salt residues before being used in the experiments. Chitosan was characterized by the degree of deacetylation (76.7 %) and viscometric average molar mass (364 ± 10 kDa). Carboxymethylcellulose was characterized in terms of the degree of substitution (0.59 ± 0.03) and viscometric average molar mass (794 ± 8 kDa) (Ferreira et al., 2022).

Methylene blue (Product ID = M9140), yellow sunset (Product ID = 465224), Congo red (Product ID = C6767), and safranin (Product ID = S2255) were also supplied by Sigma–Aldrich. As models of pollutant heavy metals, the salts $PbCl_2$ and $CdCl_2$, with purity >99 %, were studied. They were both kindly furnished by the Department of Chemistry (UFV). Hydrochloric acid (Sigma–Aldrich, Brazil, 37 wt% in H_2O) and sodium hydroxide (Sigma–Aldrich, Brazil) were of analytical grade and used without any purification process. The deionized water used in all experiments was obtained from a Milli-Q system (18.2 MΩ·cm^{-1}, 25 °C; Reference A+, Millipore, Italy).

2.2. Validation of analytical methods for determination of dye concentrations in aqueous solutions

The maximum absorption wavelengths of the dyes were determined by using the spectral scan performed from 200 to 1100 nm. In all studied pH values, the same $\lambda_{máx}$ for the dyes was obtained. Therefore, the respective peaks at the wavelengths mentioned in Supplementary Material (Table SM1) were adopted for all adsorptive tests. The adjusted coefficients, line equations for each dye, limits of detection, limit of quantification, and precision are also presented in the Supplementary Material.

For the analysis of the residual concentrations in aqueous solutions of the dyes after the adsorption onto CHS/CMC macro-PECs, standard curves were built by UV–visible spectroscopy (Kafle, 2020), monitoring the absorbance at the maximum absorption wavelengths for each dye according to Beer-Lambert law at their corresponding maximal absorption wavelengths. The calibration curves of the standard dye solutions were developed for concentrations ranging from 0.125 mg·L^{-1} to 50 mg·L^{-1} using a UV–Vis spectrophotometer (UV 1800, Shimadzu, Japan). Quartz cuvettes with an optical path equal to 1 cm were used. Absorbance analyses were performed in triplicate.

The detection limit (DL), corresponding to the lowest concentration of each substance in the sample that can be detected by this method, and the quantification limit (QL), which is equivalent to the lowest con-

centration in the sample that can be quantified, were estimated from the calibration curve resulting from the parameter linearity (Kotani et al., 2020), as represented in Eqs. (1) and (2):

$$DL = \frac{(3 \cdot SD)}{m} \quad (1)$$

$$QL = \frac{(10 \cdot SD)}{m} \quad (2)$$

In these two equations, SD is the standard deviation of the intercept for the Y axis, and m is the slope value of the analytical curve.

The accuracy of an assay is characterized by its ability to produce the correct value if an infinite number of repetitions are performed (Sahu, Rai, Rai, Banjare, et al., 2020b). The accuracy (A) was calculated through Eq. (3), which relates the concentration calculated in triplicate for a standard solution (C_c) of methylene blue and sunset yellow dyes and the expected concentration (C_e).

$$A(\%) = \frac{C_c}{C_e} \quad (3)$$

Accuracy corresponds to the variability of the results around the mean value (coefficient of variation) (Sahu, Rai, Rai, Banjare, et al., 2020a).

2.3. Determination of Pb^{2+} and Cd^{2+} concentrations in aqueous solutions

For Pb^{2+} and Cd^{2+} residual concentrations in aqueous solutions after the adsorption processes, a Perkin Elmer Model Optima 8300 DV atomic absorption spectrometer equipped with a hollow cathode lamp for cobalt as well as a deuterium lamp for background correction was used. Wavelengths of 226.506 nm for Cd^{2+} and 220.351 nm for Pb^{2+} and different standard solutions were used to construct the analytical curve for subsequent concentration calculation.

2.4. CHS/CMC macro-PEC production

Macro-PECs were prepared as described in detail by Ferreira et al. (2022), under the conditions where the highest yield of macro-PECs was observed. Briefly, at room temperature (25.0 ± 1.0 °C), appropriate volumes of CMC dispersions (pH 3.0) were added dropwise with a magnetic burette stirrer adapted to the dispersion of previously prepared CHS (pH 3.0). The mixing ratio was 1:3 (CHS:CMC). After formation, the macro-PECs were frozen, lyophilized, and ground, as schematically shown in Fig. 1.

2.5. CHS/CMC macro-PEC characterization

2.5.1. Zero-point charge (pH_{ZPC}) determination

The pH values at which the net amounts of positive and negative charges are equal on the surface of the adsorbents were estimated by direct measurements of the pH of standard solutions (pH between 1.0 and 12.0; HCl/KCl and NaOH/KCl; constant and ionic strength equal to 1 mol·L^{-1}) before and after contact with solids. The analyses were carried out as follows: 25 mL of 0.1 mol·L^{-1} KCl solution was placed in a series of Erlenmeyer flasks, and then the pH value of each container was adjusted to 1.0, 2.0, …, 11.0, or 12.0 using 0.1 mol·L^{-1} solutions of HCl or NaOH. The initial pH of the solution (pH_i) was measured and noted. One hundred milligrams of freeze-dried micro-PEC was added to each Erlenmeyer flask and stirred for 24 h. The supernatant material was filtered, and the final pH values (pH_f) of the solutions were measured. The difference between the initial and final pH values was calculated $\left[\Delta pH = pH_f - pH_i\right]$, and then the plot of $\Delta pH = f(pH_i)$ was built. The pH value where $\Delta pH = 0$ is called the zero-charge point, the pH_{pcz} of the material.

2.5.2. Scanning electron microscopy analysis

The morphology of crushed macro-PECs was obtained by scanning electron microscopy (SEM). Samples were fixed in a sample holder, covered with gold (15 nm thick) (Quorum, Q150RS, United Kingdom) (Freitas-Silva et al., 2021), and then analyzed using an LEO 1430VP scanning electron microscope (Carl Zeiss, United Kingdom) at 15 kV.

2.6. Adsorption of pollutants on CHS/CMC macro-PECs

2.6.1. Adsorption efficiency at different pH values

First, adsorption experiments were performed by varying the initial pH of the solutions of each dye or heavy metal (namely, "pollutants") to investigate the pH effect on adsorption. The dye solutions were prepared at different pH values. For this purpose, the powder dye was added

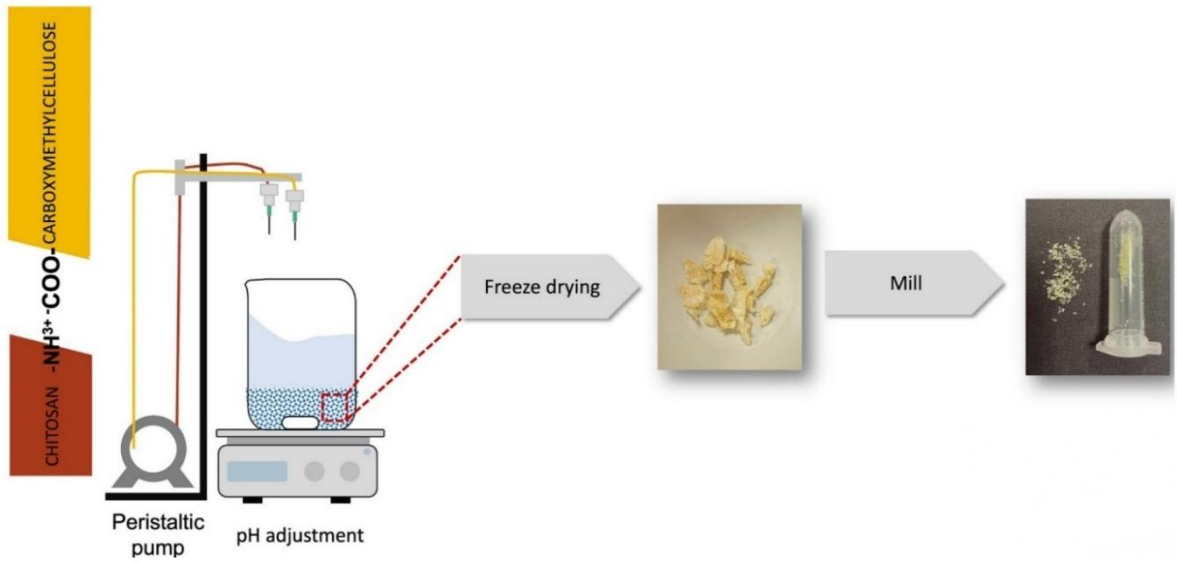

Fig. 1. Schematic representation of the methodology applied to macro-PEC preparation.

directly to the water at the target pH. Initial tests were carried out so that the intended final pH was reached when adding the dyes without the need to add any other amounts of acidic or basic solutions so that there was no interference in the final concentration of the solutions. In other words, 10 mg of the adsorbents were added to 10 mL of solution with a concentration pollutant equal to 50 mg·L^{-1} and with pH varying from 2.0 to 12.0, kept under constant agitation for 24 h and monitored periodically by UV–Vis spectroscopy for dye solutions (Section 2.2) or by atomic absorption spectrometry for heavy metal solutions (Section 2.3). Solution pH adjustments were performed with the dropwise addition of 0.1 mol·L^{-1} solutions of HCl and/or NaOH. The amounts of dye or heavy metal adsorbed (mg) per mass of material (g) (q_e) in each solution were obtained from the difference between their initial (C_0) and final or equilibrium (C_f) concentrations in solution, by the mass of adsorbent (m) used and by the volume (V) of the solution, according to Eq. (4). Additionally, the dye removal percentage (%R) was estimated by Eq. (5).

$$q_e\left(\frac{mg}{g}\right) = \frac{C_0 - C_f}{m} V \tag{4}$$

$$\%R = \frac{C_0 - C_f}{C_0} \tag{5}$$

2.6.2. Adsorption kinetics

An adsorption kinetics study was carried out to analyze the influence of the contact time of the pollutants and the adsorbate in aqueous media on the adsorbed amount of the former. Once the best adsorption pH was known (i.e., the pH at which adsorption is more favorable for each pollutant), the same procedure was used for the kinetic study, varying the contact time to determine the equilibrium time. Briefly, 10 mg samples of the adsorbents were added to 10 mL of aqueous solutions containing dyes or heavy metals at 25 mg·L^{-1} and 50 mg·L^{-1} (the concentration was varied to check for equilibrium time changes and fitted models). Next, they were kept for continuous stirring and monitored periodically (5, 10, 20, 30, 45, 60, 90, 120, 180, 240, 300, 360, 420, 480, 540, and 600 min) using UV–Vis spectroscopy for dye solutions or atomic absorption spectrometry for heavy metal solutions. The absorbance readings were taken in three replicates, and the average was used to calculate the dye concentration.

The amount of pollutant adsorbed at each time (Q_t) was calculated using Eq. (4). The experimental kinetics data were modeled using pseudo-first order, pseudo-second order, and intraparticle diffusion models as expressed in Eqs. (6), (7), and (8) (McCabe et al., 2004; Sahoo, Prelot, 2020b).

$$Q_t = Qe\left(1 - e^{-k_1 t}\right) \tag{6}$$

$$Q_t = \frac{k_2 Q_e^{\,2} t}{1 + k_2 Q_e t} \tag{7}$$

$$Q_t = k_d t^{0.5} + C \tag{8}$$

In these three equations, Q_t (mg/g) is the amount adsorbed at time t, Q_e (mg/g) is the amount adsorbed at equilibrium, k_1 (min^{-1}) is the pseudo-first order rate constant, k_2 (g/mg·min) is the pseudo-second order rate constant, k_d (mg/g.h) is the intraparticle diffusion rate constant, t (min) is the contact time, and C is the vertical axis intercept of the intraparticle diffusion plot. The values of C provide information about the thickness of the boundary layer. A larger C implies a greater effect of the boundary layer (Sahoo, Prelot, 2020a, 2020b).

2.6.3. Adsorption isotherms

The optimal pH and the equilibrium time for the adsorption of dyes and heavy metals under study were used according to data obtained in the pH study (Section 2.6.1) and the kinetic study (Section 2.6.2). The tests to obtain the adsorption isotherms were carried out similarly to those previously described but with dye concentrations varying from 1 to 100 mg·L^{-1}. For each pollutant, batch isotherms were obtained by placing 15 mL of solution in contact with 0.1 g of adsorbent, maintaining the mass of the adsorbent and varying the solution concentration (1, 5, 10, 20, 30, 40, 50, 60, 70, 80, 90, and 100 mg·L^{-1}). The systems formed were placed under mechanical agitation at 300 rpm until equilibrium was reached to obtain the amount of pollutant adsorbed and the concentration that remained in the solution. With these experimental data, the isotherms were modeled according to the Langmuir, Freundlich, and Redlich–Peterson models, represented in Eqs. (9), (10), and (11), respectively.

$$Q_e = \frac{Q_m k_L C_e}{1 + Q_m C_e} \tag{9}$$

$$Qe = k_f C_e^{\frac{1}{n}} \tag{10}$$

$$Q_e = \frac{k_R C_e}{1 + \alpha C_e^{\beta}} \tag{11}$$

In these three equations, Q_e is the amount adsorbed per gram of the adsorbent (mg.g^{-1}), Q_m (L·mg^{-1}) is a constant related to the adsorption energy, k_L (L·g^{-1}) is the Langmuir constant that gives the theoretical adsorption capacity in the monolayer, C_e (mg.g^{-1}) is the concentration at equilibrium, k_f and n are the Freundlich constants (dimensionless) that represent the adsorption capacity and the intensity of adsorption, respectively, and k_R (L/g), α (L$^{\beta}$· g$^{-\beta}$) and β (dimensionless) are the Redlich–Peterson constants.

2.6.4. Desorption assays

The recovery capacity of the adsorbed dyes was determined by saturating 10 mg of the adsorbents with 10 mL of an aqueous solution of 50 mg·L^{-1} of each dye. The dye-loaded macro-PECs were regenerated using 10 mL of 0.01 M HCl solution for methylene blue and safranin desorption and 0.01 M NaOH for yellow sunset and congo red desorption, corresponding to pH values of 2 and 10, respectively. Regeneration was carried out at room temperature for 2 h. Residual concentrations were measured, and dye desorption was calculated using Eq. (12).

$$q_D = \frac{(C_D - C_o)V}{m} \tag{12}$$

In Eq. (12), q_D (mg·g^{-1}) is the desorption capacity, C_D(mg·L^{-1}) is the equilibrium concentration after desorption, C_o (mg/L) is the initial dye concentration in solution ($C_0 = 0$), V (L) is the solution volume, and m (g) is the macro-PEC mass.

3. Results and discussion

3.1. CHS/CMC macro-PEC characterization

3.1.1. Zero-point charge (pH_{pcz})

The zero-point charge (pH_{pcz}) is a critical factor that allows predicting the net charge on the surface of the adsorbent as a function of pH and, consequently, the ease with which an adsorbent material can potentially adsorb ions. It is the value at which the net charge of the polyelectrolyte complex (PEC) is zero, that is, $\Delta pH = pH_f - pH_i = 0$. The pH of the solution is one of the factors that most strongly affects the adsorption capacity of the dye in the adsorbent. It controls the magnitude of the electrostatic charge of ionized dye molecules. Adsorbents at $pH < pH_{pcz}$ have a positive surface charge (favoring the adsorption of anions), whereas at $pH > pH_{pcz}$, they have a negative surface charge (favoring the adsorption of cations). According to our results, the pH_{pcz} of the macro-PEC under study was approximately at pH 3.3, as shown in Fig. 2.

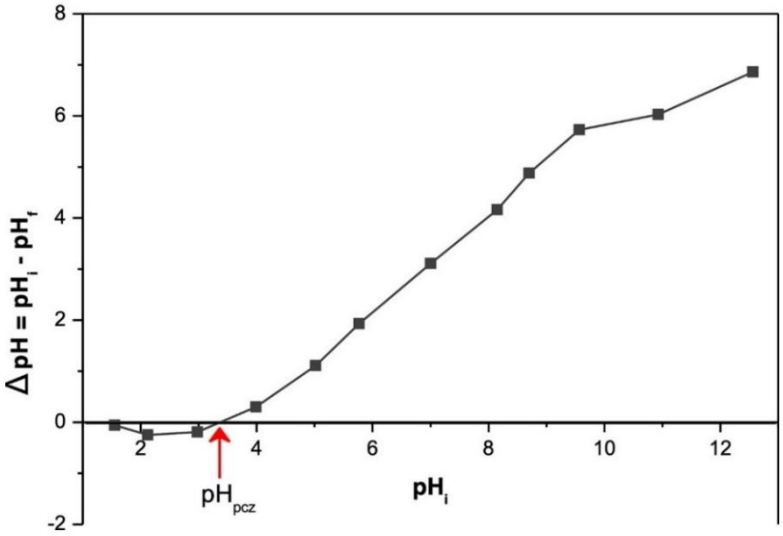

Fig. 2. Identification of the zero-point charge (pH_{pcz}) of the CHS/CMC macro-PECs.

3.1.2. Scanning Electron Microscopy (SEM)

The results of scanning electron microscopy (SEM) analysis of the CHS/CMC macro-PEC are illustrated in Fig. 3. The surface of the CHS/CMC macro-PEC particles presented a heterogeneous topology, with the presence of indentations and cavities, responsible for expanding its specific surface area (area per mass unit), thus increasing the number of potential sites for adsorption. Pores may exist on the surface of the particles but with size magnitudes smaller than the resolution limit of the available microscope.

3.2. Adsorption of pollutants on CHS/CMC macro-PECs

3.2.1. Adsorption efficiency at different pH values

Fig. 4 shows the relationship between the initial pH of the solutions and the adsorption capacity of dyes and heavy metals by macro-PEC, removing them from the aqueous media. According to these results, the YS removal capacity increased from 2.72 ± 0.03 to 60,77 ± 0.05 $mg{\cdot}g^{-1}$ when the pH changed from 10.0 to 3.0; the MB removal capacity increased from 4.52 ± 0.01 to 45.49 ± 0.03 mg·g − 1 when the pH changed from 2.0 to 11.0; the CR removal capacity increased from 2.11 ± 0.01 to 41.16 ± 0.06 $mg{\cdot}g^{-1}$ when the pH changed from 11.0 to 2.0; the S removal capacity increased from 29.16 ± 0.29 to 59.98 ± 0.09 $mg{\cdot}g^{-1}$ when the pH changed from 3.0 to 9.0; the Cd^{2+} removal capacity increased from 30.67 ± 0.10 to 68.99 ± 0.05 $mg{\cdot}g^{-1}$ when the pH changed from 2.0 to 10.0; and the Pb^{2+} removal capacity increased from 0.17 ± 0.01 to 61.65 ± 0.03 $mg{\cdot}g^{-1}$ when the pH changed from 2.0 to 9.0. These results reveal the strong impact of electrostatic effects on adsorbate-adsorbent binding. As the macro-PEC surface became more negative, the adsorption of anionic dyes was unfavored at higher pH values, whereas the cationic species had their adsorption favored.

During the formation of the macro-PEC and when these are immersed in aqueous solutions at lower pH, the electrostatic interactions between the groups of both polyelectrolytes are considered long-range; the CHS and CMC chains do not necessarily need to be relatively close for interaction between oppositely charged groups. Under these conditions, interactions only occur between the chains of the same polyelectrolyte, and the structure formed and/or maintained tends to a coiled state with a low degree of expansion. For solutions with higher pH values, the macro-PEC presents an expansion in its network due to the anion–anion repulsion between the CHS chains. There is, in these conditions, prevalence of hydrogen bonds. Interactions are no longer exclusively intrachain, so interactions between the chains of the same polyelectrolyte are also formed. The rearrangement of the chains causes most ordered regions to be formed. Samples immersed in solutions at pH 10 showed greater ordering of the chains and a consequent increase in their stability. It is also worth mentioning that the behavior of the lyophilized macro-PECs also depends on the time during which they remained immersed in each solution with different pH values.

In fact, as the pH increases, the degree of deprotonation of amino and carboxyl groups on the surface of the adsorbent becomes progressively

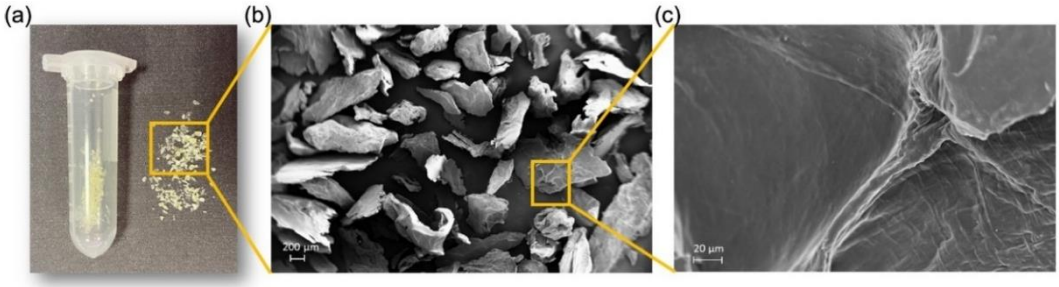

Fig. 3. (a) Visualization of micro-PECs after milling and SEM photomicrographs of PECs magnified by (b) 50× and (c) 1000×.

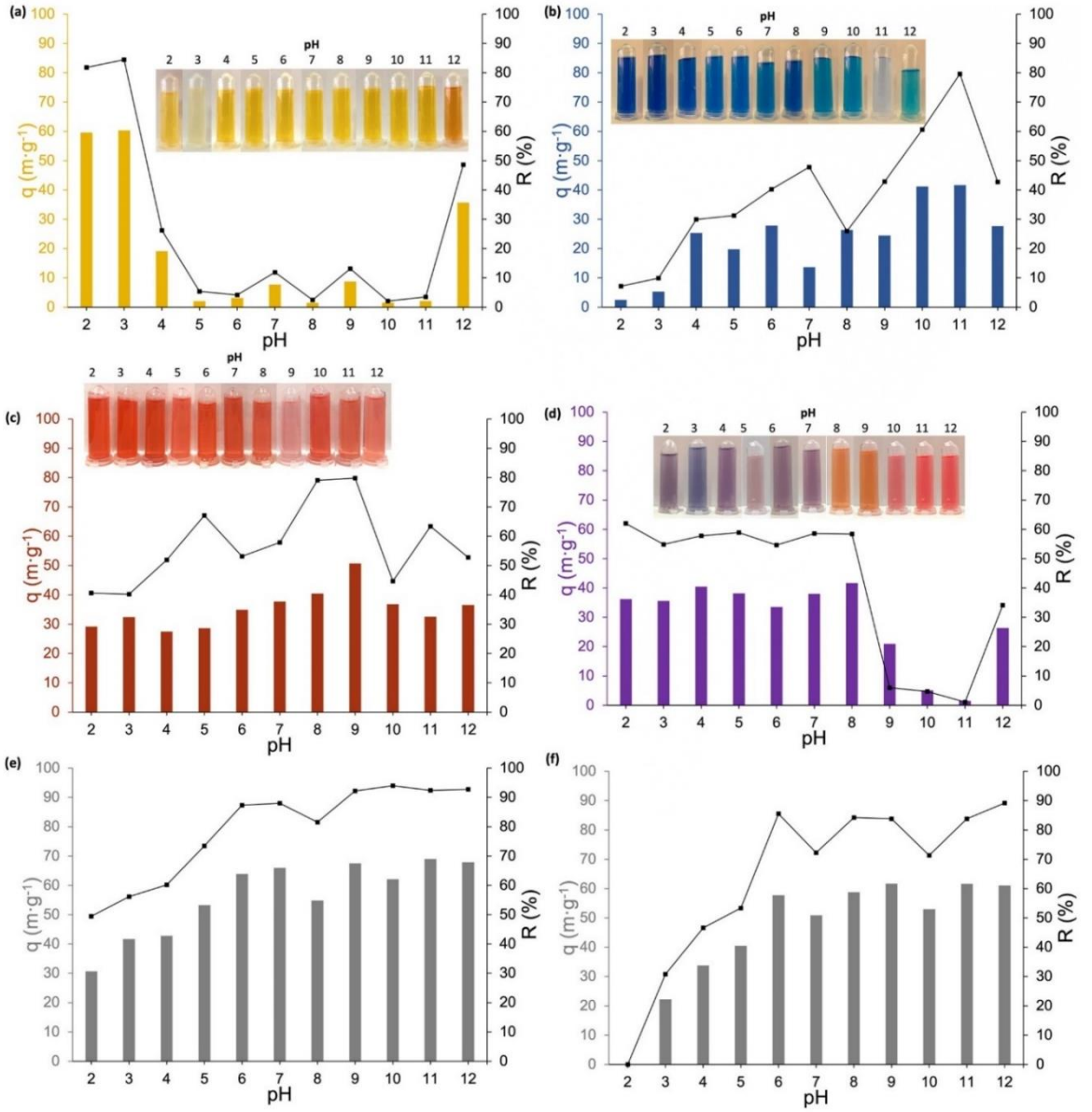

Fig. 4. Amounts of Yellow Sunset (a), Methylene Blue (b), Congo Red (c), Safranin (d), Cd^{2+} (e) or Pb^{2+} (f) adsorbed in mg per gram CHS/CMC macro-PECs (left vertical axis – bars) and their respective percentage of removal (right vertical axis – lines) at different pH values ranging from 2.0 to 12.0 and a temperature of 25 °C. (For interpretation of the references to colour in this figure legend, the reader is referred to the web version of this article.)

higher, and a greater negative charge density is generated in PECs (predominance of $-COO^-$ and $-NH_2$ over -COOH and $-NH_3^+$). This behavior increases the attractive electrostatic interactions between macro-PEC and cationic dyes. The opposite occured with anionic dyes, whose adsorption is favored at lower pH values, at which in PECs -COOH and $-NH_3^+$ groups are predominant over $-COO^-$ and $-NH_2$ (Mohammadzadeh Pakdel et al., 2022). This trend is in agreement with data depicted in Fig. 4a-d. On the other hand it is worthy emphasizsing that, since all four dyes studied are polyaromatic species (for dyes' molecular structures, please, see Suplementary Material), attractive aromatic interactions involving the aromatic rings (AR) interactions, namely anion-π and cation-π interactions – more specifically $-COO^-$…AR and $-NH_3^+$…AR – also play a non-negligeable role in these dyes adsorption onto CHS/CMS PECs' surface. This explains why there is some adsorption of all four studied dyes even when the pH of the medium lead to the predominance of charges of same sign in both PECs and dyes. Furthermore, dye molecules already adsorbed onto PECs form π-π interactions with other dye molecules coming from the solution, presumably constituting more than one layer of adsorbed molecules.

As depicted in Fig. 4e-f, the adsorption capacity of cadmium and lead

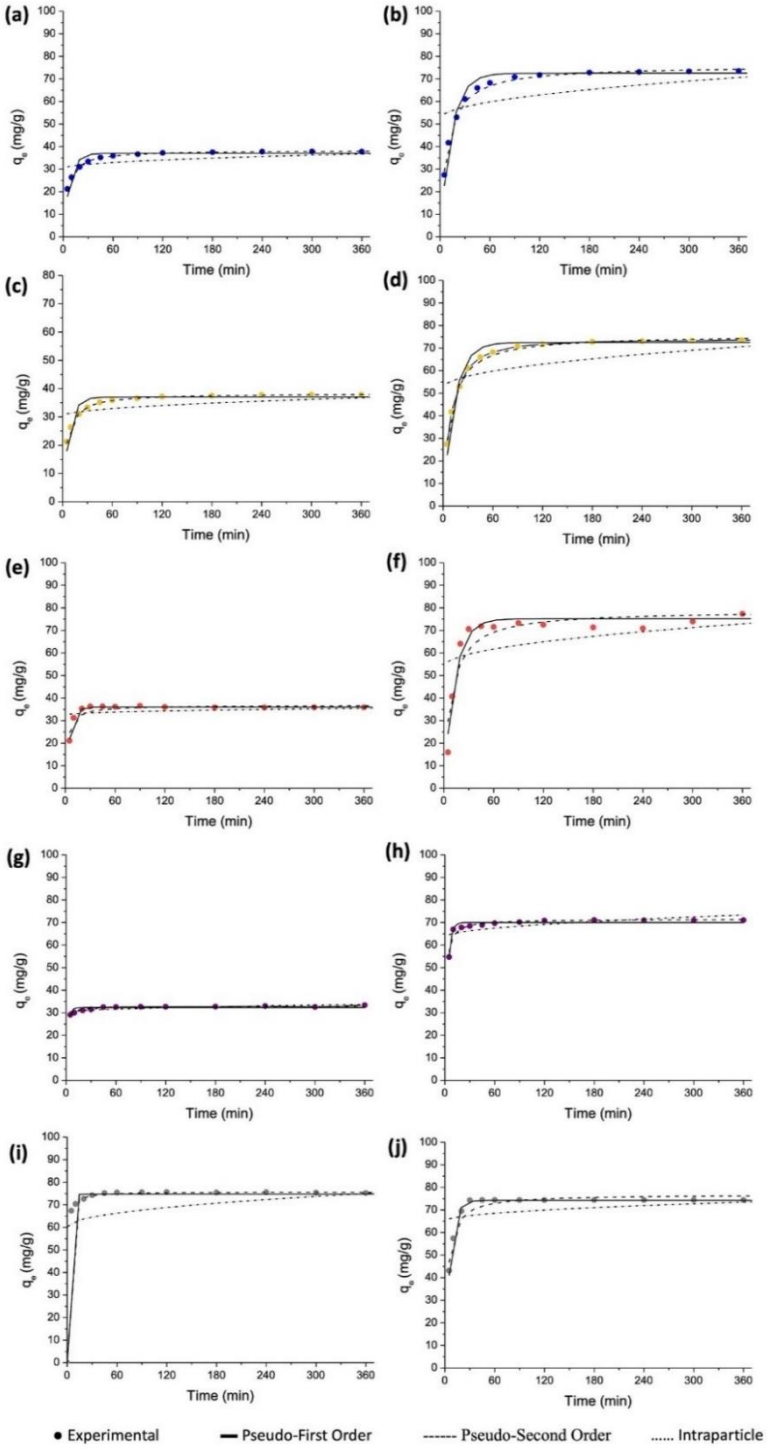

Fig. 5. Adsorption kinetics: (a) yellow sunset 25 mg/L; (b) yellow sunset 50 mg/L; (c) methylene blue 25 mg/L; (d) methylene blue 50 mg/L; (e) Congo red 25 mg/L; (f) Congo red 50 mg/L; (g) safranin 25 mg/L; (h) safranin 50 mg/L; (i) Cd^{2+} 50 mg/L; (j) Pb^{2+} 50 mg/L. (For interpretation of the references to colour in this figure legend, the reader is referred to the web version of this article.)

Table 1
Comparison of q_e, max (mg/g) for some dyes (MB, YS, and CR) and heavy metal cations (Pb^{2+} and Cd^{2+}) in adsorption on different adsorbents produced with CMC or CHS, as reported in literature.

Absorbent	Pollutant	q_e, max (mg/g)	Reference
CMC/ZIF-8 beads	MB	13.06	Marsiezade & Javanbakht, 2020
Chitosan/CMC hollow capsule		64.6	Kong et al., 2020
Chitosan grafted sodium acrylate-co-acrylamide	YS	17.97	Nagarpita et al., 2017
Chitosan grafted sodium acrylate-co-acrylamide/Nanoclay		73.41	
CMC grafted sodium acrylate-co-acrylamide		29.14	
CMC/Nanoclay grafted sodium acrylate-co-acrylamide		54.8	
Carboxymethyl chitosan hybrid montmorillonite	CR	74.01	Zhang et al., 2020
Chitosan		78.90	Wang & Wang, 2008
Carboxymethyl chitosan hybrid montmorillonite	Pb^{2+}	82.4	Zhang et al., 2020
Carboxymethyl cellulose/sugarcane bagasse/polydopamine		27.4	Furtado et al., 2022
Carboxymethylcellulose-chitosan-alkaline Ca-bentonite	Cd^{2+}	123	Wang et al., 2021
Carboxymethyl cellulose-hydroxyethyl cellulose hydrogel films		126.58	Ayouch et al., 2021

Although there are already investigations using natural materials to remove dyes from aqueous systems, sometimes the adsorption capacities of most of the reported adsorbents are limited, and sometimes the difficulty in obtaining or discarding them due to the use of crosslinking materials that contaminate hinders the use of these materials.

3.2.3. Adsorption isotherms

The experimental data and fitted isotherms are shown in Fig. 6. The calculated constants, k_L, R_L (Langmuir constant), k_f, n (Freundlich constants), k_R, α and β (Redlich–Peterson constants) – expressed in Eqs. (9), (10), and (11); Section 2.6.3 – for adsorption are shown in Table 3. As shown in Table 3, all models presented high fitting quality, as indicated by $R^2 > 0.95$ and R^2 adj > 0.952. In particular, the linear fit of the Langmuir isotherm model for the data showed that the adsorption of S, CR, Cd^{2+} and Pb^{2+} on CHS/CMC macro-PEC particles followed the Langmuir mechanism. The Langmuir isotherm assumes one-molecule-thick monolayer adsorption, with adsorption occurring at a finite number of localized specific sites, which are identical and equivalent, with no lateral interaction or steric hindrance between the adsorbed molecules, even at adjacent sites (López-Luna et al., 2019). Indeed, since R_L is the dimensionless equilibrium parameter that represents the equilibrium adsorption behavior, the adsorption phenomena are irreversible ($R_L = 0$), favorable ($0 < R_L < 1$), linear ($R_L = 1$), or unfavorable ($R_L > 1$) (Sahoo, Prelot, 2020a; Shin et al., 2021). The experimental R_L values also showed that the Langmuir model was fitted to the data and that the process was favorable for adsorption.

Chitosan–Vermiculite composite bead materials were used to efficiently remove sunset yellow FCF and brilliant blue FCF food dyes from the aqueous solution. The experimental data was better fitted the Langmuir model for YS, and the maximum adsorption capacity was 0.387 mol kg^{-1} (Şenol et al., 2020). On the other hand, methylene blue was removed by adsorption using naturally available chitin components, and the Freundlich isotherm was the model that best fitted the data (Karthi et al., 2022). The Langmuir isotherm model also showed adequacy in describing the removal of Safranin from an aqueous solution using as biosorbent a magnetic derivative of the tropical marine green calcareous algae *Cymopolia barbata* (Mullerova et al., 2019), as well as in the adsorption of Congo Red using Boehmite Microspheres (γ-AlOOH) (Wang et al., 2022). Basu et al. (2017) used cucumber peel as a bioadsorbent to remove Pb^{2+}. Satisfactory adsorption conditions were conducted at pH 5, the equilibrium time was reached in 1 h, and the kinetic model that best fitted the data were pseudo-second order. The Langmuir isotherm model was considered ideal for adsorption, with a maximum adsorption capacity of 133.60 mg/g. Khan Rao and Khatoon (2017) conducted a study to treat the bioadsorbent (leaves of *Casuarina equisetifolia*) using a 2 % solution of $NaAlO_2$ to remove Cu^{2+}, Pb^{2+}, and Ni^{2+} in aqueous solution. The maximum adsorption capacity of Pb^{2+} was 28 mg/g, following a Langmuir mechanism.

Considering that the Langmuir model is best suited to our experimental data, we can hypothesize that i) the adsorption consists mostly of monolayers of adsorbates on the CHS/CMC macro-PECs surface; ii) there is only negligible interaction between molecules adsorbed at different sites, iii) each site can contain only one adsorbed molecule; and iv) the heat of adsorption does not depend on the number of sites and is the same for all sites (Swenson & Stadie, 2019). Therefore, one can infer that the two biopolymers forming the adsorbent (CHS and CMC) were mixed in a microhomogeneous way, with no demixing on the microscopic scale and, consequently, producing an adsorbent material with a molecularly homogeneous surface. This behavior corroborates previous statements by Ferreira et al. (2022).

3.2.4. Desorption assays

Finally, this study included desorption tests for the dyes (Fig. 7a) and heavy metals (Fig. 7b). From Fig. 7a, it was noted that the maximum adsorption and desorption times for all dyes were approximately 120 min (Ci = 50 mg/L). Approximately 90 % of the YS dye was desorbed,

Table 2
Kinetic parameters obtained for the adsorption of yellow sunset, methylene blue, Congo red, safranin, Cd^{2+}, and Pb^{2+} on CHS/CMC macro-PECs at 25 °C.

Adsorbate	Concentration ($mg{\cdot}L^{-1}$)	pH	$q_{e,exp}/10^{-1}$ ($mg{\cdot}g^{-1}$)	Pseudo-first order $Q_t = Qe(1-e^{-k_1 t})$			Pseudo-second order $Q_t = \frac{k_2 Q_e^2 t}{1+k_2 Q_e t}$			Intraparticle $Q_t = k_d t^{0.5} + C$		
				$q_1/10^{-1}$ ($mg{\cdot}g^1$)	$k_1/10^1$ (min^1)	R^2	$q_1/10^1$ ($mg{\cdot}g^{-1}$)	$k_2/10^1$ ($g\ mg^{-1}\ min^{-1}$)	R^2	$k_i/10^{-1}$ ($mg{\cdot}g^{-1}{\cdot}min^{-0.5}$)	C	R^2
Yellow sunset	25	3.0	3.82	3.70	1.32	0.871	3.83	0.74	0.959	3.41	30.3	0.422
	50		7.52	7.27	0.06	0.997	7.59	0.01	0.997	9.64	52.3	0.431
Methylene blue	25	11.0	3.84	3.70	1.31	0.870	3.84	0.06	0.997	3.43	30.3	0.428
	50		7.52	7.25	0.74	0.959	7.59	0.02	0.995	9.64	52.3	0.431
Safranin	25	2.0	3.58	3.60	1.86	0.991	3.68	0.11	0.834	1.54	32.6	0.098
	50		7.74	7.51	0.77	0.953	7.89	0.02	0.889	9.97	53.9	0.306
Congo red	25	9.0	3.33	3.23	4.38	0.517	3.28	0.41	0.915	1.86	30.2	0.619
	50		7.10	7.00	3.03	0.938	7.15	0.11	0.939	5.22	63.4	0.357
Cd^{2+}	50	10.0	7.56	7.48	4.42	0.995	7.57	0.20	0.999	7.79	60.2	0.072
Pb^{2+}	50	9.0	7.40	7.43	1.59	0.988	7.69	0.04	0.927	4.43	65.1	0.126

k_1: pseudo-first order rate constant, k_2: pseudo second order rate constant, k_d: intraparticle diffusion rate constant, t: contact time, C: intercept of intraparticle diffusion plot.

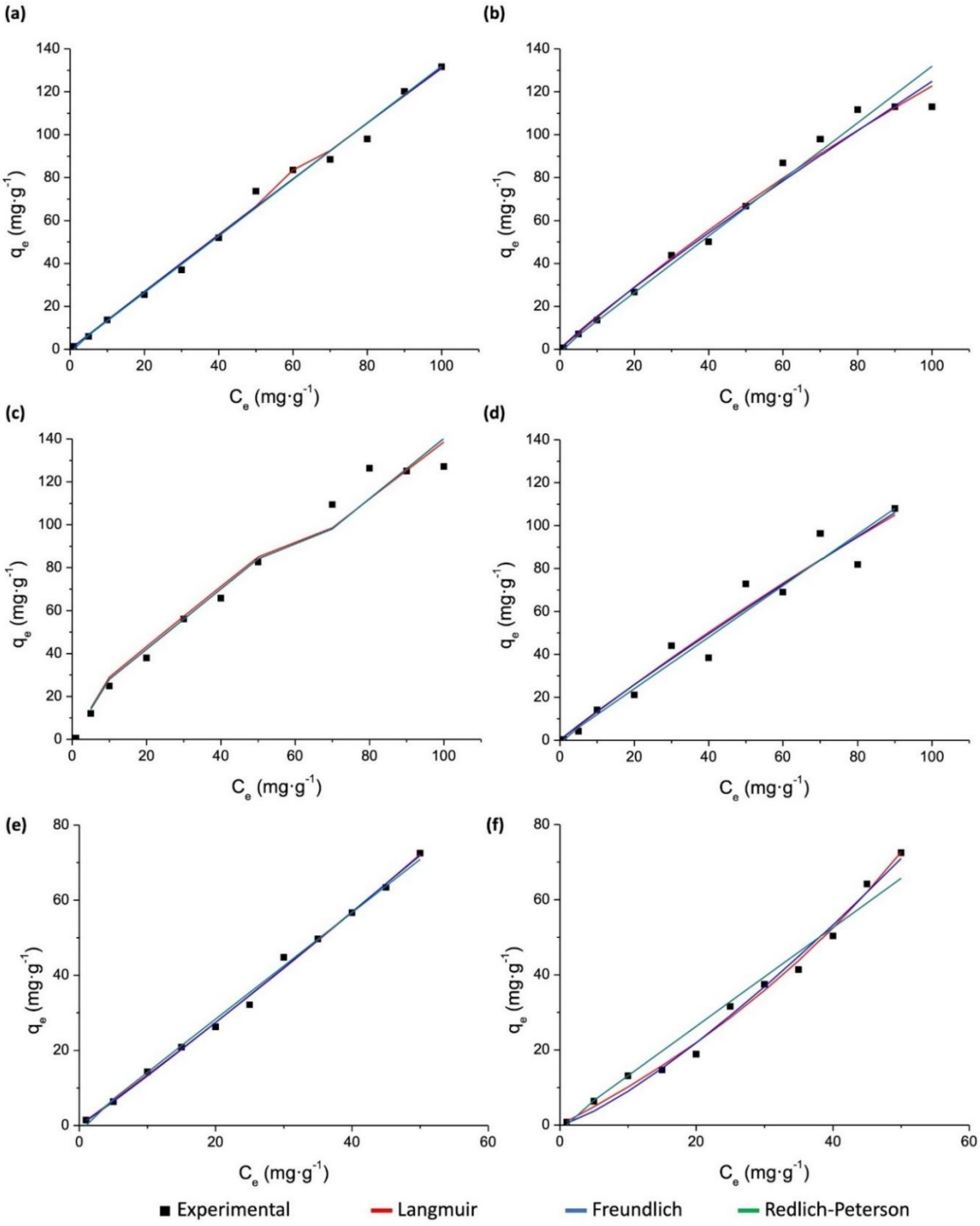

Fig. 6. Adsorption isotherms. (a) Yellow Sunset; (b) Methylene Blue; (c) Congo Red; (d) Safranin; (e) Cd^{2+}; (f) Pb^{2+}. Herein, colour lines represent the values predicted by the Langmuir, Freundlich and Redlich-Peterson equations. (For interpretation of the references to colour in this figure legend, the reader is referred to the web version of this article.)

Table 3
Kinetic parameters obtained for (a) Yellow Sunset; (b) Methylene Blue; (c) Congo Red; (d) Safranin; (e) Cd^{2+}; (f) Pb^{2+} removal using macro-PECs.

		Yellow sunset	Methylene blue	Safranin	Congo red	Cadmium	Lead
Langmuir	k_L /10^{-4} (dimensionless)	3.85	24.0	20.00	5.00	−20.00	−70.00
$Q_e = \frac{Q_m k_L C_e}{1 + Q_m C_e}$	Q_m /10^{-1} (mg·g^{-1})	2.84	9.99	3.83	4.43	3.78	5.16
	R^2	0.992	0.989	0.953	0.979	0.997	0.992
	R_{ajus}	0.990	0.989	0.952	0.977	0.997	0.990
Freundlich	k_F mg·g^{-1}) (L·mg^{-1})$^{1/n}$	1.39	1.39	1.39	1.39	1.18	0.47
$Qe = k_f C_e^{\frac{1}{n}}$	1/*n* (dimensionless)	0.99	0.91	1.00	0.94	1.05	1.29
	R^2	0.989	0.979	0.952	0.978	0.997	0.988
	R_{ajus}	0.989	0.978	0.950	0.978	0.996	0.986
Redlich-Peterson	k_R (dimensionless)	1.32	1.28	1.40	1.20	1.42	1.31
$Q_e = \frac{k_R C_e}{1 + \alpha C_e^{\beta}}$	α /10^3 (dimensionless)	7.35	−0.571	−1.18	−0.41	−1.18	−4.59
	β (dimensionless)	21.61	−3.30	−21.32	−18.00	−21.32	−26.91
	R^2	0.989	0.982	0.951	0.951	0.995	0.967
	R_{ajus}	0.988	0.981	0.950	0.949	0.995	0.966

70 % of the MB and S dyes, and 55 % of the CR dye. Cd^{2+} and Pb^{2+} were desorbed by 70 %. For the heavy metals studied, Cd^{2+} and Pb^{2+}, the adsorption took 30 min, and the desorption process took 90 min, indicating a slower desorption rate than adsorption.

Lower desorption may elucidate that adsorption is not fully reversible and that there are strong bonds between heavy metal molecules and the macro-PEC surface due to chemisorption. Therefore, the desorption mechanisms confirm that the adsorption of the studied pollutants governs both physical and chemical adsorption. In addition, these results corroborate that electrostatic interactions governed the binding of the dyes onto the surface of CHS/CMC macro-PEC particles since these substances were desorbed with NaOH or HCl solution. Reuse was possible for two cycles while maintaining the same adsorption capacity.

In addition, the desorption time was longer than the adsorption time of heavy metals by the macro-PECs, suggesting that adsorption was dominant and its environmental risk was low; that is, the adsorbed heavy metals would be released into the environment with less ease, representing a lower environmental risk. This also suggests that macro-PEC has a higher specific surface area and rich lattice structures, contributing to its high adsorption and low desorption performance. This significant retention capacity for heavy metal ions indicates the remarkable efficiency of macro-PECs as adsorbents.

The most widely used prevalent regeneration techniques for different adsorbentsare chemical and thermal regeneration. In chemical regeneration, different solvents (acid, base, or salt) mixed with used adsorbents are used to extract adsorbate. The regeneration efficiency of depleted adsorbents in the chemically modified regeneration technique depends on the adsorbate's solubility in solvents and can change the structure of the adsorbent. In our study, in acidic or basic aqueous solutions, pollutant desorption may have occurred due to the electrostatic repulsion of cations or anions (depending on the pollutant) from the adsorbent surface. Cationic pollutant molecules were attracted to negatively charged particles on the surface of the adsorbent, and anionic pollutant molecules were attracted to positively charged particles on the surface of the macro-PEC. The desorption process revealed that macro-PECs could be easily renewed and used repeatedly as recyclable and efficient adsorbents for practical use in treating effluents containing dyes and heavy metals.

Sponge-like Ti^{4+} cross-linked chitosan was synthesized for removing Orange II from wastewater. The maximum adsorption capacity was 1120 mg/g, and the adsorption and desorption times were approximately 120 min and 20 min, respectively (Co = 300 mg/L). The adsorption time was similar to that found in the present work, while the desorption time was shorter due to differences between the dyes, concentration, and adsorbent structures used. In the research by Allouss et al. (2019), approximately 83 % of the MB dye was desorbed, and the removal efficiency was maintained higher (76.07 %) even after four successive batches of adsorption-desorption cycles.

Continuous accumulation of pollutants in adsorbents gradually reduces their overall adsorption efficiency. It is a severe problem because the used adsorbent contains toxic substances that can be leached into the environment after disposal. To make adsorption a cyclical process, it is necessary, in addition to the adsorptive step, to desorb the components retained on the surface of the adsorbent, with the main objectives of restoring the adsorptive capacity of the adsorbent material and recovering the adsorbed compounds. Furthermore, the regeneration of depleted adsorbents improves the overall treatment cost and alleviates the adsorbent disposal problem. The most widely used prevalent regeneration techniques for different adsorbents are chemical and thermal regeneration. In chemical regeneration, different solvents (acid,

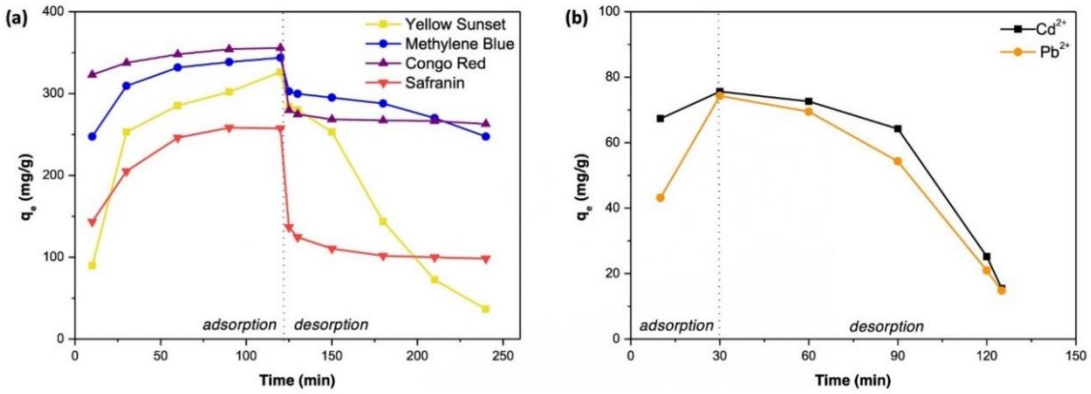

Fig. 7. Adsorption and desorption process for (a) yellow sunset, methylene blue, Congo red, and safranin dyes and (b) Cd^{2+} and Pb^{2+}. (For interpretation of the references to colour in this figure legend, the reader is referred to the web version of this article.)

base, or salt) mixed with used adsorbents are used to extract adsorbate.

The regeneration efficiency of depleted adsorbents in the chemically modified regeneration technique depends on the adsorbate's solubility in solvents and can change the structure of the adsorbent. In our study, in acidic or basic aqueous solutions, pollutant desorption may have occurred due to the electrostatic repulsion of cations or anions (depending on the pollutant) from the adsorbent surface. Cationic pollutant molecules were attracted to negatively charged particles on the surface of the adsorbent, and anionic pollutant molecules were attracted to positively charged particles on the surface of the macro-PEC. The desorption process revealed that macro-PECs could be easily renewed and used repeatedly as recyclable and efficient adsorbents for practical use in treating effluents containing dyes and heavy metals.

4. Conclusions

New applicability as adsorbents was successfully obtained for granular structures formed by the interaction between chitosan (CHS) and carboxymethylcellulose (CMC), namely CHS/CMC macro-PECs. This adsorbent demonstrated an excellent adsorption capacity for removing from aqueous medium the yellow sunset, methylene blue, Congo red, and safranin dyes, as well as the heavy metals cations Cd^{2+} and Pb^{2+}. In addition to high adsorption capacities, CHS/CMC macro-PECs showed rapid adsorption equilibrium, around 120 and 30 min for dyes and heavy metals, respectively. The Langmuir adsorption model fitted well the experimental data. The adsorption kinetics showed that the processes, depending on the type of adsorbate, followed the pseudo-first order or pseudo-second order models. Desorption assays indicated the plausibility of reuse of the CHS/CMC macro-PECs in batch processes. All the findings provide a new method for designing effective and recyclable adsorbents to improve the removal of anionic and cationic organic dyes and heavy metals. In other words, the obtained CHS/CMC macro-PECs are a promising adsorbent for the adsorption and separation of pollutants from larger volumes of industrial wastewaters. Adsortion assays in systems containing more than one pollutant are one of the next steps of this research.

CRediT authorship contribution statement

Danielle Cristine Mota Ferreira: Conceptualization, Investigation, Formal analysis, Methodology, Validation, Writing – original draft, Writing – review & editing. **Thaís Cristina dos Santos:** Conceptualization, Investigation, Formal analysis, Validation, Writing – original draft. **Jane Sélia dos Reis Coimbra:** Conceptualization, Resources, Funding acquisition, Writing – review & editing. **Eduardo Basílio de Oliveira:** Conceptualization, Methodology, Validation, Writing – review & editing, Supervision, Resources, Funding acquisition, Project administration.

Declaration of competing interest

The authors declare that they have no known competing financial interests or personal relationships that could have appeared to influence the work reported in this paper.

Data availability

Data will be made available upon reasonable request.

Acknowledgments

The authors are thankful to Brazilian research agencies CAPES for the scholarship of Ms. D. C. M. Ferreira (Process: 88882.437265/2019-01; Finance code: 001), FAPEMIG for financial support (Process: APQ-01457-18), and Professors Alexandre Gurgel and Leonardo Luiz Okumura (Department of Chemistry, UFV) who kindly provided $PbCl_2$ and $CdCl_2$ samples to perform the exploratory experiments.

Appendix A. Supplementary data

Supplementary data to this article can be found online at https://doi.org/10.1016/j.carbpol.2023.120977.

References

Abbasi, M. A., Rehman, A., Ali, Z., Atif, M., Ali, Z., & Khalid, W. (2022). Congo red removal by lanthanum-doped bismuth ferrite nanostructures. *Journal of Physics and Chemistry of Solids, 170*. https://doi.org/10.1016/j.jpcs.2022.110964

Allouss, D., Essamlali, Y., Amadine, O., Chakir, A., & Zahouily, M. (2019). Response surface methodology for optimization of methylene blue adsorption onto carboxymethyl cellulose-based hydrogel beads: Adsorption kinetics, isotherm, thermodynamics and reusability studies. *RSC Advances, 9*(65), 37858–37869. https://doi.org/10.1039/c9ra06450h

Alves, D. C. S., Coseglio, B. B., Pinto, L. A. A., & Cadaval, T. R. S. (2020). Development of Spirulina/chitosan foam adsorbent for phenol adsorption. *Journal of Molecular Liquids, 309*, Article 113256. https://doi.org/10.1016/j.molliq.2020.113256

Amran, F., & Zaini, M. A. A. (2021). Sodium hydroxide-activated casuarina empty fruit: Isotherm, kinetics and thermodynamics of methylene blue and Congo red adsorption. *Environmental Technology & Innovation, 23*, Article 101727. https://doi.org/10.1016/j.eti.2021.101727

Aragaw, T. A., & Bogale, F. M. (2021). Biomass-based adsorbents for removal of dyes from wastewater: A review. In *, 9. Frontiers in environmental science*. Frontiers Media S.A.. https://doi.org/10.3389/fenvs.2021.764958

Ayouch, I., Kassem, I., Kassab, Z., Barrak, I., Barhoun, A., Jacquemin, J., & Achaby, M. E. (2021). Crosslinked carboxymethyl cellulose-hydroxyethyl cellulose hydrogel films for adsorption of cadmium and methylene blue from aqueous solutions. *Surfaces and Interfaces, 24*, Article 101124. https://doi.org/10.1016/j.surfin.2021.1011

Basu, M., Guha, A. K., & Ray, L. (2017). Adsorption of lead on cucumber peel. *Journal of Cleaner Production, 151*, 603–615. https://doi.org/10.1016/j.jclepro.2017.03.028

Bhavyasree, P. G., & Xavier, T. S. (2021). Adsorption studies of Methylene Blue, Coomassie Brilliant Blue, and Congo Red dyes onto CuO/C nanocomposites synthesized via *Vitex negundo* Linn leaf extract. *Current Research in Green and Sustainable Chemistry, 4*, Article 100161. https://doi.org/10.1016/j.crgsc.2021.100161

Bravo-Yumi, N., Pacheco-Álvarez, M., Bandala, E. R., Brillas, E., & Peralta-Hernández, J. M. (2022). Studying the influence of different parameters on the electrochemical oxidation of tannery dyes using a Ti/IrO2-SnO2-Sb2O5 anode. *Chemical Engineering and Processing - Process Intensification, 181*, Article 109173. https://doi.org/10.1016/j.cep.2022.109173

Capanema, N. S. V., Mansur, A. A. P., Carvalho, S. M., Carvalho, I. C., Chagas, P., de Oliveira, L. C. A., & Mansur, H. S. (2018). Bioengineered carboxymethyl cellulose-doxorubicin prodrug hydrogels for topical chemotherapy of melanoma skin cancer. *Carbohydrate Polymers, 195*, 401–412. https://doi.org/10.1016/j.carbpol.2018.04.105

Chowdhury, I. R., Chowdhury, S., Mazumder, M. A. J., & Al-Ahmed, A. (2022). Removal of lead ions (Pb2+) from water and wastewater: A review on the low-cost adsorbents. *Applied Water Science, 12*(8). https://doi.org/10.1007/s13201-022-01703-6. Springer International Publishing.

Das, A., Kumar, A., Patil, N. B., Viswanathan, C., & Ghosh, D. (2015). Preparation and characterization of silver nanoparticle loaded amorphous hydrogel of carboxymethylcellulose for infected wounds. *Carbohydrate Polymers, 130*, 254–261. https://doi.org/10.1016/j.carbpol.2015.03.082

Elanchezhiyan, S. S., Karthikeyan, P., Rathinam, K., Hasmath Farzana, M., & Park, C. M. (2021). Magnetic kaolinite immobilized chitosan beads for the removal of Pb(II) and Cd(II) ions from an aqueous environment. *Carbohydrate Polymers, 261*. https://doi.org/10.1016/j.carbpol.2021.117892

Elemike, E. E., Onwudiwe, D. C., Ekennia, A. C., Ehiri, R. C., & Nnaji, N. J. (2017). Phytosynthesis of silver nanoparticles using aqueous leaf extracts of Lippia citriodora: Antimicrobial, larvicidal and photocatalytic evaluations. *Materials Science and Engineering C, 75*. https://doi.org/10.1016/j.msec.2017.02.161. Elsevier B.V.

Elgarahy, A. M., Elwakeel, K. Z., Mohammad, S. H., & Elshoubaky, G. A. (2021). A critical review of biosorption of dyes, heavy metals and metalloids from wastewater as an efficient and green process. *Cleaner Engineering and Technology, 4* (July), Article 100209. https://doi.org/10.1016/j.clet.2021.100209

Ferreira, D. C. M., Ferreira, S. O., de Alvarenga, E. S., Soares, N.d. F. F., Coimbra, J. S. d. R., & de Oliveira, E. B. (2022). Polyelectrolyte complexes (PECs) obtained from chitosan and carboxymethylcellulose: A physicochemical and microstructural study. *Carbohydrate Polymer Technologies and Applications, 3*(March). https://doi.org/10.1016/j.carpta.2022.100197

Fortunato, L., Elcik, H., Blankert, B., Ghaffour, N., & Vrouwenvelder, J. (2021). Textile dye wastewater treatment by direct contact membrane distillation: Membrane performance and detailed fouling analysis. *Journal of Membrane Science, 636*, Article 119552. https://doi.org/10.1016/j.memsci.2021.119552

Freitas-Silva, L., Diniz, N., & da Silva, L. C. (2021). Morphoanatomical and biochemical changes in Zeyheria tuberculosa exposed to glyphosate drift. *Botany, 99*, 91–98.

Furtado, L. M., et al. (20 December 2022). Carboxymethyl cellulose/sugarcane bagasse/polydopamine adsorbents for efficient removal of Pb^{2+} ions from synthetic and undergraduate laboratory wastes. *Journal of Cleaner Production, 380*(1), Article 134969. https://doi.org/10.1016/j.jclepro.2022.134969

Gadekar, M. R., & Ahammed, M. M. (2016). Coagulation/flocculation process for dye removal using water treatment residuals: Modelling through artificial neural networks. *Desalination and Water Treatment, 57*(55), 26392–26400. https://doi.org/10.1080/19443994.2016.1165150

Gupta, A., Sharma, V., Sharma, K., Kumar, V., Choudhary, S., Mankoria, P., Kumar, B., Misshra, H., Moulick, A., Ekielski, A., & Mishra, P. K. (2021). A review of adsorbents for heavy metal decontamination: Growing approach to wastewater treatment. *Materials, 14*, 4702. https://doi.org/10.3390/ma14164702

He, S., Zhong, S., Meng, Q., Fang, Y., Dou, Y., Gao, Y., & Cui, X. (2021). Sonochemical preparation of folate-decorated reductive-responsive carboxymethylcellulose-based nanocapsules for targeted drug delivery. *Carbohydrate Polymers, 266*. https://doi.org/10.1016/j.carbpol.2021.118174

Hubbe, M., Azizian, S., & Douven, S. (2019). Implications of apparent pseudo-second-order adsorption kinetics onto cellulosic materials: A review. *BioResources, 14*(3), 7582–7626. https://doi.org/10.15376/biores.14.3.7582-7626

Kafle, B. P. (2020). Theory and instrumentation of absorption spectroscopy. *Chemical Analysis and Material Characterization by Spectrophotometry, 17–38*. https://doi.org/10.1016/b978-0-12-814866-2.00002-6

Karthi, S., Sangeetha, R. K., Arumugam, K., Karthika, T., & Vimala, S. (2022). Removal of methylene blue dye using shrimp shell chitin from industrial effluents. *Materials Today: Proceedings, 66*, 1945–1950. https://doi.org/10.1016/j.matpr.2022.05.428

Khairy, M. G., Hesham, A. M., Jahin, H. E. S., El-Korashy, S. A., & Mahmoud Awad, Y. (2022). Green synthesis of a novel eco-friendly hydrochar from Pomegranate peels loaded with iron nanoparticles for the removal of copper ions and methylene blue from aqueous solutions. *Journal of Molecular Liquids, 368*. https://doi.org/10.1016/j.molliq.2022.120722

Khan Rao, R. A., & Khatoon, A. (2017). Aluminate treated Casuarina equisetifolia leaves as potential adsorbent for sequestering Cu(II), Pb(II) and Ni(II) from aqueous solution. *Journal of Cleaner Production, 165*, 1280–1295. https://doi.org/10.1016/j.jclepro.2017.07.160

Kong, Q., Wang, X., & Lou, T. (2020). Preparation of millimeter-sized chitosan / carboxymethyl cellulose hollow capsule and its dye adsorption properties. *Carbohydrate Polymers, 244*. https://doi.org/10.1016/j.carbpol.2020.116481

Kono, H., Onishi, K., & Nakamura, T. (2013). Characterization and bisphenol a adsorption capacity of β-cyclodextrin-carboxymethylcellulose-based hydrogels. *Carbohydrate Polymers, 98*(1), 784–792. https://doi.org/10.1016/j.carbpol.2013.06.065

Kotani, A., Hakamata, H., & Hayashi, Y. (2020). An automated assessment system of limits of detection and quantitation in gradient high-performance liquid chromatography with ultraviolet detection. *Journal of Chromatography A, 1621*. https://doi.org/10.1016/j.chroma.2020.461077

Kowalska, M., & Krzton-Maziopa, A. (2015). Viscoelastic effects in carrot oil emulsions thickened with carboxymethylcellulose. *Colloids and Surfaces A: Physicochemical and Engineering Aspects, 464*, 121–128. https://doi.org/10.1016/j.colsurfa.2014.10.008

Lahiri, S. K., Zhang, C., Sillanpää, M., & Liu, L. (2022). Nanoporous NiO@SiO2 photo-catalyst prepared by ion-exchange method for fast elimination of reactive dyes from wastewater. *Materials Today Chemistry, 23*. https://doi.org/10.1016/j.mtchem.2021.100677

Liu, L., Ma, Y., Yang, W., Chen, C., Li, M., Lin, D., & Pan, Q. (2020). Reusable ZIF-8@ chitosan sponge for the efficient and selective removal of Congo red. *New Journal of Chemistry, 44*(36), 15459–15466. https://doi.org/10.1039/d0nj02699a

López-Luna, J., Ramírez-Montes, L. E., Martinez-Vargas, S., et al. (2019). Linear and nonlinear kinetic and isotherm adsorption models for arsenic removal by manganese ferrite nanoparticles. *SN Applied Sciences, 1*(950). https://doi.org/10.1007/s42452-019-0977-3

Mahmoud, M. E., Abdelfattah, A. M., Tharwat, R. M., & Nabil, G. M. (2020). Adsorption of negatively charged food tartrazine and sunset yellow dyes onto positively charged triethylenetetramine biochar: Optimization, kinetics and thermodynamic study. *Journal of Molecular Liquids, 318*. https://doi.org/10.1016/j.molliq.2020.114297

Marsiezade, N., & Javanbakht, V. (2020). Novel hollow beads of carboxymethyl cellulose/ZSM-5/ZIF-8 for dye removal from aqueous solution in batch and continuous fixed bed systems. *International Journal of Biological Macromolecules, 162*, 1140–1152. https://doi.org/10.1016/j.ijbiomac.2020.06.229

McCabe, W. L., Smith, J., & Harriot, P. (2004). *Unit Operations of Chemical Engineering* (7th ed., Vol. 1). McGraw-Hill Science/Engineering/Math.

Mohammadzadeh Pakdel, P., Peighambardoust, S. J., Arsalani, N., & Aghdasinia, H. (2022). Safranin-O cationic dye removal from wastewater using carboxymethyl cellulose-grafted-poly(acrylic acid-co-itaconic acid) nanocomposite hydrogel. *Environmental Research, 212*, Article 113201. https://doi.org/10.1016/j.envres.2022.113201

Mullerova, S., Baldikova, E., Prochazkova, J., Pospiskova, K., & Safarik, I. (2019). Magnetically modified macroalgae cymopolia barbata biomass as an adsorbent for safranin O removal. *Materials Chemistry and Physics, 225*, 174–180. https://doi.org/10.1016/j.matchemphys.2018.12.074

Nagarpita, M. V., et al. (2017). Synthesis and swelling characteristics of chitosan and CMC grafted sodium acrylate-co-acrylamide using modified nanoclay and examining its efficacy for removal of dyes. *International Journal of Biological Macromolecules, 102*, 1226–1240. https://doi.org/10.1016/j.ijbiomac.2017.04.099

Nguyen, H. T., Ngwabebhoh, F. A., Saha, N., Saha, T., & Saha, P. (2022). Gellan gum/bacterial cellulose hydrogel crosslinked with citric acid as an eco-friendly green adsorbent for safranin and crystal violet dye removal. *International Journal of Biological Macromolecules, 222*, 77–89. https://doi.org/10.1016/j.ijbiomac.2022.09.040

Qi, X., Tong, X., Pan, W., Zeng, Q., You, S., & Shen, J. (2021). Recent advances in polysaccharide-based adsorbents for wastewater treatment. *Journal of Cleaner Production, 315*, Article 128221. https://doi.org/10.1016/j.jclepro.2021.128221

Qu, M., He, D., Luo, Z., Wang, R., Shi, F., Pang, Y., Sun, W., Peng, L., & He, J. (2022). Facile preparation of a multifunctional superhydrophilic PVDF membrane for highly efficient organic dyes and heavy metal ions adsorption and oil/water emulsions separation. *Colloids and Surfaces A: Physicochemical and Engineering Aspects, 637* (December 2021), Article 128231. https://doi.org/10.1016/j.colsurfa.2021.128231

Ren, H., Gao, Z., Wu, D., Jiang, J., Sun, Y., & Luo, C. (2016). Efficient Pb(II) removal using sodium alginate-carboxymethyl cellulose gel beads: Preparation, characterization, and adsorption mechanism. *Carbohydrate Polymers, 137*, 402–409. https://doi.org/10.1016/j.carbpol.2015.11.002

Revellame, E. D., Fortela, D. L., Sharp, W., Hernandez, R., & Zappi, M. E. (2020). Adsorption kinetic modeling using pseudo-first order and pseudo-second order rate laws: A review. *Cleaner Engineering and Technology, 1*(December), Article 100032. https://doi.org/10.1016/j.clet.2020.100032

Sadiq, A. C., Olasupo, A., Ngah, W. S. W., Rahim, N. Y., & Suah, F. B. M. (2021). A decade development in the application of chitosan-based materials for dye adsorption: A short review. *International Journal of Biological Macromolecules, 191*(July), 1151–1163. https://doi.org/10.1016/j.ijbiomac.2021.09.179

Sahoo, T. R., & Prelot, B. (2020a). Adsorption processes for the removal of contaminants from wastewater. In *Nanomaterials for the Detection and Removal of Wastewater Pollutants* (pp. 161–222). Elsevier. https://doi.org/10.1016/B978-0-12-818489-9.00007-4.

Sahoo, T. R., & Prelot, B. (2020b). Adsorption processes for the removal of contaminants from wastewater: The perspective role of nanomaterials and nanotechnology. In *Nanomaterials for the Detection and Removal of Wastewater Pollutants* (pp. 161–222). Elsevier. https://doi.org/10.1016/B978-0-12-818489-9.00007-4.

Sahu, D. K., Rai, J., Rai, M. K., Banjare, M. K., Nirmal, M., Wani, K., Sahu, R., Pandey, S. G., & Mundeja, P. (2020a). Detection of flonicamid insecticide in vegetable samples by UV–Visible spectrophotometer and FTIR. *Results in Chemistry, 2*, Article 100059. https://doi.org/10.1016/j.rechem.2020.100059

Sahu, D. K., Rai, J., Rai, M. K., Banjare, M. K., Nirmal, M., Wani, K., Sahu, R., Pandey, S. G., & Mundeja, P. (2020b). Detection of flonicamid insecticide in vegetable samples by UV–Visible spectrophotometer and FTIR. *Results in Chemistry, 2*. https://doi.org/10.1016/j.rechem.2020.100059

Şenol, Z. M., Gürsoy, N., Şimşek, S., Özer, A., & Karakuş, N. (2020). Removal of food dyes from aqueous solution by chitosan-vermiculite beads. *International Journal of Biological Macromolecules, 148*, 635–646. https://doi.org/10.1016/j.ijbiomac.2020.01.166

Sh. Gohr, M., Abd-Elhamid, A. I., El-Shanshory, A. A., & Soliman, H. M. A. (2022). Adsorption of cationic dyes onto chemically modified activated carbon: Kinetics and thermodynamic study. *Journal of Molecular Liquids, 346*, 118227. https://doi.org/10.1016/j.molliq.2021.118227

Shi, Y., Wang, X., Wang, X., Carlson, K., & Li, Z. (2021). Removal of toluidine blue and safranin o from single and binary solutions using zeolite. *Crystals, 11*(10). https://doi.org/10.3390/cryst11101181

Shin, J., Lee, Y.-G., Kwak, J., Kim, S., Lee, S.-H., Park, Y., Lee, S.-D., & Chon, K. (2021). Adsorption of radioactive strontium by pristine and magnetic biochars derived from spent coffee grounds. *Journal of Environmental Chemical Engineering, 9*(2), Article 105119. https://doi.org/10.1016/j.jece.2021.105119

Sousa, H. R., Silva, L. S., Sousa, P. A. A., Sousa, R. R. M., Fonseca, M. G., Osajima, J. A., & Silva-Filho, E. C. (2019). Evaluation of methylene blue removal by plasma activated palygorskites. *Journal of Materials Research and Technology, 8*(6), 5432–5442. https://doi.org/10.1016/j.jmrt.2019.09.011

Stozhko, N. Y., Khamzina, E. I., Bukharinova, M. A., & Tarasov, A. V. (2022). An electrochemical sensor based on carbon paper modified with graphite powder for sensitive determination of sunset yellow and tartrazine in drinks. *Sensors, 22*(11), 4092. https://doi.org/10.3390/s22114092

Sultana, M., Rownok, M. H., Sabrin, M., Rahaman, M. H., & Alam, S. M. N. (2022). A review on experimental chemically modified activated carbon to enhance dye and heavy metals adsorption. *Cleaner Engineering and Technology, 6*, Article 100382. https://doi.org/10.1016/j.clet.2021.100382

Swenson, H., & Stadie, N. P. (2019). Langmuir's theory of adsorption: A centennial review. *Langmuir, 35*(16), 5409–5426. https://doi.org/10.1021/acs.langmuir.9b00154

Tang, R., Wang, Z., Muhammad, Y., Shi, H., Liu, K., Ji, J., Zhu, Y., Tong, Z., & Zhang, H. (2020). Fabrication of carboxymethyl cellulose and chitosan modified magnetic alkaline ca-bentonite for the adsorption of hazardous doxycycline. *Colloids and Surfaces A: Physicochemical and Engineering Aspects, 125730*. https://doi.org/10.1016/j.colsurfa.2020.12

Wang, D., Li, Z., Lv, F., Guan, M., Chen, J., Wu, C., Li, Y., Li, Y., & Zhang, W. (2022). Characterization of microspheres γ-AlOOH and the excellent removal efficiency of Congo red. *Journal of Physics and Chemistry of Solids, 111043*. https://doi.org/10.1016/j.jpcs.2022.111043

Wang, L., & Wang. (2008). Adsorption properties of congo red from aqueous solution onto N,O-carboxymethyl-chitosan. *Bioresource Technology, 99*, 1403–1408.

Wang, Y., Zhang, H., Yaseen, M., Tong, Z., Chen, N., & Shi, H. (2021). Carboxymethylcellulose-chitosan film modified magnetic alkaline ca-bentonite for the efficient removal of Pb(II) and Cd(II) from aqueous solution. *Environmental Science and Pollution Research*. https://doi.org/10.1007/s11356-020-12156-2

Wu, C., Scott, J., & Shea, J. E. (2012). Binding of Congo red to amyloid protofibrils of the Alzheimer Aβ9-40 peptide probed by molecular dynamics simulations. *Biophysical Journal, 103*(3), 550–557. https://doi.org/10.1016/j.bpj.2012.07.008

Xu, K., Li, L., Huang, Z., Tian, Z., & Li, H. (2022). Efficient adsorption of heavy metals from wastewater on nanocomposite beads prepared by chitosan and paper sludge. *SSRN Electronic Journal, 846*(June), Article 157399. https://doi.org/10.2139/ssrn.4144064

Yayayürük, O., Erdem Yayayürük, A., Özmen, P., & Karagöz, B. (2020). PDMAEMA grafted microspheres as an efficient adsorbent for the removal of sunset yellow from pharmaceutical preparations, beverages and waste water. *European Polymer Journal, 141*. https://doi.org/10.1016/j.eurpolymj.2020.110089

Zhang, H., Ma, J., Wang, F., Chu, Y., Yang, L., & Xia, M. (2020). Mechanism of carboxymethyl chitosan hybrid montmorillonite and adsorption of Pb(II) and Congo red by CMC-MMT organic-inorganic hybrid composite. *International Journal of Biological Macromolecules*. https://doi.org/10.1016/j.ijbiomac.2020.01.201

Zhang, S., Fan, X., & Xue, J. (2023). A novel magnetic manganese oxide halloysite composite by one-pot synthesis for the removal of methylene blue from aqueous solution. *Journal of Alloys and Compounds, 930*, Article 167050. https://doi.org/10.1016/j.jallcom.2022.167050

Zhao, J., Xing, T., Li, Q., Chen, Y., Yao, W., Jin, S., & Chen, S. (2020). Preparation of chitosan and carboxymethylcellulose-based polyelectrolyte complex hydrogel via SD-A-SGT method and its adsorption of anionic and cationic dye. *Journal of Applied Polymer Science, 48980*. https://doi.org/10.1002/app.4898

Zhu, H., et al. (15 March 2023). Removal of anionic and cationic dyes using porous chitosan/carboxymethyl cellulose-PEG hydrogels: Optimization, adsorption kinetics, isotherm and thermodynamics studies. *International Journal of Biological Macromolecules, 231*, Article 123213. https://doi.org/10.1016/j.ijbiomac.2023.123213

Supplementary Material (SM) II - "Chitosan/carboxymethylcellulose polyelectrolyte complexes are an effective material for dye and heavy metal adsorption from water"

I.Dye`s information

Table SM1 - Maximum absorption wavelengths for dyes

Dye	Maximum absorption wavelength ($\lambda_{máx}$)	Structural model	pKa
Yellow Sunset	228 nm	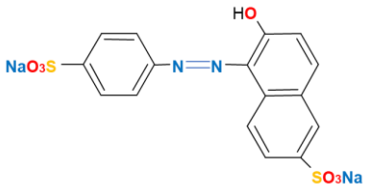	9.4 (Stozhko et al., 2022)
Methylene Blue	284 nm	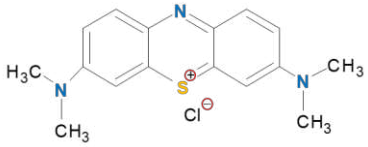	3.8 (Sousa et al., 2019)
Congo Red	277 nm	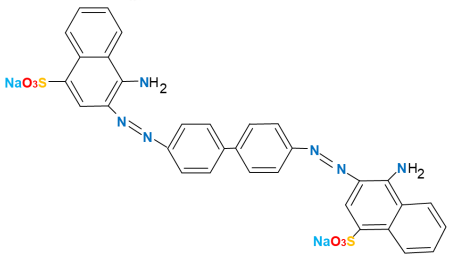	4.0 (Wu et al., 2012)
Safranin	277 nm	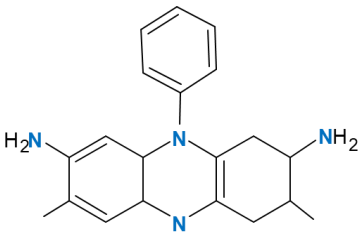	11 (Shi et al., 2021)

II. Validation of analytical methods

Figure SM1 – Calibration curve for (a) sunset yellow, (b) methylene blue, (c) congo red and (d) safranin.

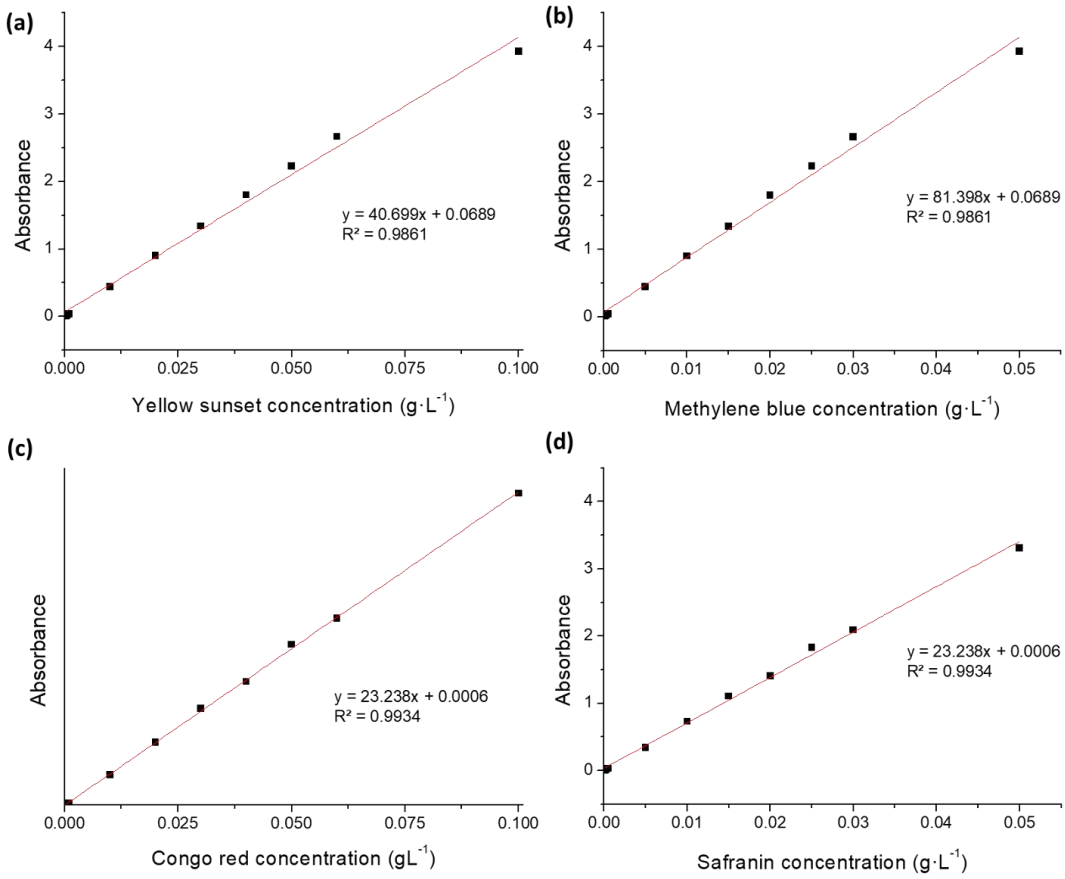

Table SM2 - Equations of straight lines, coefficient of determination (R^2), limits of detection (LD), limit of quantification (LQ) and precision (P) for Sunset Yellow (λ_{max} = 228 nm), methylene blue (λ_{max} = 284 nm), congo red (λ_{max} = 277 nm) and safranin (λ_{max} = 277 nm) .

Dye	Equation	R^2	LD	LQ	P
Yellow sunset	y=41.078 (±1.22647) x +0.057 (±0.0536)	0.9861	6,17E-05	0,0002	96% ± 0.043
Methylene blue	y=82.156 (±2.45294) x+0.0057 (±0.0536)	0.9861	1,54E-05	0,00005	93% ± 0.018
Congo red	y = 23.238 (±0.1511) x + 0.0006 (±0.0066)	0.9996	7.58E-05	0.000253	95% ± 0.040
Safranin	y=23.238 (±1.31915) x + 0.0006 (±0.02883)	0.9966	1.32E-05	4.39E-05	98% ± 0.001

CAPÍTULO 4

MICROSTRUCTURED CHITOSAN/ CARBOXYMETHYLCELLULOSE POLYELECTROLYTE COMPLEXES AS A NOVEL AND EFFICIENT MATERIAL FOR CARRYING AND CONTROLLED RELEASE OF NIACINAMIDE

Abstract

In this study, polyelectrolyte micro-complexes (micro-PECs) based on chitosan and carboxymethylcellulose, carrying niacinamide as the active component, were prepared by complex coacervation processing. The Box-Behnken experimental design was adopted to study the effects of three independent variables – processing time, namely X_1 (60, 120, and 180 min); pH, namely X_2 (3, 4, and 5); and niacinamide concentration, namely X_3 (0.02, 0.04, and 0.06 g·L-1), on the encapsulation efficiency (Y_1) and binding capacity (Y_2) of CMC/CHS micro-PECs to niacinamide. The encapsulation efficiency (Y_1) and loading capacity (Y_2) varied between 0.86 and 80.78%, and 0.03 and 3.89%, respectively. It was found that both responses studied (Y_1 and Y_2) had effects mainly from the pH of the medium. The *in vitro* digestibility of CMC/CHS micro-PECs containing niacinamide was evaluated using a static gastrointestinal model. Four kinetic models were fitted to the niacinamide release kinetics data: Zero Order, First Order, Higuchi, and Korsemeyer-Peppas. The zero-order model showed the best fit at all points (gastric and enteric digestion) with low zero-order constants ($K_0 = 0.002$ - 0.003) and similar for all systems studied, demonstrating a low release rate.

Keywords

Supramolecular structures. Vitamin B3. Carrier systems. Controlled release. Release kinetics.

List of symbols and abbreviations

A	Accuracy
K_H	Higuchi constant
K_0	Zero ordem constant
K_1	First-ordem constant
CHS	Chitosan
CMC	Carboxymethylcellulose
EE	Efficiency encapsulation
$K_{K\text{-}P}$	Korsemeyer-Peppas constant
LC	Loading capacity
LD	Limits of Detection
LQ	Limit of Quantification
m	Macro-PEC mass
Micro-PEC	Polyelectrolyte complex macroscopic
n	Diffusion or release exponent
PEC	Polyelectrolyte complex
Q	Cumulative percentage of liberated released material niacinamide
Q_0	Initial cumulative percentage of niacinamide
t	Processing time
UV	Ultraviolet
X_1	Processing time
X_2	pH
X_3	Niacinamide concentration
Y_1	Efficiency encapsulation
Y_1	Loading capacity

1. INTRODUCTION

Supramolecular structures resulting from the association of two or more different molecular species have attracted the attention of academic and industrial researchers, especially due to their differentiated properties which are generally superior to those of the forming species alone, in terms of both structural complexity and functionality scope (Hernández et al., 2020; Monteiro et al., 2016). Their formation usually occurs through the coordinated self-assembly of several macromolecular components and can be either enthalpically or entropically driven (Croguennec et al., 2017; Edwardson et al., 2020; Sing & Perry, 2020; Zhou et al., 2020). Supramolecular structures have been investigated over the last two decades as biomaterials, due to their low cytotoxicity and controllable sizes and architecture, having great relevance in the intersection of biological, chemical, and physical sciences (Hernández et al., 2020; Monteiro et al., 2016; Zhang et al., 2021).

Interactions between bioactive compounds and supramolecular structures, used as carrier systems, represent a key aspect in current scientific research in the medical-pharmaceutical, cosmetic, and food areas since the inclusion of such biologically active compounds in different carriers (or excipients) can impact their stability or even their bioavailability. Bioactive compounds, administered through a supramolecular carrier, often exhibit improved release kinetics and/or biological profiles, different from those observed when they are administered in readily bioavailable forms (Baek et al., 2021; Mejías et al., 2019; Miao & Janaswamy, 2021; Patterson & Smith, 2020). Therefore, carrier systems for bioactive compounds have been used to increase their bioavailability (Goto et al., 2015), enhance their thermal and oxidative stability (Belingheri et al., 2015; Shahparast et al., 2019), ~~to~~ overcome volatility limitations (Belingheri et al., 2015; Mamusa et al., 2021), ~~to~~ improve their stability in biological media (Peng et al., 2019), maintain and ~~to~~ control release rates (Wilson et al., 2021), and even ~~to~~ target them to specific sites in the biological environment (Rebouças et al., 2023). In view of this, efforts have been focused on improving the carrying materials and processes, including the use of new combinations of carrier systems/bioactive compounds, as recently summarized in a review paper by Premjit et al., 2022.

The inclusion of bioactive compounds in microcapsules or microparticles formed by biopolymers has been gaining ground in order to improve the carrying efficiency, controlled release accuracy, and response of these bioactives to handling conditions (Alu'datt et al., 2022). Complex coacervation, which consists of the formation of supramolecular structures from two oppositely charged polyelectrolytes, is a highly applicable technique for obtaining safe,

biocompatible, and effective carrier systems for bioactive compounds (Sing & Perry, 2020; Zhou et al., 2020). The resulting supramolecular complexes are a strategic alternative for the food industry ue to the use of food-grade proteins and/or polysaccharides to fabricate them, as well as their high encapsulation efficiency (Chen et al., 2020), production process repeatability, low processing costs, and synthesis at room temperature in aqueous media without organic solvents (Timilsena et al., 2019). Indeed, in a few words, their obtaining process involves essentially the mixing of aqueous dispersions of the negatively and the positively charged biopolymers at controlled pH, temperature, and mixing rate, to achieve an optimal biopolymers' ratio, forming polyelectrolytes complexes (micro-PECs) in dispersion.

Carboxymethylcellulose (CMC) and chitosan (CHS) are two biopolymers with outstanding biodegradability, biocompatibility, non-toxicity, low cost, and legally allowed for use in food (Agrisexport, n.d.; BRASIL, 1999). Ferreira et al. (2022) investigated the effects of the mixing ratio of chitosan (CHS) to carboxymethylcellulose (CMC) (1:0; 4:1; 3:1; 2:1; 1:1; 1:2; 1:3; 1:4; 0:1), temperature (25; 45; 65; 85 ºC) and pH (3.0; 3.5; 4.0; 4.5) in obtaining complex macro and micropolyelectrolytes (PEC). The micro-PECs presented themselves as dispersed colloidal particles, classified as amorphous and thermally stable, more stable than the biomolecules that form separately, with potential applicability in areas such as encapsulation and controlled release of bioactives. However, to the best of our knowledge, the related literature lacks reports on the application of CMC/CHS micro-PECs, without the presence of cross-linking and possibly toxic agents, as vehicles for bioactive compounds, such as vitamins.

Vitamins are essential micronutrients for the proper functioning of living organisms, acting mainly as catalysts in a plethora of physiological reactions (Maiorova et al., 2019). B vitamins play a crucial role in neurochemical pathways, including those mediated by serotonin, noradrenalin, dopamine, acetylcholine, gamma-aminobutyric acid (GABA), and glutamate (Massey et al., 2022; Rathee et al., 2022). Among B vitamins, "vitamin B3", naturally found in foods like wheat, corn, barley, rye, soybean oil meal, linseed, cowpeas, alfalfa, among others encompasses two substances: nicotinamide (or niacinamide) and nicotinic acid (or niacin) (Belitz et al., 2009; Kreetl et al., n.d.). Niacinamide is a water-soluble compound that contributes to catalyzing redox reactions involving electron and hydrogen acceptance and/or donation, essential for crucial metabolic processes (Suo et al., 2022). Furthermore, it has been suggested that niacinamide can prevent type 1 diabetes mellitus and ~~that it~~ has anti-inflammatory properties (Refat et al., 2017; Yan & Wang, 2021; Yanez et al., 2019; Yu & Zhao, 2007). Considering these biofunctionalities and health benefits of regular niacinamide consumption, either ingested or topically applied, but also its instability at processing

temperatures and usual storage conditions (Campbell et al., 2019; Fan et al., 2018), the search for improved ways to incorporate it into food and pharmaceutical formulations appears nowadays as a relevant and challenging task.

Given the scenario described so far, the novelty brought by the present study is the evaluation, for the first time, of the performance of CMC/CHS micro-PECs for carrying and controlled release of niacinamide, thus assessing the applicability of such micro-PECs as a carrier for a hydrophilic vitamin to be used in food formulations. More specifically, we investigated the influence of pH, initial niacinamide concentration within the medium, and reaction time on niacinamide-loaded CMC/CHS micro-PECs production. These micro-PECs had their performance examined in terms of encapsulation efficiency, loading capacity, and release rates of niacinamide throughout the time in an *in vitro* digestion model.

2. MATERIALS AND METHODS

2.1. Materials

Chitosan (Low Molecular Weight, Sigma-Aldrich Corporation, USA; Product ID = 448877; Batch Number = #LBG4282 V) obtained from fresh *Pandalus boralis* shrimp shell was washed three times with deionized water to reduce water-soluble chito-oligosaccharides and salt residues, before use in the experiments. Chitosan was characterized in terms of degree of deacetylation (76.7%), and viscometric average molar mass (364 ± 10 kDa). Carboxymethylcellulose was characterized in terms of degree of substitution (0.59 ± 0.03), and viscometric average molar mass (794 ± 8 kDa) (Ferreira et al., 2022). (Sigma-Aldrich Corporation, USA; Product ID=419311). The other chemical reagents used are analytical grade and used without any purification process: hydrochloric acid (Sigma-Aldrich, Brazil, 37% by weight in H2O) and sodium hydroxide (Sigma-Aldrich, Brazil). Deionized water was obtained ~~at~~ from a Milli-Q system (18.2 MΩcm^{-1}, 25 °C; Reference A+, Millipore, Italy) and it was used in all experiments. Niacinamide was supplied by Sigma-Aldrich, with higher purity at 98% (Product ID=N3376).

2.2 Determination of niacinamide concentration and validation of analytical methods

For the analysis of the niacinamide after the adsorption processes, standard curves were determined by Ultraviolet–visible spectroscopy, monitoring the absorbance at the maximum absorption wavelengths according to Lambert's Law- Beer (Kafle, 2020).

The calibration curve of the niacinamide standard solution was developed from 0.5 $g \cdot dL^{-1}$. Absorption spectra were obtained in the wavelength range of 228 nm using a UV-Vis spectrophotometer (UV 1800, Shimadzu, Japan). Quartz cuvettes, with an optical path equal to 1 cm, were used in the spectrophotometer for the analyzes. Absorbance analyzes were performed in triplicate.

The detection limit (DL), corresponding to the lowest concentration in the sample that can be detected, and the quantification limit (QL), which is equivalent to the lowest concentration in the sample that can be quantified, were estimated from the calibration curve resulting from the parameter linearity (Administration), 2014).

The calculation to determine the values corresponding to the LD and LQ was based on the standard deviation of the residual of the regression line and its relationship with the slope of the line (angular coefficient) in the analytical curve, following the Equation 1 and 2:

$$DL = \frac{(3 \cdot SD)}{m} \qquad \text{Equation 1}$$

$$QL = \frac{(10 \cdot SD)}{m} \qquad \text{Equation 2}$$

In which SD is the standard deviation of the intercept with respect to the Y axis, and m is the slope value of the analytical curve.

The accuracy of an assay is characterized by its ability to produce the correct value if an infinite number of repetitions are performed (Sahu et al., 2020). In this work, the accuracy (A) was obtained through Equation 3, which relates the concentration calculated by the calibration curve and the absorbance values read, in triplicate, for a standard solution (Cc) of vitmamin B3 and the expected concentration (Ce).

$$A(\%) = \frac{(C_c)}{C_e} \qquad \text{Equation 3}$$

Accuracy, which corresponds to the variability of the results around the mean value (coefficient of variation) (Sahu et al., 2020), was expressed as the relative standard deviation of three concentrations, calculated using the absorbance values obtained at the same concentration of a standard solution and the calibration curve.

2.3. CMC/CHS micro-PECs production

2.3.1 Experimental design

The Box-Behnken experimental design was used adopted to study the effects of three independent variables – processing time, namely X_1 (60, 120, and 180 min), pH, X_2 (3, 4, and 5) and niacinamide concentration, X_3 (0.02, 0.04, and 0.06, $g \cdot L^{-1}$), as well as the possible interaction between these independent variables among them, on encapsulation efficiency and binding capacity of CMC/CHS micro-PECs towards niacinamide. All 15 experimental series treatments are presented in Table 1. Treatment 13 represents the central point, which was performed with three repetitions, and control systems (without niacinamide) were also studied. RSM (Response Surface Methodology) was applied to experimental data to optimize the processing parameters of the carrier system and to examine the effect and/or correlation of independent variables on dependent responses. Statistica (Version 10, Stat-Soft Inc, Tulsa, EUA) was used to perform these experimental design procedures.

Table 1 - Coded and uncoded values of the three independent variables ~~of~~ studied following ~~a~~ Box-Behnken experimental planning were used to assess niacinamide encapsulation process performance.

System[a]	Coded variables			Uncoded variables		
	Time (X_1)	pH (X_2)	Niacinamide concentration (X_3)	Time (min)	pH	Niacinamide concentration ($g \cdot L^{-1}$)
10	0	1	-1	120	5.00	0.02
8	1	0	1	180	4.00	0.06
4	1	1	0	180	5.00	0.04
1	-1	-1	0	60	3.00	0.04
14	0	0	0	120	4.00	0.04
7	-1	0	1	60	4.00	0.06
12	0	1	1	120	5.00	0.06
15	0	0	0	120	4.00	0.04
5	-1	0	-1	60	4.00	0.02
9	0	-1	-1	120	3.00	0.02
2	1	-1	0	180	3.00	0.04
11	0	-1	1	120	3.00	0.06
3	-1	1	0	60	5.00	0.04
6	1	0	-1	180	4.00	0.02
13	0	0	0	120	4.00	0.04

The systems' numbering was generated randomly by the software (Statistica, Version 10, Stat-Soft Inc, Tulsa, EUA).

2.3.2 Preparation of chitosan (CHS) and carboxymethylcellulose (CMC) acidic dispersions

2.3.3

Firstly, a hydrochloric acid solution (1.0 mM) was prepared. Then, chitosan (0.5 $g \cdot dL^{-1}$) was added to this solution in order to obtain a chitosan stock dispersion (CSD). The resulting system was stirred at 25.0 ± 2 °C for 12 h using a magnetic stirrer (MA-039, Marconi, Brazil). A similar procedure was performed for the preparation of CMC dispersions; distilled water with a pH adjusted to 3.0 was used The CMC dispersion, once prepared, was added with niacinamide to the desired final concentration values (0.02, 0.04, and 0.06 $g \cdot L^{-1}$). Pure CMC dispersions were also maintained for the preparation of controls. All dispersions were placed in closed flasks and stored in a refrigerator (Consul, PRACTICE 410, Brazil) at 7 ± 2 °C, until use in the subsequent experiments.

2.3.3 Production of CMC/CHS micro-PECs carrying niacinamide

Micro-PECs were prepared as described in detail elsewhere by Ferreira et al. (2022). Micro-PECs were synthesized from the simultaneous drop-by-drop addition of the biopolymer dispersions (0.5 $g \cdot dL^{-1}$) under agitation. Briefly, CMC dispersion containing niacinamide was allowed to stir for 30 minutes. Soon after, this dispersion was added, with the help of a pneumatic pump, to the CHS dispersion in a 1:1 ratio. After total addition, the final resulting mixtures had their pH corrected to the target pH (3, 4, or 5) using a solution of NaOH 0.01M, and were kept under the studied stirring times (magnetically stirred for 60, 120, or 180 minutes). The micro-PECs were lyophilized (Terroni, LS 3000, Brazil) for subsequent analyses.

2.4 Assessment of CMC/CHS micro-PECs for carrying and controlled release of niacinamide

2.4.1 Encapsulation efficiency – EE (%)

1500 µL aliquots were taken from each sample and placed in Eppendorf tubes (AUY220, Shimadzu, Japan), previously weighed empty. Then, the tubes loaded were centrifuged at 10,000 *g* at 4 ± 2 °C for 1 h under refrigeration (centrifuge 4K15 Sigma, Germany). After centrifugation, 30 µL of the supernatant of each sample was pipetted and added to 270 µL of Ultra pure MiliQ water in quartz cuvettes for UV-Vis spectrophotometric analyses (UV 1800, Shimadzu, Japan). The control micro-PEC treatment (without niacinamide)

was used as a reference. Total niacinamide content was quantified from an average of three standard curves built as for the concentration range ~~of~~ from 5– to 100 $mg \cdot L^{-1}$ (See Supplementary material). The coefficients, the respective equations of the line for each repetition, as well as the Limits of Detection (LD), the Limit of Quantification (LQ), and the precision values are presented in Supplementary Material. Spectrophotometric analyzes were performed in triplicates at 228 nm. From the absorbance values read from each sample, the concentration of niacinamide in the supernatant and the encapsulation efficiency EE (%) were calculated using equation (4), according to Venkachalam et al. (2011) and Li et al. al. (2009).

$$EE(\%) = \left(\frac{W_{total} - W_{free}}{W_{total}}\right) \qquad \text{Equation 4}$$

In Equation 4, EE (%) is the encapsulation efficiency, W_{total} (g) was the total of niacinamide added in the micro-PECs and W_{free} (g) was the total of free niacinamide found in the supernatant.

2.4.2 Loading capacity – LC (%)

The supernatant present in the Eppendorf tube was carefully removed with the aid of a micropipette and the decanted present remaining solid was lyophilized. Subtracting the final weight from the initial weight of the Eppendorf tube, we obtain the value of W_{np} for equation (5). Then the value of the loading capacity (LC) of niacinamide was calculated by equation (5).

$$LC(\%) = \left(\frac{W_{total} - W_{free}}{W_{np}}\right) \qquad \text{Equation 5}$$

In Equation 5, LC (%) corresponds to binding capacity and loading, W_{total} (g) is the total niacinamide added to the micro-PECs, W_{free} (g) is the total free niacinamide found in the supernatant, and W_{np} (g) is the value of bound niacinamide to micro-PECs.

Due to analytical issues (low yield of some systems after the lyophilization process), only systems with encapsulation efficiency greater than 10% were taken to the loading capacity analysis.

2.4.3-Niacinamide release kinetics during an *in vitro* simulated digestion

The *in vitro* digestibility of niacinamide-carrying loaded in CMC/CHS micro-PECs was evaluated according to the methodology reported by e Oliveira et al. (2020), using a gastrointestinal model static. Briefly, dispersions of CMC/CHS micro-PECs containing niacinamide [3.0 g·dL^{-1} (w/v)] were prepared in deionized water. Upon reaching 37 ± 2 °C, in a controlled environment, the simulated gastric digestion stage began. At this stage, the pH was adjusted to 2 with HCl (2 mol·L^{-1}) and then pepsin (2.0 g·dL^{-1}% w/w, protein base) was added. The solution resulted was incubated at 37 ± 2 °C, for 1 h, in a thermostatic bath with agitation (Dubnoff TE-053, Tecnal, Brazil). Then, the material was submitted to the step of simulated enteric digestion. The pH was adjusted to 7 with NaOH (2 mol·L^{-1}), and pancreatin (2 g·dL^{-1} w/w; protein base) was added. The dispersion was incubated at 37 ± 2 °C for 2 h, and then submerged in a boiling water bath for 5 min to stop the activity of the digestive enzymes, inactivating it by thermal denaturation. Aliquots of 3 mL were taken for UV-VI spectroscopy analysis before starting the first step of the digestion (gastric digestion), with 30 min after beginning the gastric phase step, and in the eminence of the end of the gastric phase, (30, 60, and 180 min). These aliquots were centrifuged at 10,000*g* for 10 min at 25 ± 2 °C (Centrifuge 5430, Eppendorf, Germany), and the supernatants were collected and analyzed by UV-Vis spectroscopy.

To provide the release kinetics, ~~the~~ experimental data of average curves for niacinamide concentration in the supernatants liberation, based on the experimentally determined release profile sat the times above mentioned, were modeled to according to four mathematical models: Zero Order, First Order, Higuchi, Hixson-Crowell, and Korsemeyer-Peppas, as expressed in Eqs. (6), (7), (8), (9) and (10), respectively (Abbasnezhad et al., 2021; Anwar et al., 2022; Bruschi, 2015; Yang et al., 2022).

$$Q = K_0(t) + Q_0 \qquad \text{Equation 6}$$

$$lnQ = K_1(t) + lnQ_0 \qquad \text{Equation 7}$$

$$Q = K_H(t^{0.5}) + Q_0 \qquad \text{Equation 8}$$

$$Q^{\frac{1}{3}} = Q_0{}^{\frac{1}{3}}(t) - K_{hc} \qquad \text{Equation 9}$$

$$Q = K_{K-P}(t^n) \qquad \text{Equation 10}$$

In Equations 6 to 10: Q (%) is the cumulative percentage of liberated released material niacinamide ~~in~~ at the time t; Q_0 (%) is the initial cumulative percentage of niacinamide; K_0 is the zero-order constant (dimensionless), K_1 is the first-ordem constant (dimensionless), K_H is the Higuchi constant (dimensionless), K_h is the Hixson-Crowell constant (dimensionless) and, $K_{K\text{-}P}$ is the Korsemeyer-Peppas constant (dimensionless) and n: diffusion or release exponent (dimensionless).

2.5. Data analysis

Regression models were developed to analyze the encapsulation efficiency (Y_1) and loading capacity (Y_2) responses as a function of processing time (X_1 - 60, 120, and 180 min), pH (X_2 - 3, 4, and 5), and niacinamide concentration (X_3 - 0.02, 0.04, and 0.06, $g \cdot L^{-1}$). The adequacy of the models was evaluated in terms of significance (p-value ≤ 0.05), coefficient of determination (R^2), and coefficient adjusted R^2. Scatter plots were observed, and the best-fit models of response surface were evaluated. The standardized effects of the independent variables and their interactions on the response were analyzed using Pareto charts. It was decided to build models with simple linear and quadratic complexity. The most suitable model was chosen considering the highest-order polynomial, in which the additional terms are significant. Analysis of variance (ANOVA) were performed to examine the statistical significance of terms in the regression equations for each dependent variable. After establishing the best model, contour plots were generated using Statistica (Version 10, Stat-Soft Inc, Tulsa, EUA). Each response came from at least one triplicate, and the center point was expressed as a mean ± standard deviation of 3 replicates.

3. RESULTS AND DISCUSSION

3.1 Encapsulation efficiency – EE (%)

As mentioned in item 2.4.2, only systems with encapsulation efficiency greater than 10% were taken to a deeper analysis and discussion: 1, 2, 7, 8, 9, and 11 (Table 1). In fact, in developing delivery systems for bioactive compounds, considering the encapsulation efficiency (EE) is crucial to ensure that ~~an~~ enough compound amount is delivered at the target location.

This parameter measures the percentage of carrier systems that effectively encapsulate the bioactive compound (either on the surface or inside the particle's core), and is, therefore, a critical analysis in the design of systems for delivery systems and compound release studies carrying a compound of interest (Sharma et al., 2021). Encapsulation efficiency can be influenced by the carrier's properties and the encapsulated compounds themselves, in addition to as well as by the parameters of the encapsulation process, such as pH, contact time, concentrations used, and mechanical stress (Piacentini, 2016).

In the system considered in the present analysis, encapsulation efficiencies of niacinamide in CMC/CHS micro-PECs ranged from 0.86% (S11) to 80.78% (S-6) (Table SM1). A Pareto chart (Figure 1a) was constructed to assess which factors significantly influenced EE values. As shown, all studied variables – stirring time, pH, and niacinamide concentration – had significant effects on EE, at a 95% confidence level. The mathematic model obtained for the effect of these factors on EE is presented in Eq. 11:

$$Y_1 = 0.297 - 0.064X_1 - 0.65X_{2-} - 0.264X_2^2 + 0.223X_3 - 0.079X_3^2 + 0.159X_1X_2 + 0.133X_1X_2^2 + 0.111X_1X_3 - 0.082X_1^2X_3 \quad \text{Equation 11}$$

It is worth remembering that, in this adjusted model, Y_1 is encapsulation efficiency (%), X_1 is processing time (60, 120, or 180 min), X_2 is pH (3, 4, or 5), and X_3 is niacinamide concentration (0.02, 0.04, or 0.06, g·L^{-1}). Furthermore, both R^2 (0.999) and adjusted R^2 (0.998) were also close to unity 1, whereas (adjusted R^2 minus adjusted R^2)/R^2 is equal to 0.0011. This indicates that when the model is applied to a new dataset, it can shrink by a small factor of 0.01. A positive or negative value coefficient is related to a positive augmenting or negative diminishing effect on the studied response, respectively. However, the effect of quadratic terms on the response can be inferred according to their sign, while for the main effect and interaction terms, their contribution to increasing or decreasing the response cannot be simply determined because at different levels of each variable, encoded values can be negative or positive. Therefore, a single pattern for increase or decrease in response by these model components could not be defined.

Agitation time exhibited a negative linear effect on EE. During the first hour of the interaction reaction, the complexation process was presumably sufficient for the maximum interaction between chitosan, carboxymethylcellulose, and niacinamide to occur. From that moment on, all active micro-PECs' binding sites would already be filled by niacinamide.

Seemingly, a further increase in stirring time caused an increase in excessive collisions between molecules and the formed vitamin-loaded micro-PECs, modifying the interactions and allowing some niacinamide desorption and thus decreasing the encapsulation efficiency (EE) response. Another reliable hypothesis to explain these findings would be that increasing the stirring time favors the solubilization of niacinamide in water, as it is a well-known hydrophilic vitamin.

Figure 1 - Pareto chart of the normalized effects from the independent variables analyzed on encapsulation efficiency (A) and loading capacity (B).

* (Q) quadratic effect and (L) linear effect.

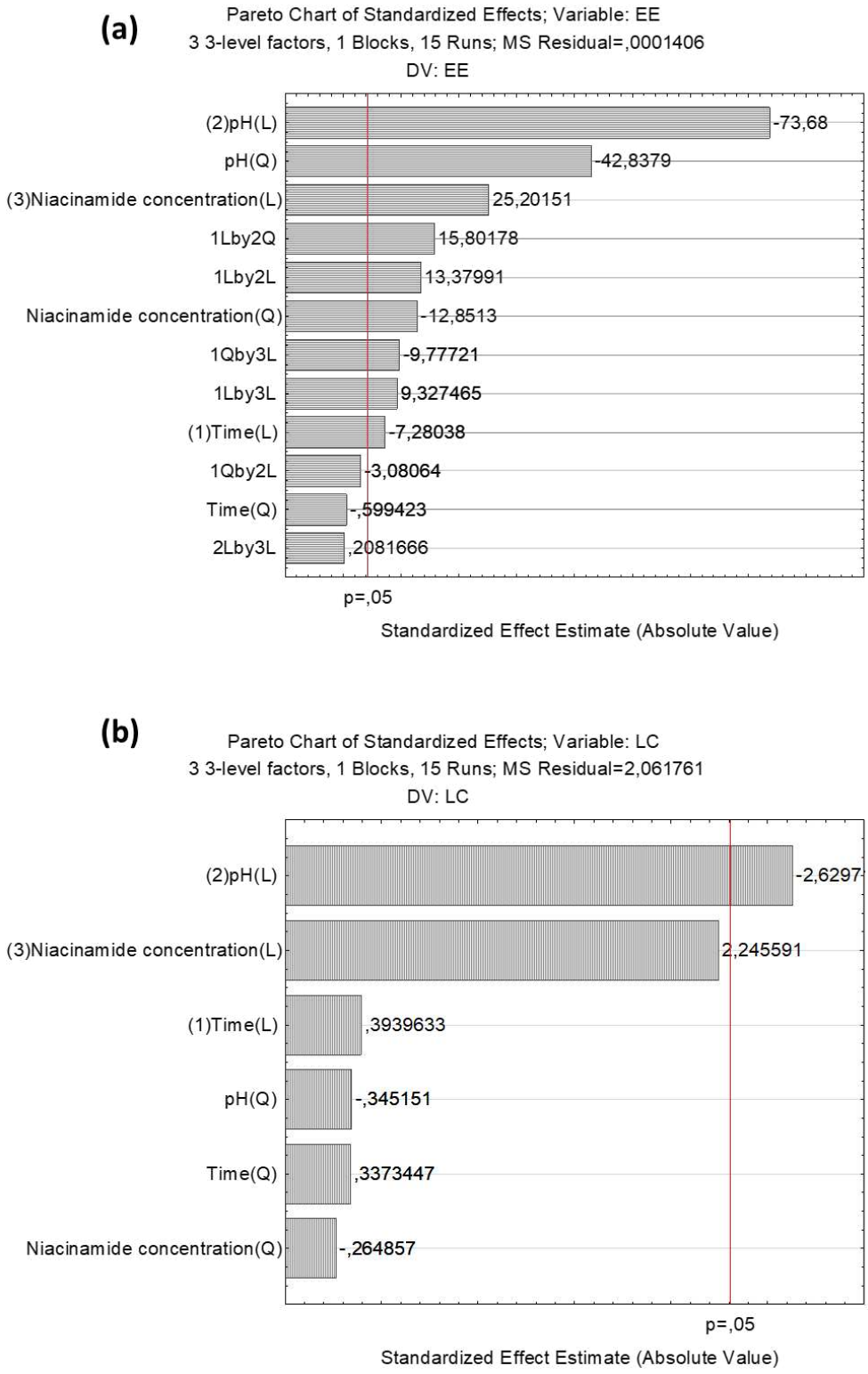

The pH exhibited a negative linear effect on EE. It is well-known that CHS amino groups are a weak base with pK_a at pH ~ 6.5, being this biopolymer insoluble in neutral and alkaline pH media (Dogsa et al., 2014). In an acidic media, these biopolymer's primary amino groups are progressively protonated by hydrogen ions as the pH drops, thus acquiring a high crescent positive charge density. At the lowest pH value studied (3.0), the CHS polymer chains can more easily extend after dissolution in water; however, when the pH was adjusted to 5.0, partial deprotonation of NH_3^+ groups was favored, leading to a decrease of the positive charges density and, hence, the favoring the folding of the CHS chains (Xiong et al., 2020). Indeed, ~~as~~ less protonated NH_3^+ groups were available to interact with CMC anionic chains, which in turn resulted in weaker electrostatic attractive interactions, less compact micro-PECs' structures and, eventually, the observed lower encapsulation efficiency. Furthermore, at higher pH values, micro-PECs are more likely to form aggregates, which precipitate forming macro-PECs (Ferreira et al., 2022b).

The niacinamide concentration had a positive effect on EE. This is consistent with the fact that the interaction rates are dependent on the concentration of niacinamide. Therefore, interactions between the micro-PECs and this bioactive compound must occur faster at higher concentrations of this last. When the niacinamide:micro-PEC ratio is low, the bioactive amount is insufficient to load the micro-PEC particles, which will eventually release the bioactive compound. As the niacinamide:micro-PEC ratio increases, more niacinamide molecules are available to interact with the surface and/or pores of the micro-PECs.

The interactive effects of independent variables on the encapsulation efficiency response (Y_1) were further investigated by constructing three-dimensional response surface plots (Figure 2) and two-dimensional contour plots (Figure 4). The graphs in Figure 2 are derived from Equation 7 keeping a constant variable at its central level for each plot. As observed in Figure 4, pH had the greatest influence on encapsulation efficiency, being greater at lower pH values, which is in line with the previously explained results. Also, at lower pHs, a greater influence of the agitation time was observed, with shorter times being favorable to the niacinamide encapsulation process.

From these results, it can be inferred that pH 3.0, 1 hour of agitation, and a concentration of 0.06 mg/g niacinamide are the conditions that will lead to greater encapsulation efficiencies.

Figure 2 - Response surface plots showing effect of time, pH, and niacinamide concentration on encapsulation efficiency.

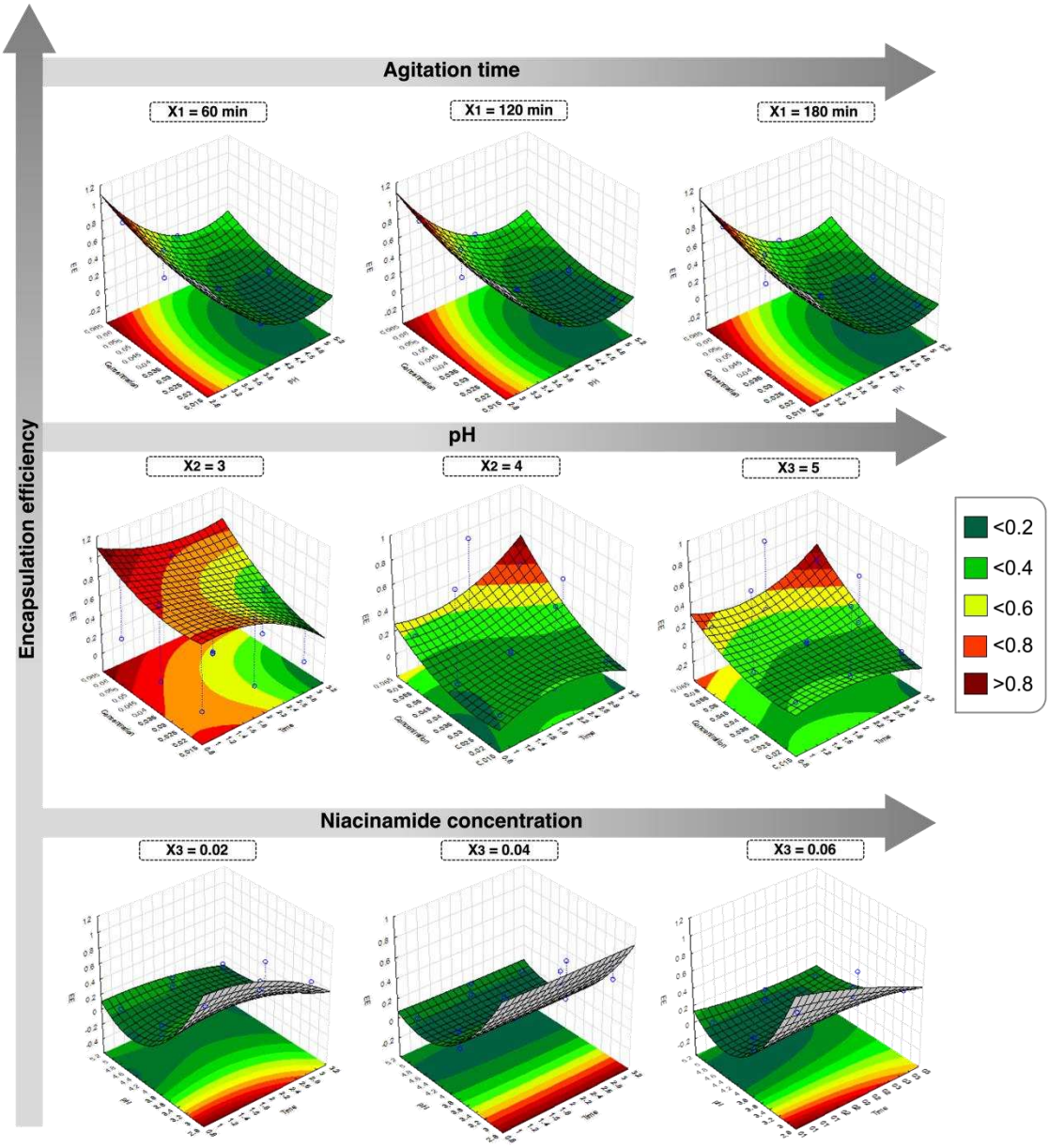

3.2. Loading capacity – LC (%)

Loading capacity is another important parameter to be quantified when studying the inclusion of a given compound into a carrier system since it refers to the total amount of trapped compound divided by the total weight of the carrier systems. In carrying systems, the LC, given as a percentage, is the amount of drug delivered per encapsulated amount (Rankin-Turner et al., 2021).

Loading capacity ranged from 0.02% (S-15) to 4.85% (S-11) (Table SM1). Only pH had a significant effect on LC. The corresponding mathematic model to predict the effect of factors on LC as a function of the independent variables is presented in Eq. 12:

$$Y_2 = 0.1433 - 2.67X_2 \qquad \text{Equation 12}$$

In this adjusted model, Y_1 is loading capacity (%), X_1 is processing time (60, 120, or 180 min), X_2 is pH (3, 4, or 5), and X_3 is niacinamide concentration (0.02, 0.04, or 0.06, g·L^{-1}). The predicted R^2 (0.931) and adjusted R^2_{ajus} (0.961) values obtained from the ANOVA (Tabel SM3) test suggested that this model provides excellent representation of LC experimental values as a function of the independent variables.

This can be credited to the impact of the pH value on the behavior of niacinamide and the dominant charges on the surface of the micro-PECs. Acidic conditions induce niacinamide ionization into structures with more stable properties and cause an increase in ionic interactions with micro-PEC and increase its loading capacity.

Response surface analysis, combined with experimental data and the developed model, allowed a better understanding of the individual and combined effects of independent variables on the loading capacity response. As depicted in Figure 3, when the agitation time values were kept constant, the increase in molar concentration and the decrease in pH caused an increase in loading capacity. Elevated pH at any concentration negatively affected the LC. Keeping the pH constant, in any agitation times studied, the LC was higher in higher concentrations of encapsulated bioactive. When the niacinamide concentration was kept constant, the pH of up to approximately 3.4 favored LC. In general, pH is ~~the~~ preponderant in the LC, such predicted results is in accordance with the experimental results.

Figure 3 - Response surface plots showing the effect of time, pH, and niacinamide concentration on loading capacity.

Figure 3 - Response surface plots showing the effect of time, pH, and niacinamide concentration on loading capacity.

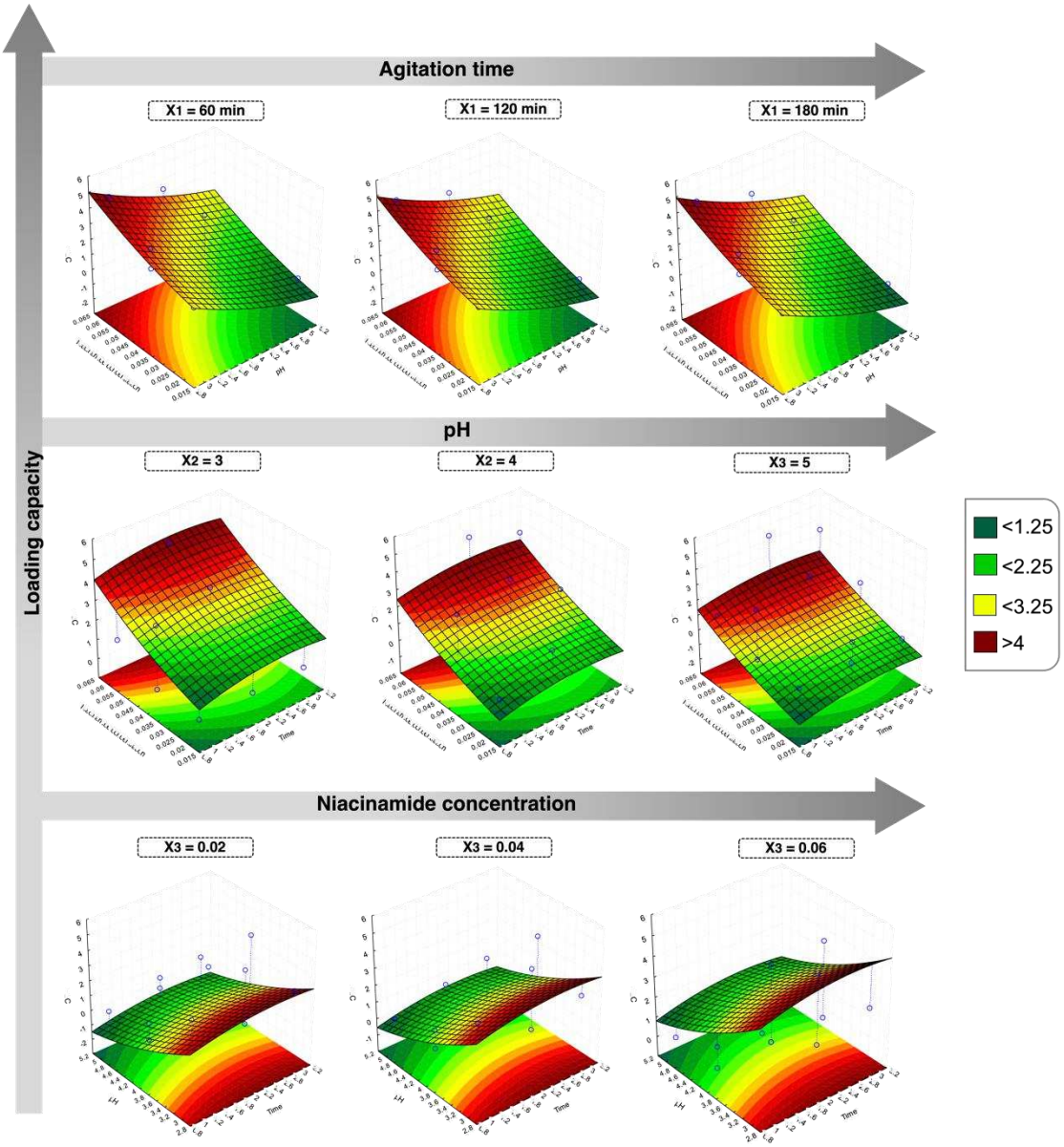

3.3 Niacinamide release kinetics during an *in vitro* simulated digestion

The objectives of carrier systems are to maintain the concentration of the carried bioactive compound in a target location at a desired value for as long as possible, exerting control over the rate and duration of the compound's release. Normally, the controlled release systems promote the release of an amount of the compound in order to reach the desired concentration, and, then, the modulated release rates are responsible for keeping the effective level of concentration close to this reached value (Bruschi, 2015).

The release behavior of niacinamide from the micro-PECs (observed and predicted) with EE above 10% is shown in Figure 4. During the first hour, systems 12 and 1 (Table 1) showed respectively the lowest and highest niacinamide release, which were 43.7% and 33.8%. For the loaded micro-PECs, maximum release occurred after about 4.5 h (270 min) in all systems studied. The percentages of niacinamide released at t = 270 min were 89.3, 87.7, 96.8, 89.6, 91.6, 88.0, and 97.8% for systems 1, 2, 7, 8, 9, 10, and 11, respectively. The different release rates may be associated with the strength of the different interactions, either between the biopolymers that form the carrier systems (CMC and CHS) or between niacinamide and the carrier systems.

In the beginning, it is assumed that the niacinamide desorption process takes place from the surface of the carrier system; it occurs quickly (rapid release phenomenon) causing the profile curves shown in Figure 4 to present a steep initial slope. However, with the changes in the microcarrier structure during the digestion, the release rate – and the consequent release curves' slopes – remain high, even though smaller than the initial ones. As discussed by Bhagya Raj & Dash (2022), one can hypothesize that niacinamide molecules encapsulated in CHS/CMC micro-PECs are released by three sequential mechanisms: 1) desorption of niacinamide from the particles' surface; 2) diffusion and resorption of niacinamide through the pores of the polymeric network or the intermediate layer of the micro-PEC and; 3) degradation and erosion of the polymeric network.

Figure 4 - *In vitro* niacinamide release observed and predicted from CMC/CHS micro-PECs during a simulated digestion encompassing a gastric phase (0 to 90 min) followed by an enteric phase (90 to 270 minutes); Systems (a) 1, (b) 2, (c) 7, (d) 8, (e) 9, (f) 12.

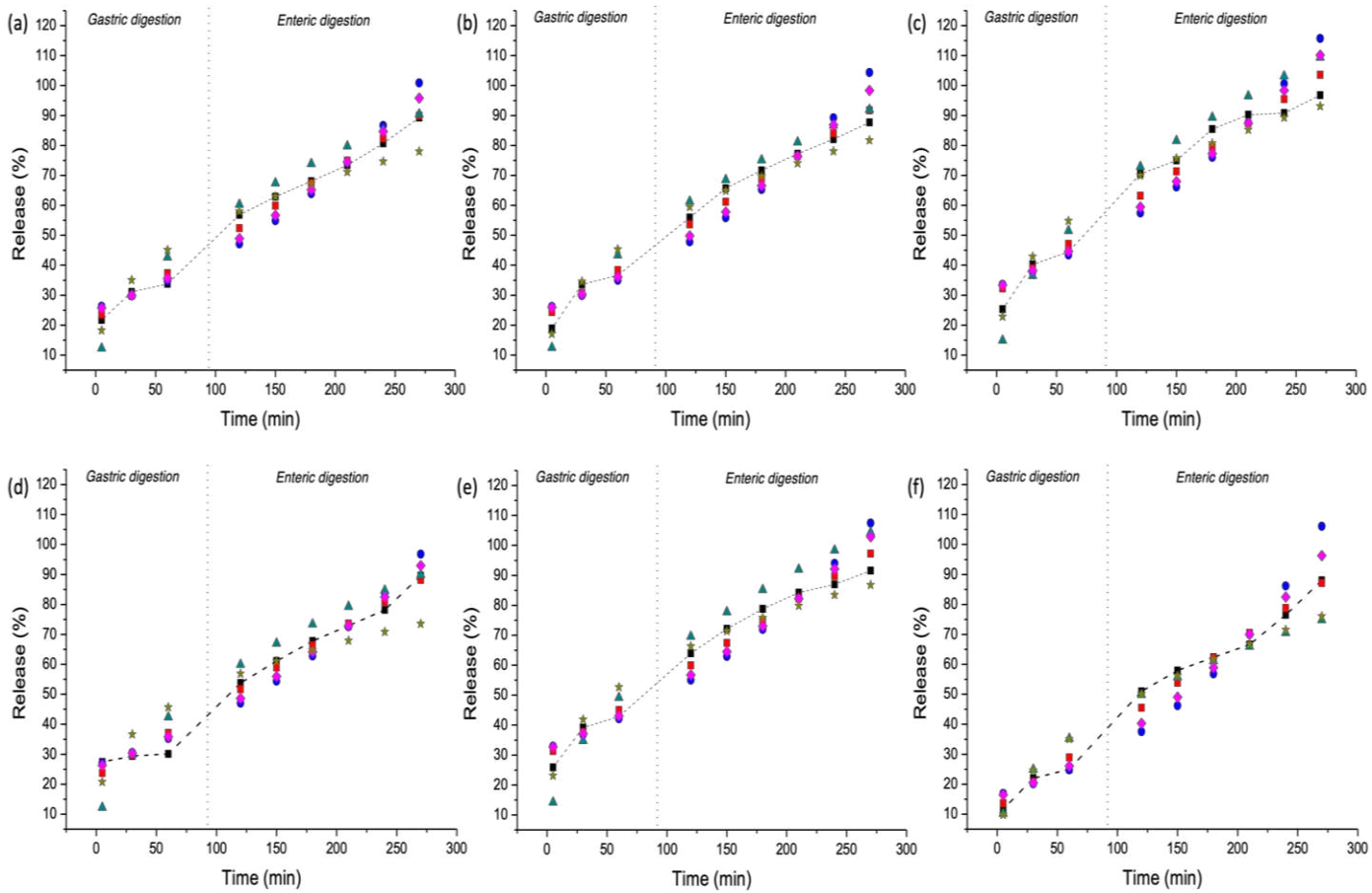

The overall rate of niacinamide release tends to become superior in systems with higher niacinamide initial concentrations (7, 8, and 11). It was initially thought that larger amounts of niacinamide would disfavor the formation of CHS and CMC carriers, because the amino group of niacinamide also interacts with the carboxyl groups of carboxymethylcellulose, competing with chitosan's amino groups in such interactions, leading to a faster niacinamide release from micro-PECs. However, the initial concentration of niacinamide used did not affect the final release. On the other hand, carriers produced at lower pH values had lower release rates compared to those fabricated at higher pH values. This may be due to the more intense attractive interactions between the two biopolymers molecules, as explained in section 3.1.

Aiming for a better understanding of the release behavior of niacinamide from CMC/CHS micro-PECs, five different empirical models were fitted from the experimental data (Figure 6 and Table 2). The five models used to mathematically describe the niacinamide release from the micro-PEC particles provided an adequate correspondence to the experimental data, presenting a high value of R^2 (except for the Korsmeyer-Peppas model adjusted from data of system 11; Table 1). These kinetic models allow inferences on whether the niacinamide release is dissolution-dependent or diffusion dependent. It can seem contradictory that more than one empirical model fits the experimental data; however, as explained by Gouda et al. (2017), the release kinetics does not perfectly follow one/the model used, although one or few of them can be approached. This observation suggests that the niacinamide was released due to a combination of different microscopic phenomena. Hereafter, we reported the main findings and discussions considering each tested model. However, observing Figure 6, it is noted that the best model that fitted ~~in~~ the highest number of points was the zero-order model for all systems studied.

Table 2 - Fitted kinetic models for niacinamide release from CMC/CHS micro-PECs during the *in vitro* simulated digestion, separately for the gastric phase and the enteric phase parameters of drug release models of niacinamide micro-PEC complexes

		Systems					
Release model	Parameters	1	9	2	8	7	12
Zero order $Q = K_0(t) + Q_0$	K_0	0.002	0.003	0.002	0.002	0.003	0.003
	R^2	0.979	0.956	0.981	0.970	0.984	0.978
First order $lnQ = K_1(t) + lnQ_0$	K_1	0.005	0.005	0.005	0.004	0.007	0.004
	R^2	0.896	0.885	0.956	0.907	0.906	0.953
Higuchi $Q = K_H(t^{0.5}) + Q_0$	K_h	0.056	0.500	0.500	0.500	0.043	0.069
	R^2	0.957	0.889	0.867	0.855	0.950	0.737
Hixson-Crowell $Q^{\frac{1}{3}} = Q_0{}^{\frac{1}{3}}(t) - K_{hc}$	K_{hc}	0.134	0.127	0.125	0.121	0.165	0.115
	R^2	0.933	0.914	0.968	0.933	0.945	0.963
Korsmeyer-Peppas $Q = K_{K-P}(t^n)$	K_K	0.091	0.129	0.125	0.135	0.047	0.185
	n	0.392	0.353	0.317	0.332	0.414	0.281
	R^2	0.967	0.962	0.791	0.955	0.723	0.861
Zero order $Q = K_0(t) + Q_0$	K_0	0.003	0.003	0.002	0.002	0.003	0.003
	R^2	0.979	0.956	0.980	0.970	0.984	0.978
First order $lnQ = K_1(t) + lnQ_0$	K_1	0.005	0.005	0.005	0.004	0.007	0.004
	R^2	0.896	0.885	0.956	0.907	0.906	0.953
Higuchi	K_H	0.909	0.067	0.055	0.065	0.065	0.069

$Q = K_H(t^{0.5}) + Q_0$	R^2	0.967	0.889	0.867	0.855	0.945	0.737
Hixson-Crowell	K_{hc}	0.134	0.128	0.126	0.121	0.165	0.115
$Q^{\frac{1}{3}} = Q_0{}^{\frac{1}{3}}(t) - K_{hc}$	R^2	0.933	0.914	0.968	0.933	0.945	0.963
Korsmeyer-Peppas $Q = K_{K-P}(t^n)$	K_K	0.909	0.129	0.125	0.135	0.043	0.184
	n	0.392	0.352	0.317	0.332	0.414	0.281
	R^2	0.766	0.962	0.791	0.955	0.950	0.861

K_0: zero ordem constant (dimensionless), K_1: first-ordem constant (dimensionless), K_H: Higuchi constant, K_{hc}: Hixson-Crowell constant (dimensionless), K_{K-P}: Korsemeyer-Peppas constant (dimensionless), n: diffusion or release exponent (dimensionless), R^2: correlation coefficient.

- The zero-order model fitted the highest number of points (gastric and enteric digestion), besides presenting the highest correlation coefficients and lowest error parameters. The zero-order constants (K_0) were low (0.002 - 0.003) and similar for all studied systems, suggesting low release rates. Observing the zero-order model, we can assume that the release of niacinamide is independent of its concentration, which is in agreement with the results discussed so far and happens by diffusion. This model has generally used adequately when the carrier system does not break down and releases the compost compound slowly (Wójcik-Pastuszka et al., 2019). This type of behavior occurs mainly typical of formulations in the form of tablets with poorly soluble compounds and coated forms, it can hypothesize that a part of the niacinamide was initially found inside of micro-PECs (Bruschi, 2015; Paarakh et al., 2019). Similar results were obtained for K_1 values (0.004 – 0.007), which were similar for all systems and remained constant from the astric to enteric phase.

- The Higuchi dissolution constant K_H corresponds to the slope of the graph (cumulative percentage of drug release versus square root of time). It is noted, therefore, that systems 2, 8, and 9 showed more inclination in the gastric phase (K_h

= 0.500), decreasing this value in the enteric phase (K_H = 0.055, 0.065, and 0.067 for 2, 8, and 9, respectively). System 1 had an increase in slope (K_H) from 0.056 to 0.909. The system had an insignificant increase in the Kh value (0.043 to 0.65), while system 12 presented the K_H parameter unchanged (0.069). In general, for the systems under study, the constants of the Higuchi model were higher in the enteric digestion step. The value of K_H (Higuchi constant) is directly proportional to the release of the active component from the carrier system. In other words, the higher the K_h value, the faster ~~was~~ will be the release of niacinamide. This fact, according to the release profile, in which, after initial desorption of niacinamide from CHS/CMC micro-PECs, initiates the degradation and erosion of the polymeric network, promoting rapid release (Bhagya Raj & Dash, 2022). The equation described in the Higuchi model assumes that the initial concentration of the carried compound in the studied system is greater than its solubility in the surrounding medium. Furthermore, it considers that the compound spreads only in one dimension and that the swelling and dissolution of the system carrier particles and their dissolution are negligible (Higuchi, 1963).

- Release data were also plotted according to the Hixon-Crowell model. The Hixson-Crowell dissolution rates (K_{hc}) had values between 0.121 (System 8) and 0.165 (System 7) in the gastric phase, maintaining the same maximums and minimums for the enteric phase. There were no changes in these values considering the same system, indicating similar dissolution rates at the different pHs (2 and 7) studied. The possibility of describing the release of niacinamide from CHS/CMC micro-PECs using the Hixon-Crowell model may indicate that the change in surface area and mean particle diameter during the dissolution process affects the release of the compound (Bruschi, 2015).

- According to the Korsmeyer-Peppas model, when the diffusional release exponent (n) is ≤ 0.5, Fickian diffusion is considered, whereas if $0.5 < n < 1.0$, anomalous non-Fickian transport is considered (Korsmeyer et al., 1983). It was observed, therefore, that for the release of niacinamide both under acidic (gastric digestion) and basic (enteric digestion) conditions $n < 0.5$, indicating that the release of niacinamide from CHS/CMC micros-PECs occurs through the Fickian diffusion transport route (Korsmeyer et al., 1983).

Juhász et al. (2021) presented a method of simple encapsulation of vitamin B1 in asolectin-based liposomes at pH = 7.4 and in acidic conditions. The authors also evaluated the effects of the amount of lipid carrier, vitamin B1, and sonication time. It was observed that EE decreased with increasing lipid carrier concentration, with the best EE % (63.5 ± 1.8% and 65.8 ± 2.1%, in PBS and acid medium, respectively) being achieved with the use of 0. 50 mg/mL of the carrier. Higher amounts of vitamin B1 led to higher EE (74.6 ± 2.4%) at pH = 3.00. However, under physiological conditions, increasing the amount of vitamin B1 resulted in a decrease in EE (62.1 ± 1.9%). The best sonication time found was 60 min to reach EE% ~~is~~ of 62.0 ± 1.31%. Similar to what was found in the present work, no significant difference was observed in the profile of the dissolution curves. After 100 min, 92% of the control non-formulated vitamin molecules diffused, whereas the vitamin B1 nanocarriers showed better drug retention, achieving up to 4.5 times greater release time compared to non-encapsulated vitamin B1. The kinetic model with the best fit was the second-order kinetic model.

Jan et al. (2022) developed a low-temperature-aided sonication method to incorporate vitamin D3 into the oil-in-water emulsion. Response Surface Methodology revealed that a sonication time of 30 s, agitation rate of 1500 rpm, and mixing time of 10 min produced the optimal nanoemulsion with an encapsulation efficiency of 91%. Furthermore, it was found from the release study that 26.30% and 78.15% of ~~the~~ vitamin D3 were released, in simulated gastric solution and simulated intestinal solution, respectively. The Korsmeyer-Peppas was the most suitable model to define the release of vitamin D3 from the nanoemulsion. Microcapsules were prepared by the spray-drying technique by the coacervation method, using a mixture of chitosan and sodium lauryl ether sulfate to transport vitamin E. High encapsulation efficiency values were found for formulations without cross-linking reagent (73.17 ± 0.64) and in the presence of ~~when~~ crosslinking agents (100.00 ± 3.55). The initial release of vitamin E from the microcapsules followed the Korsmeyer-Peppas model, which was based on a complex process that, in addition to simple diffusion, involved the direct release of the active substance from the surface of the microcapsules (Budinčić et al., 2021). In their research, Mohammed et al. (2021) examined the release of vitamin B9 (folic acid - FA) from sporopollenin microcapsules. The loading capacity and the encapsulation efficiency of the FA were 8.63% and 21.6%, respectively. The *in vitro* release study was carried out under different pH conditions, mimicking the gastrointestinal tract. The slow release was achieved in the simulated gastric fluid, while it was faster in the simulated intestinal fluid, meaning ~~that~~ the release was pH dependent. The Higuchi model exhibited a higher R^2 for vitamin B9 release in both simulated gastric fluid (SGF) and simulated intestinal fluids (SIF) media, indicating that the release

kinetics followed the diffusion mechanism. From the Korsmeyer-Peppas model and the exponent of diffusional release (n), it was discovered the release of vitamin B9 in acidic conditions of simulated gastric fluid, $n < 0.5$, indicated the release ~~occurs~~ through the Fickian diffusion transport route. However, the vitamin release from simulated intestinal fluid,$-0.5 < n < 1.0$ suggests anomalous non-Fickian transport. This behavior can be attributed to the difference in media solubility.

To the best of our knowledge, no similar studies were found regarding ~~on~~ niacinamide carrying and controlled release using CMC/CHS excipients. However, some studies described above obtained varied results about the carrying and controlled release of different other vitamins in different carrier systems, demonstrating the importance and specificity of this type of study. Each release system is unique and needs to be studied in depth.

4. Conclusion

The use of micro-PECs produced from chitosan and carboxymethylcellulose ~~have~~ has been shown to be effective in niacinamide delivery systems. It can be concluded that only the pH factor had a greater influence on the encapsulation efficiency and loading capacity, with the production process of carrier structures being favored at lower pH values (3.0). Therefore, the use of shorter process times would favor practical and economic terms. The zero-order constants, the model that best fitted the *in vitro* release data under conditions of the gastrointestinal tract, were low and similar for all studied systems, demonstrating a low release rate, indicating that the process of niacinamide release from the micro-PECs CHS/CMC occurs mainly by diffusion. Indeed, the present work shows that a relatively simple process can be used to carry niacinamide. However, before being able to carry out the process on an industrial level it would be necessary to evaluate the microcapsules' stability over time as well as the bioavailability and applicability of the encapsulated compounds in different food matrices.

5. References

Abbasnezhad, N., Zirak, N., Shirinbayan, M., Kouidri, S., Salahinejad, E., Tcharkhtchi, A., & Bakir, F. (2021). Controlled release from polyurethane films: Drug release mechanisms. *Journal of Applied Polymer Science*, *138*(12). https://doi.org/10.1002/app.50083ï

Alu'datt, M. H., Alrosan, M., Gammoh, S., Tranchant, C. C., Alhamad, M. N., Rababah, T., Alzougl, R., Alzoubi, H., Ghatasheh, S., Ghozlan, K., & Tan, T.-C. (2022). Encapsulated-

based films for bioactive compounds and their application in the food industry: A roadmap for food-derived functional and healthy ingredients. *Food Bioscience*, *50*(PA), 101971. https://doi.org/10.1016/j.fbio.2022.101971

Anwar, A., Imran, M., Ramzan, M., Khan, F. A., Ismail, N., Hussain, A. I., Hussain, S. M., Alsanie, W. F., & Iqbal, H. M. N. (2022). Chitosan-based Dy2O3/CuFe3O4 bio-nanocomposite development, characterization, and drug release kinetics. *International Journal of Biological Macromolecules*, *220*, 788–801. https://doi.org/10.1016/j.ijbiomac.2022.08.119

Baek, J., Ramasamy, M., Willis, N. C., Kim, D. S., Anderson, W. A., & Tam, K. C. (2021). Encapsulation and controlled release of vitamin C in modified cellulose nanocrystal/chitosan nanocapsules. *Current Research in Food Science*, *4*, 215–223. https://doi.org/10.1016/j.crfs.2021.03.010

Belingheri, C., Giussani, B., Rodriguez-Estrada, M. T., Ferrillo, A., & Vittadini, E. (2015). Oxidative stability of high-oleic sunflower oil in a porous starch carrier. *Food Chemistry*, *166*, 346–351. https://doi.org/10.1016/j.foodchem.2014.06.029

Belitz, H. D., Grosch, W., & Schieberle, P. (2009). Food chemistry. In *Food Chemistry*. Springer Berlin Heidelberg. https://doi.org/10.1007/978-3-540-69934-7

Bhagya Raj, G. V. S., & Dash, K. K. (2022). Microencapsulation of betacyanin from dragon fruit peel by complex coacervation: Physicochemical characteristics, thermal stability, and release profile of microcapsules. *Food Bioscience*, *49*(May), 101882. https://doi.org/10.1016/j.fbio.2022.101882

Brasil. Resolução nº 18, de 30 de abril de 1999. Diário Oficial da União; Poder Executivo, Brasília.

Bruschi, M. L. (2015). Mathematical models of drug release. In *Strategies to Modify the Drug Release from Pharmaceutical Systems* (1st ed., pp. 63–86). Woodhead Publishing. https://doi.org/10.1016/b978-0-08-100092-2.00005-9

Budinčić, J. M., Petrović, L., Đekić, L., Fraj, J., Bučko, S., Katona, J., & Spasojević, L. (2021). Study of vitamin E microencapsulation and controlled release from chitosan/sodium lauryl ether sulfate microcapsules. *Carbohydrate Polymers*, *251*. https://doi.org/10.1016/j.carbpol.2020.116988

Campbell, M. T. D., Jones, D. S., Andrews, G. P., & Li, S. (2019). Understanding the physicochemical properties and degradation kinetics of nicotinamide riboside, a promising vitamin B3nutritional supplement. *Food & Nutrition Research*, *63*(0). https://doi.org/10.29219/fnr.v63.3419

Chen, G., Dong, S., Chen, Y., Gao, Y., Zhang, Z., Li, S., & Chen, Y. (2020). Complex coacervation of zein-chitosan via atmospheric cold plasma treatment: Improvement of encapsulation efficiency and dispersion stability. *Food Hydrocolloids*, *107*. https://doi.org/10.1016/j.foodhyd.2020.105943

Croguennec, T., Tavares, G. M., & Bouhallab, S. (2017). Heteroprotein complex coacervation: A generic process. In *Advances in Colloid and Interface Science* (Vol. 239, pp. 115–126). Elsevier B.V. https://doi.org/10.1016/j.cis.2016.06.009

de Oliveira, A. P. H., Omura, M. H., Barbosa, É. de A. A., Bressan, G. C., Vieira, É. N. R., Coimbra, J. S. dos R., & de Oliveira, E. B. (2020). Combined adjustment of pH and ultrasound treatments modify techno-functionalities of pea protein concentrates. *Colloids and Surfaces A: Physicochemical and Engineering Aspects*, *603*(June). https://doi.org/10.1016/j.colsurfa.2020.125156

Edwardson, T. G. W., Tetter, S., & Hilvert, D. (2020). Two-tier supramolecular encapsulation of small molecules in a protein cage. *Nature Communications*, *11*(1), 1–9. https://doi.org/10.1038/s41467-020-19112-1

Fan, B., You, J., Suo, Y., & Qian, C. (2018). A novel and sensitive method for determining vitamin B3 and B7 by pre-column derivatization and high-performance liquid chromatography method with fluorescence detection. *PLOS ONE*, *13*(6), e0198102. https://doi.org/10.1371/journal.pone.0198102

FDA, Food and Drug Administration. (2014). International Conference on Harmonisation. *Encyclopedia of Toxicology: Third Edition*, *2* (November 1994), 1070–1072. https://doi.org/10.1016/B978-0-12-386454-3.00861-7

Ferreira, D. C. M., Ferreira, S. O., de Alvarenga, E. S., Soares, N. de F. F., Coimbra, J. S. dos R., & de Oliveira, E. B. (2022b). Polyelectrolyte complexes (PECs) obtained from chitosan and carboxymethylcellulose: A physicochemical and microstructural study. *Carbohydrate Polymer Technologies and Applications*, *3*. https://doi.org/10.1016/j.carpta.2022.100197

Goto, Y., Masuda, A., & Aiba, T. (2015). In vivo application of chitosan to improve bioavailability of cyanocobalamin, a form of vitamin B12, following intraintestinal administration in rats. *International Journal of Pharmaceutics*, *483*(1–2), 250–255. https://doi.org/10.1016/j.ijpharm.2015.02.016

Gouda, R., Baishya, H., & Qing, Z. (2017). Application of Mathematical Models in Drug Release Kinetics of Carbidopa and Levodopa ER Tablets. *Journal of Developing Drugs*, *06*(02). https://doi.org/10.4172/2329-6631.1000171

Hernández, H. L. H., Santos, I. J. B., Oliveira, E. B. de, Teófilo, R. F., Soares, N. de F. F., & Coimbra, J. S. dos R. (2020). Nanostructured conjugates from tara gum and α-lactalbumin. Part 1. Structural characterization. *International Journal of Biological Macromolecules*, *153*, 995–1004. https://doi.org/10.1016/j.ijbiomac.2019.10.229

Jan, Y., Al-Keridis, L. A., Malik, M., Haq, A., Ahmad, S., Kaur, J., Adnan, M., Alshammari, N., Ashraf, S. A., & Panda, B. P. (2022). Preparation, modelling, characterization and release profile of vitamin D3 nanoemulsion. *LWT*, *169*. https://doi.org/10.1016/j.lwt.2022.113980

Juhász, Á., Ungor, D., Várkonyi, E. Z., Varga, N., & Csapó, E. (2021). The ph-dependent controlled release of encapsulated vitamin b1 from liposomal nanocarrier. *International Journal of Molecular Sciences*, *22*(18). https://doi.org/10.3390/ijms22189851

Korsmeyer, R. W., Gurny, R., Doelker, E., Buri, P., & Peppas, N. A. (1983). Mechanisms of solute release from porous hydrophilic polymers. *International Journal of Pharmaceutics*, *15*(1), 25–35. https://doi.org/10.1016/0378-5173(83)90064-9

Kreetl, W. A., De, J., Huerga, L. A., Elvehjem, C. A., & Hart, E. B. (n.d.). *THE DISTRIBUTION OF NIACINAMIDE AND NIACIN IN NATURAL MATERIALS**.

Maiorova, L. A., Erokhina, S. I., Pisani, M., Barucca, G., Marcaccio, M., Koifman, O. I., Salnikov, D. S., Gromova, O. A., Astolfi, P., Ricci, V., & Erokhin, V. (2019). Encapsulation of vitamin B12 into nanoengineered capsules and soft matter nanosystems for targeted delivery. *Colloids and Surfaces B: Biointerfaces*, *182*(July). https://doi.org/10.1016/j.colsurfb.2019.110366

Mamusa, M., Resta, C., Sofroniou, C., & Baglioni, P. (2021). Encapsulation of volatile compounds in liquid media: Fragrances, flavors, and essential oils in commercial formulations. In *Advances in Colloid and Interface Science* (Vol. 298). Elsevier B.V. https://doi.org/10.1016/j.cis.2021.102544

Massey, D., Cunniffe, N., & Noorani, I. (2022). *Carpenter's Neurophysiology: A Conceptual Approach* (6th ed., Vol. 1). CRC Press.

Mejías, F. J. R., Gutiérrez, M. T., Durán, A. G., Molinillo, J. M. G., Valdivia, M. M., & Macías, F. A. (2019). Provitamin supramolecular polymer micelle with pH responsiveness to control release, bioavailability enhancement and potentiation of cytotoxic efficacy. *Colloids and Surfaces B: Biointerfaces*, *173*, 85–93. https://doi.org/10.1016/j.colsurfb.2018.09.057

Miao, M., & Janaswamy, S. (2021). Editorial: Advances and Challenges of Carrier Architectures for Bioactive Delivery Systems. *Frontiers in Chemistry*, *9*. https://doi.org/10.3389/fchem.2021.739946

Mohammed, A. S. Y., Dyab, A. K. F., Taha, F., & Abd El-Mageed, A. I. A. (2021). Encapsulation of folic acid (vitamin B9) into sporopollenin microcapsules: Physico-chemical characterisation, in vitro controlled release and photoprotection study. *Materials Science and Engineering C*, *128*. https://doi.org/10.1016/j.msec.2021.112271

Monteiro, A. A., Monteiro, M. R., Pereira, R. N., Diniz, R., Costa, A. R., Malcata, F. X., Teixeira, J. A., Teixeira, Á. v., Oliveira, E. B., Coimbra, J. S., Vicente, A. A., & Ramos, Ó. L. (2016). Design of bio-based supramolecular structures through self-assembly of α-lactalbumin and lysozyme. *Food Hydrocolloids*, *58*, 60–74. https://doi.org/10.1016/j.foodhyd.2016.02.009

Paarakh, M. P., Jose, P. A. N. I., Setty, C. M., & Peter, G. V. (2019). Release Kinetics – Concepts and Applications. *International Journal of Pharmacy Research & Technology*, *8*(1), 12–20. https://doi.org/10.31838/ijprt/08.01.02

Patterson, A. K., & Smith, D. K. (2020). Two-component supramolecular hydrogel for controlled drug release. *Chemical Communications*, *56*(75), 11046–11049. https://doi.org/10.1039/d0cc03962d

Peng, S., Liu, J., Qin, Y., Wang, H., Cao, B., Lu, L., & Yu, X. (2019). Metal-Organic Framework Encapsulating Hemoglobin as a High-Stable and Long-Circulating Oxygen Carriers to Treat Hemorrhagic Shock. *ACS Applied Materials and Interfaces*, *11*(39), 35604–35612. https://doi.org/10.1021/acsami.9b15037

Premjit, Y., Pandhi, S., Kumar, A., Rai, D. C., Duary, R. K., & Mahato, D. K. (2022). Current trends in flavor encapsulation: A comprehensive review of emerging encapsulation techniques, flavour release, and mathematical modelling. *Food Research International*, *151*(November 2021), 110879. https://doi.org/10.1016/j.foodres.2021.110879

Rankin-Turner, S., Vader, P., O'Driscoll, L., Giebel, B., Heaney, L. M., & Davies, O. G. (2021). A call for the standardised reporting of factors affecting the exogenous loading of extracellular vesicles with therapeutic cargos. *Advanced Drug Delivery Reviews*, *173*, 479–491. https://doi.org/10.1016/j.addr.2021.04.012

Rathee, S., Nayak, V., Singh, K. R., & Ojha, A. (2022). Nanofortification of vitamin B-complex in food matrix: Need, regulations, and prospects. *Food Chemistry: Molecular Sciences*, *4*(2), 100100. https://doi.org/10.1016/j.fochms.2022.100100

Rebouças, L. M., Sousa, A. C. C., Sampaio, C. G., Silva, L. M. R., Costa, P. M. S., Pessoa, C., Brasil, N. V. G. P. S., & Ricardo, N. M. P. S. (2023). Microcapsules based on alginate and guar gum for co-delivery of hydrophobic antitumor bioactives. *Carbohydrate Polymers*, *301*. https://doi.org/10.1016/j.carbpol.2022.120310

Refat, M. S., El-Megharbel, S. M., Hussien, M. A., Hamza, R. Z., Al-Omar, M. A., Naglah, A. M., Afifi, W. M., & Kobeasy, M. I. (2017). Spectroscopic, structural characterizations and antioxidant capacity of the chromium (III) niacinamide compound as a diabetes mellitus drug model. *Spectrochimica Acta - Part A: Molecular and Biomolecular Spectroscopy*, *173*, 122–131. https://doi.org/10.1016/j.saa.2016.08.053

Shahparast, Y., Eskandani, M., Rajaei, A., & Khosroushahi, A. Y. (2019). Preparation, physicochemical characterization and oxidative stability of omega-3 fish oil/α-tocopherol-co-loaded nanostructured lipidic carriers. *Advanced Pharmaceutical Bulletin*, *9*(3), 393–400. https://doi.org/10.15171/apb.2019.046

Sing, C. E., & Perry, S. L. (2020). Recent progress in the science of complex coacervation. *Soft Matter*, *16*(12), 2885–2914. https://doi.org/10.1039/d0sm00001a

Suo, J., Gao, Y., Zhang, H., Wang, G., Cheng, H., Hu, Y., Lou, H., Yu, W., Dai, W., Song, L., & Wu, J. (2022). New insights into the accumulation of vitamin B3 in Torreya grandis nuts via ethylene induced key gene expression. *Food Chemistry*, *371*(April 2021), 131050. https://doi.org/10.1016/j.foodchem.2021.131050

Timilsena, Y. P., Akanbi, T. O., Khalid, N., Adhikari, B., & Barrow, C. J. (2019). Complex coacervation: Principles, mechanisms and applications in microencapsulation. In *International Journal of Biological Macromolecules* (Vol. 121, pp. 1276–1286). Elsevier B.V. https://doi.org/10.1016/j.ijbiomac.2018.10.144

Wilson, B. K., Sinko, P. J., & Prud'Homme, R. K. (2021). Encapsulation and Controlled Release of a Camptothecin Prodrug from Nanocarriers and Microgels: Tuning Release Rate with Nanocarrier Excipient Composition. *Molecular Pharmaceutics*, *18*(3), 1093–1101. https://doi.org/10.1021/acs.molpharmaceut.0c01012

Yan, X., & Wang, S. (2021). The efficacy of niacin supplementation in type 2 diabetes patients. *Medicine*, *100*(12), e22272. https://doi.org/10.1097/md.0000000000022272

Yanez, M., Jhanji, M., Murphy, K., Gower, R. M., Sajish, M., & Jabbarzadeh, E. (2019). Nicotinamide Augments the Anti-Inflammatory Properties of Resveratrol through PARP1 Activation. *Scientific Reports*, *9*(1). https://doi.org/10.1038/s41598-019-46678-8

Yang, M., Abdalkarim, S. Y. H., Yu, H.-Y., Asad, R. A. M., Ge, D., & Zhou, Y. (2022). Thermo-sensitive composite microspheres incorporating cellulose nanocrystals for regulated drug release kinetics. *Carbohydrate Polymers*, 120350. https://doi.org/10.1016/j.carbpol.2022.120350

Yu, B. lian, & Zhao, S. ping. (2007). Anti-inflammatory effect is an important property of niacin on atherosclerosis beyond its lipid-altering effects. *Medical Hypotheses*, *69*(1), 90–94. https://doi.org/10.1016/j.mehy.2006.11.026

Zhang, Q., Zhou, Y., Yue, W., Qin, W., Dong, H., & Vasanthan, T. (2021). Nanostructures of protein-polysaccharide complexes or conjugates for encapsulation of bioactive compounds. In *Trends in Food Science and Technology* (Vol. 109, pp. 169–196). Elsevier Ltd. https://doi.org/10.1016/j.tifs.2021.01.026

Zhou, L., Shi, H., Li, Z., & He, C. (2020). Recent Advances in Complex Coacervation Design from Macromolecular Assemblies and Emerging Applications. In *Macromolecular Rapid Communications* (Vol. 41, Issue 21). Wiley-VCH Verlag. https://doi.org/10.1002/marc.202000149

Supplementary Material (SM) III - "Microstructured chitosan/carboxymethylcellulose polyelectrolyte complexes for carrying and controlled release of niacinamide"

I. Validation of analytical methods

Figure SM1. Standard curves straight equations, coefficient of determination (R2), limits of detection (LD), the limit of quantification (LQ), and precision (P) for niacinamide (λmax = 228 nm).

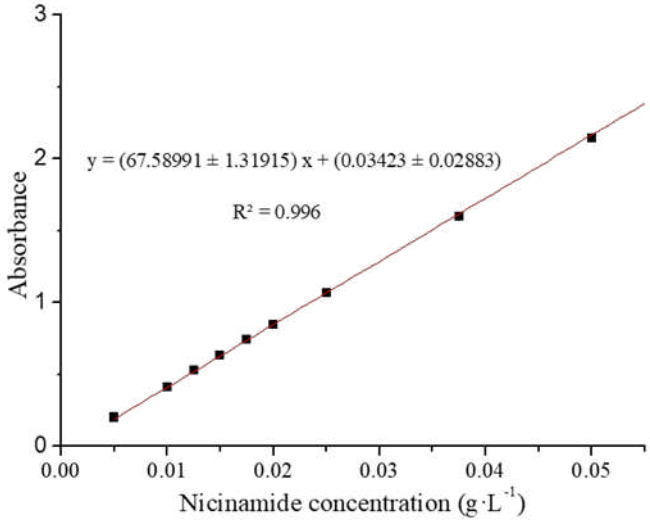

Equation	R^2	LD	LQ	P
y = = (67.58991 ± 1.31915) x + (0.03423 ± 0.02883)	0.996	3.71E-05	1.24E-04	95% ± 0.040

II. Box Behnken results

Table SM1. Box–Behnken design matrix and corresponding results for the dependent variables.

System (S)	Time(min)	pH	Niacinamide concentration (g/L)	EE (%)	LC (%)
10	120	5.00	0.02	0.86	0.20
8	180	4.00	0.06	39.89	3.89
4	180	5.00	0.04	1.98	0.02
1	60	3.00	0.04	80.65	3.23
14	120	4.00	0.04	7.90	0.04
7	60	4.00	0.06	17.60	1.06
12c	120	5.00	0.06	72.45	3.75
15	120	4.00	0.04	5.63	0.02
5	60	4.00	0.02	0.92	0.03
9	120	3.00	0.02	69.68	1.39
2	180	3.00	0.04	49.52	1.98
11c	120	3.00	0.06	80.78	4.85
3	60	5.00	0.04	1.38	0.05
6	180	4.00	0.02	1.09	0.20
13c	120	4.00	0.04	76.20	3.89

Note: “c” indicates the replicates at design center point.

III. ANOVA

Table SM2. Analyses of variance for regression models to Eficience Encapsulation (Y_1).

	SS	F	p	R^2	R^2_{ajus}
(1) Time – L+Q	0.007505	26.682	0.036125	0.99979	0.9985
(2) pH – L+Q	1.0211539	3631.912	0.000275		
(3) Niacinamide concentration – L+Q	0.112545	400.137	0.002493		
1*2	0.061627	146.069	0.006807		
1*3	0.025679	91.298	0.010836		
2*3	0.000006	0.043	0.854373		
Error	0.000281				
Total SS	1.308285				

Table SM3. Analyses of variance for regression models to Loading Capacity (Y_2).

	SS	F	p	R^2	R^2ajus
Time – L	0.23463	0.23463	0.113801	0,961	0,931
Time – Q	14.25780	14.25780	6.915349		
pH – L	0.24562	0.24562	0.119129		
pH - Q	10.39680	10.39680	5.042678		
Niacinamide concentration - L	0.14463	0.14463	0.070149		
Niacinamide concentration - Q	16.49409	2.06176			
Error	42.13457				
Total SS	0.23463	0.23463	0.113801		

CONCLUSÕES GERAIS

Face aos resultados obtidos no presente trabalho é possível concluir que:

Foi possível confirmar a construção de sistemas macro e micro-estruturados a partir da mistura entre CHS (polieletrólito catiônico) e CMC (polieletrólito aniônico). Macro-PECs se apresentaram como estruturas macroscopicamente visíveis e visualmente estáveis em solução aquosa por semanas, o que sugeriu a aplicação potencial em áreas como adsorção de contaminantes, como por exemplo corantes e metais pesados, e na engenharia de tecidos, como plataformas para reparo de tecidos. Por outro lado, os micro-PECs se apresentaram como partículas coloidais dispersas, classificadas como amorfas e termicamente estáveis, com potencial aplicabilidade em áreas como encapsulamento e liberação controlada de bioativos termossensíveis, como vitaminas, antioxidantes, fitoesteróis, probióticos, entre outros.

Foi possível confirmar a técnico-funcionalidade dos macro-PECs de CHS-CMC por sua ação como adsorventes rápidos, eficazes e recicláveis de corantes orgânicos aniônicos e catiônicos, bem como de metais pesados. Macro-PECs de CHS e CMC demonstrou excelente capacidade de adsorção para a remoção dos corantes Amarelo Crepúsculo, Azul de Metileno, Vermelho Congo e Safranina, bem como para os metais pesados Cd^{2+} e Pb^{2+}. O modelo de adsorção de Langmuir sugeriu homogeneidade da superfície das partículas do macro-PEC. A cinética de adsorção mostrou que os processos podem seguir o modelo de pseudo-primeira ou pseudo-segunda ordem. Acredita-se que os macro-PECs obtidos podem ser usados como um bom adsorvente promissor para adsorção e separação de poluentes de grandes volumes de águas residuais de corantes industriais.

Foi possível confirmar a formação do sistema de carreamento de micro-PECS formados por CHS e CMC em solução, bem como a eficácia do processo de entrega controlada e sustentada de niacinamida. A capacidade máxima de carga (LC) e a eficiência de encapsulamento (EE) alcançaram 4,85% e 80,78%, respectivamente. O fator pH teve maior influência nas respostas (EE e LC) estudadas, sendo o processo de produção de estruturas carreadoras favorecido em valores de pH mais baixos (3,0). A utilização de tempos de processo mais curtos favoreceu a formação dos sistemas de carreamento em termos práticos e econômicos. O estudo de liberação *in vitro* de micro-PECs de CHS/CMC ~~de~~ e niacinamida foi realizado em diferentes condições de pH, mimetizando a condição do trato gastrointestinal. O estudo indicou que a liberação máxima de niacinamida ocorreu após cerca de 4,5 horas (270 min). As porcentagens máximas de niacinamida liberadas foram 89,29%, 87,68%, 96,76%, 89,57%, 91,58%, 88,02% e 97,78% para os sistemas 1, 2, 7, 8,9, 10 e 11, respectivamente. As

constantes do modelo de ordem zero (K_0) foram baixas e semelhantes para todos os sistemas estudados, demonstrando uma baixa taxa de liberação, indicando que o processo de liberação de niacinamida dos micro-PECs de CHS/CMC ocorre principalmente por difusão.

O impacto promissor dos sistemas macro e micro-estruturados de quitosano e carboximetilcelulose em sistemas-modelo de adsorção de poluentes em meio aquoso e em sistemas-modelo de liberação controlada de compostos bioativos hidrofílicos foi demonstrado apontando, por conseguinte, ampla gama de técnico-funcionalidades em diversos setores, como por exemplo indústria alimentícia, química, têxtil e farmacêutica.

Diante do exposto, conclui-se que a presente tese comtemplou a importância da produção e aplicação de novas estruturas supramoleculares. Os resultados aqui obtidos abrem perspectiva para a otimização dos sistemas aqui propostos, com adição de novos compostos e/ou modificações estruturais nos já existentes. Além disso, podem ser realizados, por exemplo, estudos desses sistemas como agentes estabilizantes de emulsão pickering, a fim de se verificar o potencial dos macro e micro-PECs como alternativa à agentes emulsionantes ou tensioactivos.